

# **A Fragment-Based Approach to the Identification of Novel Ketopantoate Reductase Inhibitors**

Submitted in total fulfilment of the requirements of the degree of

**Doctor of Philosophy**

by

**Amelia Vom**

B. Med. Chem. (Hons)

Department of Medicinal Chemistry and Drug Action

Monash Institute of Pharmaceutical Sciences

Monash University

January 2012

*The following corrections have all been made:*

- Page xiii            Abbreviation "ADP" listed as "ammonium dihydrogen phosphate" should be "adenosine diphosphate"
- Page 2                Change: *M. tuberculosis* to *Mycobacterium tuberculosis*; *S. aureus* to *Staphylococcus aureus*; and *P. aeruginosa* to *Pseudomonas aeruginosa*
- Page 9, line 3        Insert: comma after (Figure 1-4)
- Page 11              In 2<sup>nd</sup> paragraph, line 5 remove space in "5,10-methylene-tetrahydrofolate"
- Page 12              In Scheme 1-2, the structures **24**, **29**, **27**, **28**, & **31** in the ribose ring where it shows "OR" attached through the "R" group should actually be attached through the oxygen atom
- Page 13, line 8        Change: "bacteria" to "species"
- Page 15, line 5        Change: "(Scheme 1-6B)" to "(Scheme 1-4B)"
- Page 15              Change in Scheme 1-4:  $K_i$  for "*E. coli*" to  $K_i$  for "*M. tuberculosis*"
- Page 22              In Figure 1-6, structure **41** with the "OR" attached to the ribose ring should be changed as described above for Scheme 1-2
- Page 53, line 9        Change: "..the cells my lyse.." to "..the cells may lyse.."
- Page 54              Change Figure 2-2 legend: "protein expression level" to "cell density"
- Page 62, line 5        Insert: "indicating" after the sentence "...addition of NADPH (**24**),"
- Page 76, line 6        Insert: "(refer to section 7.1.6.4 Glide docking for a description of SP and XP)." after "...extra-precision (XP) mode were examined"
- Page 77              In Figure 2-13, structures **24**, **29**, **27**, **28**, **31**, **118**, **119**, **41** with the "OR" attached to the ribose ring should be changed as described above for Scheme 1-2
- Page 88, line 7        Change: " X-axis" to "Y-axis"
- Page 96              Insert in 2<sup>nd</sup> paragraph, line 1: "may" after "Non-competitive inhibitors"
- Page 103             Insert in 2<sup>nd</sup> paragraph, line 3: "inhibitory" before "activity"

- Page 200      Insert after the 1<sup>st</sup> paragraph: "Additionally, it would be interesting to retest the thienothiophene series with the optimised detergent-based enzyme assay. Particularly for compounds **166**, **167** and **176**, which were shown to be quite active (based on the initial enzyme assay). To determine whether the thienothiophene series are worth pursuing, there are two important issues that need to be addressed. The first is to establish that inhibition is not aggregation based and second is to determine that the inhibition is not due to the presence of the minor active impurity."
- Page 233      Change the compound number for pyrrolidine: "**141a**" to "**141b**"
- Page 244      Change: "m2ethanol-ether" to "methanol-ether"
- Page 254      Change compound **160**: LRMS (ESI) *m/z* 213 "(M-H)<sup>+</sup>" to "(M+H)<sup>+</sup>"
- Page 296      Change in Appendix II: the IC<sub>50</sub> values for **220** and **221** are 13 µM and 6 µM, respectively
- Chapter 2 and 3      Insert a footnote for the following Tables in Chapter 2 and 3 (Table 2-1, page 73; Table 3-2, page 104; Table 3-3, page 112; Table 3-6, page 123; Table 3-7, page 137; Table 3-8, page 139; Table 3-9, page 141; Table 3-10, page 146; Table 3-11, page 148 and Table 3-12, page 150): "The data shown were analysed by standard KPR assay conditions: NADPH (**24**, 20 µM), ketopantoate (**22**, 1 mM), and KPR (3 nM) in 100 mM HEPES buffer (pH 7.6) with 2% DMSO (vol/vol)."
- Chapter 4 and 5      Insert a footnote for the following Tables in Chapter 4 and 5 (Table 4-4, page 184; Table 5-1, page 192 and Table 5-2, page 194): "The data shown were analysed by optimised detergent-based conditions: NADH (**29**, 25 µM), ketopantoate (**22**, 1 mM), and KPR (3 nM) in 100 mM HEPES buffer (pH 7.6) with 0.01% Tween-20 and 2% DMSO (vol/vol)."

**Notice 1**

*Under the Copyright Act 1968, this thesis must be used only under the normal conditions of scholarly fair dealing. In particular no results or conclusions should be extracted from it, nor should it be copied or closely paraphrased in whole or in part without the written consent of the author. Proper written acknowledgement should be made for any assistance obtained from this thesis.*

**Notice 2**

*I certify that I have made all reasonable efforts to secure copyright permissions for third-party content included in this thesis and have not knowingly added copyright content to my work without the owner's permission.*

# Declaration

I hereby declare that this thesis contains no material which has been accepted for the award of any other degree or diploma at any university or equivalent institution and that to the best of my knowledge and belief, this thesis contains no material previously written by another person, except where due reference is made in the text of the thesis.

Amelia Vom

---

# Table of contents

<b>Declaration</b> .....	<b>i</b>
<b>Acknowledgements</b> .....	<b>viii</b>
<b>Abstract</b> .....	<b>xi</b>
<b>Abbreviations and acronyms</b> .....	<b>xiii</b>
<b>1 Introduction</b> .....	<b>2</b>
1.1 The need for new antimicrobial agents .....	2
1.1.1 Bacterial resistance to antibiotics .....	2
1.1.2 The decline of antimicrobial research and development in the pipeline ....	3
1.1.3 The targets of current antimicrobial agents .....	4
1.1.4 Mechanisms of bacterial resistance .....	7
1.2 Pantothenate .....	9
1.2.1 The biosynthesis of pantothenate.....	11
1.2.2 Inhibition of pantothenate biosynthesis .....	13
1.3 Ketopantoate reductase .....	18
1.3.1 Proposed catalytic mechanism of KPR.....	18
1.3.2 The structure of <i>E. coli</i> KPR.....	19
1.3.3 KPR catalytic activity .....	25
1.4 Fragment-based lead discovery .....	29
1.4.1 Chemical space .....	31
1.4.2 Ligand complexity .....	31

---

1.4.3	Ligand efficiency .....	32
1.4.4	Fragment library design .....	33
1.4.5	Fragment screening and confirming hits .....	34
1.4.6	Converting fragment hits into leads.....	41
1.4.7	Fragments in the clinic.....	45
<b>2</b>	<b>Protein expression, screening and hit validation .....</b>	<b>50</b>
2.1	Introduction .....	50
2.2	Protein expression .....	50
2.2.1	His <sub>6</sub> -KPR .....	51
2.2.2	His <sub>6</sub> - <sup>15</sup> N KPR.....	54
2.2.3	Purification (unlabelled and <sup>15</sup> N-KPR).....	55
2.3	Fragment library.....	56
2.4	STD-NMR fragment screening .....	57
2.4.1	STD-NMR analysis .....	57
2.4.2	STD NMR screening hits.....	58
2.5	<sup>1</sup> H/ <sup>15</sup> N-HSQC NMR .....	60
2.5.1	NADPH test study .....	60
2.5.2	Fragment hit confirmation .....	63
2.6	Functional assay .....	67
2.6.1	Assay development and optimisation .....	67
2.6.2	KPR inhibition by fragment hits.....	71
2.7	Computational modelling.....	73

---

2.7.1	Analysis of water molecules in the binding site .....	74
2.7.2	Docking NADP <sup>+</sup> and analogues .....	75
2.7.3	Fragment docking .....	81
2.8	Conclusions .....	83
<b>3</b>	<b>SAR development of fragment hits .....</b>	<b>85</b>
3.1	Introduction .....	85
3.2	Sulfonamides .....	86
3.2.1	Mode of inhibition .....	87
3.2.2	Preliminary SAR.....	88
3.2.3	Chemical shift mapping .....	91
3.2.4	3-(Piperidin-1-ylsulfonyl)aniline.....	93
3.2.5	Synthesis of sulfonylaniline derivatives .....	97
3.2.6	Inhibition analysis of sulfonamide analogues.....	101
3.2.7	Summary.....	104
3.3	Thienopyrroles .....	105
3.3.1	Mode of inhibition .....	105
3.3.2	Preliminary SAR.....	106
3.3.3	Chemical shift mapping .....	108
3.3.4	Thieno[3,2- <i>b</i> ]thiophene-2-carboxylic acid .....	110
3.3.5	Synthesis of thieno[3,2- <i>b</i> ]thiophenes .....	112
3.3.6	Inhibition analysis of thienothiophene analogues.....	121
3.3.7	Summary.....	130

---

3.4	Phenylthiophenes .....	131
3.4.1	SAR for phenylthiophenes.....	135
3.4.2	Chemical shift mapping.....	141
3.4.3	SAR for phenylfurans .....	144
3.4.4	Summary.....	150
3.5	Conclusions .....	152
<b>4</b>	<b>Screening evaluation and optimisation.....</b>	<b>155</b>
4.1	Introduction .....	155
4.1.1	What is aggregation? .....	155
4.1.2	Proposed mechanism of aggregation-based inhibition .....	156
4.1.3	Characteristics of aggregation-based inhibition .....	157
4.2	Characterisation of aggregation-based false positives .....	161
4.2.1	Steep dose-response curves: sulfonamide series .....	161
4.2.2	Non-specific interactions: bovine serum albumin .....	162
4.2.3	Dynamic light scattering.....	164
4.3	UV-Vis assay.....	166
4.3.1	Detergent selection .....	167
4.3.2	NADPH and NADH .....	170
4.3.3	Test case .....	171
4.4	STD-NMR optimisation .....	175
4.4.1	Detergent selection .....	175
4.4.2	Test case .....	176

---

4.4.3	Analysis of ligand binding.....	178
4.4.4	Rescreen.....	181
4.5	Detergent-based enzyme assay.....	182
4.6	Fragment binding evaluation and mapping.....	184
4.7	Conclusions.....	185
<b>5</b>	<b>Fragment hit development.....</b>	<b>187</b>
5.1	Introduction.....	187
5.1.1	Mode of inhibition of the nicotinic acid derivatives.....	188
5.1.2	Chemical shift mapping.....	188
5.1.3	Preliminary SAR for nicotinic acids.....	190
5.1.4	Conclusions.....	194
<b>6</b>	<b>Conclusions and future directions.....</b>	<b>196</b>
<b>7</b>	<b>Experimental.....</b>	<b>201</b>
7.1	Biochemistry.....	201
7.1.1	Materials.....	201
7.1.2	Molecular methods.....	204
7.1.3	Functional assay.....	217
7.1.4	Dynamic light scattering.....	220
7.1.5	NMR methods.....	221
7.1.6	Computational docking.....	225
7.2	Chemistry.....	228
7.2.1	General experimental.....	228

---

7.2.2	Synthesis of sulfonamides .....	231
7.2.3	Synthesis of thieno-thiophene/pyrrole analogues .....	251
7.2.4	Synthesis of phenyl-furan/thiophene analogues .....	265
<b>References</b>	.....	<b>274</b>
<b>Appendices</b>	.....	<b>293</b>
Appendix I	.....	293
Appendix II	.....	295
Appendix III	.....	303
A: HPLC chromatograms for synthesised sulfonamide analogues	.....	303
B: HPLC chromatograms for synthesised thienothiophene analogues	.....	308
C: HPLC chromatograms for synthesised phenylfuran analogues	.....	311

# Acknowledgements

I am truly indebted and thankful to my supervisor Dr Jamie Simpson. His enthusiasm for research is inspiring and his breadth of knowledge in chemistry and more generally astounds me. This has taught me to appreciate science and research so much more. I am grateful for his guidance in keeping me on track but also allowing me the opportunities to learn, explore and grow to be a better scientist. While I only thank him now formally, I appreciate the times he has challenged and pushed the boundaries. This has strengthened my ability to critically analyse and solve problems. One of my favourite memories I'll never forget is the time he fused my name with fragments and called me 'fragameliment'! Additionally, I would like to thank my co-supervisors, Dr Ben Capuano and Dr Elizabeth Yuriev. To Ben, his suggestions and advice on chemistry were invaluable as well as his support in family matters. His enthusiasm, positive attitude and encouragement always put a smile on my face. To Elizabeth, thank you for providing useful advice and suggestions in computational docking. I am very grateful for all the support and encouragement through-out my candidature and I very much enjoyed the interesting discussions over coffee.

A special thanks to Associate Professor Martin Scanlon for all his invaluable advice, suggestions and considerable support for all the biochemical aspects during my PhD studies. His focus and passion towards research is inspiring. It has been a privilege both working and learning from him. In his lab, I was spoilt with lab space and felt very much a part of his research team. For me, Martin's love for NMR was undeniable when he saw the first  $^1\text{H}/^{15}\text{N}$ -HSQC spectrum of KPR and described it as 'sexy'!

I thank Dr Tony Velkov for showing me how to express and purify protein. I thank Dr Stephen Headey, Dr Kieran Rimmer and Dr James Horne for their help, advice and guidance with NMR related experiments. Particularly to Steve, I am thankful for his patience and persistence in teaching me NMR theory and for assigning the backbone resonances of

KPR. His never ending facts and statistics; discussions of history, culture, psychology and philosophy were all enlightening and entertaining. I thank past and present students Mr Duy Pham, Mr Hai Tao Zhao and especially Mr Tony Wang, who helped with biochemical testing and useful discussions. I thank Dr David Chalmers for all his help and advice in computational docking and scripting work; Dr Jason Dang for MS analysis and Dr Charlie Dong for his technical support and assistance setting up the DLS experiments.

I thank Simpson's group: Mr Brad Doak, Mr Chris Opie, Miss Natalie Vinh and Mr Chris Schreurs for their helpful chemistry discussions, suggestions and advice along the way. Additionally, I am grateful to Scanlon's group: Miss Yanni Chin, Dr Pooja Sharma, Mr Martin Williams, Miss Mansha Vazirani, Dr Aisha Laguerre, Miss Jennifer La, Mr Sandeep Chhabra and Dr Maria Hughes for their help and advice in the biochemistry lab. To Yanni, Pooja and Aisha, thanks for creating a unique lab experience with lots of laughter and tears shared over the years.

Thanks to my office colleagues Dr Michelle Camerino, Dr Jo-Anne Pinson, Dr Gemma Ferguson and Mr Joshua Gosling for sharing the PhD life and the friendships gained. Our obsession and over-use of fruity deodorant room sprays, canned soup and 2-minute noodles will remain with me always. Thanks to my coffee and ski buddies Mr Will Nguyen, Mr Tim Blackmore, Chris, Michelle, Josh and Jen for all the good times and memories.

I thank my mother Lan Sam and father Fem Vom for being so supportive, understanding and patient through-out my studies. Thank you for all the takeaway dinners! I thank Richard Vom, my baby brother for always believing in me and for being there whenever and wherever I needed help. Last but not least, I thank my husband Jonathan Lay, for his patience and understanding of my 'student' status. Thank you for the invaluable support and sharing the life I only dreamt of as a little girl.

---

*For 'po-po' - Lay Kiu Jung,  
my strength and courage*

# Abstract

Pantothenate (Vitamin B5) is a key precursor to coenzyme A, an essential cofactor for fatty acid biosynthesis and other metabolic processes. The pathway for pantothenate biosynthesis is only present in microorganisms and plants, suggesting it may be a target for developing novel antimicrobial agents. Ketopantoate reductase (KPR), a 34 kDa protein, is a key enzyme on this pathway, catalysing the NADPH-dependent reduction of ketopantoate to pantoate.

In this study, a fragment-based lead design (FBLD) approach was used to identify small molecule inhibitors of KPR. The expression and purification of labelled and unlabelled KPR was optimised to give high yields suitable for screening and kinetic studies. NMR based screening of 500 fragments using STD-NMR identified 47 hits that were validated by  $^1\text{H}/^{15}\text{N}$ -HSQC NMR, resulting in 14 confirmed fragment hits, correlating to a hit rate of 3%. These hits were assessed for inhibitory activity, with 4 compounds showing an  $\text{IC}_{50} < 500 \mu\text{M}$ .

The fragment hits were prioritised based on ligand efficiency (the quality of binding interactions between the fragment and target protein) and tractability for synthetic elaboration and derivatisation. Preliminary SAR was established for three series by testing simple analogues of the initial hit. Further analogues based on the scaffolds - sulfonamide, thienopyrrole and phenylthiophene were designed and synthesised to optimise binding to the active site and improve the potency. Binding locations of the fragment hits were identified using  $^1\text{H}/^{15}\text{N}$ -HSQC NMR based on the assigned backbone resonances of *E. coli* KPR.

This thesis also describes the risks of false positives in fragment-based identification of KPR inhibitors. The lead series were identified to be inhibiting through a non-specific mechanism, which was confirmed to be aggregation based, by comparison with literature studies of aggregating compounds. As a result, an NMR-based fragment screening approach and enzyme assay was developed to overcome many of the challenges posed by false positives. Post elimination of false positives, a number of fragment hits has been confirmed to inhibit KPR activity in an *in vitro* assay.

---

## Abbreviations and acronyms

<b>1D</b>	one-dimensional
<b>2'-P-ADP-ribose</b>	2'-monophosphoadenosine 5'-diphosphoribose
<b>2D</b>	two-dimensional
<b>2'-P-AMP</b>	2'-phosphoadenosine-5'-monophosphate
<b>3D</b>	three-dimensional
<b>A<sub>280</sub></b>	absorbance at 280 nm
<b>AcOH</b>	acetic acid
<b>ADC</b>	aspartate decarboxylase
<b>ADP</b>	adenosine diphosphate
<b>ADP-ribose</b>	adenosine diphosphate ribose
<b>AHAIR</b>	acetohydroxyacid isomeroeductase
<b>Amp</b>	ampicillin
<b>AMP</b>	adenosine monophosphate
<b>APB</b>	alternative pyrimidine biosynthetic
<b>ATP</b>	adenosine triphosphate
<b>BCG</b>	<i>bacille</i> Calmette-Guérin
<b>BSA</b>	bovine serum albumin
<b>CMC</b>	critical micelle concentration
<b>CoA</b>	coenzyme A
<b>COSY</b>	correlation spectroscopy
<b>CSP</b>	chemical shift perturbations
<b>CV</b>	column volume
<b>DCM</b>	dichloromethane
<b>DHFR</b>	dihydrofolate reductase
<b>DHPS</b>	dihydropteroate synthase
<b>DLS</b>	dynamic light scattering
<b>DMF</b>	<i>N,N</i> -dimethylformamide
<b>DMSO</b>	dimethyl sulfoxide
<b>DTT</b>	dithiothreitol
<b>EDTA</b>	ethylenediaminetetraacetic acid
<b>ESI</b>	electrospray ionisation

---

<b>FBLD</b>	fragment-based lead discovery
<b>FDA</b>	Food and Drug Administration
<b>FKBP</b>	FK506-binding protein
<b>GDP</b>	guanosine diphosphate
<b>GTP</b>	guanosine-5'-triphosphate
<b>h</b>	hour
<b>HAC</b>	heavy atom count
<b>HCS</b>	high content screening
<b>HEPES</b>	2-[4-(2-hydroxyethyl)piperazin-1-yl]ethanesulfonic acid
<b>HIV</b>	human immunodeficiency virus
<b>HMBC</b>	heteronuclear multiple bond correlation
<b>HPLC</b>	high performance liquid chromatography
<b>HRMS</b>	high resolution mass spectroscopy
<b>HSQC</b>	heteronuclear single quantum correlation
<b>HTS</b>	high-throughput screening
<b>IPTG</b>	isopropyl-1-thio- $\beta$ -D-galactopyranoside
<b>ITC</b>	isothermal titration calorimetry
<b>KPHMT</b>	ketopantoate hydroxymethyltransferase
<b>KPR</b>	ketopantoate reductase
<b>LB</b>	luria broth
<b>LE</b>	ligand efficiency
<b>M</b>	molarity
<b>MALDI-TOF</b>	matrix-assisted laser desorption/ionization-time of flight
<b>min</b>	minutes
<b>MIPS</b>	Monash Institute of Pharmaceutical Sciences
<b>mp</b>	melting point
<b>MS</b>	mass spectrometry
<b>NADH</b>	nicotinamide adenine dinucleotide
<b>NADPH</b>	nicotinamide adenine dinucleotide phosphate
<b>Ni-NTA</b>	nickel-nitrilotriacetic acid
<b>NMR</b>	nuclear magnetic resonance
<b>NROT</b>	number of rotatable bonds
<b>OD</b>	optical density
<b>PABA</b>	<i>p</i> -aminobenzoic acid

<b>PDB</b>	Protein Data Bank
<b>ppm</b>	parts per million
<b>PSA</b>	polar surface area
<b>PtS</b>	pantothenate synthetase
<b>PyBOP</b>	(benzotriazol-1-yloxy)tripyrrolidinophosphonium hexafluorophosphate)
<b>RECAP</b>	retrosynthetic combinatorial analysis procedure
<b>RMSD</b>	root-mean-square distance
<b>rpm</b>	revolutions per minute
<b>S</b>	svedberg
<b>SAR</b>	structure-activity relationships
<b>SDS-PAGE</b>	sodium dodecyl sulphate-polyacrylamide gel electrophoresis
<b>SP</b>	standard-precision
<b>SPR</b>	surface plasmon resonance
<b>STD</b>	saturation transfer difference
<b>TEMED</b>	tertramethylethylenediamine
<b>THF</b>	tetrahydrofuran
<b>TLC</b>	thin layer chromatography
<b>UV</b>	ultraviolet
<b>XP</b>	extra-precision
<b><math>\beta</math>-NMN</b>	nicotinamide mononucleotide

# Chapter 1

---

## Introduction

# 1 Introduction

## 1.1 The need for new antimicrobial agents

### 1.1.1 Bacterial resistance to antibiotics

Identified as one of the greatest threats to human health, the problem with antibiotic-resistant pathogenic bacteria continues to worsen.<sup>1-2</sup> The prevalence of resistant pathogens has virtually extended to all currently available drugs. Global examples of drug-resistant bacteria include multidrug-resistant *Mycobacterium tuberculosis*, methicillin-resistant and multidrug-resistant *Staphylococcus aureus*, penicillin- and macrolide-resistant *Pneumococci*, vancomycin-resistant *Enterococci*, as well as multidrug-resistant Gram-negative bacteria such as *Pseudomonas aeruginosa*.<sup>3-5</sup>

One of the factors responsible for most resistance problems is patient-to-patient spread in hospitals.<sup>6</sup> A study has shown 1.7 million Americans in the year 2002 acquired infections in hospitals after being hospitalised for another reason.<sup>7</sup> Of these, 6% of patients died of their infections. Most of these infections were caused by antibiotic resistant bacteria. Hospital acquired infections are the consequence of concentrating sick patients, transmission of pathogens from patient to patient *via* the hands of health care workers<sup>8</sup> and the use of invasive procedures and devices becoming more frequent. For example, sticking a catheter through the skin and into the veins to allow drainage, administration of fluids or gases or access by surgical instruments are common techniques used in hospitals. Having the skin open increases the chance of bacterial infections as it enables them to bypass the most protective layer of our body.

### 1.1.2 The decline of antimicrobial research and development in the pipeline

New classes of antimicrobial agents approved by the Food and Drug Administration (FDA) have decreased alarmingly over the past 30 years. In fact, only two completely new classes of antimicrobials (shown in Figure 1-1) have been introduced: the oxazolidinone linezolid (Zyvox (**1**); Pfizer) in 2000 and the cyclic lipopeptide daptomycin (Cubicin (**2**); Cubist) in 2003.<sup>9</sup> One of the principal reasons for the decline of antibacterial research and development in pharmaceutical companies is the lack of financial incentives.<sup>10</sup> Drug discovery efforts are focused on agents that treat chronic medical conditions (where a better return on investment can be made) such as hypertension, depression, dementia, and rheumatoid arthritis. These agents act only to suppress symptoms which are non-curable. In contrast, antibiotics are used for short periods of time that cure their target disease and are subject to the emergence of resistance.

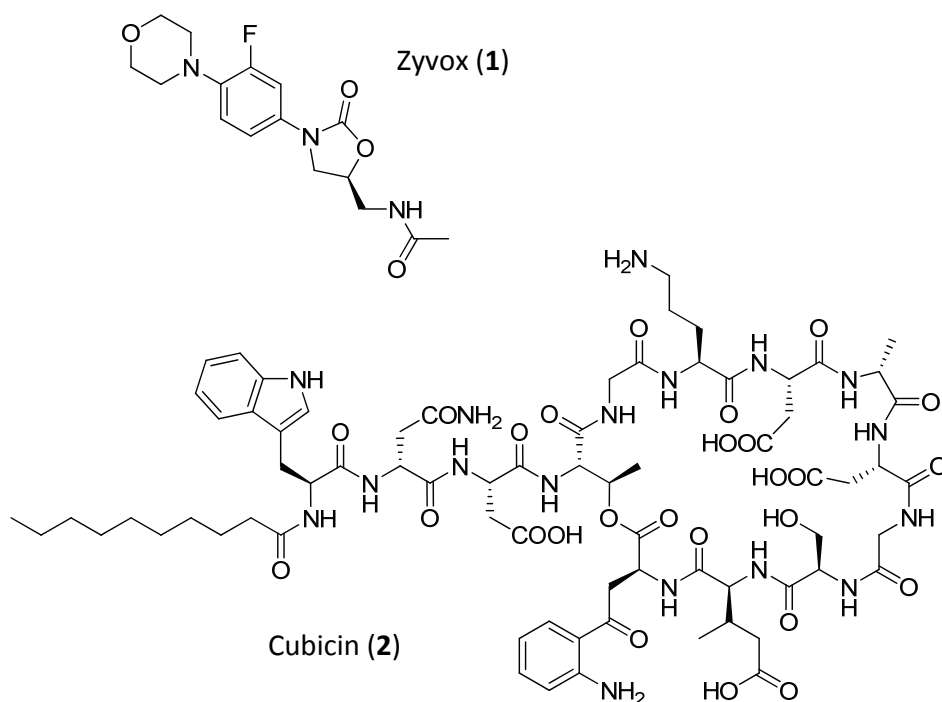


**Figure 1-1.** Chemical structures of new antimicrobial chemical classes

Regulatory authorities have also played a part in the decline of antibacterial development. Concerns have been raised about the FDA's decision making and 'changing the rules' after providing advice on the development and approval of new antimicrobials.<sup>3,11-12</sup> The FDA were criticised for uncertainty or unclear regulatory guidance particularly in defining safety requirements of novel agents, acceptable sample sizes for statistical significance in clinical trial and acceptable outcome measures. The demand by the FDA for appropriate labelling to prevent 'unnecessary use' of antibacterial agents was a positive move for the community however, had negatively impacted sales for pharmaceutical companies. In 2002 the use of antibacterial agents was estimated to be 100,000 – 200,000 tonnes per annum worldwide.<sup>11-13</sup> Since the label was introduced, the consumption rate of antibiotics has decreased. France and Japan have shown the strongest decline of antibiotic usage between 2000 and 2009 by 21% and 15%, respectively.<sup>14</sup>

The decline in antibacterial research and development at a time of increasing emergence and spread of resistant pathogens raises a major concern for the availability of effective therapy options in the future.

### **1.1.3 The targets of current antimicrobial agents**

Existing antimicrobial agents predominately target a few cellular functions. The antimicrobial agents act either to induce cell death (bactericidal drugs) or inhibit cell growth (bacteriostatic drugs) by targeting cell-wall biosynthesis (**3 – 5**), protein biosynthesis (**6 – 9**), folate metabolism (**10 – 11**), DNA or RNA synthesis (**12 – 15**).<sup>15</sup> Table 1-1 and Table 1-2 briefly describe the mechanisms of action for antibiotics targeting biosynthetic pathways and the resistance mechanisms developed, respectively.

**Table 1-1.** The mechanisms of action of antimicrobial agents (structures are shown in Figure 1-2)

Antimicrobial	Mechanisms of action
$\beta$ -Lactams	<ul style="list-style-type: none"> <li>- Interfere with cell-wall biosynthesis</li> <li>- Compromise cell shape and size, causing cell stress responses and ultimately lead to cell lysis<sup>16-17</sup></li> <li>- E.g. Penicillins (<b>3</b>), Carbapenems (<b>4</b>) and Cephalosporins (<b>5</b>)</li> </ul>
Macrolides	<ul style="list-style-type: none"> <li>- Inhibit protein biosynthesis</li> <li>- Act on the large ribosomal subunit and interferes with the catalysis of peptide bond formation and/or the progression of the nascent peptide toward the exit tunnel</li> <li>- E.g. Erythromycin (<b>6</b>)</li> </ul>
Aminoglycosides	<ul style="list-style-type: none"> <li>- Inhibit protein biosynthesis</li> <li>- Facilitate mRNA miscoding,<sup>18</sup> inhibit mRNA and tRNA translocation<sup>19-20</sup> and inhibit ribosome recycling<sup>21</sup></li> <li>- E.g. Gentamicin (<b>7</b>), Neomycin (<b>8</b>) and Paromomycin (<b>9</b>)</li> </ul>
Trimethoprim - Sulfonamides	<ul style="list-style-type: none"> <li>- The synergism with Sulfamethoxazole (<b>10</b>) and Trimethoprim (<b>11</b>) targets the folic acid pathway</li> <li>- The sulfonamides operate as structural analogues of <i>p</i>-aminobenzoic acid (PABA) and inhibit dihydropteroate synthase (DHPS), while trimethoprim forms tight binding to dihydrofolate reductase (DHFR)<sup>22-23</sup></li> </ul>
Quinolones	<ul style="list-style-type: none"> <li>- Interfere with DNA synthesis</li> <li>- Bind to DNA gyrase and/or topoisomerase IV and disrupt the integrity of the supercoiled DNA helix during replication and transcription<sup>24</sup></li> <li>- E.g. Sparfloxacin (<b>12</b>) and Moxifloxacin (<b>13</b>)</li> </ul>
Rifampicin	<ul style="list-style-type: none"> <li>- Interfere with RNA synthesis</li> <li>- Binds tightly to non-conserved part of the RNA polymerase (more than 12 Å away from the active site) which inhibits the extension of the nascent RNA chain after the first or second condensation step<sup>25-26</sup></li> <li>- E.g. Rifamycin SV (<b>14</b>) and Rifampicin (<b>15</b>)</li> </ul>

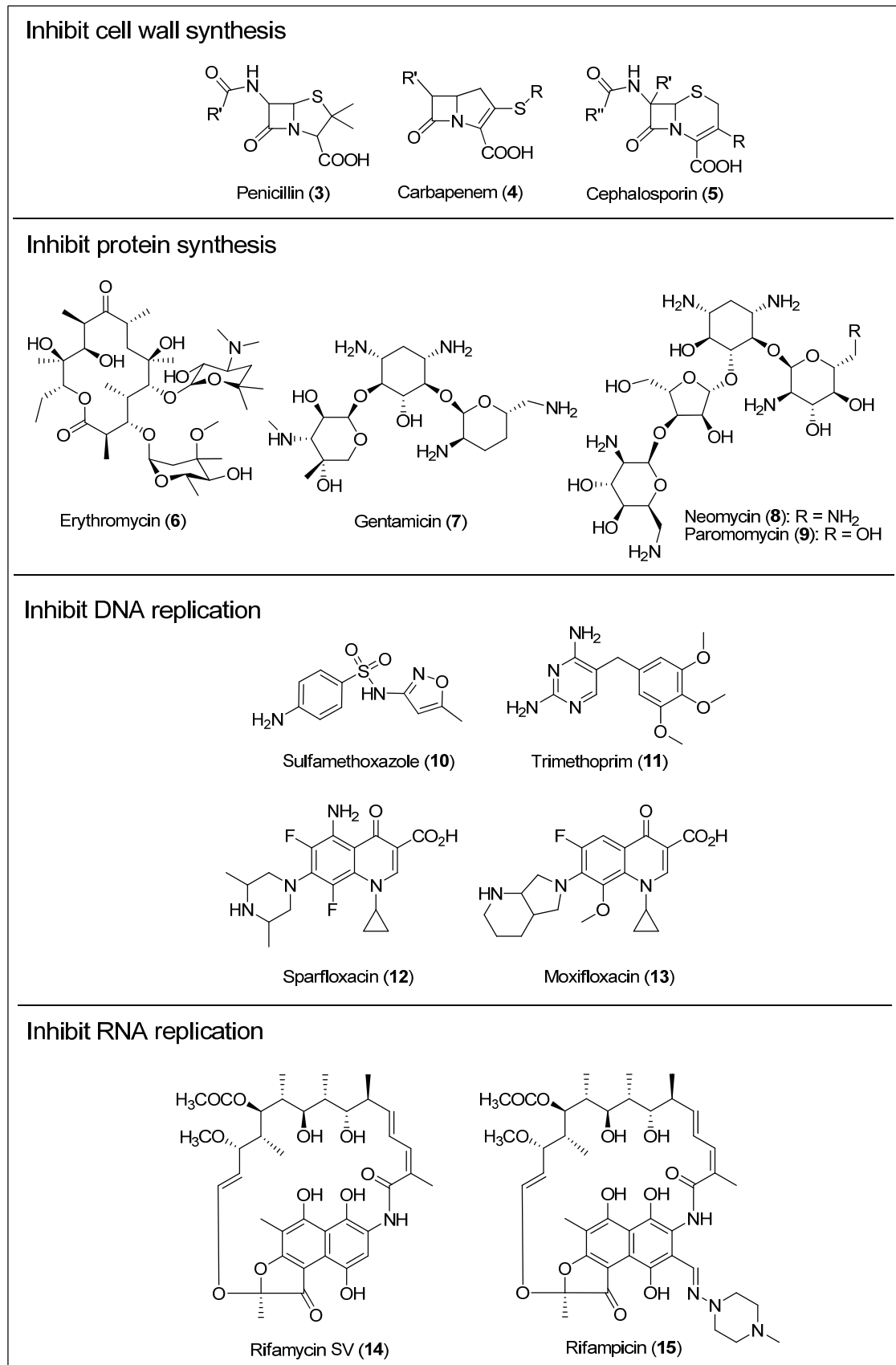
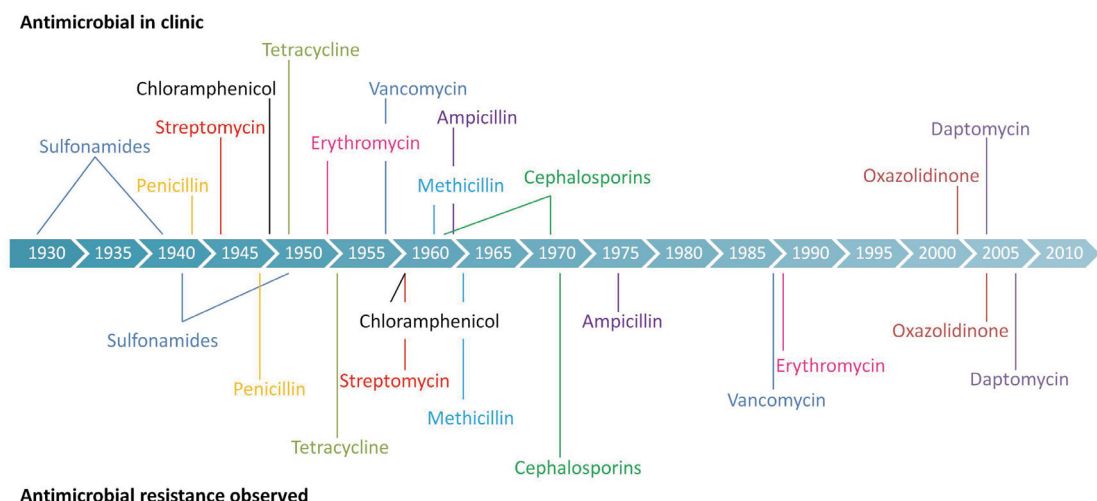


Figure 1-2. Structures of antimicrobial agents

### 1.1.4 Mechanisms of bacterial resistance

The emergence of resistance to antimicrobial agents occurs through a variety of mechanisms. Depending on the genetic event for acquiring an antimicrobial resistance phenotype, they are termed vertical or horizontal evolution.<sup>27-28</sup> Vertical evolution is when the bacteria are inherently resistant to one or more classes of antimicrobial agents or acquire resistance following chromosomal mutation and selection. Horizontal evolution occurs when bacteria acquire new genetic material from other resistant organisms. The genetic exchange mechanism for the latter event can occur *via* conjugation, transformation or transduction.<sup>28-29</sup> The biochemical antimicrobial resistance mechanisms are similar and can be divided into five categories: (1) drug inactivation, (2) decreased accessibility, (3) altered target, (4) metabolic bypass, and (5) tolerance.<sup>28,30</sup> Since the introduction of the sulfa drugs, penicillins and subsequent novel antimicrobial agents, various forms of resistance also followed in as little as a few years (as illustrated in Figure 1-3). The mechanisms of resistance to antimicrobial agents are summarised in Table 1-2.



**Figure 1-3.** Timeline of antimicrobials available in the clinic (above indicated year) and the first report of antimicrobial resistance (below indicated year)<sup>31</sup>

**Table 1-2.** Mechanisms of bacterial resistance to antimicrobial agents

Antimicrobial	Resistance Mechanisms
$\beta$ -Lactams <sup>32-36</sup>	<ul style="list-style-type: none"> <li>- Inactivation by <math>\beta</math>-lactamases as it cleaves the amide bond</li> <li>- Decreased accessibility by lowering membrane permeability</li> <li>- Efflux pumps</li> <li>- Alteration of active site (penicillin binding proteins)</li> </ul>
Aminoglycosides <sup>37-38</sup>	<ul style="list-style-type: none"> <li>- Inactivation by acetylases, adenylases, phosphorylases</li> <li>- Reduced uptake or decreased membrane permeability</li> <li>- Modification of active site (30S ribosomal subunit)</li> </ul>
Macrolides <sup>39</sup>	<ul style="list-style-type: none"> <li>- Efflux pump</li> <li>- Modification of active site (23S ribosomal subunit)</li> <li>- Modification of macrolide antibiotic</li> </ul>
Trimethoprim - Sulfamethoxazole <sup>28,30</sup>	<ul style="list-style-type: none"> <li>- Decreased membrane permeability</li> <li>- Bypassing of drug action by new DHFR and DHPS</li> </ul>
Quinolones <sup>40</sup>	<ul style="list-style-type: none"> <li>- Efflux pump</li> <li>- Modification of active site (DNA gyrase and topoisomerase IV)</li> </ul>
Rifampicin <sup>25</sup>	<ul style="list-style-type: none"> <li>- Alteration of target (RNA polymerase, rpoB)</li> </ul>

Clearly, there is a need for novel antibacterial targets to prevent and control resistant bacterial infection. Undeniably, overcoming antibiotic resistance is an enormous challenge. However, a novel antibacterial target increases the potential to identify new ways to prevent bacterial infection and minimise the induction of bacterial resistance mechanisms.

## 1.2 Pantothenate

It has been suggested in the literature<sup>41-42</sup> that the biosynthesis of pantothenate (**16**), vital to coenzyme A (CoA, **17**) and acyl carrier proteins such as phosphopantetheine (**18**) (Figure 1-4), as an attractive target for the development of a potential broad spectrum antimicrobial agent and herbicides due to its absence in humans.

Pantothenate (**16**) is the key precursor to CoA (**17**) that is a ubiquitous and essential cofactor in all organisms and is involved in numerous reactions central to cellular metabolism. CoA (**17**) functions as an acyl group carrier and carbonyl-activating group in many biochemical transformations. CoA (**17**) is the source of the 4'-phosphopantetheine moiety incorporated into the prosthetic group of the acyl carrier proteins in fatty acid synthases, polyketide synthases and non-ribosomal peptide synthetases.<sup>43</sup>

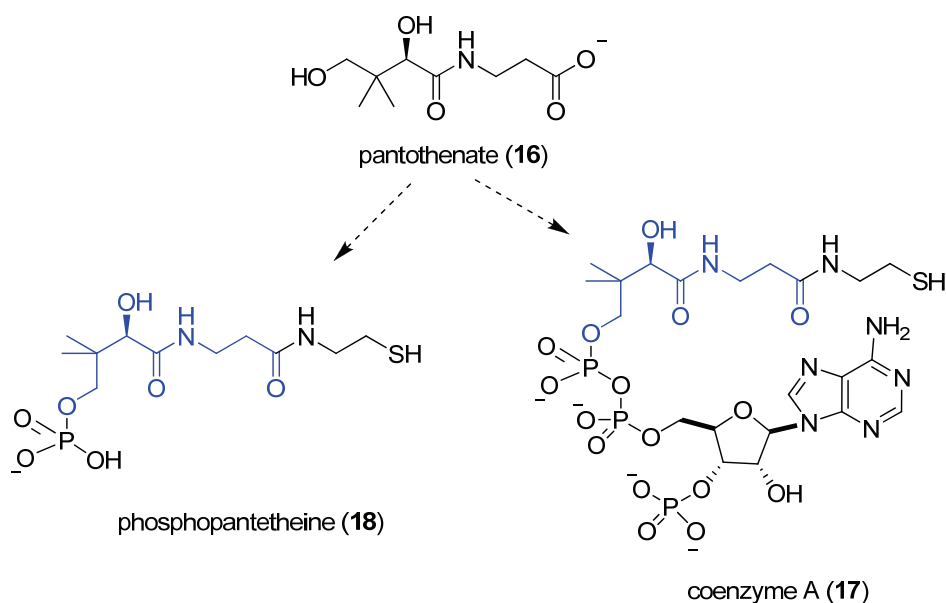
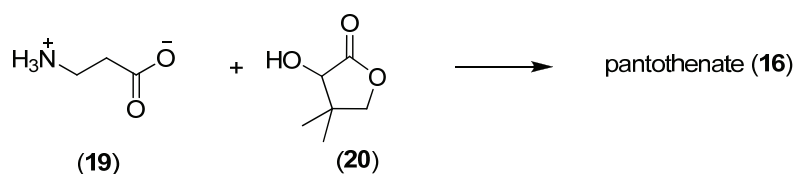


**Figure 1-4.** Chemical structures of pantothenate (**16**), CoA (**17**) and phosphopantetheine (**18**)

Pantothenate (**16**) was initially identified in 1933 by Williams *et al.*<sup>44</sup> while investigating the nutritional requirements of yeast. They discovered this acidic substance which promoted the growth to a strain of *S. cerevisiae*. Further probing of this stimulant in samples from many different sources led to the name ‘pantothenate’.<sup>45</sup> The term comes from the Greek word pantothen, meaning ‘from everywhere’ as pantothenate (**16**) was very widespread, present in tissues of bacteria, plants to animals. With the limited characterisation techniques of the time, the structure of pantothenate (**16**) was not elucidated for some years. After many studies,  $\beta$ -alanine (**19**) was recognised as one of the cleavage products and a collaboration between Williams *et al.* and Merck Research Laboratories discovered  $\alpha$ -hydroxy- $\beta,\beta$ -dimethyl- $\gamma$ -butyrolactone (**20**) condensed with  $\beta$ -alanine (**19**) to form pantothenate (**16**).<sup>46</sup>

**Scheme 1-1.** First elucidated step to pantothenate



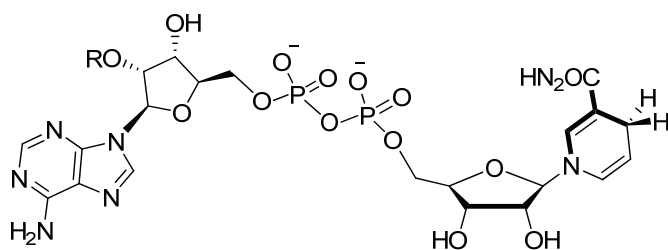
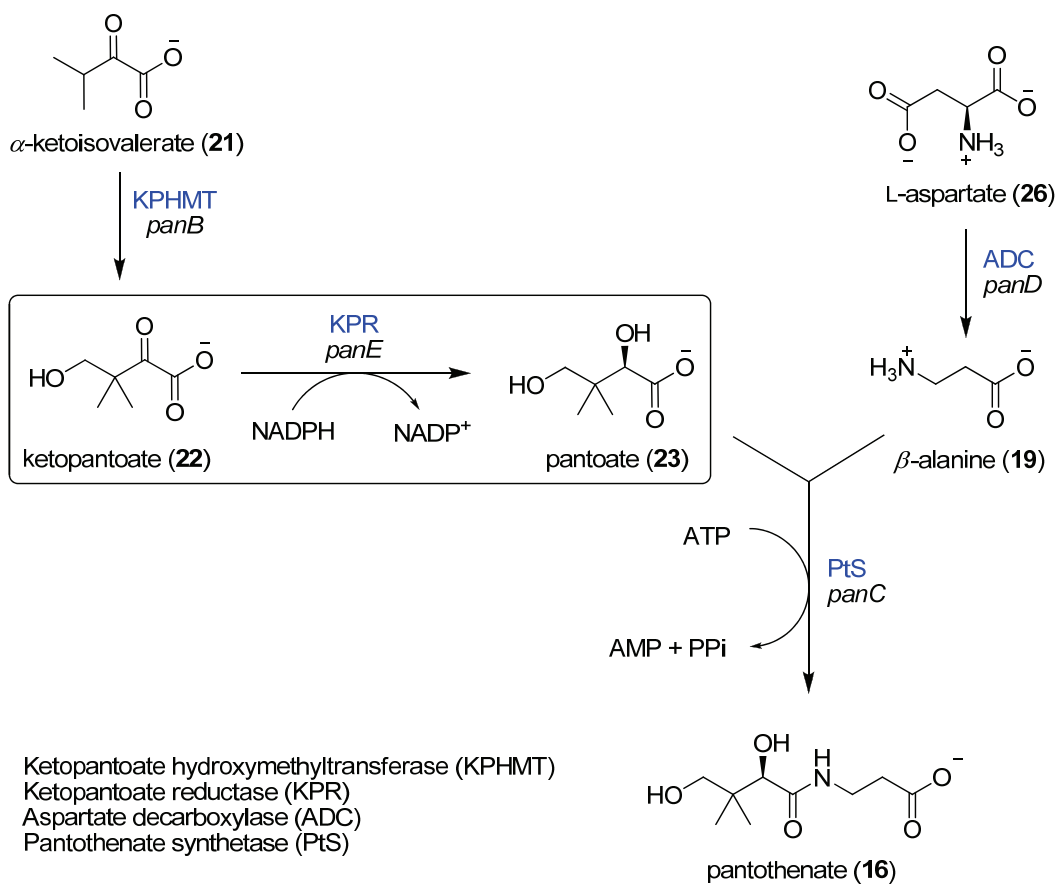
Since the discovery of pantothenate (**16**), much attention was focussed on elucidating its biosynthetic pathway as the enzymes make attractive targets for non-toxic antimicrobials, fungicides and herbicides. Furthermore, there is major industrial use of pantothenate (**16**) as a food supplement and its derivatives are used in cosmetic hair and beauty products.<sup>47</sup>

### 1.2.1 The biosynthesis of pantothenate

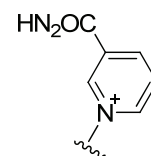
The pantothenate biosynthesis pathway was determined gradually over a number of years. For plant pantothenate biosynthesis, advances in plant molecular biology have facilitated the understanding of how plants make pantothenate (**16**). Pantothenate synthesis in plants has been reviewed by a number of groups and will not be discussed here.<sup>48-52</sup> The current production of pantothenate (**16**) is *via* chemical synthesis, however biotransformation where plants are engineered with elevated vitamin B<sub>5</sub> is being developed as a means to eliminate the need for costly procedures such as separating racemic intermediates.<sup>50</sup>

The pantothenate biosynthetic pathway in bacteria has been completely elucidated and is best studied in *E. coli*<sup>41,53-54</sup> where it consists of two branches. In *E. coli* four enzymes are involved in the pantothenate biosynthetic pathway (Scheme 1-2). The first step involves the enzyme ketopantoate hydroxymethyltransferase (KPHMT) that converts  $\alpha$ -ketoisovalerate (**21**) into ketopantoate (**22**) using 5,10-methylene-tetrahydrofolate.<sup>55</sup> Then ketopantoate (**22**) is reduced to pantoate (**23**) by ketopantoate reductase (KPR) using NADPH (**24**) as the hydride donor which forms NADP<sup>+</sup> (**25**).<sup>56</sup> In a separate branch, L-aspartate (**26**) is decarboxylated to produce  $\beta$ -alanine (**19**) using aspartate decarboxylase (ADC).<sup>57</sup> Finally, adenosine triphosphate (**27**) is consumed to give adenosine monophosphate (**28**) when pantothenate synthetase (PtS) catalyses the condensation of pantoate (**23**) and  $\beta$ -alanine (**19**) to form the product pantothenate (**16**).<sup>53</sup> All four genes for the enzymes involved in the pathway (*panB*, *panE*, *panD* and *panC*) have been cloned, the recombinant proteins overexpressed and purified, and their 3D structures determined.<sup>58-61</sup>

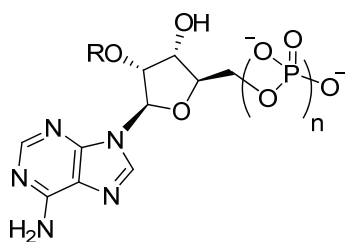
**Scheme 1-2.** Pantothenate biosynthesis pathway in bacteria: Enzyme names are given in blue with the corresponding genes in italics. The structures of NADPH (**24**) and its analogues are shown below.



NADPH (**24**) R = PO<sub>3</sub><sup>2-</sup>  
 NADH (**29**) R = H



NADP<sup>+</sup> (**25**) R = PO<sub>3</sub><sup>2-</sup>  
 NAP<sup>+</sup> (**30**) R = H



ATP (**27**) n = 3, R = H  
 AMP (**28**) n = 1, R = H  
 ADP (**31**) n = 2, R = H

### 1.2.2 Inhibition of pantothenate biosynthesis

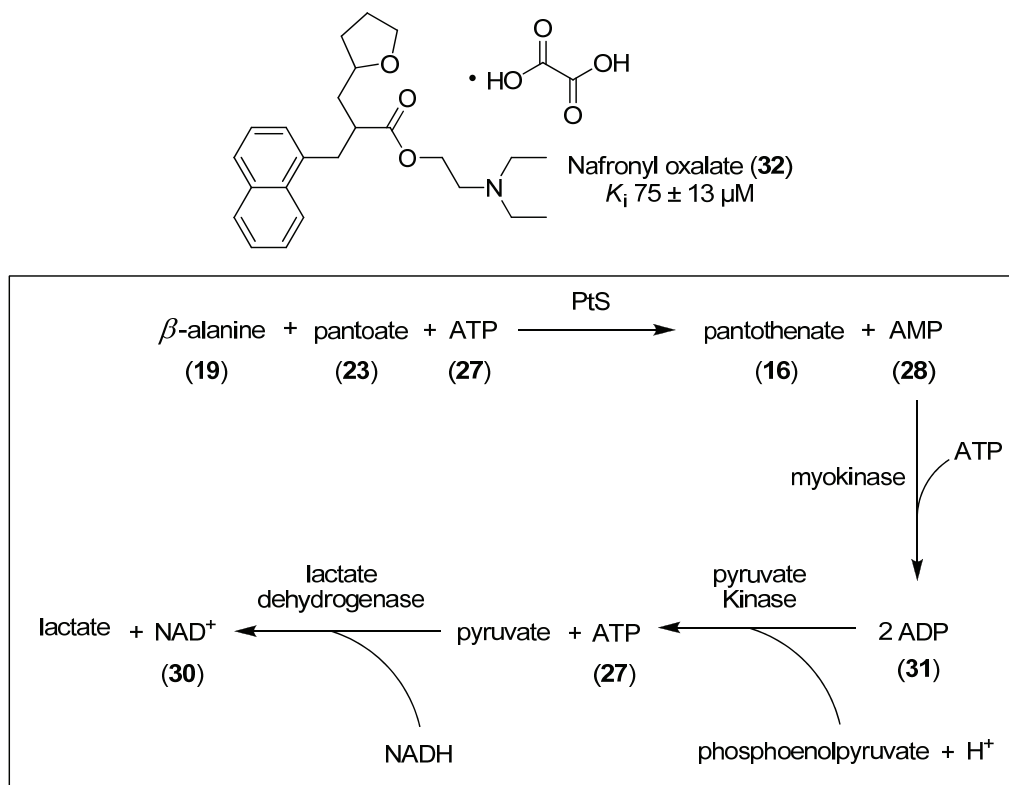
Supporting the theory that pantothenate (**16**) is a necessity to most, if not all organisms, bioinformatics analysis has identified this pathway as a potential target for antimicrobial agents.<sup>62-64</sup> The *de novo* pantothenate biosynthetic pathway is only present in bacteria, fungi and plants and its absence in mammals suggests that inhibitors could be selective with a reduced risk of side effects. Additionally, the enzymes in the pathway have been thoroughly studied biochemically and genetically.

A potential drawback of inhibiting the pantothenate biosynthesis pathway is the ability of certain species, such as *P. falciparum*<sup>65</sup> and *E. coli*<sup>66</sup> to acquire exogenous pantothenate (**16**) through pantothenate permease (*panF*). However, the validity of targeting this pathway is highlighted by genetic studies, where Sambandamurthy *et al.*<sup>67</sup> have shown that a *panCD* null strain of *M. tuberculosis*, with deletions to the genes for both PtS and ADC greatly attenuated virulence. Indeed, the *panCD* mutant helped protect immunocompromised mice against virulent *M. tuberculosis* more effectively than *bacille* Calmette-Guérin (BCG) vaccination. The immunocompromised mice injected with the *panCD* mutant lived seven times longer than those injected with the wildtype *M. tuberculosis*. Sambandamurthy *et al.*<sup>68</sup> have since developed an attenuated strain of *M. tuberculosis* that deletes both *panCD* and the primary attenuating mutations of the BCG strain which is being considered as a human vaccine candidate for protection against *M. tuberculosis*.<sup>68-69</sup> Since small molecule inhibitors of PtS and ADC have been reported they will be discussed in greater detail.

### 1.2.2.1 Inhibition of pantothenate synthetase

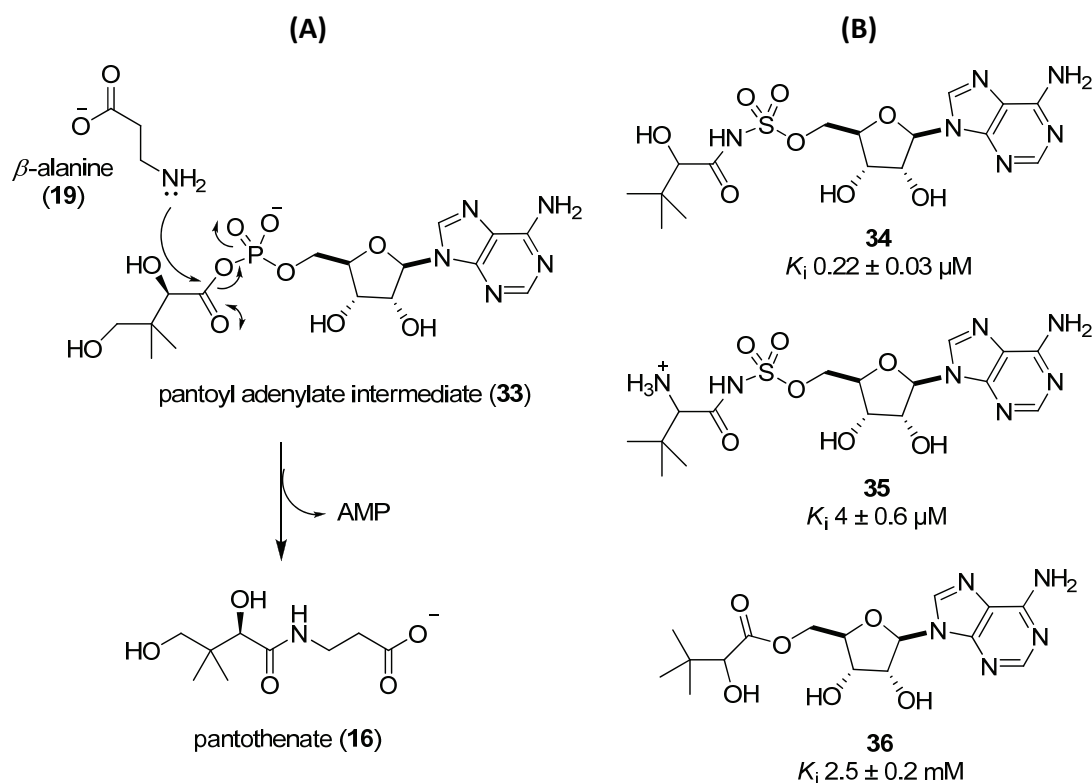
A range of approaches have been adopted in the search for PtS inhibitors. Early efforts in designing inhibitors for PtS focussed on analogues of either pantoate (**23**) or  $\beta$ -alanine (**19**).<sup>70-73</sup> White and co-workers<sup>74</sup> developed the first small molecule inhibitor targeting PtS of *M. tuberculosis*. A high-throughput screen was set up to monitor the oxidation of NADH (**29**) to NAD<sup>+</sup> (**30**) spectrophotometrically at 340 nm, through an enzymatic cascade involving PtS, myokinase, pyruvate kinase and lactate dehydrogenase (Scheme 1-3) and a range of nucleosides (**27** – **31**). A screen of 4080 compounds led to the lead compound, nafronyl oxalate (**32**), a competitive inhibitor with  $K_i$  of  $75 \pm 13 \mu\text{M}$ .<sup>74</sup> Nafronyl oxalate is also a vasodilator utilised in the treatment of vascular and cerebral disorders.

**Scheme 1-3.** Structure of nafronyl oxalate (**32**) and the coupled enzyme assay for PtS activity



The Abell group employed modern approaches of rational drug design to discover inhibitors for PtS of both *E. coli* and *M. tuberculosis*.<sup>75-76</sup> As illustrated in Scheme 1-4A, the inhibitors were designed as analogues of the reaction intermediate pantooyl adenylate (33), where the phosphodiester is substituted for either a sulfamoyl or an ester group (Scheme 1-4B). To examine the kinetics and inhibition, a combination of biophysical techniques such as isothermal titration calorimetry (ITC), thermal denaturation assays and kinetic assays were employed. X-ray crystallography was used to assess binding modes and interactions. The sulfamoyl derivatives (34 and 35) were found to be approximately 100-fold more potent than the ester analogues (e.g. 36). The sulfamoyl analogue (34) that most closely resembles the pantooyl adenylate reaction intermediate was the most potent inhibitor with a  $K_i$  of  $0.3 \pm 0.05 \mu\text{M}$  (*E. coli*) and  $0.22 \pm 0.03 \mu\text{M}$  (*M. tuberculosis*).

**Scheme 1-4.** (A) The reaction between  $\beta$ -alanine and the pantooyl adenylate intermediate catalysed by PtS. (B) Structures of sulfamoyl and ester analogues with their respective  $K_i$  for *M. tuberculosis* PtS.

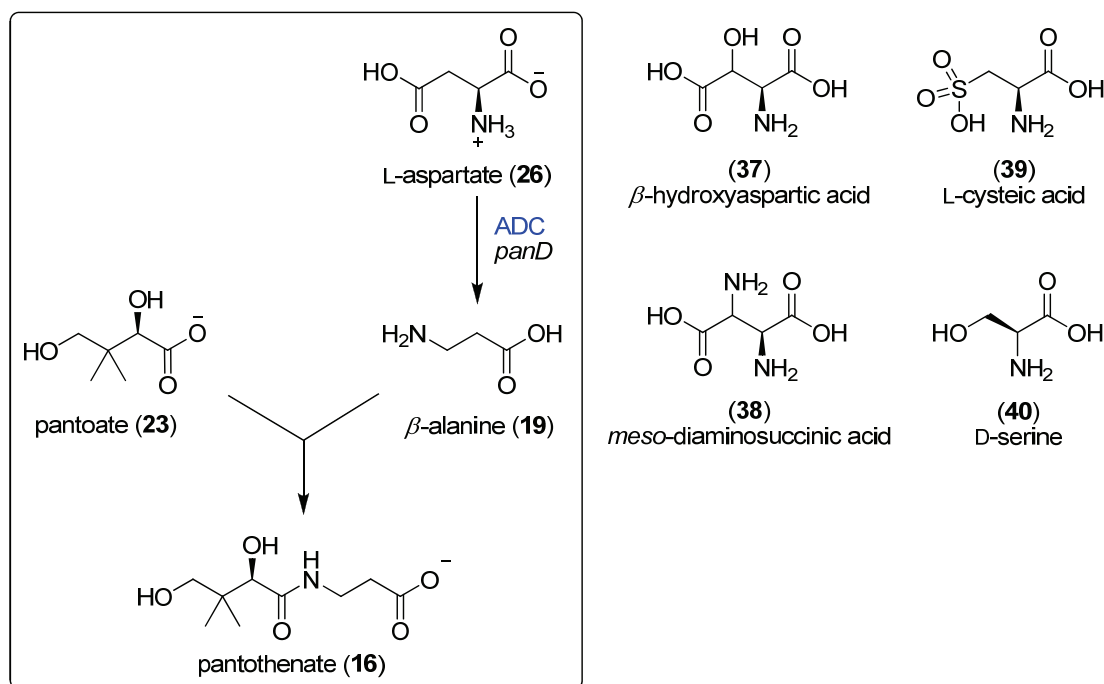


The Abell and Ciulli groups<sup>77-79</sup> have since reported new series of inhibitors for *M. tuberculosis* PtS while advancing strategies in rational drug design especially using fragment-based methods. The fragment-based approach will be discussed in greater detail in section 1.4.

### 1.2.2.2 Inhibition of aspartate decarboxylase

Efforts towards the design of ADC inhibitors have been slow presumably due to the small active site and narrow selectivity that allow only close structural analogues of aspartate to bind.<sup>41,80-81</sup> The earliest studies of ADC inhibition show L-aspartic acid analogues (Scheme 1-5)  $\beta$ -hydroxyaspartic acid (**37**), *meso*-diaminosuccinic acid (**38**) and L-cysteic acid (**39**) all inhibit the growth of *E. coli in vivo*.<sup>82-83</sup> This inhibition was reversed by the addition of aspartic acid indicating that the inhibitors were competing directly with L-aspartate.  $\beta$ -Alanine (**19**) and pantothenate (**16**) can also reverse the inhibition at lower concentrations of inhibitor (**37 – 39**). Similarly, Maas *et al.*<sup>84</sup> showed that D-serine (**40**) also inhibited this step, while the mechanism of inhibition was unknown. Expanding on these findings, Williamson *et al.*<sup>85</sup> determined a  $K_i$  of 0.08 mM for L-cysteic acid (**39**), making it the most potent competitive inhibitor of ADC in *E. coli* followed by  $\beta$ -hydroxyaspartic acid (**37**) and D-serine (**40**) with  $K_i$  values of 0.13 mM and 0.16 mM, respectively.

**Scheme 1-5.** Reaction scheme for aspartate decarboxylase is shown in the box and the structures of ADC inhibitors on the right



Using a different strategy to those described above, Webb *et al.*<sup>86</sup> employed matrix-assisted laser desorption/ionization-time of flight (MALDI-TOF) mass spectroscopy to screen for compounds that covalently bind to *E. coli* ADC. Including previously identified inhibitors, a library of 55 compounds, selected on the basis of their size and structural similarity to the natural substrate L-aspartate (26) and possessing the primary amine functionality were tested for binding. At 2 mM only a small handful of compounds bound to ADC; these were L-aspartate, β-alanine, L-cysteine, methyl L-aspartate, D-serine, β-glutamate, β-leucine, β-hydroxyaspartate and glycine. These results help validate earlier findings and additionally provide a useful pharmacophore model for future ADC inhibitor design.

Most recently, Strauss and co-workers<sup>87</sup> synthesised substrate analogues L-erythro and L-threo isomers of 3-fluoroaspartate to probe the reactivity and binding to ADC of *E. coli* and *M. tuberculosis* ADC. The preliminary study found little difference in the activity of *E. coli* ADC treated with either 3-fluoroaspartate isomer. In *M. tuberculosis* ADC, the L-erythro-isomer also had no effect. However, the treatment with L-threo isomer showed an approximate 25% reduction in activity. Strauss and co-workers<sup>87</sup> suggested the L-threo 3-fluoroaspartate closely resembled the bound conformation of the native substrate.

### 1.3 Ketopantoate reductase

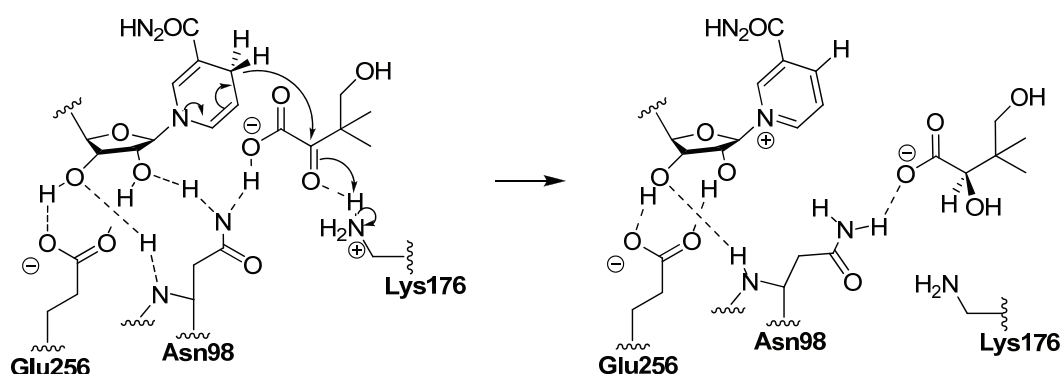
The target selected in this project is the second enzyme of the biosynthetic pathway, KPR. KPR has been purified and extensively characterised both biochemically and structurally, particularly in *E. coli*.<sup>59,88-92</sup> However, no inhibitors of KPR have been reported in the literature to date. In the SCOP database, KPR belongs to the 6-phosphogluconate dehydrogenase superfamily and has properties of both class A and B secondary alcohol dehydrogenases.<sup>93</sup>

#### 1.3.1 Proposed catalytic mechanism of KPR

A catalytic mechanism of *E. coli* KPR has been proposed using a combination of biochemical and structural studies (Scheme 1-6).<sup>59,88-92,94</sup> The forward and reverse KPR activity can be monitored by the disappearance/appearance in absorbance for NADPH at 340 nm. A sequential ordered bi:bi kinetic mechanism is reported for *E. coli* KPR as NADPH (**24**) is demonstrated to bind first, followed by ketopantoate (**22**) and once the

product pantoate (**23**) is released, the release of  $\text{NADP}^+$  (**25**) ensues.<sup>88-90</sup> The observed pH dependence of catalysis suggested a general acid-base chemical mechanism.

**Scheme 1-6.** Proposed catalytic mechanism of *E. coli* KPR



It is proposed that upon NADPH binding, the phosphate groups of NADPH are recognised by the side chains of Arg31 and the conserved Lys72, which induce subtle conformational changes favouring ketopantoate (**22**) binding. An extended hydrogen bonding network involving the conserved residues Glu256 and Asn98 orientates the cofactor in the conformation required for optimal hydride transfer (Scheme 1-6). Reprotonation of Lys176 and the loss of hydrogen bonds facilitate the release of pantoate (**23**). The subsequent release of  $\text{NADP}^+$  (**25**) ends the catalytic cycle. Site directed mutagenesis has revealed two conserved residues, Lys176 and Glu256 to be important in the catalytic cycle.<sup>88</sup>

### 1.3.2 The structure of *E. coli* KPR

Matak-Vinkovic *et al.*<sup>59</sup> solved the first crystal structure of (unliganded) KPR to 1.7 Å resolution. The crystal structure revealed a 34 kDa monomeric enzyme composed of a coenzyme binding domain and a substrate binding domain separated by a large cleft. It

has 12  $\alpha$ -helices, three  $3_{10}$ -helices, and 11  $\beta$ -strands. The N-terminal domain has the  $\alpha\beta$  Rossmann fold characteristic to many nucleotide-binding proteins (Figure 1-5), with a glycine-rich region ( ${}^7\text{GCGALG}^{12}$ ) for nucleotide recognition, whilst the C-terminus is an  $\alpha$ -helical domain. The crystal structure validated the importance of residues Lys176 and Glu256, found in mutagenesis studies, as they were located in the active site. It was proposed that Lys176 stabilised substrate binding and Glu256 was the required general acid/base.

The crystal structure of KPR with NADP<sup>+</sup> (**25**) bound at the active site (2.1 Å resolution) was solved by Lobley *et al.*<sup>91</sup> Surprisingly, NADP<sup>+</sup>-KPR shared the same open conformation as *apo*-KPR (unliganded). NADP<sup>+</sup> (**25**) bound closely to the N-terminal Rossmann fold domain forming hydrogen bonds with the pyrophosphate in NADP<sup>+</sup> (**25**). Hydrophobic interactions were observed as the adenine portion of NADP<sup>+</sup> (**25**) sits in the hydrophobic pocket containing Arg31, Leu71 and Gln75. Glu256 was indeed making hydrogen bond interactions with the nicotinamide ribose 2'- and 3'-hydroxyls (Figure 1-5). Conserved residues (Lys72, Lys176, Glu210, Asp248 and Glu256) close to the active site were mutated to probe their function. Results were consistent with previous studies in which K176A and E256A mutant proteins resulted in approximately 78,000- and 2,600-fold decrease in  $k_{\text{cat}}/K_{\text{m}}$  for ketopantoate (**22**), respectively. The other three mutants displayed wildtype activity. Asn98 mutated to N98A also showed a decrease of about 4,000-fold in  $k_{\text{cat}}/K_{\text{m}}$ .

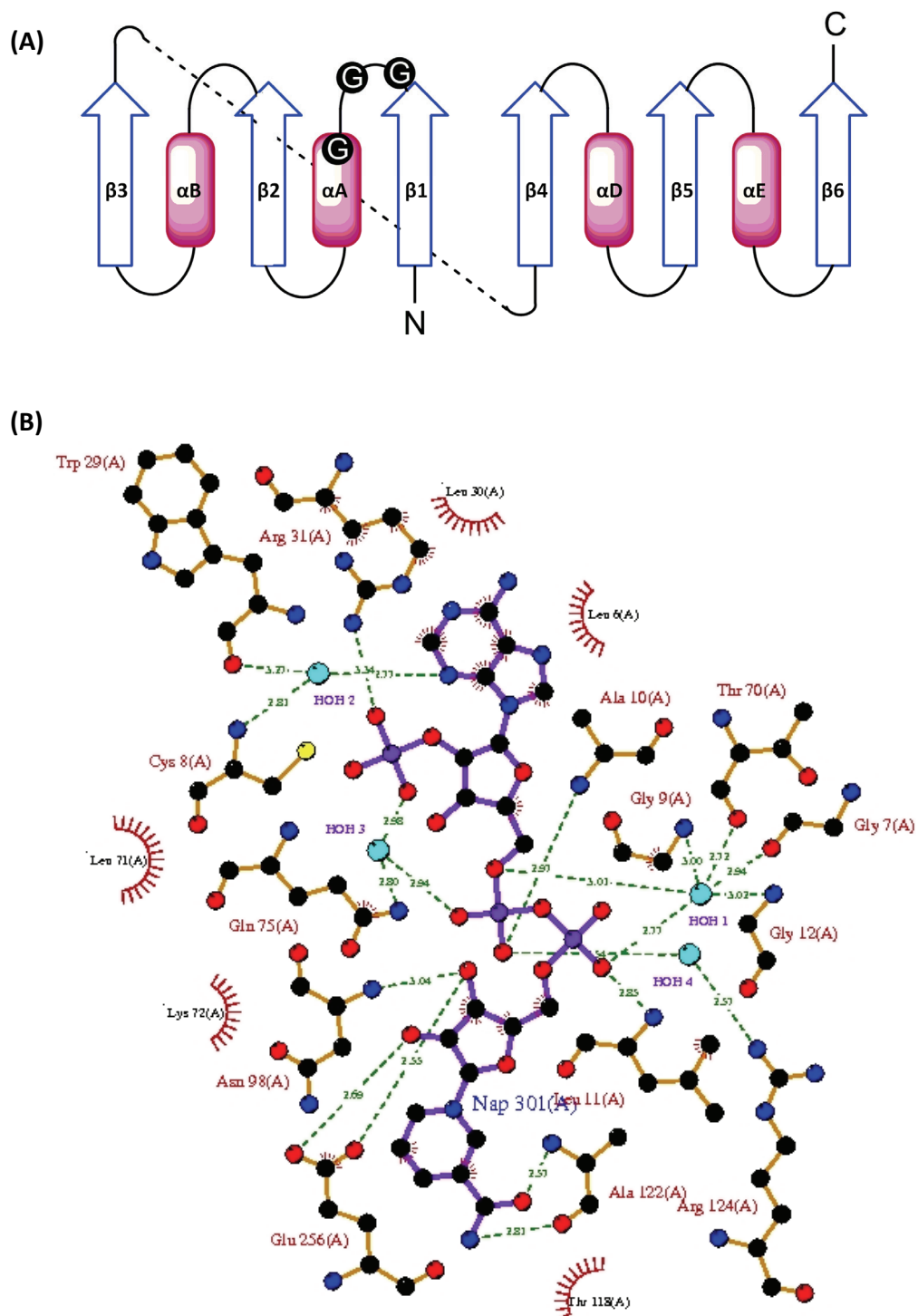


**Figure 1-5.** (A) Classic Rossmann fold topology. Blue arrows designate  $\beta$ -strands and purple rectangles denote  $\alpha$ -helices. Circles represent conserved glycine residues. (B) Schematic 2D plot of the intermolecular interactions between  $\text{NADP}^+$ , KPR and water molecules. Non-polar interactions: vdW displayed as spokes; hydrogen bonds displayed as dashed lines [the length of each bond ( $\text{\AA}$ ) is printed in the middle]. This image is generated by LIGPLOT.<sup>95</sup>

In an attempt to crystallise the ternary complex of KPR with NADP<sup>+</sup> (**25**) and pantoate (**23**), Ciulli *et al.*<sup>94</sup> unexpectedly crystallised and solved KPR in complex with 2'P-ADP-ribose (**41**), a fragment of NADP<sup>+</sup> (**25**) without the nicotinamide ring (1.95 Å resolution). NADPH was hydrolysed to 2'P-ADP-ribose (**41**) under the acidic conditions (pH 4.0 – 5.0) used in the co-crystallisation experiments. Interestingly, under these acidic conditions, 2'P-ADP-ribose (**41**) actually bound in a ‘reversed binding mode’ compared to NADP<sup>+</sup> (Figure 1-6).

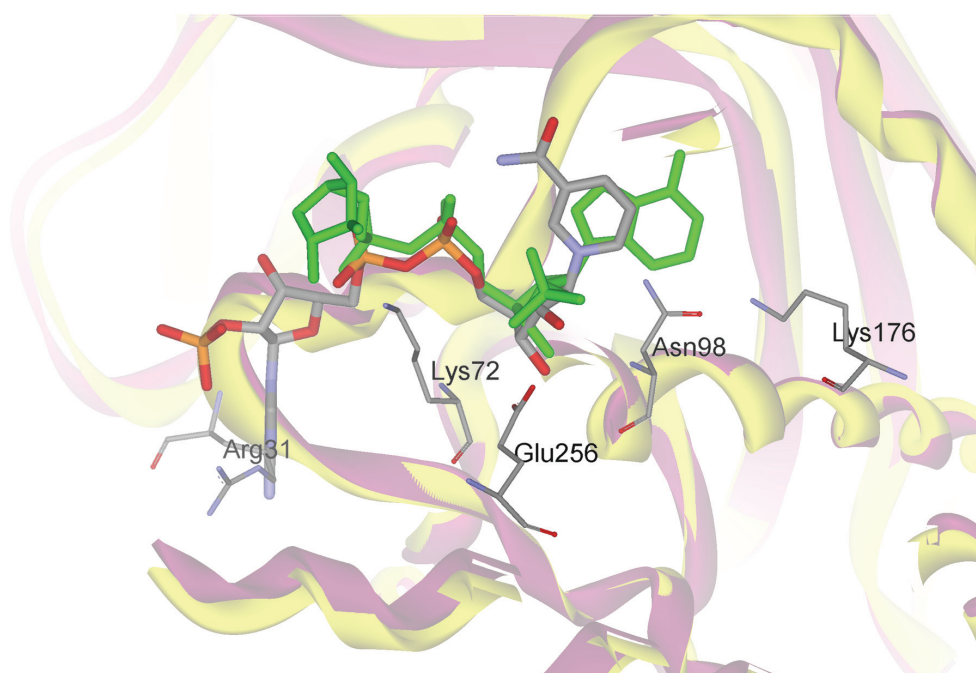
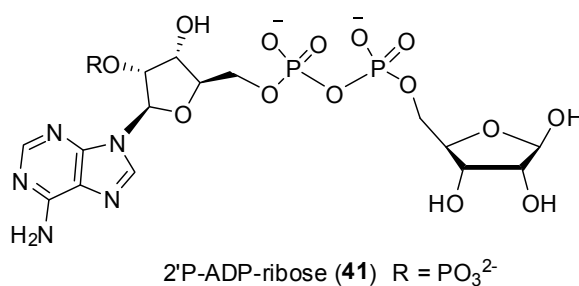


**Figure 1-6.** Superimposed crystal structures of NADP<sup>+</sup> (shown as grey carbons) and 2'P-ADP-ribose (green structure) in the enzyme active site (PDB ID: 1YJQ and 1YON, respectively)

The ternary complex of KPR with NADP<sup>+</sup> (**25**) and pantoate (**23**) bound (2.3 Å resolution)<sup>92</sup> was recently determined (Figure 1-7). Two monomers were found captured in a pre-catalytic ternary complex, one in an open conformation (monomer A) and the other in a closed conformation (monomer B). The extent of conformational changes of the protein backbone was measured between KPR structures and summarised in Table 1-3. The comparison reveals that the C-terminal domain of the hinge region (Ile169 – Lys176) is where the movement occurs. The main interactions of NADP<sup>+</sup> (**25**) in monomer A and B are similar to NADP<sup>+</sup>-KPR. This structure is also the first insight into substrate binding, showing a hydrogen bond between Lys176 and the oxygen of pantoate (**23**) confirming that Lys176 functions to stabilise the substrate. Lys176 makes further hydrogen bonds with Asn98 and Thr118. In monomer B, pantoate (**23**) is fully enclosed between the two domains preventing solvent entry. In this conformation, pantoate (**23**) makes hydrogen bonds with Ser244 and Asn98 while the dimethyl group of pantoate (**23**) sits in a hydrophobic pocket (Thr119, Val179, Ile183, Val234 and Thr238).

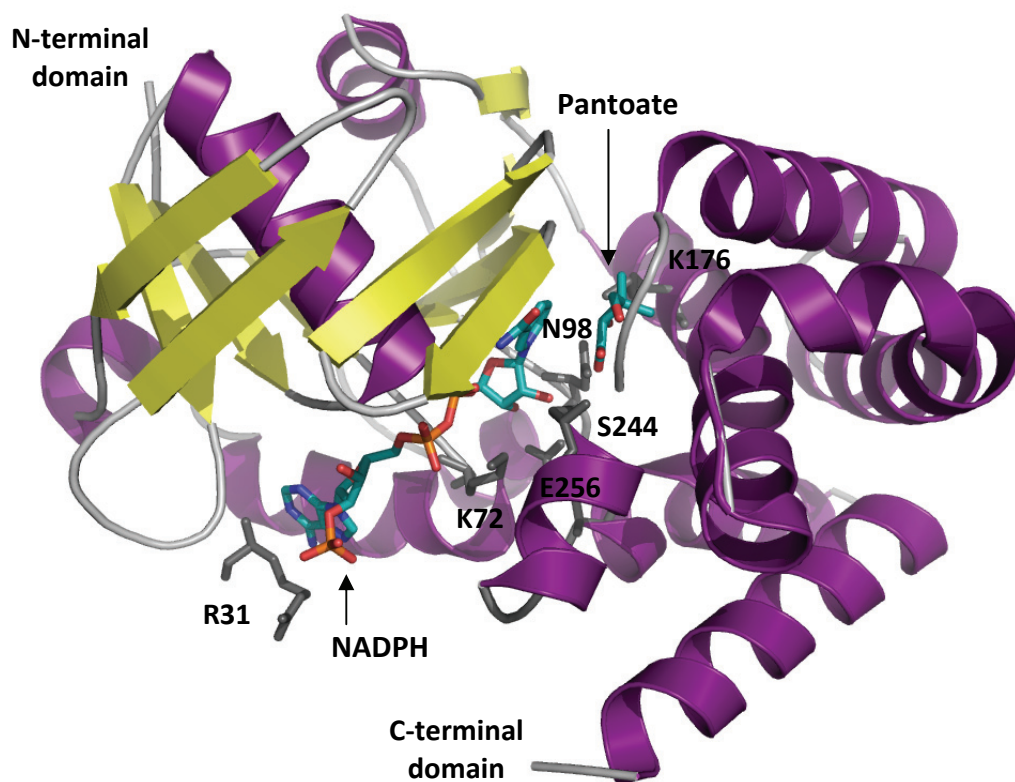


**Figure 1-7.** The crystal structure of KPR-NADP<sup>+</sup>-pantoate ternary complex (PDB ID: 2OFP)

**Table 1-3.** Root mean square deviations from superposition of KPR structures<sup>92</sup>

Superposition on main chain atoms	RMSD (main chain atoms, Å)		
	NADP <sup>+</sup> -KPR	Monomer A	Monomer B
<b><i>N-terminal domain only (residues 1 – 169)</i></b>			
<i>apo</i> -KPR	0.58	0.61	0.61
NADP <sup>+</sup> -KPR		0.47	0.48
Monomer A			0.23
<b><i>C-terminal domain only (residues 170 – 292)</i></b>			
<i>apo</i> -KPR	1.56	2.63	5.54
NADP <sup>+</sup> -KPR		1.85	5.01
Monomer A			3.45

### 1.3.3 KPR catalytic activity

On studying the alternative pyrimidine biosynthetic (APB) pathway, precursor to thiamine in *Salmonella typhimurium*, Downs and Peterson<sup>96</sup> identified an *apbA* gene that led to thiamine auxotrophy. Interestingly, the growth of the *apbA*<sup>-</sup> mutant was affected by pantothenate (**16**) and thiamine, suggesting that pantothenate (**16**) is required for the APB pathway. However, it was later concluded that ApbB is KPR when the overexpressed protein ApbB had KPR activity and that *apbA* and *panE* both mapped to 10 minutes on both the *E. coli* and *S. typhimurium* chromosomes.<sup>97</sup>

The biosynthesis of isoleucine (involving substrates **42** – **45**), valine and leucine (with substrates **46** – **48**, **21**) is catalysed by three common enzymes (Scheme 1-7). However, the acetohydroxyacid isomeroreductase (AHAIR) encoded by *ilvC* can also catalyse the same reaction as KPR. The ability of AHAIR to use ketopantoate (**22**) as a substrate can be appreciated and best explained by the close resemblance of ketopantoate (**22**) to the isomerisation intermediates (acetohydroxybutyrate (**43**) and acetolactate (**47**), Scheme 1-7) in the normal reaction of AHAIR. The occurrence of, and extent to which AHAIR displays KPR activity varies in different species and is summarised in Table 1-4.

Scheme 1-7. Biosynthetic pathways of branched chain amino acids

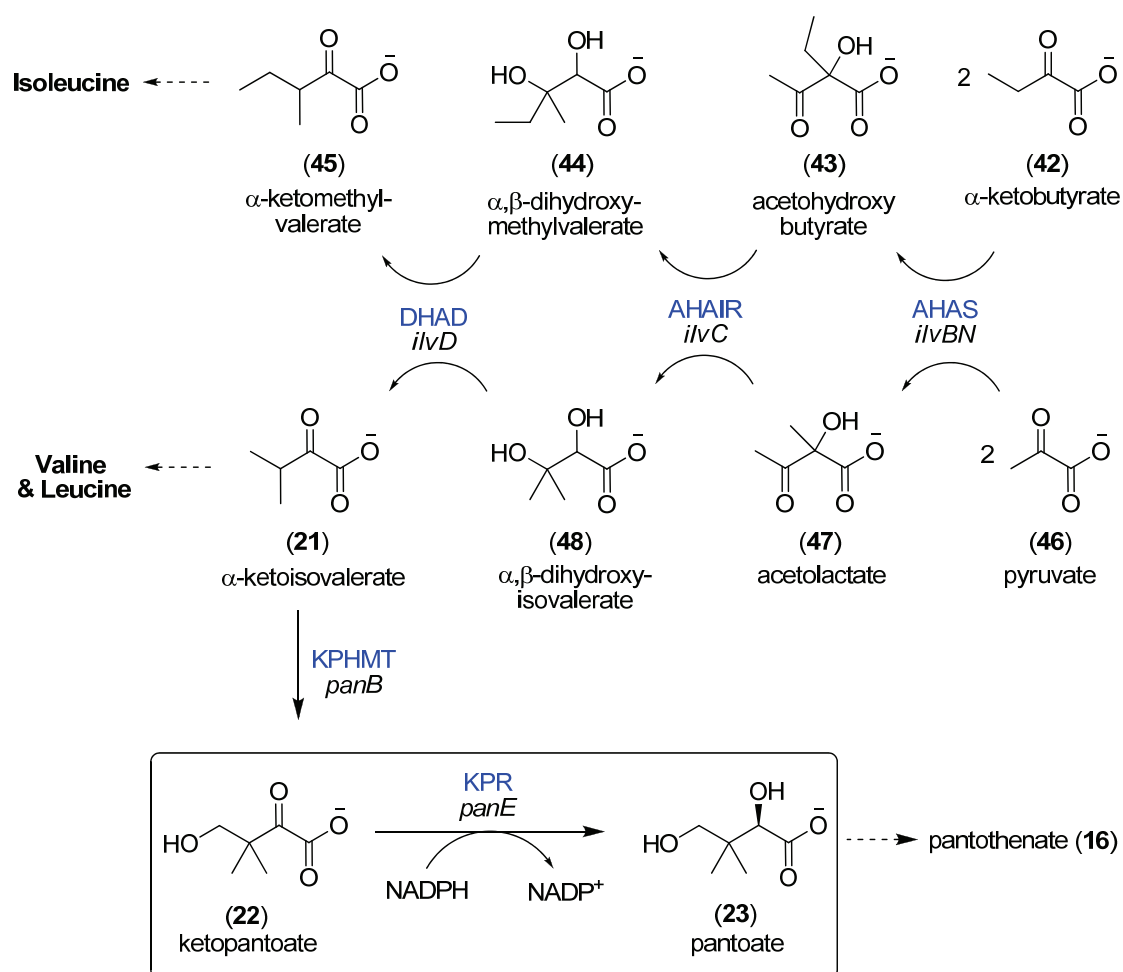


**Table 1-4.** Summary of *ilvC* ability to catalyse KPR activity in different organisms

Group and species	Summary
Primerano <i>et al.</i> <sup>98</sup> (1983) <i>S. typhimurium</i>	<p><i>panE</i><sup>-</sup> and <i>ilvC</i><sup>-</sup> double mutants of <i>S. typhimurium</i> were only able to grow in minimal media supplemented with either pantoate (<b>23</b>) or pantothenate (<b>16</b>) in addition to isoleucine and valine. Introducing a wildtype <i>ilvC</i> gene restored the amino acid auxotrophy, however were still unable to grow in the absence of either pantoate (<b>23</b>) or pantothenate (<b>16</b>) unless provided with ketopantoate (<b>22</b>).</p> <p>Normal AHAI activity is insufficient to provide adequate levels of pantothenate (<b>16</b>).</p>
Shimizu <i>et al.</i> <sup>99</sup> (1988) <i>P. maltophilia</i>	<p><i>panE</i><sup>-</sup> mutants of <i>P. maltophilia</i> were only able to grow when the media was supplemented with either pantoate (<b>23</b>) or pantothenate (<b>16</b>) in the media.</p> <p>No alternative enzyme was observed to catalyse the conversion of ketopantoate (<b>22</b>) to pantoate (<b>23</b>).</p>
Baigori <i>et al.</i> <sup>100</sup> (1991) <i>B. subtilis</i>	<p><i>panE</i><sup>-</sup> mutants of <i>B. subtilis</i> were unable to grow in the absence of pantothenate (<b>16</b>) even with 2 mM of ketopantoate (<b>22</b>) in the culture.</p> <p>Normal AHAI activity is insufficient to provide pantothenate (<b>16</b>) in this bacterium.</p>
Elischewski <i>et al.</i> <sup>101</sup> (1999) <i>E. coli</i>	<p>The <i>E. coli ilvC</i><sup>-</sup> mutant showed the same KPR activity as the <i>E. coli</i> wildtype suggesting <i>ilvC</i> gene had little, if any, role in pantothenate (<b>16</b>) production in this bacterium.</p>
Merkamm <i>et al.</i> <sup>102</sup> (2003) <i>C. glutamicum</i>	<p><i>ilvC</i> is the only KPR - encoding gene in <i>C. glutamicum</i> responsible for reduction of ketopantoate (<b>22</b>).</p>

AHAIR's ability to catalyse KPR activity does not preclude KPR from being a potential antimicrobial target because as indicated in Table 3, most species studied suggest that normal levels of AHAIR activity are unable to provide adequate levels of pantothenate (**16**) for bacteria to grow. Perhaps this is due to the competition between the three substrates of AHAIR (Scheme 1-7), as it catalyses the reduction of acetohydroxybutyrate (**43**) to dihydroxymethylvalerate (**44**) in the isoleucine pathway, the reduction of acetolactate (**47**) to dihydroxyisovalerate (**48**) in the valine and leucine biosynthetic pathway, and the reduction of ketopantoate (**22**) to pantoate (**23**) in the pantothenate pathway. The *ilvC panE* double mutants in *E. coli* and *S. typhimurium* have no detectable KPR activity, indicating that there are no other genes encoding for the enzymes able to convert ketopantoate (**22**) to pantoate (**23**).<sup>98,101</sup> For species where low KPR activity is catalysed by AHAIR, it is more important to determine whether the surviving bacterial organism is no longer virulent, similarly to studies demonstrated by Sambandamurthy *et al.*<sup>67</sup> in the *panCD* mutant of *M. tuberculosis*.

Notably, KPR activity has been shown to represent a bottleneck in pantothenate biosynthesis, where Elischewski *et al.*<sup>101</sup> found that a 3-fold overexpression of *panE* in *E. coli* led to a corresponding 3.5-fold increase in pantothenate (**16**) excretion. The value of finding small molecule inhibitors for the pantothenate pathway includes using these compounds to investigate the role of KPR in the development of antimicrobials. Currently, no inhibitors of KPR have been reported in the literature.

## 1.4 Fragment-based lead discovery

Despite significant investments over the years in improving the quality and efficiency of the drug discovery process, there is a rise in attrition rate of drugs in development. Success in drug discovery requires the lead compound to be novel, possess good potency, be selective and have desirable physicochemical (solubility, permeability and chemical stability) and pharmacokinetic properties including toxicity. There have been many approaches in obtaining lead compounds that may satisfy the drug-like profile. For example, identifying a compound from an existing lead or drug,<sup>103</sup> natural product with known biological activity,<sup>104</sup> combinatorial chemistry<sup>105</sup> and high-throughput screening (HTS).<sup>106</sup> HTS is currently one of the main approaches in lead identification. However, challenges in HTS have been associated with low hit rates and identifying drug-sized compounds that are difficult to optimise due to high molecular weight and/or unfavourable physical properties.<sup>107</sup> In addition, these larger compounds have complicated structures that often restrict the presented functional groups from binding optimally. The fragment-based lead discovery (FBLD) is an alternative to HTS.<sup>108</sup> In FBLD, optimisation begins with a low molecular weight fragment (150 – 300 Da) that is engaged in efficient binding in which the complexity and physical property are easier to control and optimise.<sup>108-109</sup>

The theoretical framework for this fragment-based approach was first suggested by Jencks<sup>110</sup> three decades ago. Jencks pointed out that the binding of a fragment molecule to a protein target results in considerable translational and rotational entropy penalty in solution. However, this entropy barrier is similar for larger molecules; hence in linking two smaller molecules, this penalty is only paid once (Figure 1-8).



**Figure 1-8.** Schematic representation of fragment hits **1** (red) and **2** (green) in a binding pocket: The last box (on the right) corresponds to an optimised fragment linking.

In 1996, the publication by Shuker, Hajduk, Meadows, and Fesik from Abbott Laboratories demonstrated the first practical fragment-based approach, called SAR by NMR (structure-activity relationships by nuclear magnetic resonance), capturing serious interest.<sup>111</sup> An NMR screen of 1,000 fragments against the FK506-binding protein (FKBP) identified a number of weak fragment binders. The fragments were assessed by  $^1\text{H}/^{15}\text{N}$ -amide chemical shift perturbations (CSP) in two-dimensional  $^{15}\text{N}$ -heteronuclear single quantum correlation (2D  $^1\text{H}/^{15}\text{N}$ -HSQC) NMR. Upon analysis, the pipercolinic acid (**49**,  $K_d = 2\ \mu\text{M}$ ) and diphenylamide (**50**,  $K_d = 100\ \mu\text{M}$ ) were found binding in proximal binding pockets. After a few iterations of linker designs, a potent 49 nM FKBP inhibitor (**51**) was developed (Figure 1-9).

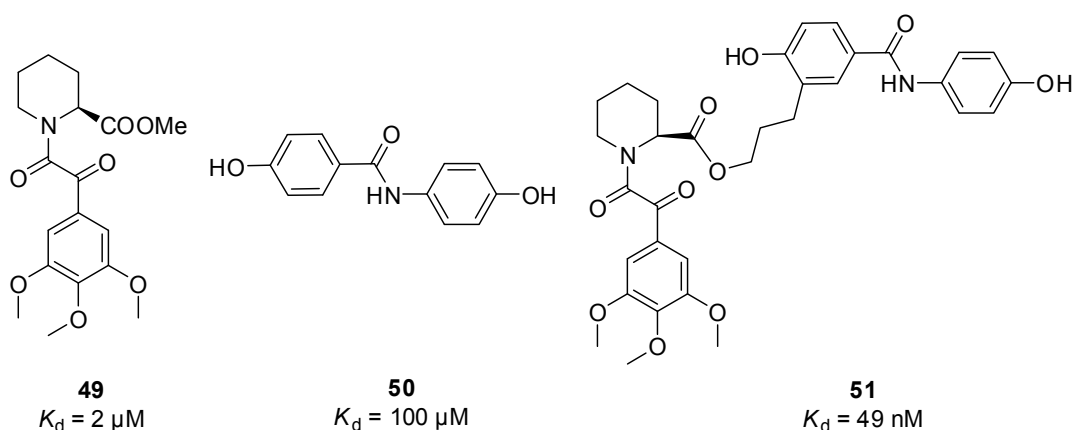


**Figure 1-9.** Potent inhibitors of FKBP discovered through the SAR by NMR method

### 1.4.1 Chemical space

Accessing chemical space is important to identify novel molecules for new protein targets and ensure efficient discovery of high-quality drug leads. Given that there are approximately  $10^{63}$  possible small drug-like molecules, a HTS screen of  $10^6$  does not come close to the available chemical space.<sup>112</sup> On the other hand, the total number of ‘drug-like’ molecules with 11 heavy atoms or fewer have been estimated to be  $10^9$ .<sup>113-114</sup> Therefore, screening a fragment library of 10,000 compounds allows considerably more access to chemical space than a HTS screen.

### 1.4.2 Ligand complexity

Molecules with lower complexity (fragments) in a ligand-protein receptor interaction would give rise to higher hit rates than molecules that are more complex (drug-sized molecules). The reason for this is because the complex molecules are more likely to have interfering functionality that would prevent them from binding to a target protein or unfavourable interactions or clashes with the receptor. Larger and more lipophilic molecules exploiting hydrophobic interactions to increase potency can also compromise pharmacokinetics and pharmacodynamics.<sup>115-116</sup> Therefore, screening small molecules (typically 150 – 300 Da, with reduced complexity) reduces the search space wherein the activity and other properties of the initial lead can then be optimised by increasing the complexity.<sup>117</sup> However, a degree of complexity is needed to provide enough potency to be able to measure the binding.

### 1.4.3 Ligand efficiency

Fragments are small and less complex, therefore are less likely to engage in unfavourable steric or electrostatic interactions and the use of unnecessary chemical moieties during binding. ‘Ligand efficiency’ (LE) is a useful measure to assess whether the ligand derives its potency from efficient binding with the protein target or making many contacts through electrostatic interactions. Introduced by Hopkins *et al.*,<sup>118</sup> LE is a ratio of the binding energy to the number of non-hydrogen atoms or heavy atom count (HAC) in a ligand (Equation 1-1). LE values greater than 0.3 kcal/mol per non-hydrogen atom are desirable (based on a 500 Da compound with a binding constant of 10 nM).<sup>118</sup>

**Equation 1-1.** LE is used to guide the optimisation of fragments into lead compounds

$$LE = -\Delta G/HAC \approx RT \ln(IC_{50})/N_{\text{non-hydrogen atoms}}$$

A study by Hadjuk<sup>119</sup> compared the potency and molecular weight of 18 highly optimised inhibitors which were systematically deconstructed. Notably, along the path of an ideal optimisation, the binding efficiency was maintained and a linear relationship between the potency and molecular size was observed.<sup>119</sup> Therefore, to avoid pursuing potency gains through unnecessary chemical groups that add excess mass, Hadjuk suggested that for every 64 mass units added a 10-fold increase in binding is expected. Moreover, as the fragment size is increased during synthetic elaboration, a drop in the binding efficiency of more than 10% suggests that the modification is not ideal even when modest gains in activity are observed.

The next section addresses the fragment-based approach described in three phases, (a) design of fragment libraries; (b) fragment screening and validation of the hits; (c) elaboration of fragments into more potent inhibitors.

#### 1.4.4 Fragment library design

The first step in FBLD is to develop a library of fragments. There are many approaches that have been used, for example, Vertex Pharmaceuticals computationally deconstructed commercially available therapeutics and took common chemical features to build a library of 200 fragments specifically for NMR (SHAPES).<sup>120</sup> Another group identified recurring fragments from known drugs and described the procedure as ‘retrosynthetic combinatorial analysis procedure’ (RECAP).<sup>121</sup> The fragment libraries designed by Hajduk and co-workers<sup>122</sup> were enriched with ‘privileged molecules,’ such as biphenyls, that have been shown to bind to proteins frequently.

A number of factors are considered in the design of a fragment library,<sup>123-125</sup> for example:

1. *Physical properties*: ‘Lipinski’s rule of five’ has become a common filter in assessing whether compounds are likely to be ‘drug-like’.<sup>126</sup> In a similar approach, Congreve *et al.*<sup>127</sup> proposed the ‘rule of three’ for fragments. Congreve *et al.*<sup>127</sup> examined the properties of 40 fragment hits identified against a range of targets using high-throughput X-ray crystallographic screening technology. The hits seem to obey, on average, a ‘rule of three’, in which molecular weight is < 300 Da, the number of hydrogen bond donors is  $\leq 3$ , the number of hydrogen bond acceptors is  $\leq 3$  and ClogP is  $\leq 3$ . In addition, the

results suggested the number of rotatable bonds (NROT)  $\leq 3$  and polar surface area (PSA)  $\leq 60$  might also be useful criteria for fragment selection.<sup>127</sup>

2. *Chemical group*: Compounds with unwanted functionalities that are reactive or known to interfere with the screening technique are removed, for example, nitro, acyl halides or acrylates.
3. *Chemical diversity*: Having a set of fragments which are able to cover a large chemical space using a small number of compounds. Maximising the chemical diversity increases the chance of identifying novel scaffolds.
4. *Synthetic feasibility*: Plausible synthetic routes allowing elaboration of a hit compound with substituents. Affordable starting materials.

#### 1.4.5 Fragment screening and confirming hits

As fragments are small and bind to their target with relatively low affinity between 0.1 mM and 10 mM, a reliable detection method is essential. Several different screening techniques have been carried out, all of which allow high concentrations of fragments to detect their weak binding. These methods include biochemical assays,<sup>128-129</sup> NMR spectroscopy,<sup>130</sup> mass spectrometry (MS),<sup>131</sup> X-ray crystallography<sup>132</sup> and surface plasmon resonance (SPR)<sup>133</sup> or a combination of all these methods. The range of detection methods and their effective affinity ranges have been surveyed by Hubbard and Murray,<sup>134</sup> who highlighted that the most commonly employed techniques recently are NMR and X-ray crystallography which will be discussed in more detail.

### 1.4.5.1 Nuclear magnetic resonance

Solution-state NMR is a versatile tool for the study of binding interactions between small molecules and macromolecular targets,<sup>135-136</sup> whereby numerous research groups use NMR as part of their primary screen and/or secondary method.<sup>137-139</sup> NMR screening can be divided into two general methods: ligand- and target-based methods.<sup>140-141</sup> Ligand-based methods measure changes in NMR signals of the ligand upon binding to a protein target. Target-based methods measure the changes of the receptor resonances in the presence and absence of ligands.

For ligand-based methods, WaterLOGSY and saturation transfer difference (STD) are most commonly used. Ligand-based methods require less target protein, which can be of almost any molecular size and the target needs no isotopic labelling. On the downside, this method is limited to weak and medium binders as tight binders may not be distinguished from the target and consequently its signal is suppressed resulting in false negatives. Additionally, non-specific binding can result in the appearance of false positives.

In 2D  $^1\text{H}/^{15}\text{N}$ -HSQC NMR, ligand binding to  $^{15}\text{N}$ -labelled protein is detected from the change in  $^{15}\text{N}$  chemical shifts indicating which amide protons are perturbed.<sup>141-143</sup>  $^1\text{H}/^{15}\text{N}$ -HSQC NMR of the target allows reliable and robust detection of even weakly bound ligands ( $K_D > \sim 10 \mu\text{M}$ ).<sup>144</sup> When full chemical shift assignments are available, the binding location of the ligand to the target can be determined and used to guide fragment optimisation and elaboration.<sup>145</sup> The disadvantage of  $^1\text{H}/^{15}\text{N}$ -HSQC NMR is that it is generally resource intensive, requiring large amounts of protein and the targets usually have to be labelled with  $^{15}\text{N}$ .

#### 1.4.5.1.1 Saturation transfer difference

STD-NMR is a very useful screening technique described by Mayer *et al.*<sup>146</sup> It takes the difference of two experiments, (1) ‘on-resonance’ in which the irradiation frequency is set to a value where only the protein nuclei are located (-2 to 0 ppm) and hence selectively excited and (2) ‘off-resonance’ is a reference experiment where irradiation frequency is set to a value far from any signal, ligand or protein (40 ppm).<sup>143</sup> The selective magnetisation of the high field  $^1\text{H}$  resonance results in the saturation of the protein and eventually to any bound ligands *via* spin diffusion (Figure 1-10). When the bound ligand dissociates from the target protein into solution, the magnetisation change transferred in the bound state is retained in the free ligand. The resulting difference spectrum provides signals for only perturbed ligands.

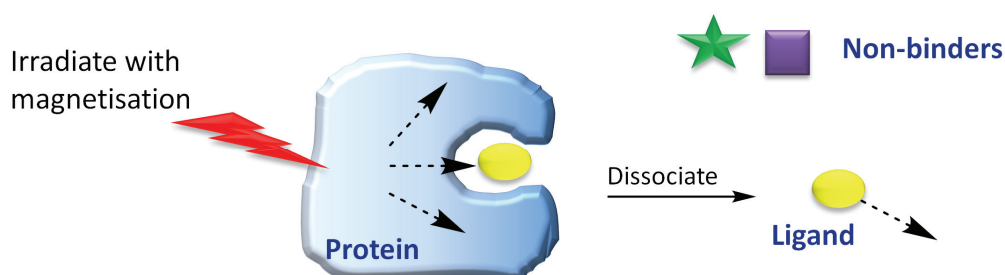


**Figure 1-10.** Illustration of the effect of on-resonant irradiation of protein signals: Due to spin diffusion, the resulting magnetisation spreads out across the target molecule and is transferred to the bound ligand. On dissociation into solution, the ligand retains the acquired magnetization.

STD-NMR is widely applied in FBLD screening due to its fast detection and screening of fragment cocktails without the need for subsequent deconvolution. For a primary screen, the STD-NMR approach is useful for rapid cost-effective acquisition of data.

### 1.4.5.1.2 2D Heteronuclear single quantum correlation

Target-based methods are lower throughput and typically used as a follow-up for primary screen. A binding event between protein and ligand can be monitored by the CSP in an overlaid *apo*-protein (unbound) and *holo*-protein (ligand bound)  $^1\text{H}/^{15}\text{N}$ -HSQC spectra. The nuclei of the atoms directly involved in the interactions usually show the greatest change in CSP. An advantage of this approach is that detection of binding and even binding affinity is possible without any backbone assignments. However to identify which amino acids are involved in the interactions, the protein backbone needs full chemical shift assignments. To identify the residues of the target involved in the protein-ligand interactions, the method requires relatively large amounts of isotopically labelled protein (50 – 300  $\mu\text{M}$ ). The advantages and disadvantages are summarised in Table 1-5.

**Table 1-5.** Advantages and disadvantages of  $^1\text{H}/^{15}\text{N}$ -HSQC NMR

Advantages	Disadvantages
- Detect high- and low-affinity ligands ( $K_D > \sim 10 \mu\text{M}$ )	- Limited to smaller protein targets (< 30 – 40 kDa)
- Obtain binding affinity of ligands	- Target protein require isotope-labelling
- Yield ligand binding site information	- High protein concentration (50 – 300 $\mu\text{M}$ ) is required
- Very reliable	- Knowledge of 3D structure of target protein and NMR assignments (or map) of at least active site residues required

Target-based NMR methods used in fragment-based approach have extended to academia, for example; Monash Institute of Pharmaceutical Sciences (MIPS, Monash University) have reported fragment based screening on the integrase enzyme of human immunodeficiency virus 1 (HIV)<sup>147</sup> and Leiden University screened against FKBP.<sup>148</sup>

An example of a successful use of the target-based NMR method was reported by Schering-Plough on hepatitis C virus.<sup>149</sup> On designing non-peptidic inhibitors for hepatitis C virus protease, Schering-Plough screened a fragment library containing 3639 compounds using 2D NMR methods.<sup>149</sup> From over 50 hits, 16 compounds were confirmed binding in the active site by <sup>1</sup>H/<sup>15</sup>N-HSQC NMR CSP. To improve potency, 5 different scaffolds (e.g. diiodophenol **52** and benzophenone **53**) found binding in adjacent pockets (S1 – S3 and S2') were selected and optimised. In the S1 – S3 region, 64 analogues of the diiodophenol hit indicated removal of the phenyl group **54** gave the highest affinity and the acidic phenol and iodide atoms appeared to be essential for affinity. Analogues of the benzophenone hit **53** binding in the S2' region were evaluated. Most variations decreased activity except converting the *para*-hydroxyl substituent to a methoxy as in methoxybenzophenone **55**, which improved activity slightly. Since the CSP demonstrated the simultaneous binding of diiodophenol **54** and benzophenone **55** to proximal substrate binding sites, a linking strategy was employed (Figure 1-11). The linked compound **56** was 175-fold to 2000-fold more potent than the individual fragments. Although the linked compound **56** represents a significant increase in potency, the binding energies were not additive. This example highlights the difficulty in achieving efficient linking however, demonstrates that through fragment linking, the potency can be improved starting from weak affinity fragments.

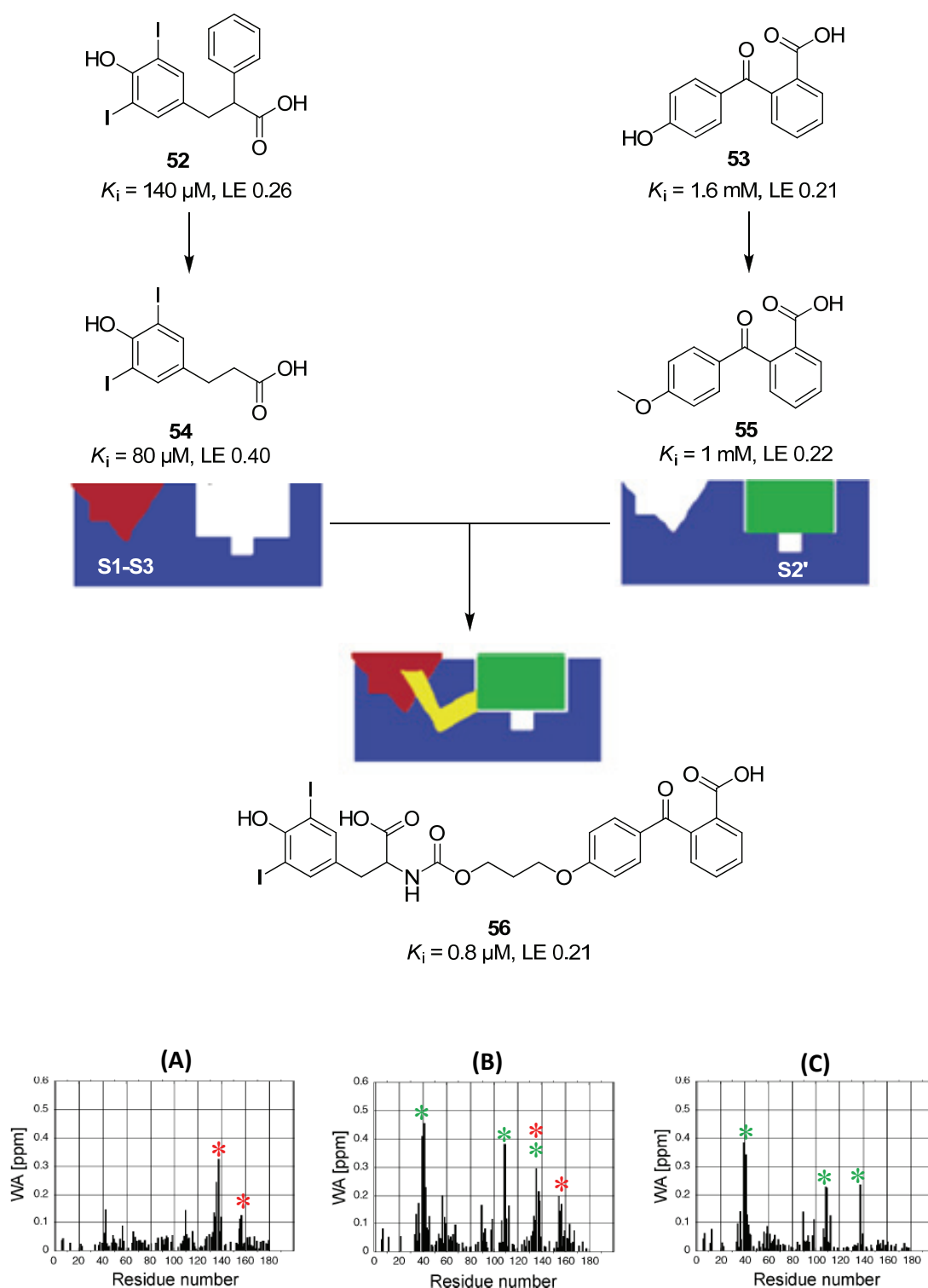


**Figure 1-11.** (Top) Fragments **52** and **53** that bind in proximal subsites were optimised before linking with further improvements in potency.<sup>149</sup> (Bottom) The graphs represent per residue weighted average CSP of  $^{15}\text{N}$ -labelled protein in the presence of 1 mM each of diiodophenol ‘\*’ (left), diiodophenol and benzophenone (middle), and benzophenone ‘\*’ (right). The middle graph illustrates that both diiodophenol and benzophenone can bind simultaneously. Adapted with permission from *J. Med. Chem.* 2004, 47 (10), 2486-2498. Copyright (2012) American Chemical Society

### 1.4.5.2 X-ray crystallography

X-ray crystallography is a valuable tool in providing detailed structural ligand-binding information. Such information has been exploited in lead optimisation to enable hit validation and optimisation of ligand potency and selectivity.<sup>150</sup> The use of X-ray crystallography to identify hits by co-crystallising target-protein with fragments was first demonstrated in 2000 by researchers at Abbott.<sup>151</sup> The process involved soaking crystals of *apo*-target protein with mixtures of fragments with high shape diversity (up to 100 fragments per cocktail) for 1 – 24 h.

Advances in technology, software and molecular biology have significantly increased the speed and power of protein crystallography.<sup>152</sup> However, there are considerable challenges in X-ray crystallography including many false negatives results presumably due to the thermodynamically controlled process; the binding site must be accessible in the crystal packing form; crystals of the *apo*-target protein are suitable quality for high concentrations of ligands and X-ray diffraction.<sup>134,153</sup> Therefore, as a primary screening tool, X-ray crystallography is not widely used because it is low throughput and resource intensive. Instead X-ray crystallography is utilised in validating hits in which the three-dimensional (3D) structure of the fragment hit interacting with the protein target can be used to compare binding modes of various fragments to develop valuable SAR information.<sup>134</sup>

### 1.4.6 Converting fragment hits into leads

Validation of fragment hits after a primary screen can be critical for hit-to-lead optimisation. Therefore, alternative complementary techniques such as SPR, biochemical assay, target-based NMR or X-ray crystallography may be used. A validation step is especially important when STD-NMR is used as the screening method, since it is more susceptible to false positives. Once a fragment hit is confirmed, the next step involves testing structurally similar analogues, where SAR may be established around the initial fragment hit. Structural information from X-ray crystallography or  $^1\text{H}/^{15}\text{N}$ -HSQC NMR can identify the fragments binding mode or location on the target protein which may become critical for hit progression. Notably, the preferred binding mode within a chemical series may be affected as substituents are changed, thus confusing SAR development. In the absence of structural information, the binding site can be located by competition experiments with a known ligand or site directed mutagenesis.<sup>42</sup> SAR can then be used to direct synthesis of larger molecules to optimise binding to adjacent regions of the active site and improve the potency. During this early phase, an iterative approach is adopted, where syntheses of molecules, potency and binding location may be tracked at each stage. LE may be used as a quantitative measure to ensure that effective interactions are being made as a fragment is evolved.

Three main strategies used to elaborate the initial fragment hit into lead compounds include fragment growing, merging or linking.<sup>108,154</sup> The more common approach is fragment growing. Starting at a single point, structural information such as fragment binding orientation and/or SAR is used to guide the direction to grow the fragment and hence pick up additional interactions, and gradually increase potency. Fragment merging takes optimal features of two individual fragments binding in adjacent or overlapping

positions in the active site to create a larger, higher affinity compound. Fragment linking, requires that two (or more) fragments bind to proximal parts of the active site. A suitable linker is used to join the individual fragments forming a larger, higher affinity molecule.<sup>155</sup> For this approach, structural information is imperative to avoid large combinatorial and random search to find an effective linking scheme.

An example where the two strategies, fragment linking and growing have been compared was reported by Hung and co-workers<sup>77</sup> for the *M. tuberculosis* enzyme PtS. A range of biophysical techniques were used in this study including thermal shift assay, ligand-based NMR, ITC and X-ray crystallography. Hung *et al.*<sup>77</sup> identified 5-methoxyindole **57**, a weak binder, in a preliminary screen using WaterLOGSY. A screen of structurally related fragments indicated a narrow SAR as the replacement of the methoxy group with either a hydroxy group or a methyl group, or the replacement of the indole core with a benzopyridine or benzimidazole heterocycle led to an approximate 10-fold decrease in the binding affinity. The initial fragment hit was taken into the next phase: the fragment growing approach. X-ray crystallography revealed that the 5-methoxyindole **57** binds in the ATP adenine motif binding site. As a result, synthetic modifications by introducing negatively charged moieties (**58** – **60**) were made in an attempt to capture electrostatic interactions in the triphosphate binding site for ATP, which indeed led to modest improvements in potency (Figure 1-12). The crystal structure of the complex of compound **60**, which incorporated an acyl sulfonamide, was found in the same binding mode as the initial fragment hit at the P2 pocket, making further hydrogen-bonding interactions. To their advantage, there was also room for further growing from the methyl substituent of the sulfonamide. Converting the methyl group to a 4-methylpyridine ring **61** (on the sulfonamide) and introducing an alkyl

carboxyl group at the N1 position of the indole, led to compound **62**, and improved the affinity by approximately two orders of magnitude while maintaining LE.

At the same time, a benzofuran **63** was identified by a thermal shift screen. Confirmed as a hit through WaterLOGSY, NMR spectroscopy and ITC, the benzofuran was discovered to bind in the P1 pocket in close proximity to the indole **59**, suggesting that the two fragments can be linked. Flexible linkers such as alkyl ester **64** and sulfonamide **65** were introduced (Figure 1-12). The indole and benzofuran fragments were linked with the sulfonamide **66** which closely resembles the 4-methylpyridine (**62**) final compound from fragment growing. The final compound from fragment growing (**62**) was marginally more potent and ligand efficient than the fragment linking (**66**).

Hung *et al.*<sup>77</sup> concluded that despite both strategies resulting in similar compounds and similar potency, ‘...the linking strategy appears more elegant...’ but the small collection of linkers available could compromise how the original fragments bind. On the other hand, the fragment growing strategy allowed ‘...more freedom for development... more room for further optimisation.’ There is still further development needed for the linking strategy. It is challenged by many factors, such as maintaining the binding orientation and position of the fragments,<sup>156</sup> energy lost as a result of linker strain,<sup>157-158</sup> or the chemical nature of the linker influencing binding.<sup>148</sup>

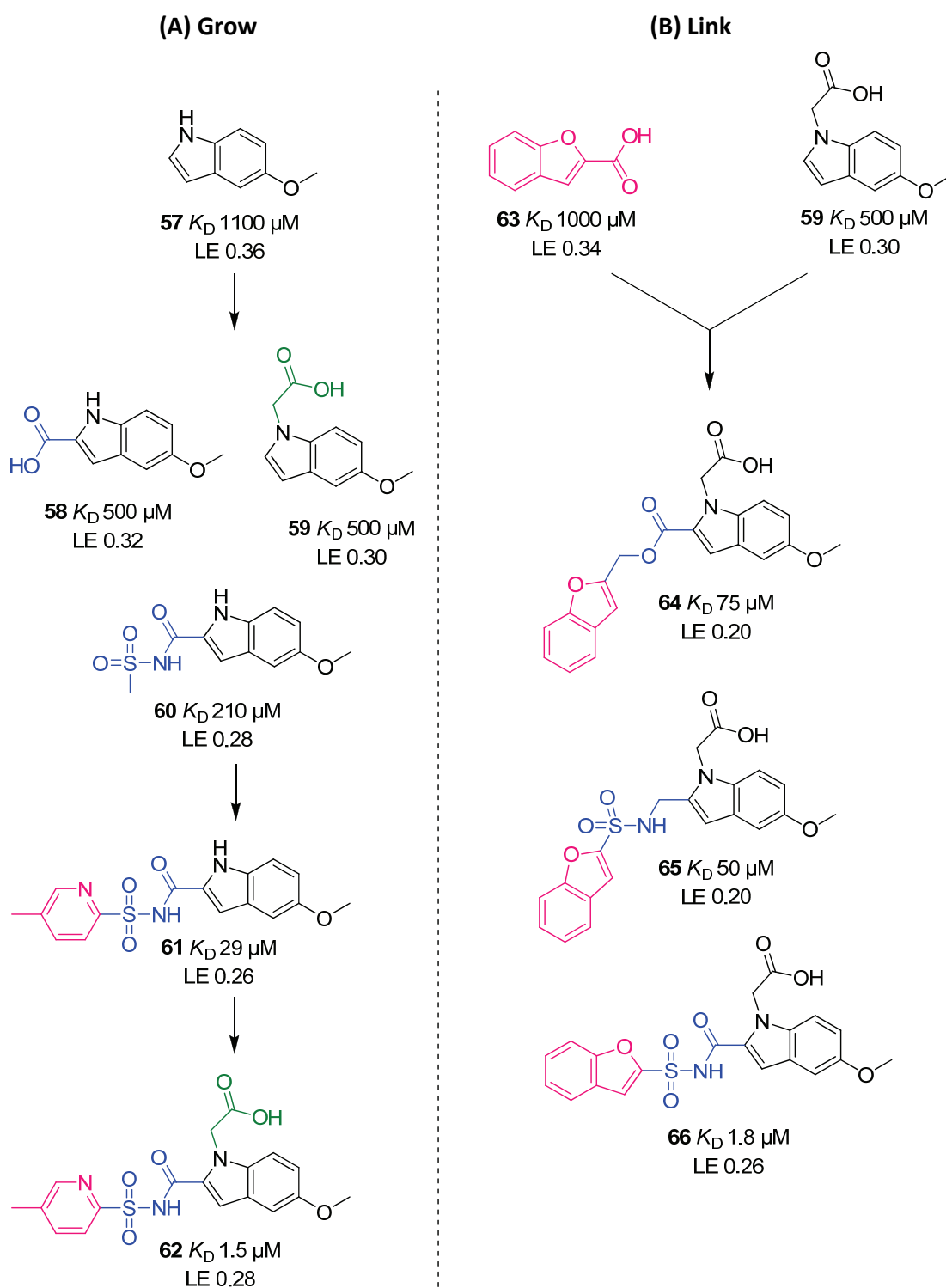


**Figure 1-12.** A fragment growing strategy is compared to a fragment linking strategy for *M. tuberculosis* PtS<sup>77</sup>

### 1.4.7 Fragments in the clinic

FBLD has significantly developed over the past fifteen years and is now taken up at universities, large pharma and biotech companies.<sup>159</sup> There have been a number of reviews recently documenting successes and summarising programs that have generated clinical candidates from fragments and also the challenges that need to be addressed.<sup>160-</sup>  
<sup>163</sup> Lead compounds derived from fragments currently in clinical development are summarised in Table 1-6.

**Table 1-6.** Lead compounds derived from fragments currently in clinical development<sup>162</sup>

Compound	Company	Target	Progress	Detection Method
ABT-263	Abbott	Bcl-X <sub>L</sub>	Phase 2	NMR
AT9283	Astex	Aurora	Phase 2	X-ray
LY-517717	Lilly/Protherics	FXa	Phase 2	Computational/X-ray
NVP-AUY-922	Novartis/Vernalis	Hsp90	Phase 2	NMR
Indeglitazar	Plexxikon	PPAR agonist	Phase 2	HCS/X-ray
ABT-518	Abbott	MMP-2 & 9	Phase 1	NMR
AT7519	Astex	CDK2	Phase 1	X-ray
AT13387	Astex	Hsp90	Phase 1	NMR/X-ray
IC-776	Lilly/ICOS	LFA-1	Phase 1	NMR
PLX-5568	Plexxikon	Kinase Inhibitor	Phase 1	HCS/X-ray
SGX-523	SGX Pharmaceuticals	Met	Phase 1	X-ray/HCS
SNS-314	Sunesis	Aurora	Phase 1	MS

(HCS = high content screening)

In August 2011, the FDA approved the first drug candidate to come out of fragment-based screening.<sup>164</sup> The discovery started with a biochemical screen against a panel of kinases using the Plexxikon library containing 20,000 compounds (molecular weight approximately 150 – 350 Da).<sup>165</sup> Fragment hits were judged based on their ability to inhibit the activity of three kinases, Pim-1, p38 and CSK by at least 30% at 200  $\mu$ M. The selection resulted in 238 hits that were then co-crystallised with one of the three kinases. In complex with Pim-1 was 7-azaindole **67**, however, interestingly a few binding modes were identified for this fragment (Figure 1-13). A subsequent analogue screen yielded the 3-aminophenyl analogue **68** with improved affinity and only one binding mode observed, although the 3-aminophenyl analogue **68** showed non-selective kinase binding. Therefore, a series of analogues with varying substituents were synthesised and screened against a panel of kinases, including the B-Raf<sup>V600E</sup> mutant. After iterations of crystallography and optimisation chemistry, a highly selective lead compound **69** with nanomolar affinity for B-Raf<sup>V600E</sup> was discovered. In fact, **69** displayed remarkable selectivity against a diverse panel of 70 other kinases. Despite being less potent and ligand efficient, Zelboraf (**70**) performed more favourably in terms of pharmacokinetics in animal models and therefore was selected over **69**.<sup>166</sup> The discovery program started in February 2005 highlighting that discovery to approved drug candidate can happen in just 6 years!

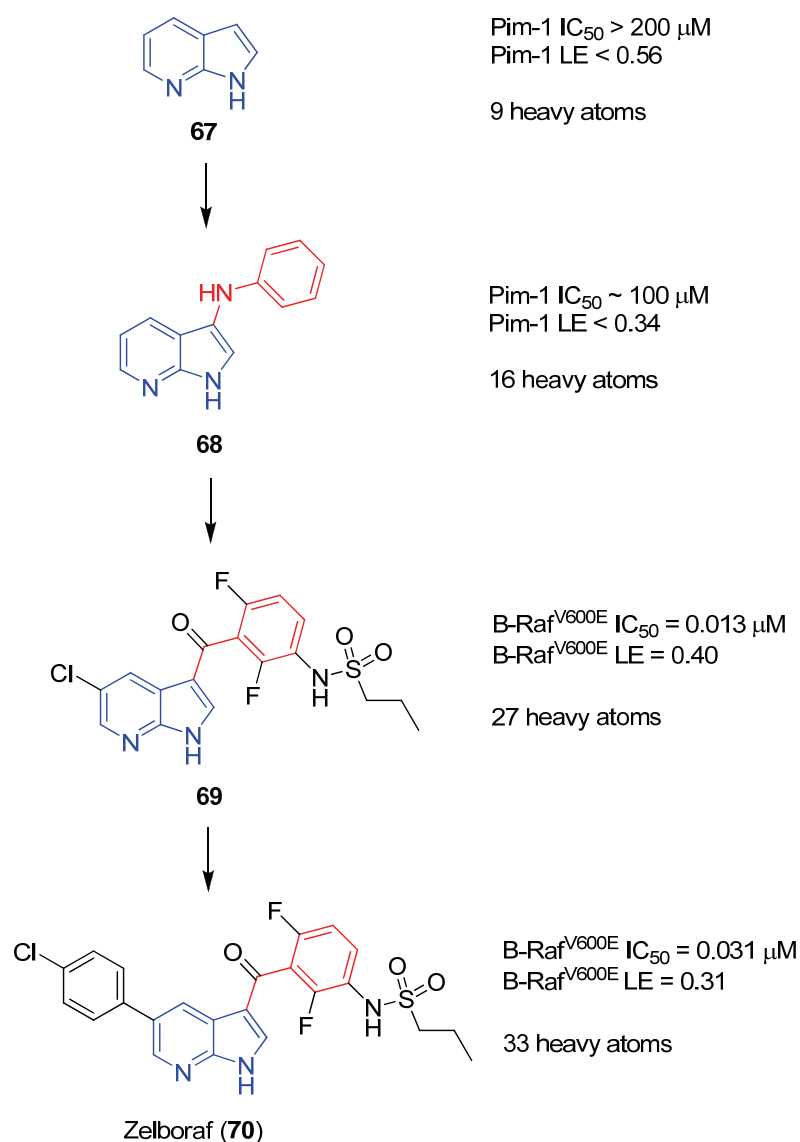


**Figure 1-13.** From fragment to lead compound and approved drug Zelboraf (**70**) using fragment growing method

The contribution of FBLD to modern drug discovery is largely due to strong collaborative efforts between biologists, medicinal chemists, biophysicists and modellers. The significant advancements in technology across all major screening platforms with improvements such as enhanced sensitivity, higher throughput and applicability to broader biological targets have enabled considerable progress in FBLD.

Since FBLD is design-intensive, it is an ideal technique for application in academic medicinal chemistry groups. In this study, a FBLD approach is used to identify small molecule inhibitors of KPR. KPR is the second enzyme in the pantothenate pathway and has been shown to be a critical step of the pantothenate biosynthesis.<sup>101</sup> Despite the extensive structural and mechanistic information being available,<sup>59,88-92</sup> no inhibitors of KPR have been reported in the literature to date. The benefits of finding a small molecule inhibitor for the pantothenate pathway include using these compounds to investigate the role of KPR in the development of antimicrobials.

# Chapter 2

---

## Protein expression, screening and hit validation

# 2 Protein expression, screening and hit validation

## 2.1 Introduction

In this study, a FBLD program was carried out to identify small molecule inhibitors of KPR. The approach involved an STD-NMR screen for fast detection of fragments binding to KPR followed by  $^1\text{H}/^{15}\text{N}$ -HSQC NMR to confirm the fragment hits. The activity of the confirmed fragment hits was assessed using *in vitro* assays. This requires pure protein and the ability to incorporate isotope labels. This chapter describes the optimisation of the expression system for unlabelled and labelled KPR. The initial expression construct was a pRSETA plasmid containing the *panE* gene and was provided as a kind gift from Prof. Chris Abell (Cambridge University).

## 2.2 Protein expression

Binding and kinetic studies of a receptor target require relatively pure, correctly folded protein; often in large amounts to enable the downstream screens and structural work. For primary screen follow-up, an efficient expression system is important when incorporating isotopes for NMR to minimise production cost. The yield is often lower when the protein is expressed in *E. coli* grown in minimal media with defined nutrients, as required for isotopic labelling. In this study, an *E. coli* expression system was used due to the ease of handling, rapid growth and high-yield protein production. A tag for affinity purification (His<sub>6</sub>-tag) was incorporated into the recombinantly expressed KPR. The His<sub>6</sub>-tag enables efficient purification of the protein by exploiting its high affinity for Ni-NTA (nickel-nitrilotriacetic acid).

### 2.2.1 His<sub>6</sub>-KPR

Initial attempts to express the His<sub>6</sub>-KPR construct in a number of cell lines were challenged by the limited level of expression. To establish the best expression conditions for the KPR construct, the construct was analysed by Dr Noelene Quinesy (Department of Biochemistry and Molecular Biology, Monash University) in 12 different strains of *E. coli*. The best expression was observed in *E. coli* C41(DE3) cells when grown at 28 °C (Figure 2-1). Many cell lines were not suitable for KPR expression, possibly suggesting that the expression of large amounts of KPR is toxic to the cells, as C41(DE3) are typically used for expressing toxic recombinant proteins.<sup>167</sup>

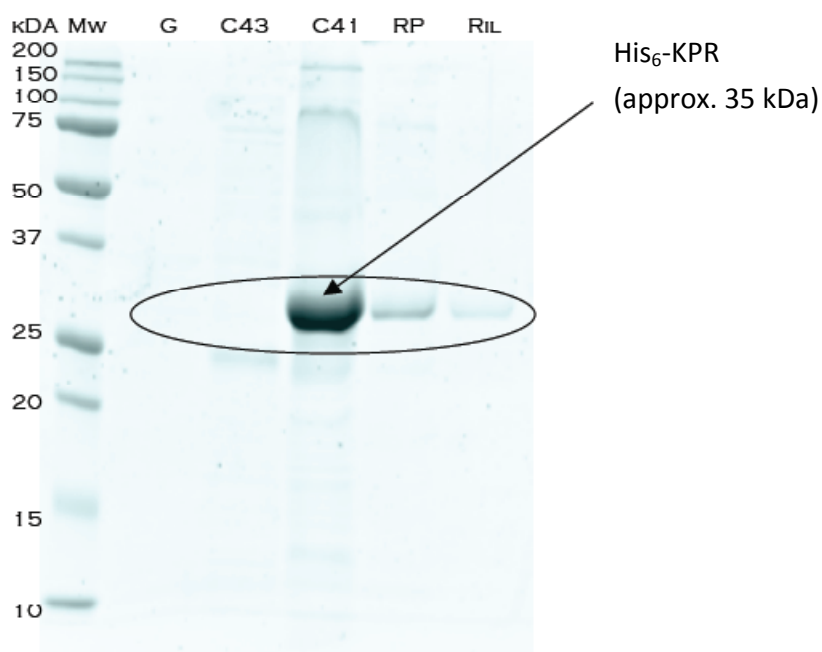


**Figure 2-1.** SDS gel (15%) of His<sub>6</sub>-KPR construct expressed in a variety of *E. coli* cell lines including BL21 Gold, C43, C41, BL21 codon plus RP and BL21 codon plus RIL

To express unlabelled KPR, competent cells of *E. coli* strain C41(DE3) are transformed with the pRSETA plasmid using the heat shock method.<sup>168</sup> An isolated colony of freshly transformed *E. coli* competent cells were grown overnight in a starter culture (5 – 10 mL of Luria Broth (LB) broth containing ampicillin (Amp, 100 µg/mL)) and then used to inoculate the main culture in 1 L LB/Amp. The cells were grown at 28 °C to mid-log phase (optical density at 600 nm (OD<sub>600</sub>) of 0.6) when expression was induced with 1 mM isopropyl-1-thio-β-D-galactopyranoside (IPTG). The cells were incubated for an additional 4 h at 28 °C before harvesting.

Alternatively, KPR expression was performed by transferring the starter culture into auto-induction media using a method described by Studier.<sup>169</sup> Auto-induction is a more convenient method than IPTG induction. Briefly, the T7 expression system is widely used in *E. coli* for recombinant protein expression. In the absence of an inducer, the *lac repressor* is bound to the *lac operator* preventing transcription of the T7 RNA polymerase gene and consequently target protein expression. So when an inducer (e.g. IPTG) is added, the *lac repressor* is relieved and the cells can express T7 RNA polymerase. Alternatively, lactose has been used to induce protein expression. Studier<sup>169</sup> has shown that with the appropriate balance of glucose and glycerol as carbon source, the cells will grow to reach high cell density until their depletion which then allows the α-lactose present in the medium to finally induce expression.<sup>169</sup> Therefore, in an auto-inducing medium, the cells are grown to saturation without the need to monitor the cell density to catch the cells at log phase to induce protein expression.

A comparative study of KPR expression yields between an IPTG induction and auto-induction revealed intriguing results (Figure 2-2). The expression level when using

IPTG started to plateau 4 h post induction and therefore the cells were harvested with cell density  $OD_{600}$  of 2.5. The auto-induction method showed continual cell growth for more than 20 h reaching an  $OD_{600}$  of 8.5, after which it was harvested. The purified yield from IPTG method was 30 – 40 mg/L, while auto-induction yielded 122 mg/L (both yields are after purification). The lower yield from the IPTG method may be due to basal expression of small amounts of T7 RNA polymerase leading to expression of KPR. Since KPR is suspected to be toxic towards the host, the cells may lyse KPR resulting in a lower yield. However, in the auto-inducing media the basal expression of target protein is minimised due to the presence of glucose.<sup>169</sup>

A fresh transformation of KPR construct into C41(DE3) cells of *E. coli* provided more consistent expression levels of KPR compared to using frozen glycerol stocks of pre-transformed KPR cells, thus the optimised method employs a fresh transformation for each protein expression. Auto-induction expression was the method of choice due to its ease, convenience and superior expression level.

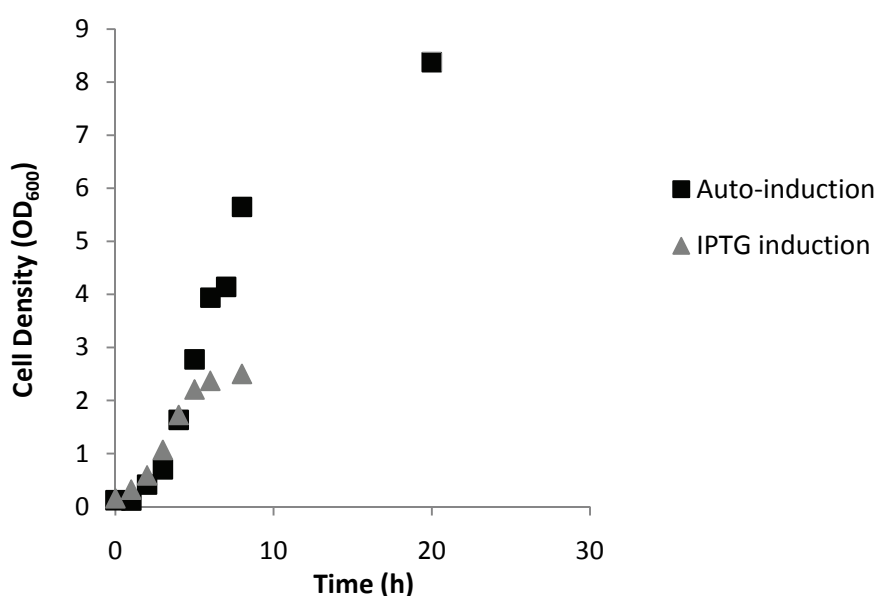


**Figure 2-2.** The effect of auto-induction and IPTG induction on cell density

### 2.2.2 His<sub>6</sub>-<sup>15</sup>N KPR

For nitrogen labelling, the initial growth phase was in LB before transferring to a defined minimal media and initiating protein expression. The theory behind the approach is that *E. coli* grown rapidly in unlabelled rich media (LB) contain more ribosomes.<sup>170</sup> The native *E. coli* proteins, including the ribosomes, do not need to be isotopically labelled in order to produce labelled recombinant protein. Therefore, the high cell density is optimised to produce maximal labelled recombinant protein expression once in defined minimal media.<sup>170</sup>

The method for high-level expression and efficient isotopic labelling of His<sub>6</sub>-<sup>15</sup>N KPR involved selecting a single colony of freshly transformed cells to inoculate an unlabelled starter culture (LB/Amp), which was grown overnight at 37 °C. After centrifuging, the pelleted cells were transferred into a larger fresh media (LB/Amp) and incubated until the cell density reached log phase with OD<sub>600</sub> of 0.6 prior to pelleting and resuspension in one quarter of the volume of defined, labelled minimal media (Chapter 7, section 7.1.2). The *E. coli* cells were incubated at 28 °C until growth recovery (OD<sub>600</sub> ~2.4) was observed when expression was then induced by the addition of 1 mM IPTG (Figure 2-3). Once the cell density had plateaued, typically 5 – 6 h post-induction, the cells were harvested.

Initial attempts to obtain high-yielding expression of His<sub>6</sub>-<sup>15</sup>N KPR utilised the M9 minimal media recipe according to Sambrook *et al.*,<sup>171</sup> however, the expression levels were insufficient for economical isotopic labelling for NMR studies. When the cells were grown in minimal media prepared according to the recipe described by Marley and co-workers,<sup>170</sup> the yields were much higher. The improved minimal media recipe

contained five times the stock solution of M9 salts ( $\text{KH}_2\text{PO}_4$ ,  $\text{Na}_2\text{HPO}_4$ ,  $\text{NaCl}$ ,  $\text{NH}_4\text{Cl}$ ) and 4 g/L glucose compared to the initial recipe of one times the stock solution of M9 salts and 2 g/L glucose. The *E. coli* cells grew at a high rate upon transferring to minimal media and reached an  $\text{OD}_{600} > 8.0$  (Figure 2-3). Protein yields were as high as 53 mg/L post purification.

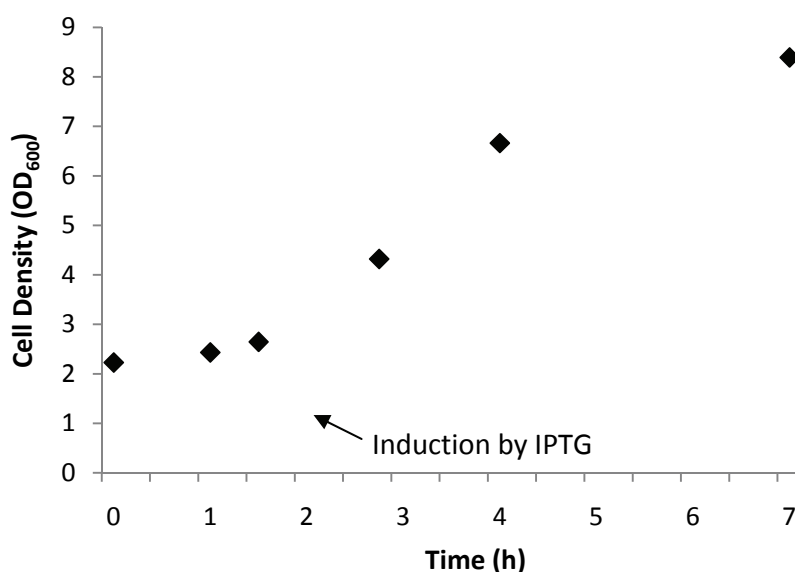


**Figure 2-3.** Growth curve of cells in minimal media

### 2.2.3 Purification (unlabelled and $^{15}\text{N}$ -KPR)

Purification of His<sub>6</sub>-KPR was a three-step process; after lysing the cells and removing the cell debris by centrifugation, the supernatant containing KPR was first applied to a HisTrap HP nickel affinity column then a HiPrep 26/10 desalting column and a HiLoad Superdex 75 HR 16/60 size exclusion column. The nickel affinity column allows separation of proteins based on the affinity of the His<sub>6</sub>-tag for the Ni-NTA resin. His<sub>6</sub>-KPR was applied to the Ni-NTA column in buffer A (10 mM potassium phosphate pH 8.0), containing low imidazole concentration (10 mM). After a wash step in buffer A, His<sub>6</sub>-KPR was eluted at a gradient of 0 – 100% buffer B (500 mM imidazole). Fractions

containing purified KPR, as assessed by sodium dodecyl sulphate-polyacrylamide gel electrophoresis (SDS-PAGE), were pooled and exchanged into 100 mM HEPES (buffer C or D, chapter 7 section 7.1.2) using a desalting column. The final step in the purification was a size exclusion column (in buffer C or D) to separate lower molecular weight protein impurities from His<sub>6</sub>-KPR. Fractions containing His<sub>6</sub>-KPR were identified by SDS-PAGE and concentrated. The mass of the protein calculated from the predicted amino acid sequence with His<sub>6</sub>-tag (35791.9 Da), compared well to the electrospray mass spectrometry (ES-MS, 35790.21 Da).

In summary, a 1 L culture was sufficient to obtain 50 – 120 mg/L of purified (unlabelled/labelled) KPR over three chromatographic purification steps. The protein behaved as a monomer on a size exclusion column, and its identity was confirmed by SDS-PAGE and MS (Chapter 7, section 7.1.2.6).

### **2.3 Fragment library**

With the target protein in hand, a fragment screen using STD-NMR was undertaken. The fragment library used in the preliminary screen contained 500 structurally diverse compounds purchased from Maybridge. The fragments had an average molecular weight of 200 Da and were ‘rule of three’ compliant, as introduced in Chapter 1. The library included chemical cores with 1 – 3 substituents attached with at least one polar substituent such as an amine, acid or hydroxyl.

The fragments were prepared in neat <sup>2</sup>H<sub>6</sub>-dimethyl sulfoxide (DMSO) to generate a concentrated stock solution and stored at 4 °C. Initially, the fragments were assessed

individually for purity and solubility by one-dimensional (1D)  $^1\text{H}$  NMR. Those that were less than 90% pure, had questionable identity or were not soluble (based on the chemical shifts, coupling and intensity of peaks in the 1D  $^1\text{H}$  NMR spectra) were noted and removed from analysis.

A 1D  $^1\text{H}$  NMR reference spectrum for each of the 500 fragments in the library was acquired individually by Zhao.<sup>172</sup> The samples were prepared in phosphate buffer (20 mM  $\text{KH}_2\text{PO}_4$ , 80 mM NaCl pH 7.4) to avoid changes in chemical shifts in the reference spectra due to changes in the pH of the sample. The reference spectra also served as a quality check to ensure correct fragment identity, purity and solubility. For primary screening, a previous STD-NMR study performed by Zhao<sup>172</sup> suggested fragments screened in groups of 10 (50 cocktails) sometimes complicated identifying hits due to overlapping signals. Therefore, each cocktail contained a group of 5 fragments.

## **2.4 STD-NMR fragment screening**

The samples were prepared using 25  $\mu\text{M}$  unlabelled KPR with mixtures of 5 fragments (1 mM each) added from 100 mM stocks in DMSO.

### **2.4.1 STD-NMR analysis**

The strategy used to filter the 100 acquired STD spectra involved overlaying 10 STD spectra at a time and comparing the relative intensities of signals. Those that displayed stronger STD signals were selected for a more in depth analysis, resulting in 32 spectra. An example of an individual analysis is shown in Figure 2-4. The 1D  $^1\text{H}$  NMR spectrum of the individual fragments in solution (A – E) is shown for reference. The 1D  $^1\text{H}$  NMR spectrum of the fragment mixture (containing 5 fragments) in the presence of KPR (blue

spectrum) is compared with the STD (red spectrum). The resonance signals observed in the STD spectrum are indicative of a fragment binding. In this case fragment (C) is a KPR fragment binder.

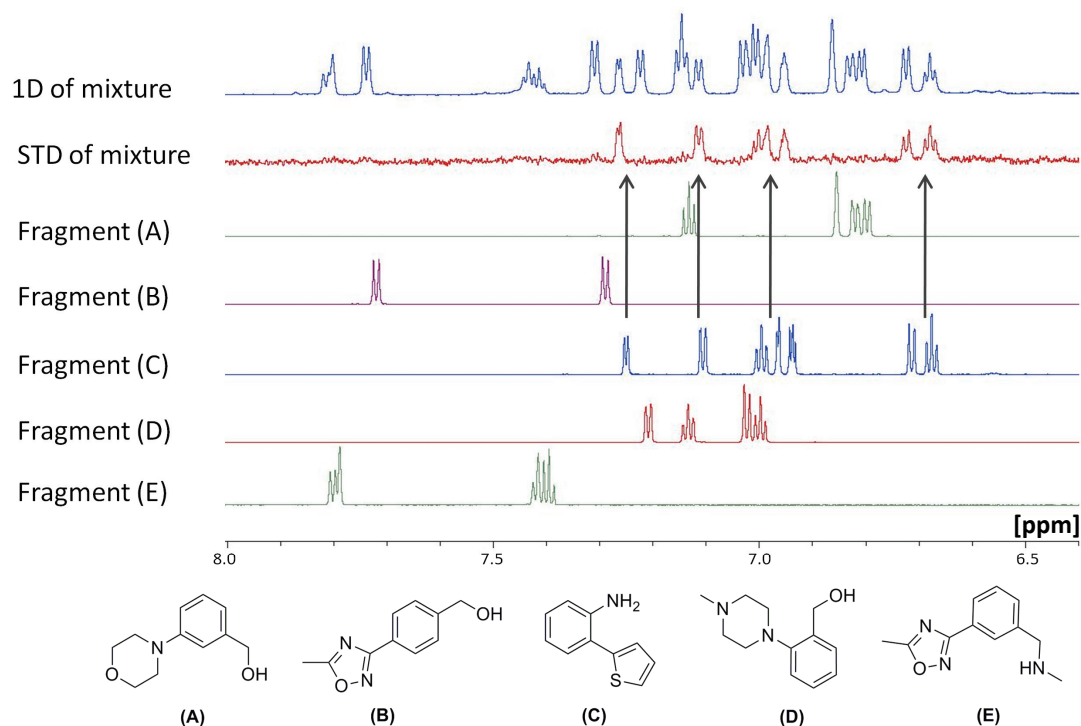


**Figure 2-4.** Detection of ligand binding to KPR using STD-NMR: The arrows highlight fragment C proton signals matching those observed in the STD spectrum indicating fragment C is binding to KPR.

#### 2.4.2 STD NMR screening hits

In this study a primary screen using STD-NMR spectroscopy was carried out and approximately 10% of the compounds in the library gave a positive STD result (Figure 2-5). From the 47 STD hits (71 – 117), 36% shared a similar chemical framework; a phenyl ring substituted with a five-membered heteroaromatic ring. Some examples include the phenylthiophene, phenylpyrrole, phenylthiazole and phenylpyrazole cores.



## 2.5 $^1\text{H}/^{15}\text{N}$ -HSQC NMR

As discussed in Chapter 1,  $^1\text{H}/^{15}\text{N}$ -HSQC NMR is a reliable and robust technique and an ideal method for validating the fragment hits identified in the preliminary screens. However, given that KPR is a relatively large protein (35 kDa) by NMR standards, it was important to determine whether the  $^1\text{H}/^{15}\text{N}$ -HSQC NMR spectrum of KPR was of sufficiently high quality for this purpose. An investigation involving KPR and its natural cofactor NADPH (**24**) was carried out to ensure that high quality 2D spectra were achievable and chemical shift perturbations (CSPs) were clear and observable.

### 2.5.1 NADPH test study

Upon addition of NADPH (300  $\mu\text{M}$ ,  $K_{\text{d(NADPH)}} = 0.26 \mu\text{M}$ ) to  $^{15}\text{N}$ -labelled KPR (100  $\mu\text{M}$ ), the NMR protein spectrum displayed significant perturbations (Figure 2-6). The amino acids affected by NADPH (**24**) binding were identified since the assignments of the backbone resonances of *apo*-KPR expressed in *E. coli* were completed by Dr Stephen J. Headey (MIPS, Monash University).<sup>173</sup> Binding was analysed using the weighted combined  $^1\text{H}$  and  $^{15}\text{N}$  amide shifts ( $\Delta\delta$ ) using Equation 2-1, where  $\delta\text{H}_{\text{boundKPR}}$ ,  $\delta\text{H}_{\text{unboundKPR}}$ ,  $\delta\text{N}_{\text{boundKPR}}$  and  $\delta\text{N}_{\text{unboundKPR}}$  are the CSPs in the bound and unbound states for the amide proton ( $\delta\text{H}$ ) and the amide nitrogen ( $\delta\text{N}$ ); The factor of 0.154 is used to account for the differences in the spectral width for  $^1\text{H}$  and  $^{15}\text{N}$  amide shifts which is in the ratio of  $\sim 1:0.154$ .

**Equation 2-1:**

$$\Delta\delta = \sqrt{(\delta\text{H}_{\text{bound KPR}} - \delta\text{H}_{\text{free KPR}})^2 + 0.154 (\delta\text{N}_{\text{bound KPR}} - \delta\text{N}_{\text{free KPR}})^2}$$

The CSPs mapped on the KPR structure (Figure 2-6) were localised around the catalytic site consistent with the crystal structure of NADPH (**24**) bound to KPR (PDB ID: 1YJQ).<sup>91</sup> Signals belonging to residues Leu6 – Gly7, Leu30, Leu68 – Gln75 and His97 (Figure 2-6) in the NADPH (**24**) binding site of the *apo* protein disappeared upon addition of NADPH (**24**), indicating that these residues are in intermediate exchange on the NMR time scale. Most of these residues are directly involved in the binding interactions suggested in biochemical studies (described in Chapter 1). For example, the residues Leu6 and Gly7 are part of the glycine-rich region (<sup>7</sup>GCGALG<sup>12</sup>) for nucleotide recognition and Leu30, Leu68 – Gln75 form hydrophobic interactions with the adenine ring of NADP<sup>+</sup> (**25**).

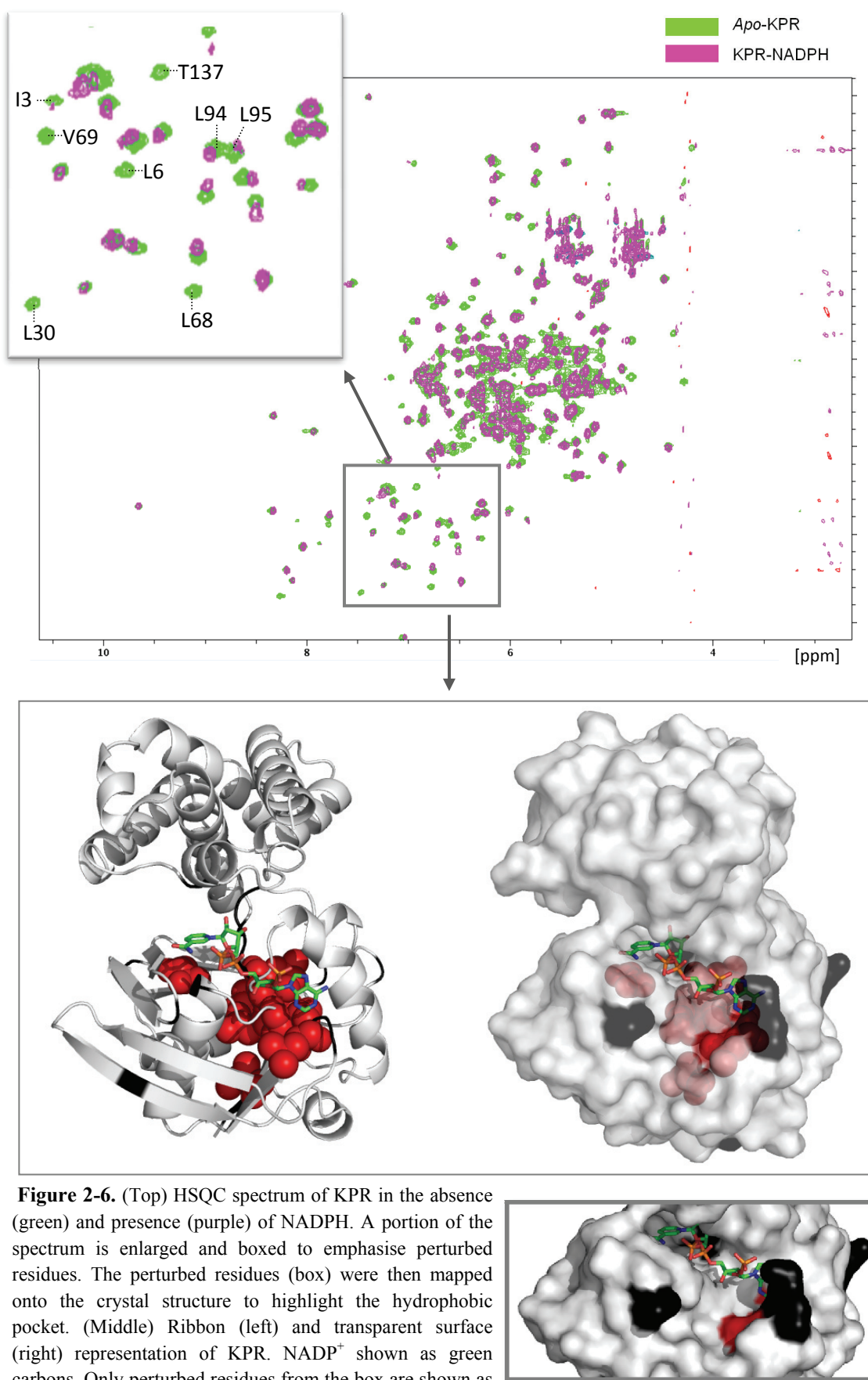


**Figure 2-6.** (Top) HSQC spectrum of KPR in the absence (green) and presence (purple) of NADPH. A portion of the spectrum is enlarged and boxed to emphasise perturbed residues. The perturbed residues (box) were then mapped onto the crystal structure to highlight the hydrophobic pocket. (Middle) Ribbon (left) and transparent surface (right) representation of KPR. NADP<sup>+</sup> shown as green carbons. Only perturbed residues from the box are shown as red spheres. Unassigned residues are coloured black. (Bottom right) Solid surface to demonstrate that perturbed residues were not all on the surface of binding cavity.

### 2.5.2 Fragment hit confirmation

The clear CSPs observed upon the binding of NADPH (**24**) to KPR confirmed that  $^1\text{H}/^{15}\text{N}$ -HSQC NMR could be used as a complementary technique to STD-NMR. As such we proceeded to investigate the effect on CSPs on addition of the fragment hits identified in the STD-NMR screen and validate their binding.  $^1\text{H}/^{15}\text{N}$ -HSQC spectra were acquired individually for each hit compound. Compounds were tested at 1 mM (0.2% DMSO) with 100  $\mu\text{M}$  of uniformly  $^{15}\text{N}$ -labelled KPR in buffer C and 10%  $\text{D}_2\text{O}$ .

Addition of fragments to  $^{15}\text{N}$ -labelled KPR resulted in detectable changes in chemical shifts for 14 out of 47 fragments, signifying fragment binding to KPR. An example of a spectrum resulting from fragment binding is shown in Figure 2-7. The 14 fragments (Figure 2-8) were retained for further characterisation. For these fragments, the CSPs were categorised as strong ( $\Delta\delta > 0.04$  ppm), medium ( $0.04 > \Delta\delta > 0.01$  ppm) or weak ( $\Delta\delta > 0.01$  ppm).

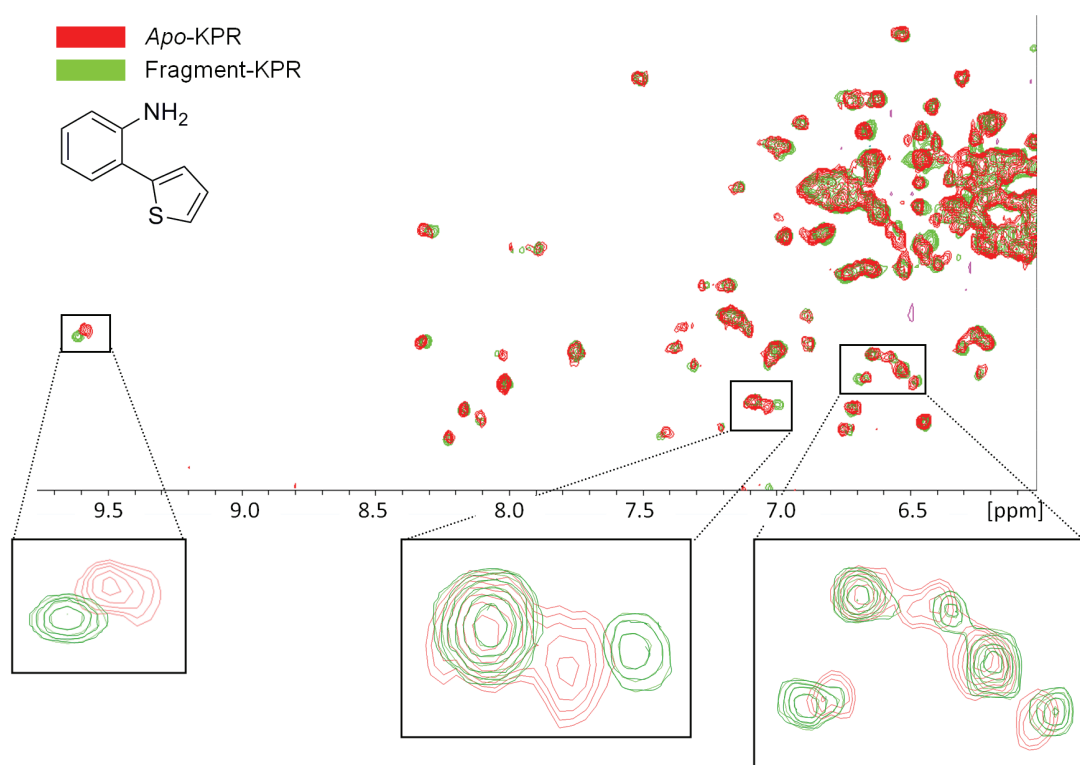


**Figure 2-7.** Portion of a  $^1\text{H}/^{15}\text{N}$ -HSQC spectrum of KPR in the absence (red contours) and presence (green contours) of 2-(thiophen-2-yl)aniline (**73**)

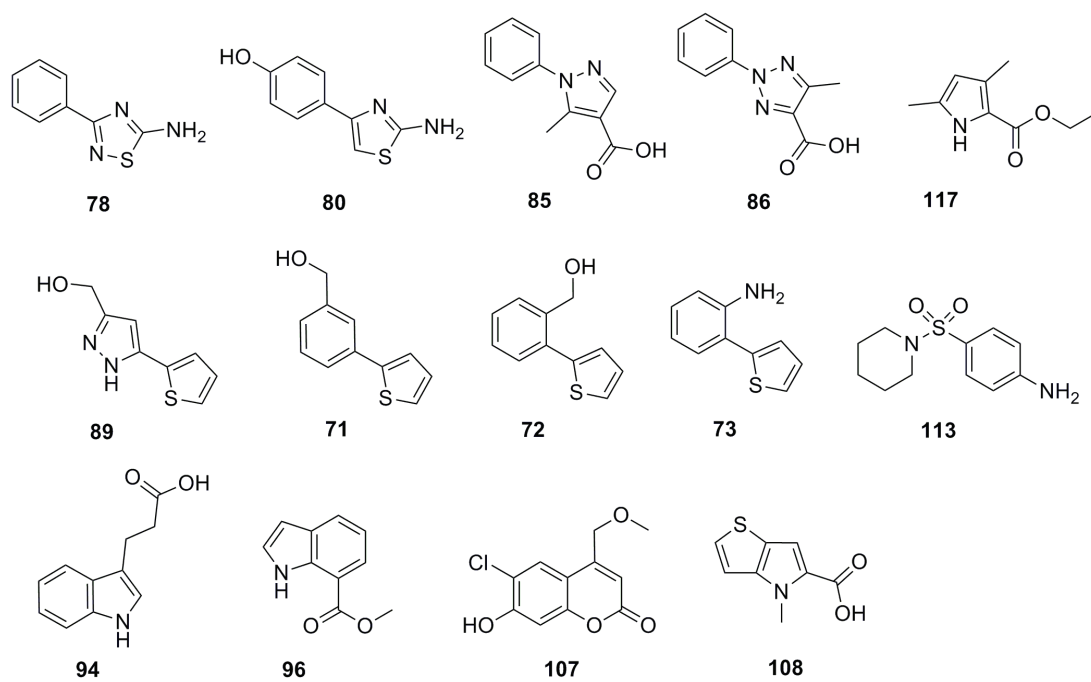


**Figure 2-8.** Structures of confirmed fragments from  $^1\text{H}/^{15}\text{N}$ -HSQC NMR

The CSPs were subsequently mapped onto the KPR crystal structure (PDB ID: 1YJQ). The 2-(thiophen-2-yl)aniline (**73**), (3-(thiophen-2-yl)phenyl)methanol (**71**), methyl 1*H*-indole-7-carboxylate (**96**), coumarin **107** and aminothiazole **80** displayed interactions with residues at the hydrophobic pocket where the adenine portion of the NADPH (**24**) binds (Figure 2-9). Of these fragments, (3-(thiophen-2-yl)phenyl)methanol (**71**) and 2-(thiophen-2-yl)aniline (**73**) displayed an additional cluster of perturbations suggesting either another binding site or the effects of conformational change. The thienopyrrole **108** and sulfonamide **113** were found to perturb residues close to the nicotinamide portion of the NADPH (**24**) binding site (Figure 2-9). Thienopyrrole **108** also showed CSPs in regions of the protein distant from the active site. When the CSP map displays good clustering on the protein, the binding site can be inferred with confidence.<sup>174</sup> However, in some circumstances, resonances at remote locations or even the majority of the resonances may be affected.<sup>175</sup> <sup>1</sup>H/<sup>15</sup>N-HSQC NMR is very sensitive to environmental changes and the CSPs are often caused by direct local interactions as well as indirect interactions such as conformational changes within the protein. Therefore it is not always possible to extract precise binding location information. As a result, the data can only be used as an approximate guide to binding location.

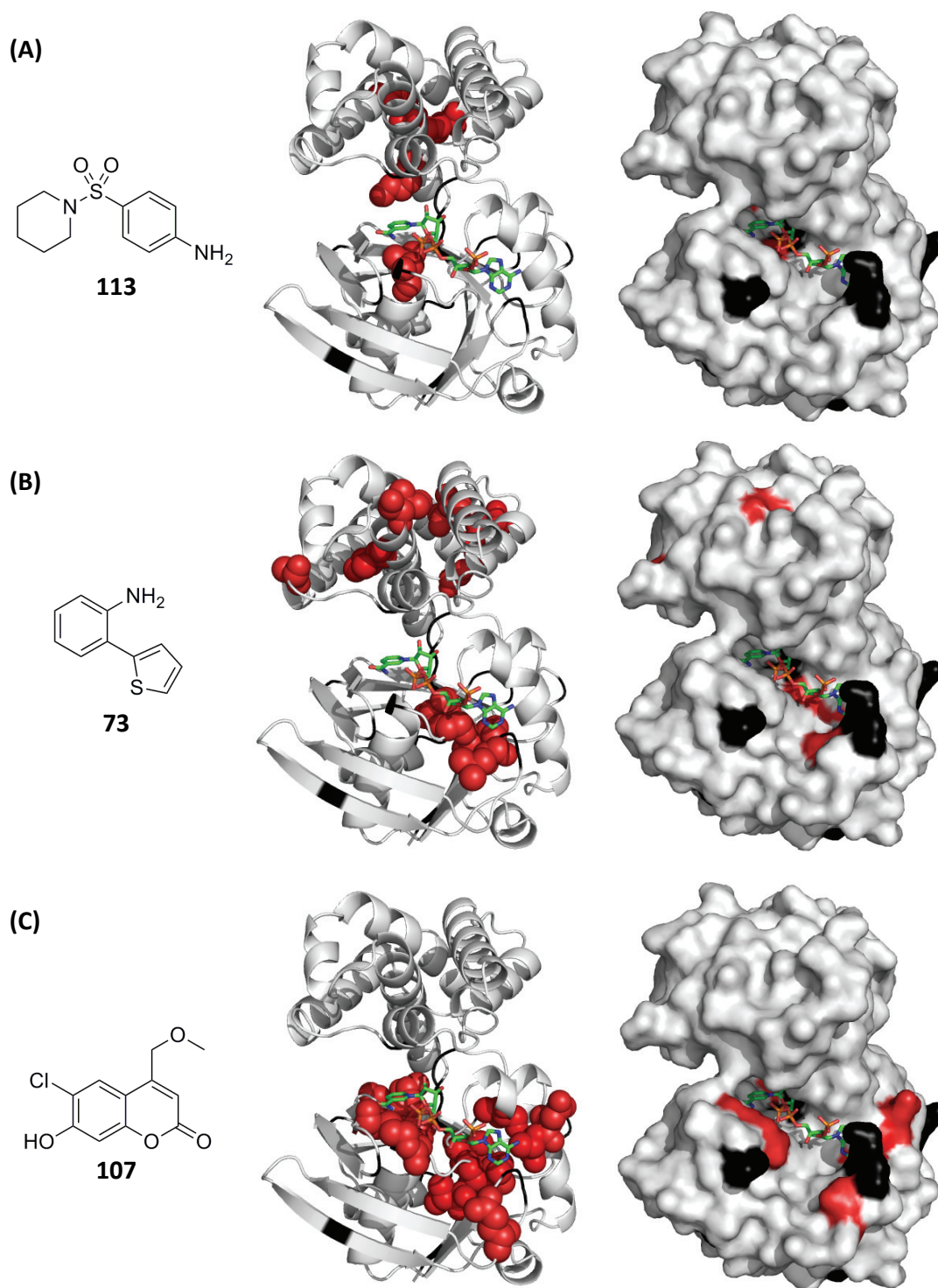


**Figure 2-9.** Residues perturbed on addition of fragments (**113**, **73**, and **107**) were mapped onto the crystal structure (PDB ID: 1YJQ): Ribbon (left) and surface (right) representation of KPR. Perturbations are shown as red spheres. Unassigned residues are coloured black. NADP<sup>+</sup> (**25**) shown as green carbons.

Note: NADP<sup>+</sup> (**25**) was not included in the actual experiment but is included here to help visualise the binding pocket.

## 2.6 Functional assay

STD-NMR and  $^1\text{H}/^{15}\text{N}$ -HSQC NMR identify fragments that bind to KPR. However it is critical to evaluate the hits in terms of their biological activity. A UV-based enzymatic assay was used to assess the ability of the fragments to inhibit KPR activity. The 14 fragments with confirmed binding to KPR (by  $^1\text{H}/^{15}\text{N}$ -HSQC NMR) were assayed for KPR inhibition at 1 mM. The enzymatic assay was carried out as described in Ciulli *et al.*,<sup>42</sup> wherein inhibition activity was determined by monitoring the decrease in absorbance at 340 nm over time due to the enzyme-catalysed oxidation of NADPH to  $\text{NADP}^+$  ( $\epsilon_{340}$  for NADPH =  $6220 \text{ M}^{-1} \text{ cm}^{-1}$ ).

### 2.6.1 Assay development and optimisation

#### 2.6.1.1 NADPH preparation

If an inhibitor competes with the substrate for the same active site of the enzyme, it is deemed to be a competitive inhibitor and its effectiveness is based on its relative concentration to the substrate and the affinity with which it binds to the enzyme. Therefore an accurate substrate concentration is crucial in replicating true inhibition measurements. Since NADPH (**24**) is particularly susceptible to hydrolysis and degradation, the preparation of solutions of known concentrations of NADPH (**24**) was investigated. The NADPH (**24**) concentration was measured using UV absorbance at 340 nm based on the literature extinction coefficient. To confirm the activity of the enzyme and this concentration measurement, the  $K_m$  for NADPH (**24**) was compared to the literature value ( $K_m = 36 \text{ }\mu\text{M}$ ).<sup>90</sup> NADPH (**24**) concentrations 10, 25, 50, 80, 100, 150, 200 and 300  $\mu\text{M}$  were used in the kinetic assay.

The  $K_m$  measurement for NADPH (**24**) using the UV-based method was 28  $\mu\text{M}$  (Figure 2-10), comparable to the literature value.<sup>90</sup> In contrast, when NADPH (**24**) was prepared based on the weighed mass, a 2-fold greater  $K_m$  value was obtained ( $K_m = 54 \mu\text{M}$ ), suggesting that the actual concentration of NADPH (**24**) used was lower than anticipated, due to hydrolysis or the presence of impurities. Therefore by using the UV-based method, the NADPH (**24**) concentration can be measured accurately and consistently for every inhibition measurement.

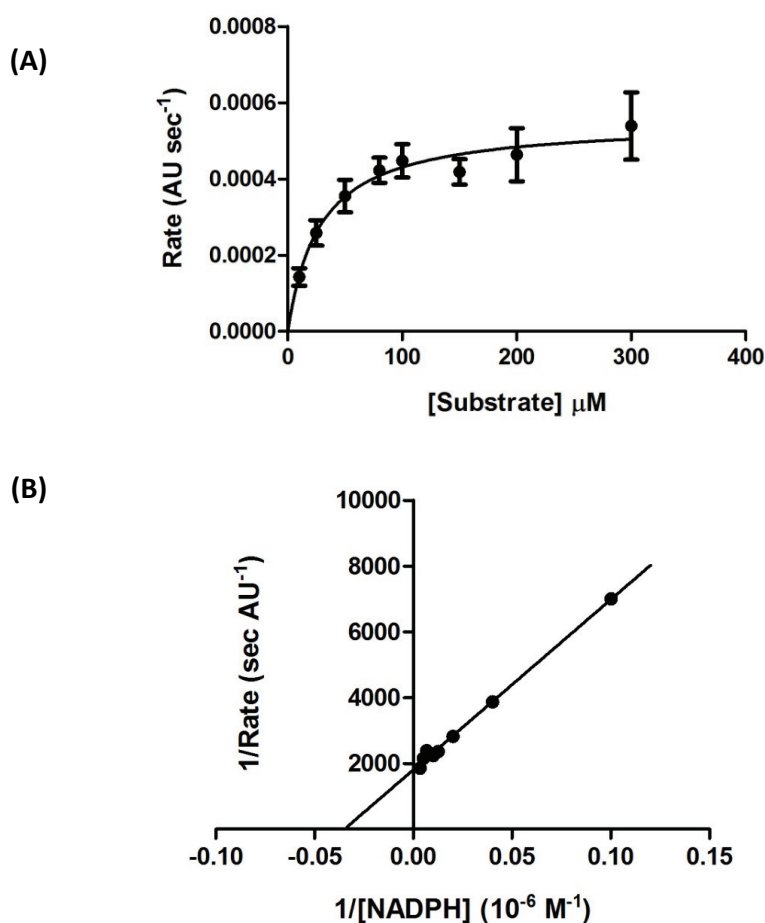


**Figure 2-10.**  $K_m$  determination of NADPH (**24**): (A) Michaelis-Menten plot and (B) Lineweaver-Burk plot.

### 2.6.1.2 KPR concentration

Next, the enzyme concentration was investigated to ensure that the observed activity was proportional to the amount of enzyme present and to select an appropriate enzyme concentration that allowed consistent collection of data in the linear portion of the enzyme reaction. To study the effect of KPR concentrations (1.5, 3 and 6 nM) upon the rate of reaction, the rate was examined in the presence of saturating concentrations of NADPH (300  $\mu$ M) and ketopantoate (1 mM). The results show that the rate is dependent on the enzyme concentration (Figure 2-11). When NADPH (25  $\mu$ M) became the limiting factor in the reaction, KPR concentrations 1.5 nM and 3 nM had longer linearity range in the initial velocity region of the enzymatic reaction (Figure 2-11). However, 3 nM KPR was found most appropriate to allow more reproducible measured rates.

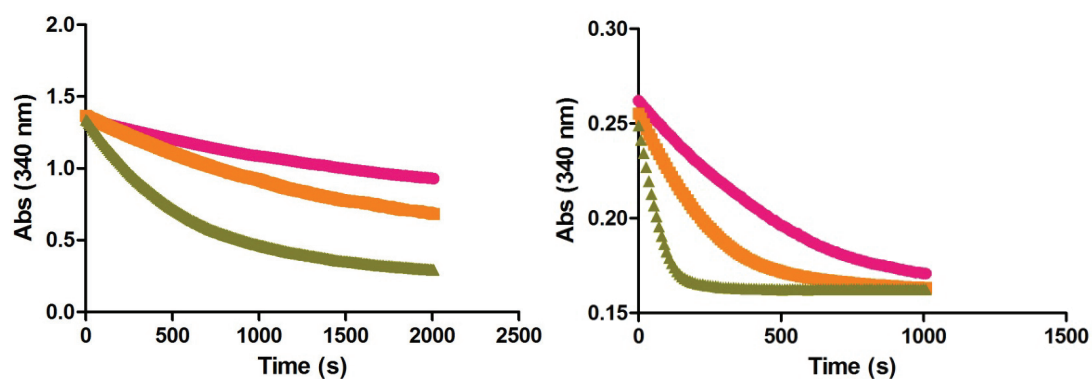


**Figure 2-11.** Effect of KPR concentrations (● 1.5, ■ 3 and ▲ 6 nM): (Left) at saturating NADPH concentration (300  $\mu$ M); (Right) at non-saturating NADPH concentration (25  $\mu$ M).

### 2.6.1.3 Effect of DMSO

All the fragments in the Maybridge library were obtained as solids or oils which were dissolved in neat DMSO to generate concentrated stock solutions. Therefore, it was crucial to determine the tolerance of KPR to DMSO levels and the potential side effects of DMSO in the functional assay. The assay was conducted with increasing concentrations of DMSO (0 – 5%) against KPR (Figure 2-12).

The KPR activity or the turnover rate remained relatively constant and unaffected through the DMSO concentration range tested. Given the flexibility in DMSO concentrations, 2% DMSO was sufficient to solubilise the fragments hence all assays were carried out with a final concentration of 2% DMSO vol/vol.

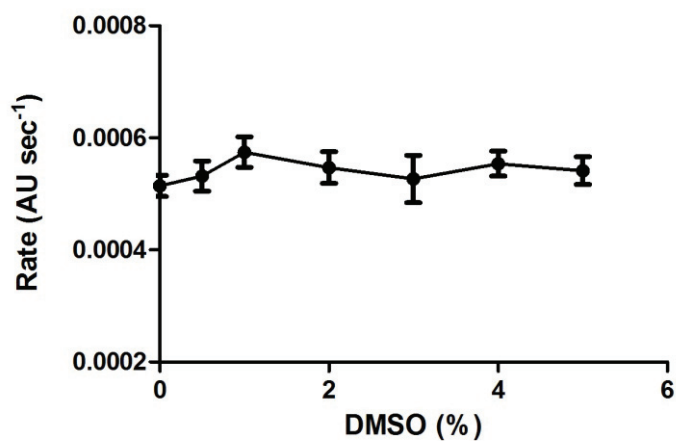


**Figure 2-12.** Effect of increasing DMSO concentration (0 – 5%) on KPR activity

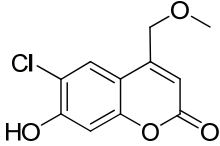
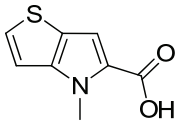
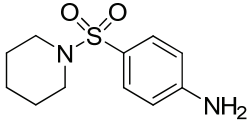
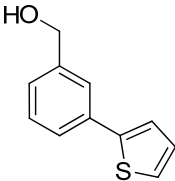
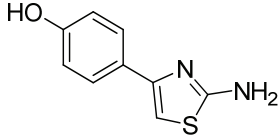
### 2.6.2 KPR inhibition by fragment hits

The 14 fragments identified as hits by perturbations in  $^1\text{H}/^{15}\text{N}$ -HSQC were assayed using the UV-based kinetics assay to determine the fragments' ability to inhibit KPR activity. The fragments were first tested at a final concentration of 1 mM for inhibition activity. The assays were reported as percentage inhibition (%). For fragments that exhibited greater than 50% inhibition, their  $\text{IC}_{50}$  was determined.

The % inhibition at 1 mM suggested that less than half of the 14 fragments were inhibiting at greater than 50% (Table 2-1). Interestingly, thienopyrrole **108**, sulfonamide **113** and phenylthiophene **71** all inhibited at approximately 82%, yet their  $\text{IC}_{50}$  varied quite remarkably (40 – 226  $\mu\text{M}$ ). The inconsistency between the % inhibition and  $\text{IC}_{50}$  value could be the result of solubility, given that the single point was measured at a high concentration. Nevertheless, an  $\text{IC}_{50}$  value from a dose response is a more reliable measurement of inhibition activity.

The assay revealed some exciting results, for example 4 of the 5 fragments selected for further analysis gave an  $\text{IC}_{50}$  value less than 0.5 mM corresponding to high LE (Table 2-1). The thienopyrrole **108** showed significantly greater inhibition with an  $\text{IC}_{50}$  of 40  $\mu\text{M}$  and remarkably high LE of 0.50 kcal/mol per HAC suggesting a large proportion of this molecule is contributing to the overall binding. Despite the difference in  $\text{IC}_{50}$  between the sulfonamide **113**, phenylthiophene **71** and aminothiazole **80**, (65  $\mu\text{M}$ , 226  $\mu\text{M}$  and 416  $\mu\text{M}$ , respectively) their corresponding LE were very similar (0.36 – 0.38 kcal/mol per HAC). This emphasises the usefulness and importance of the LE metric to ensure that the most ligand efficient compounds are selected for progression.

**Table 2-1.** % Inhibition of fragments at 1 mM with corresponding IC<sub>50</sub> and LE values<sup>1</sup>

	Structure	Inhibition (%)	IC <sub>50</sub> (μM)	LE (kcal/mol per HAC)
107		100*	-	-
108		83	40	0.50
113		82	65	0.36
71		82	226	0.38
80		56	416	0.36

\* A curve could not be fitted due to limited solubility above 250 μM preventing a reliable IC<sub>50</sub> determination.

<sup>1</sup> The data shown were analysed by standard KPR assay conditions: NADPH (**24**, 20 μM), ketopantoate (**22**, 1 mM), and KPR (3 nM) in 100 mM HEPES buffer (pH 7.6) with 2% DMSO (vol/vol).

## 2.7 Computational modelling

Knowledge of the fragment's binding mode may be critical for compound elaboration and optimisation; in the absence of experimental structural information, computational methods may be used. Docking is a computational technique that predicts a ligand's binding mode and estimates affinity relative to the receptor target. However, *in silico* selection of compounds that bind to a protein active site is difficult.<sup>176</sup> Commonly, the docking accuracy in predicting a ligand pose is based by comparison to an available experimental structure. A predicted ligand pose with a root-mean-square distance (RMSD) of  $< 2\text{\AA}$  to the experimental structure is considered reasonable.<sup>177</sup> Efforts are constantly being made to increase the accuracy of docking; for example, Gonzalez-Ruiz and Gohlke<sup>178</sup> have applied CSPs from NMR studies to score ligand poses with respect to their agreement with experimental CSP data.

Herein, the ability of docking to reproduce the experimentally determined binding mode for the target KPR is described. The effects of conserved water molecules on docking accuracy were examined. Validation of the predicted binding modes would provide confidence in the docking accuracy and later provide a basis for inhibitor design using the predicted binding modes. This could greatly enhance productivity and potentially reduce developmental costs.

### 2.7.1 Analysis of water molecules in the binding site

A visual inspection of 4 crystal structures of KPR (Table 2-2) was performed to identify water molecules that participate in water-mediated hydrogen bonds between the protein and the ligand. LIGPLOT<sup>95</sup> was used for 2D analysis to identify these waters and then all the crystal structures were superimposed to determine whether these water molecules were also in the same position in the binding site across all the structures including *apo*-KPR (Table 2-2).

Only H<sub>2</sub>O-1 appeared to be consistent both structurally and functionally among all the KPR crystal structures (refer to Chapter 1, Figure 1-5). In the *holo*- and ternary complex of KPR, H<sub>2</sub>O-1 was found bridging NADP<sup>+</sup> (**25**) with the well-known glycine-rich phosphate-binding loop. It formed hydrogen bonds to the dinucleotide pyrophosphate, two of the three conserved glycine residues of the phosphate-binding loop, and Thr70. This water molecule is also present in the high-resolution structure of *apo*-KPR. This is important since water molecules can sometimes be artefacts of the crystallographic refinement process.<sup>179-180</sup>

**Table 2-2.** Water molecules involved in hydrogen bond bridging between the protein and NADP<sup>+</sup> (**25**) or 2'P-ADP-ribose (**41**)

PDB codes	H <sub>2</sub> O-1	H <sub>2</sub> O-2	H <sub>2</sub> O-3	H <sub>2</sub> O-4
<b>1YON</b> - KPR-2'P-ADP-ribose complex (1.7 Å)	✓	-	-	✓
<b>2OFP</b> - KPR-NADP <sup>+</sup> -Pantoate complex (2.3 Å)	✓	✓	✓	✓*
<b>1YJQ</b> - <i>holo</i> -KPR (2.1 Å)	✓	✓	✓	✓*
<b>1KS9</b> - <i>apo</i> -KPR (1.7 Å)	✓	-	✓	-

Refer to Chapter 1 (Figure 1-5), for the 2D representation of the water-mediated hydrogen bonds between the protein and the ligand. '-' indicates that the water molecule was not observed. '\*' indicates that the water was not in the exact location, it was approximately 1 Å away.

### 2.7.2 Docking NADP<sup>+</sup> and analogues

Ciulli *et al.*<sup>42</sup> used a fragment-based approach to probe hot spots at the cofactor-binding site of KPR. NADPH (**24**) and smaller fragments and analogues (Figure 2-13) were used in their experiment. For our purpose, the same ligands were used and compared to the experimental findings of Ciulli *et al.*<sup>42</sup> NADP<sup>+</sup> (**25**) and analogues were docked into the cofactor binding site of KPR using Glide.<sup>181</sup> Both Glide standard-precision (SP) and extra-precision (XP) mode were examined (refer to section 7.1.6.4 Glide docking for a description of SP and XP). The effect of the presence and absence of the identified conserved water molecule was investigated. The binding modes of docked structures were evaluated by superimposing them on to crystal structures of KPR with NADP<sup>+</sup> (**25**) and/or 2'P-ADP-ribose (**41**) (PDB ID: 1YJQ and 1YON, respectively).

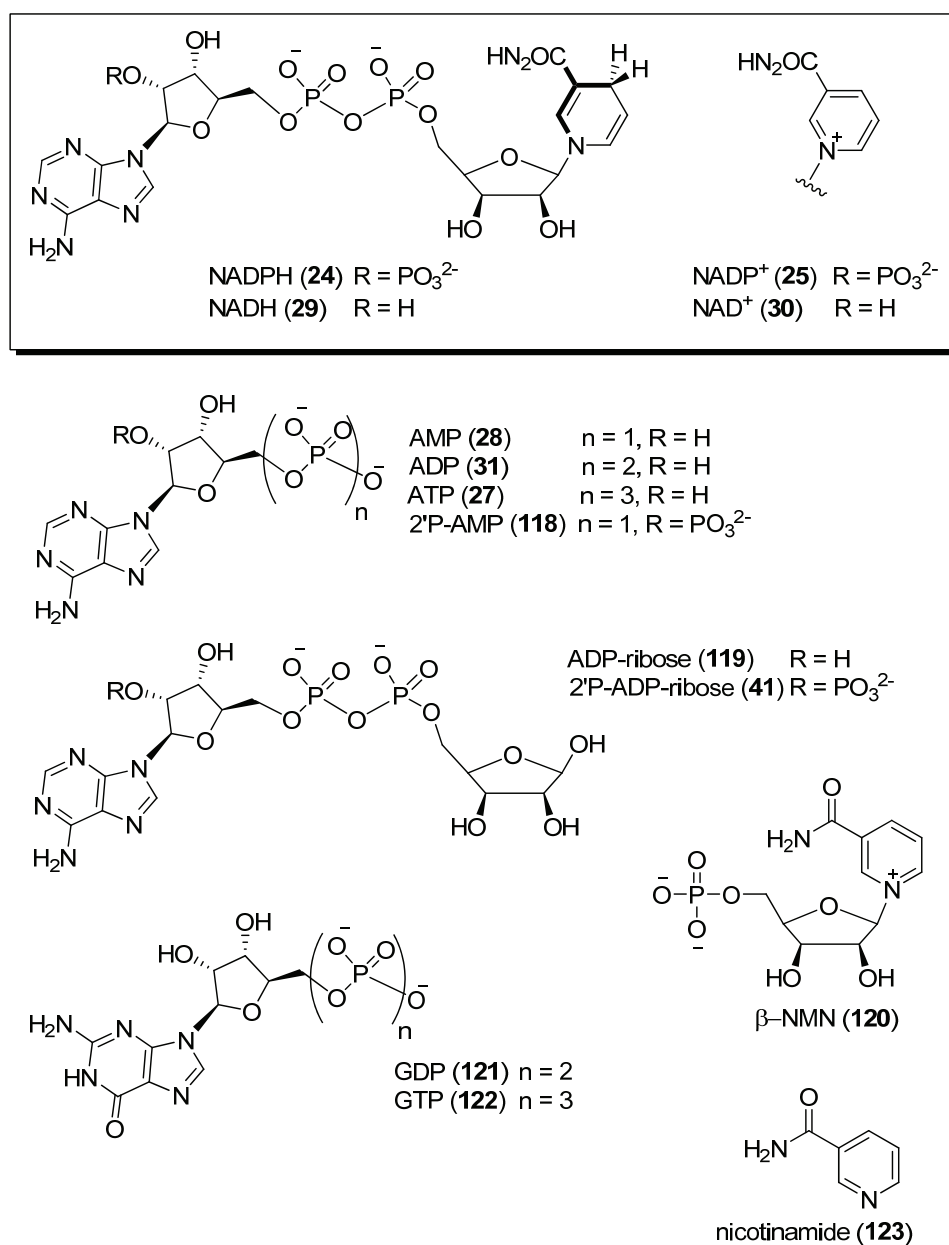


**Figure 2-13.** Chemical structures of NADP<sup>+</sup> (**25**) and analogues. Figure adapted from Ciulli *et al.*<sup>42</sup>

Docking in XP mode generally provided a lower RMSD between the docking solution and the experimental binding mode. In the XP mode, the cofactor NADP<sup>+</sup> (**25**) docked in the presence of the conserved water (H<sub>2</sub>O-1) superimposed with the crystal structure (*holo*-KPR, PDB ID: 1YJQ) giving an RMSD of 1.7 Å compared to 2.6 Å (for SP mode). This was also observed for the cofactor docked in the absence of the water,

where the XP mode gave a better RMSD value than SP mode (3.6 Å and 5.8 Å, respectively).

The conformation (*apo*, *holo* and modelled structure) of 10 different enzymes were studied in docking screens involving a library of 95,000 small molecules.<sup>182</sup> Since the library contained at least 35 ligands (known actives) for each of the 10 enzymes, they were used to assess the ability of each enzyme structure to enrich the known active ligands over random selection. The docking screens revealed that the *holo*-form gave the best results (70% enrichment), followed by *apo* (20%) and finally the modelled form (10%).<sup>182-183</sup> For this reason, the crystal structure of the *holo*-form (PDB ID: 1YJQ) was used in the docking experiments.

For most of the NADP<sup>+</sup> (**25**) analogues, the conserved water (H<sub>2</sub>O-1) helped maintain the ligands in an extended conformation in the binding site. The interactions observed for the docked NADP<sup>+</sup> (**25**) were consistent with the crystal structure (Figure 2-14A). In the presence of the conserved water, docked NADPH (**24**), NADP<sup>+</sup> (**25**), NADH (**29**), 2'P-ADP-ribose (**41**), 2'P-AMP (**118**), ADP-ribose (**119**), and  $\beta$ -NMN (**120**) hydrogen bonded to the water molecule (Figure 2-14B – C), giving conformations relatively consistent with the crystal structure of NADP<sup>+</sup> (**25**). The docked ligands ATP (**27**), AMP (**28**), GDP (**121**) and GTP (**122**) which all lack the nicotinamide-ribose moiety of NADP<sup>+</sup> (**25**) were found to be bound at the enzyme active site in the opposite orientation to that observed for NADP<sup>+</sup> (**25**). Their purine ring was occupying the lipophilic nicotinamide pocket (Chapter 1). This reversed binding mode has been reported for the crystal structure complex KPR-2'P-ADP-ribose, however under acidic conditions

(pH 4.0 – 5.0).<sup>94</sup> The nicotinamide (**123**) on its own showed no specificity for the binding site as several different orientations were observed.

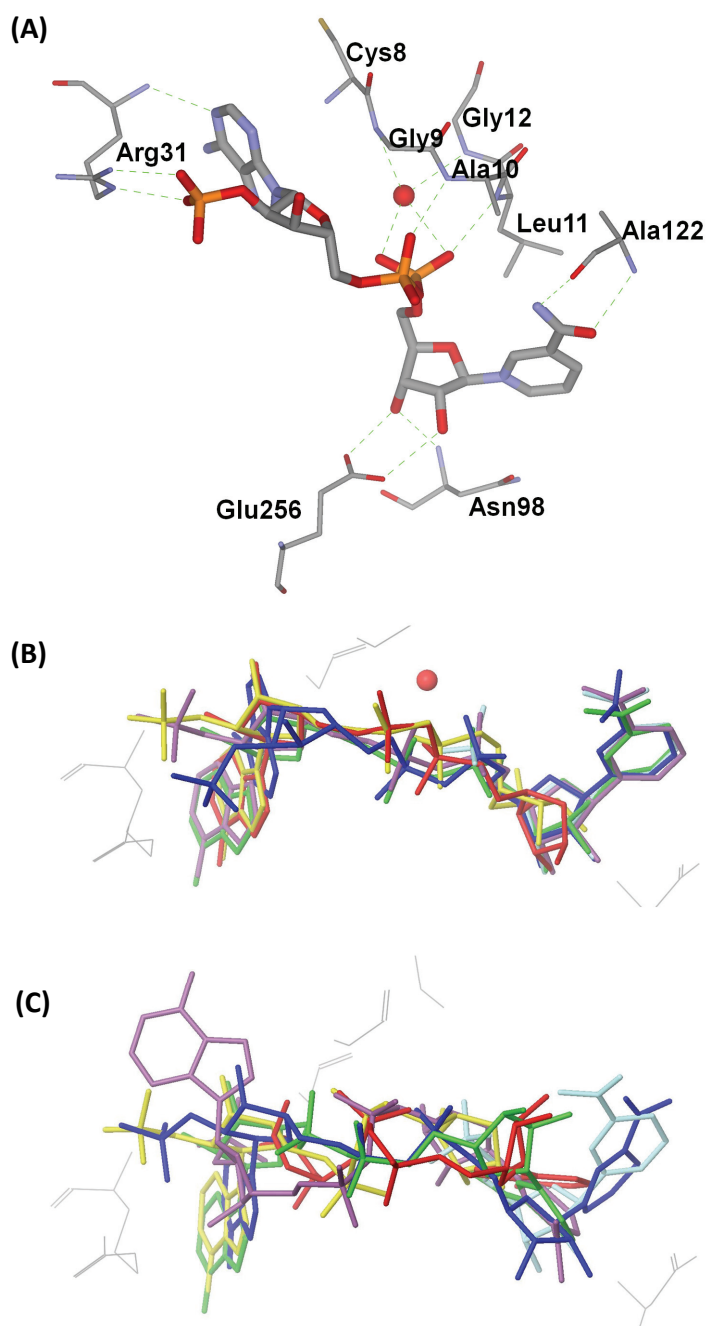


**Figure 2-14.** (A) Hydrogen bonding interaction between the cofactor, conserved water and KPR in docked solution. (B). Overlay of the docked ligands (XP mode) NADPH (**24**), NADP<sup>+</sup> (**25**), 2'P-ADP-ribose (**41**), NADH (**29**), 2'P-AMP (**118**), ADP-ribose (**119**) and  $\beta$ -NMN (**120**). The conserved water molecule is rendered in CPK, coloured in red. (C). Same as (B) however, docking was carried out in the absence of the conserved water.

The study by Ciulli *et al.*<sup>42</sup> identified the 2'-phosphate and 1,4-dihyronicotinamide ring as the most ligand efficient groups, as their incorporation (e.g. AMP to 2'-P-AMP) led to large increases in affinity and consequently LE. The 2'-phosphate group of NADP<sup>+</sup> (**25**) is involved in two hydrogen-bond interactions with Arg31. To identify the binding mode of fragments containing the 2'-phosphate group, 2'-P-AMP (**118**) and 2'-P-ADP-ribose (**41**) were studied in KPR where Arg31 was mutated to Ala. The binding affinity decreased by 30 – 60 fold suggesting that these fragments adopt the same binding mode as NADP<sup>+</sup> (**25**).

In our study, the docking of analogues containing the 2'-phosphate group in the presence of the conserved water in either SP or XP mode showed the 2'-phosphate group of 2'-P-AMP (**118**) and 2'-P-ADP-ribose (**41**) forming a hydrogen-bond interaction with Arg31 and also adopting the same binding mode as NADP<sup>+</sup> (**25**) (Table 2-3). Verdonk *et al.*<sup>184</sup> have demonstrated that compounds with high LE (> 0.4 kcal/mol per HAC) were docked with greater success than those with lower LE. They proposed that compounds with high LE form high-quality interactions with the target, which may be easier to detect in docking through scoring functions. The correct binding mode predicted by docking may be related to molecules containing the 2'-phosphate group being ligand efficient. The reasonable docking results of the NADP<sup>+</sup>-like analogues warranted an attempt at fragment docking.

**Table 2-3.** The conformation and/or orientation of the docked NADP<sup>+</sup>-like analogues: Visual analysis was performed with the crystal structure of NADP<sup>+</sup> (**25**) superimposed.

<b>Fragments</b>	<b>*H<sub>2</sub>O (SP)</b>	<b>*H<sub>2</sub>O (XP)</b>	<b>w/o-H<sub>2</sub>O (SP)</b>	<b>w/o-H<sub>2</sub>O (XP)</b>
NADPH ( <b>24</b> )	✓	✓	✓	✓ D
NADP <sup>+</sup> ( <b>25</b> )	✓	✓	✓ D	✓ D
NADH ( <b>29</b> )	✓	✓	✓	C
2'P-ADP-ribose ( <b>41</b> )	✓	✓	✓	✓
2'P-AMP ( <b>118</b> )	✓	✓	A	A
ADP-ribose ( <b>119</b> )	✓	✓	B, D	✓ D
AMP ( <b>28</b> )	B	B, C	B	B
ADP ( <b>31</b> )	A	B	B	B
ATP ( <b>27</b> )	B	B	B	B
β-NMN ( <b>120</b> )	✓	✓	✓	✓
GDP ( <b>121</b> )	B	B, C	B, C	B, C
GTP ( <b>122</b> )	B	C	B	B
Nicotinamide ( <b>123</b> )	A	A	A	A

\*' denotes with H<sub>2</sub>O and 'w/o' denotes without H<sub>2</sub>O.

- ✓ Ligand in the cofactor binding site and adopting the same orientation as the crystal structure NADP<sup>+</sup> (**25**) in the binding site
- A. Non-specific orientation
- B. Purine group in the nicotinamide pocket
- C. Folded conformation
- D. Substituent has slightly different orientation to NADP<sup>+</sup> (**25**)

### 2.7.3 Fragment docking

The  $^1\text{H}/^{15}\text{N}$ -HSQC validated fragment hits were docked against KPR using the XP docking mode with the inclusion of the conserved water molecule. The importance of this study was to analyse whether the docked poses were consistent with the NMR perturbations. Docking of thienopyrrole **108** and sulfonamide **113** suggested that both fragments bound in the same pocket as the nicotinamide substituent of  $\text{NADP}^+$  (**25**). However, the NMR CSP maps and the docking solutions for both the thienopyrrole **108** and sulfonamide **113** were not in agreement. Similarly, the docked binding locations of phenylthiophene **71** and thiophenylaniline **73** were not in agreement with the NMR CSP map (Figure 2-15A). The coumarin **107** and aminothiazole **80** docked in the cavity that the adenine portion of the cofactor occupies (Figure 2-15B – C). The docking solutions of **107** and **80** were in agreement with the NMR CSPs. Superposition shows the benzene portion of **107** and **80** overlapping with the pyrimidine of  $\text{NADP}^+$  (**25**). The two fragments also shared a common hydrogen bond interaction to Cys8 in the glycine-rich region. The NMR mapping data for coumarin **107** illustrated perturbation occurring across the binding cavity of KPR. This suggests either coumarin **107** can bind in two different sites or a single binding event has caused adjacent residues to be affected. Interestingly, the docking result fits with the former idea suggesting coumarin **107** may bind in two different sites. Additionally, the predicted binding sites from docking overlaid well to the NMR perturbation map. However, given that the docking data was consistent with the experimental information in only 2 out of 6 cases, sufficiently reliable docking results for a range of fragments and analogues seemed unlikely. As such, the predictive value of docking was too limited and so not used in further analyses.

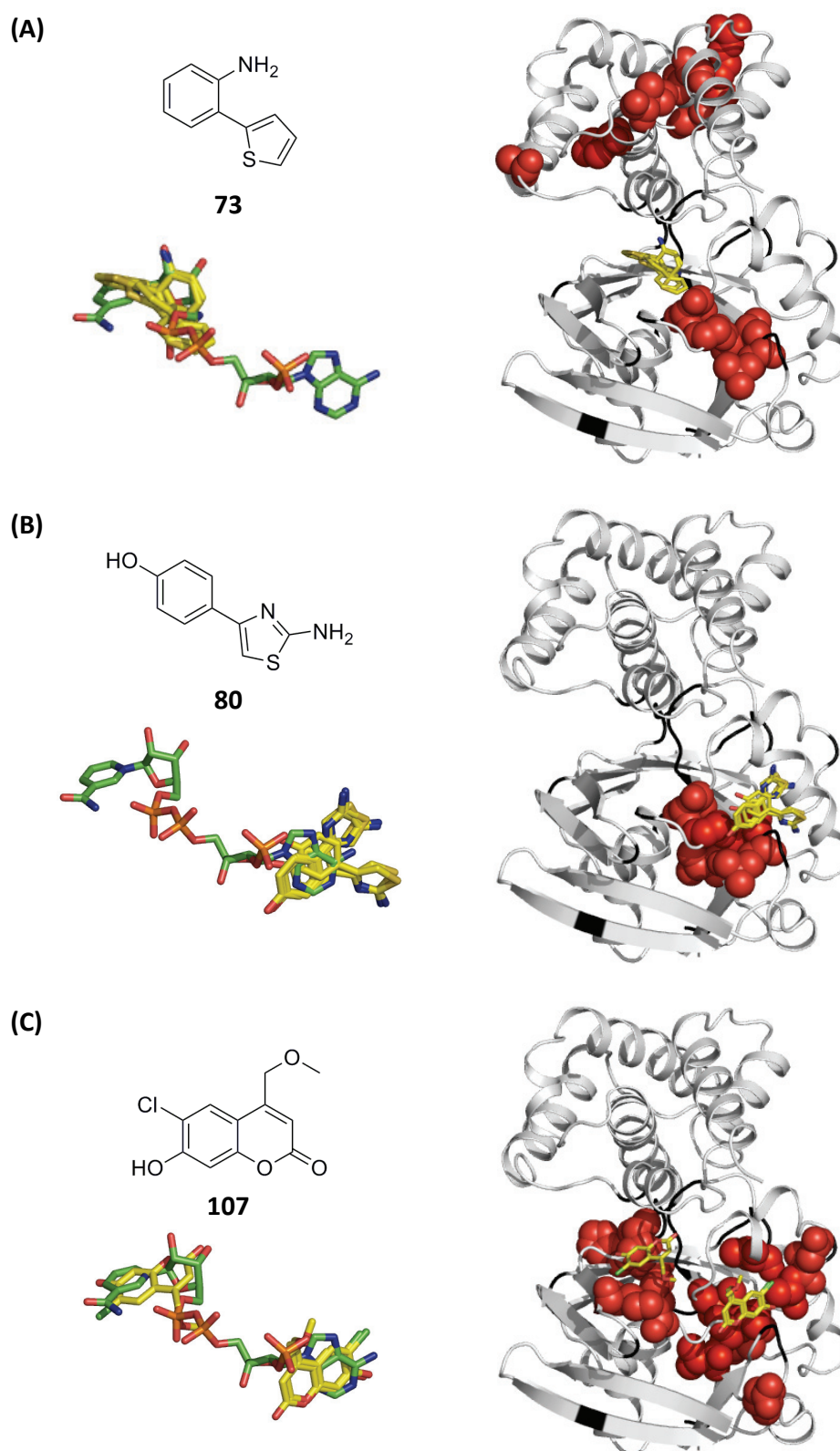


**Figure 2-15.** Superposition of docking solution to  $^1\text{H}/^{15}\text{N}$ -HSQC NMR mapped CSPs: (Left) Overlay of the fragment docking solution to  $\text{NADP}^+$  (**25**). Fragments shown as yellow carbons and  $\text{NADP}^+$  (**25**) shown as green carbons. (Right) The perturbed residues were mapped onto the *holo*-KPR crystal structure (PDB ID: 1YJQ). Ribbon representation of KPR with perturbations ( $> 0.03$  ppm) shown as red spheres. Unassigned residues are coloured black. Docked fragments shown as yellow carbons.

## 2.8 Conclusions

A protocol has been developed to express high levels of KPR and  $^{15}\text{N}$  KPR which is important for many steps involved in the fragment-based approach. A primary screen of 500 fragments by STD-NMR found 47 hits and their binding was validated in the subsequent step involving  $^1\text{H}/^{15}\text{N}$ -HSQC. The resultant 14 fragment binders of KPR were subsequently evaluated by UV-Vis based assay to inhibit KPR activity. The thienopyrrole **108** was the most active fragment found with an  $\text{IC}_{50}$  of 40  $\mu\text{M}$  and was shown to bind in the active site of KPR by NMR methods. A total of 4 fragments were found to have  $\text{IC}_{50} < 500 \mu\text{M}$ . These ligands represent novel starting points for fragment-based design of KPR inhibitors.

Glide docking with the XP mode was better than the SP mode in providing smaller RMSDs between the docked solutions to the crystal structure. Docking with the conserved water and docking of larger ligands also gave more accurate results. In this study, the NMR and docking data did not agree well, i.e. the predicted fragment binding site from docking often did not correlate with the  $^1\text{H}/^{15}\text{N}$ -HSQC suggested binding location. Therefore, docking for KPR may not be reliable in predicting the binding mode for fragments.

A combination of experimental data was used to guide the fragment selection for further development. From the top 5 fragments, which not only bind to but also inhibit KPR, the sulfonamide **113**, thienopyrrole **108** and phenylthiophene **71** fragment hits were selected for further investigation, which is detailed in Chapter 3.

# Chapter 3

---

## SAR development of fragment hits

## 3 SAR development of fragment hits

### 3.1 Introduction

There are three important factors to consider when selecting hits for follow-up. Firstly, LE measures the quality of binding interactions between the fragment and target protein. LE values above 0.3 kcal/mol per HAC are desirable through the process of optimisation (1 kcal  $\approx$  4.184 kJ).<sup>162</sup> Secondly, the tractability for synthetic elaboration and derivatisation of the fragment hits to characterise and/or enhance binding is considered. Finally, the novelty of the chemical scaffold is also important, particularly if the target has been extensively studied by other groups.

Once the fragment hits have been identified and prioritised, preliminary SAR may be quickly progressed by testing simple analogues of the initial hit from readily available commercial suppliers or internal fragment collections. This SAR is then used to direct synthesis of larger molecules to optimise binding to adjacent regions of the active site and improve the potency. Ideally, the design and elaboration of hits is also guided by the binding modes from X-ray crystallography and/or <sup>1</sup>H/<sup>15</sup>N-HSQC NMR. Careful consideration in selecting hits for follow-up, SAR interpretation and binding site or binding mode evaluation is critical for successful fragment optimisation.

In Chapter 2, the use of NMR methods identified 14 fragments bound to KPR from a library of 500 fragments correlating to a hit rate of 3%. Of those 14 hits, a total of 4 fragments have IC<sub>50</sub> < 500  $\mu$ M and LE values > 0.35 kcal/mol per HAC. This chapter describes the hit development for selected fragments sulfonamide **113**, thienopyrrole **108** and phenylthiophene **71** shown in Figure 3-1. Initial SAR was obtained by testing

analogues from readily available external and/or internal sources. An iterative process was adopted, compounds were synthesised, their potency and LE tracked and elaboration was done incrementally. The binding location of these fragments on KPR was evaluated by  $^1\text{H}/^{15}\text{N}$ -HSQC NMR.

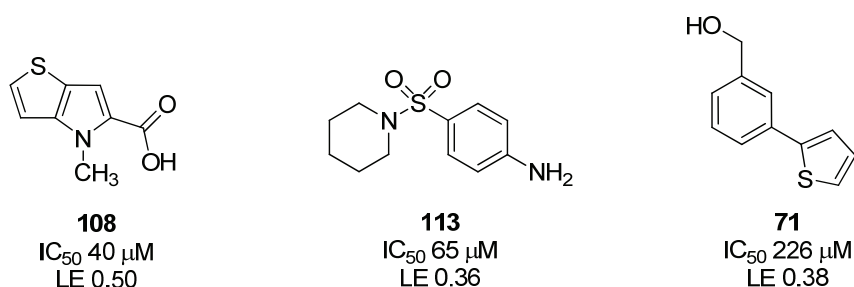


**Figure 3-1.** Selected fragment hits taken for further development.

### 3.2 Sulfonamides

The first fragment investigated in hit development was 4-(piperidin-1-ylsulfonyl)aniline (**113**). With reasonable inhibitory activity ( $\text{IC}_{50}$  65  $\mu\text{M}$ ) and LE (0.36 kcal/mol per HAC), the sulfonamide was a good starting point to develop more potent inhibitors against KPR. Compared to other fragment hits, the sulfonamide was not the most potent or ligand efficient, however, the internal fragment collection and availability of close structural analogues from commercial suppliers allowed quick access to preliminary SAR. Additionally, the ease of synthesis afforded further analogues to investigate the binding of the sulfonamides to KPR.

### 3.2.1 Mode of inhibition

The mode of inhibition by the sulfonamide **113** against KPR activity was examined. The assay was carried out on a 96-well plate in which the sulfonamide **113** was tested at final concentrations of 5, 25, 50 and 100  $\mu\text{M}$  in the reaction containing NADPH (**24**, 5 – 100  $\mu\text{M}$ ), ketopantoate (**22**, 1 mM), and KPR (3 nM) in 100 mM HEPES buffer (pH 7.6) with 2% DMSO (vol/vol). The data were fitted to a one site competition model from GraphPad Prism. The Lineweaver-Burk plot (Figure 3-2) shows data points at different inhibitor concentrations converge at the Y-axis, indicating that the sulfonamide **113** is competitive against NADPH (**24**) with  $K_i$  value of 33  $\mu\text{M}$ .

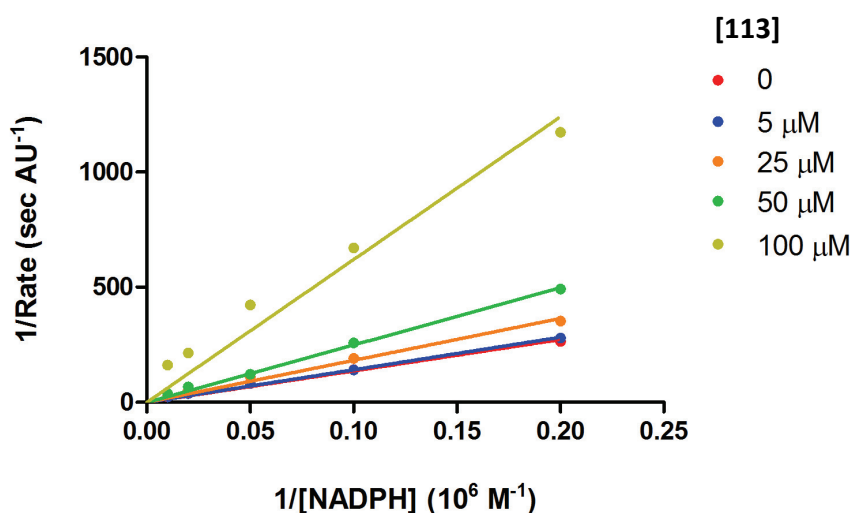
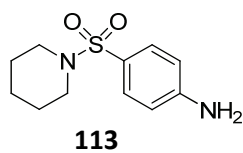


**Figure 3-2.** Inhibition analysis (plotted in double reciprocal form): NADPH (**24**) titration of steady state velocity for KPR in the presence of sulfonamide **113** at varying concentrations.  $K_i$  of 33  $\mu\text{M}$  was obtained.

### 3.2.2 Preliminary SAR

Among the 14 fragment hits, the sulfonamide scaffold is distinctive as all the other scaffolds were made up of either two aryl rings connected by one rotatable bond or fused bicyclic structures. Notably, the sulfonamides were the first truly effective antimicrobial agent that targeted the folate pathway and inhibited the formation of specific DNA bases (discussed in Chapter 1).<sup>22-23</sup>

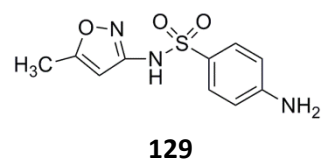
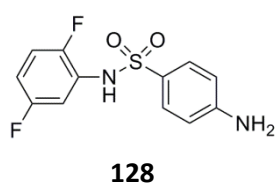
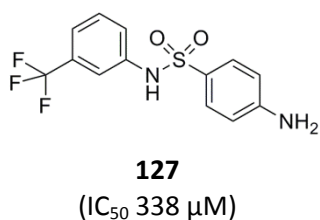
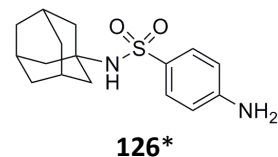
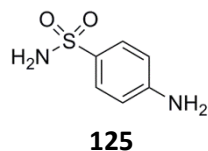
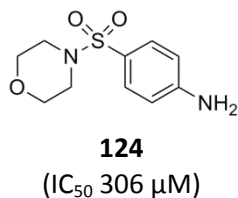
Given that the sulfonamide **113** showed good potency and competitive inhibition, close structural analogues were investigated. To begin with, 17 sulfonamide analogues (**124** – **140**) from commercial suppliers were selected by employing a similarity search with a threshold of 0.7 (where 0 is completely dissimilar and 1 is identical).<sup>185</sup> Four compounds (**124**, **125**, **135** and **138** shown in Figure 3-3) were selected from the internal fragment collection while thirteen were purchased. There were 6 analogues which had variations at the piperidine portion while the rest of the molecule was kept constant, 8 analogues had variations at the aniline portion while the rest of the molecule was kept constant and 3 analogues had variations at both ends of the sulfonamide (Figure 3-3). The sulfonamide analogues were tested at a final concentration of either 300 or 500  $\mu\text{M}$  (depending on solubility) for KPR inhibition and the assays were reported as percentage inhibition (%). Compounds that exhibited greater than 30% inhibition against KPR were tested for  $\text{IC}_{50}$ .




---

**Variation at the piperidine portion**

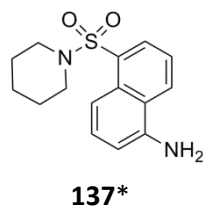
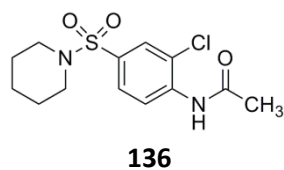
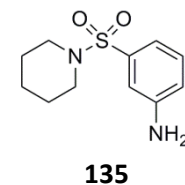
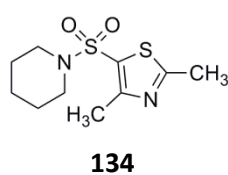
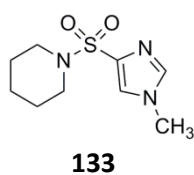
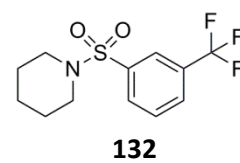
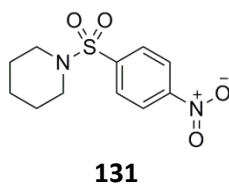
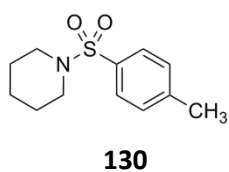

---




---

**Variation at the aniline portion**


---




---

**Variation of both substituents**


---

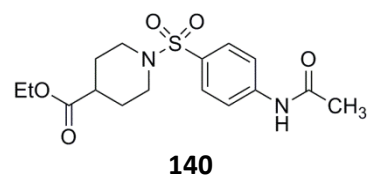
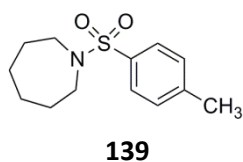
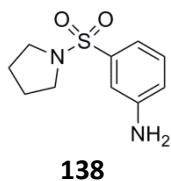


**Figure 3-3.** Sulfonamide analogues obtained from internal library or purchased: ‘\*’ Indicates inhibitory activity could not be measured due to low compound solubility.

One of the greatest challenges associated with the sulfonamide analogues were their limited solubilities. To begin with, we attempted to test the analogues at 500  $\mu\text{M}$  in the % inhibition assay. However, more than half of the compounds showed limited solubility and as a result, were tested at a lower concentration (300  $\mu\text{M}$ ). Particularly, for the adamantyl derivative **126** and the naphthyl derivative **137** the limited solubility at 300  $\mu\text{M}$  prevented their inhibitory activity from being measured.

Surprisingly, only two sulfonamide analogues displayed KPR inhibition greater than 30% at either 300  $\mu\text{M}$  or 500  $\mu\text{M}$  (Appendix I). These were the morpholino derivative **124** with 85% inhibition at 500  $\mu\text{M}$  and (trifluoromethyl)phenyl derivative **127** with 43% inhibition at 300  $\mu\text{M}$ . Interestingly, the analogues containing the acetamide moiety (**136** and **140**) appeared to increase the rate of turnover. The catalytic turnover rate of KPR was enhanced by approximately 45% in the presence of these acetamides at 300  $\mu\text{M}$ . Small molecule activators of enzymes are well reported. For example, recent studies include discovering a glucokinase activator as a clinical candidate for the treatment of type 2 diabetes mellitus and another on histone deacetylase activators.<sup>186-187</sup> Both studies have suggested small molecule activators bind to an allosteric site on the enzyme and alter the enzyme's kinetic profile. In addition to increasing the catalytic turnover rate of the enzyme, another feature of activators includes an observed decrease in the  $K_m$  value of the enzymes substrate.<sup>186-187</sup> However, in the interest of focussing on KPR inhibitors no further studies were carried out.

For the morpholino derivative **124** and (trifluoromethyl)phenyl derivative **127** with KPR inhibition > 30%, the  $\text{IC}_{50}$  was determined to be 306  $\mu\text{M}$  and 338  $\mu\text{M}$ , respectively. Although these sulfonamide analogues are less potent than the initial sulfonamide hit

(**113**, IC<sub>50</sub> 65 μM), they suggest that the piperidine portion is amenable to changes while the aniline substituent is critical for activity. Small changes such as replacing the aniline with a toluene derivative abolished inhibitory activity suggesting the presence of important hydrogen-bond interactions. Moreover, changing the position of the aniline from *para* to *meta* also eliminated inhibitory activity suggesting the amino group is positioned for optimal hydrogen-bond interaction.

### 3.2.3 Chemical shift mapping

The series of sulfonamide analogues studied in the preliminary SAR were analysed using <sup>1</sup>H/<sup>15</sup>N-HSQC NMR to characterise their binding, in the same manner as described in chapter 2 section 2.5. Residues that experience the greatest changes in chemical shift were mapped onto the crystal structure of KPR (PDB ID: 1YJQ).<sup>91</sup>

Binding analysis is straightforward when the CSP map is consistent across a compound series. This allows the effects of structural modifications of the ligand on binding be monitored and used to guide the design for subsequent analogues. The lead fragment **113** showed modest perturbations at the nicotinamide portion of the NADPH binding site, but did not share common perturbation patterns with its analogues (**124** and **138** shown as an example in Figure 3-4). A simple replacement of the piperidine for morpholine ring **124** or the aniline substitution from *para* to *meta* (**135**, Figure 3-5) presented such different CSP maps. In fact, the affected residues from analogues **124** and **138** did not form clear clusters on the surface making it difficult to assign a likely binding location (Figure 3-4).

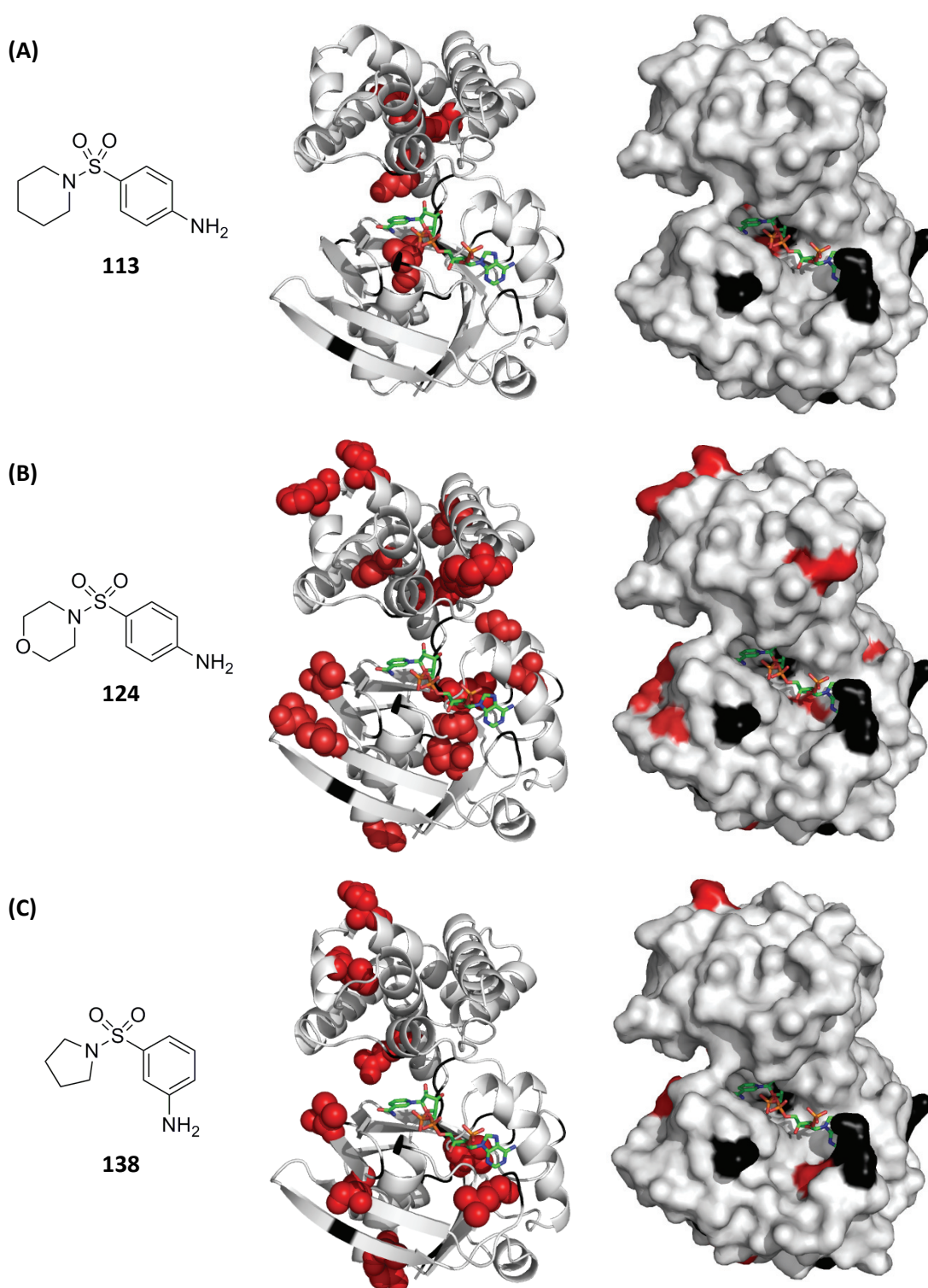


**Figure 3-4.** The residues that were perturbed on addition of (A) **113**, (B) **124** and (C) **138** were mapped onto the crystal structure (PDB ID: 1YJQ): Ribbon (left) and surface (right) representation of KPR. Perturbations ( $\Delta\delta > 0.03$  ppm) are shown as red spheres. Unassigned residues are coloured black. NADP<sup>+</sup> shown as green carbons.

Note: NADP<sup>+</sup> was not included in the actual experiment but is included here to help visualise the binding pocket.

### 3.2.4 3-(Piperidin-1-ylsulfonyl)aniline

The most striking perturbation map was observed for 3-(piperidin-1-ylsulfonyl)aniline (**135**). Changing the aniline substitution from *para* to *meta* not only revealed that the two compounds (**113** and **135**) bind at different sites on KPR, but the measured amide shifts were significantly stronger for the *meta* substituted analogue. Compared to other analogues in the sulfonamide series, the magnitude of the largest chemical shifts on addition of the *m*-aniline analogue **135** were up to 10-fold more intense. Typically a strong weighted amide shift is approximately  $\Delta\delta$  0.04 ppm. However, the *m*-aniline analogue **135** was demonstrating amide shifts of almost  $\Delta\delta$  0.2 ppm. The CSPs were localised in or close to the pantoate-binding pocket, which is approximately 6.5 Å from NADP<sup>+</sup> (Figure 3-5).<sup>92</sup> A close inspection of the affected residues revealed that the perturbed residues do not correspond to the pantoate-binding pocket. The binding characteristics of pantoate have not been studied by 2D NMR, however, based on biochemical studies<sup>92</sup> discussed in chapter 1 section 1.3, important residues in this pocket (Thr119, Val179, Ile183, Val234 and Thr238, while Ile96 – Gly99, and Ser244 have not been assigned) were largely unaffected. Instead the perturbed residues on the addition of the *m*-aniline analogue **135** clustered along the hinge region (residues 169 – 176) and above the pantoate pocket with considerable perturbations observed for residues 203 – 233 (Figure 3-5, see graph of weighted amide shifts vs. residue number for KPR). To date, there are only two known binding sites on KPR which belong to the substrate and cofactor.<sup>42,92</sup> Therefore, the information from <sup>1</sup>H/<sup>15</sup>N-HSQC NMR suggests **135** may be bound at a previously unreported binding site on KPR. Kinetic studies were employed to understand the interactions between the *m*-aniline analogue **135** and KPR.

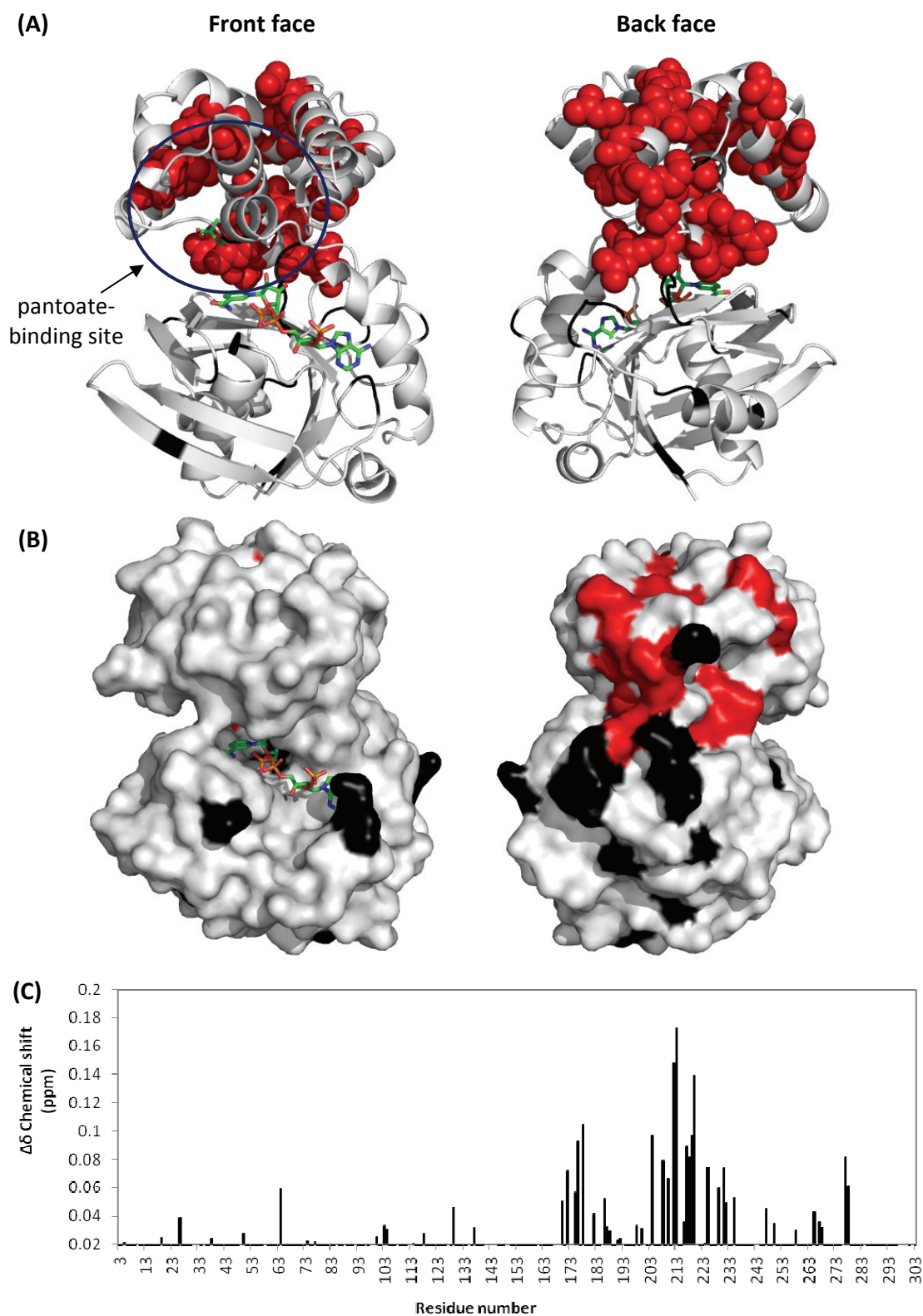


**Figure 3-5.** Induced CSPs on the addition of **135** mapped onto the crystal structure (PDB ID: 2OFP): (A) Ribbon and (B) surface representation of KPR. Strongly perturbed residues ( $\Delta\delta > 0.05$  ppm) are shown as red spheres. Unassigned residues are coloured black. NADP<sup>+</sup> and pantoate are shown as green carbons. (C) Plot of weighted average chemical shift change vs. residue number for KPR.

Note: NADP<sup>+</sup> and pantoate were not included in the actual experiment but is included here to help visualise their binding pockets.

In the preliminary SAR study, the *m*-aniline analogue **135** was tested in an inhibition assay at a final concentration of 500  $\mu$ M. The final concentrations in the reaction were 20  $\mu$ M NADPH (**24**), 1 mM ketopantoate (**22**), and 3 nM KPR in 100 mM HEPES buffer (pH 7.6), 2% DMSO (vol/vol). Under these conditions, the *m*-aniline analogue **135** inhibited KPR activity by 28%. The effect of **135** on KPR activity was further examined by measuring the enzyme velocity at varying ketopantoate (**22**) concentrations. The final concentrations in the reaction were 500  $\mu$ M of **135**, 100  $\mu$ M NADPH (**24**), 3 nM enzyme and concentration range 15 – 1000  $\mu$ M ketopantoate (**22**) in 100 mM HEPES buffer (pH 7.6). In the presence of the *m*-aniline analogue **135**, inhibition was not overcome even at high concentrations of ketopantoate (**22**) (Figure 3-6A). Notably, when the data was converted to a Michaelis-Menten plot (Figure 3-6B), the apparent  $V_{\max}$  was lower in the presence of **135** than in the absence ( $V_{\max}$  0.008 and 0.012  $\mu$ mol/sec/mg, respectively), while the  $K_m$  was unchanged. The fact that increasing the substrate concentration could not overcome inhibition and the observed lower  $V_{\max}$  and unchanged  $K_m$  in the presence of **135** implies non-competitive inhibition.

Non-competitive inhibitors may bind at a site away from the catalytic active site and cause a reduction in the catalytic rate.<sup>188</sup> Thus, the kinetic analysis of the *m*-aniline analogue **135** is in agreement with the  $^1\text{H}/^{15}\text{N}$ -HSQC NMR CSP map, suggesting that the *m*-aniline analogue **135** does indeed bind to an allosteric site. Furthermore, binding of the *m*-aniline analogue **135** caused large perturbations on KPR along the hinge region indicative of a conformational change. A conformational change can affect the formation of the usual enzyme-substrate complex since the catalytic binding site and allosteric binding site are conformationally linked.<sup>189</sup> The potential advantage of

targeting an allosteric site is that they can achieve high selectivity against other enzymes that utilise the same substrate.<sup>190</sup>

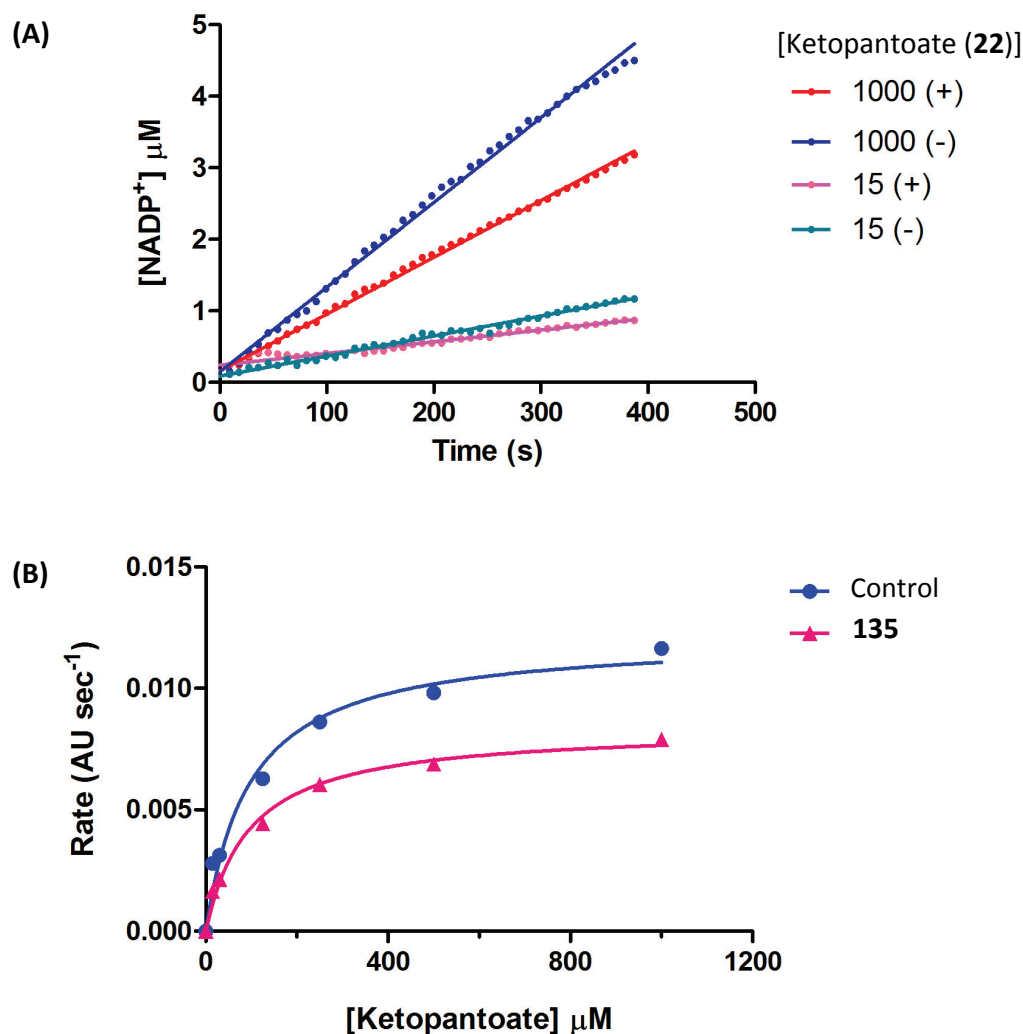


**Figure 3-6.** Kinetic study of **135**: (A) At ketopantoate (**22**) concentrations 15 and 1000 μM, the effect of KPR activity is measured (–) in the absence of **135** and (+) in the presence of **135**. (B) Michaelis-Menten plot in the presence (▲) and absence (●) of **135**.

The design of allosteric inhibitors of KPR using SAR around the *m*-aniline analogue **135** was rather challenging. For example, the initial lead sulfonamide **113** showed modest perturbations at the nicotinamide portion of the NADPH binding site and inhibition was competitive. While a simple modification of the aniline from *para* to *meta* changed binding in the catalytic site to an allosteric site and inhibition became non-competitive

(Figure 3-7). Then the change from piperidine derivative **135** to the corresponding pyrrolidine **138** affected the binding such that the pyrrolidinesulfonamide exhibited much weaker perturbations (**138**  $\Delta\delta_{\max}$  0.03 ppm compared to **135**  $\Delta\delta_{\max}$  0.18) and no clear clustering of CSPs were observed to identify its binding location. Therefore, further studies of allosteric inhibitors based on the **135** template were set aside.

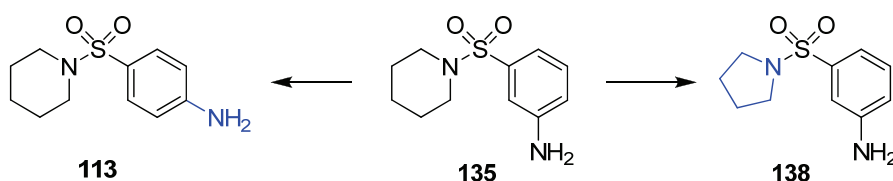
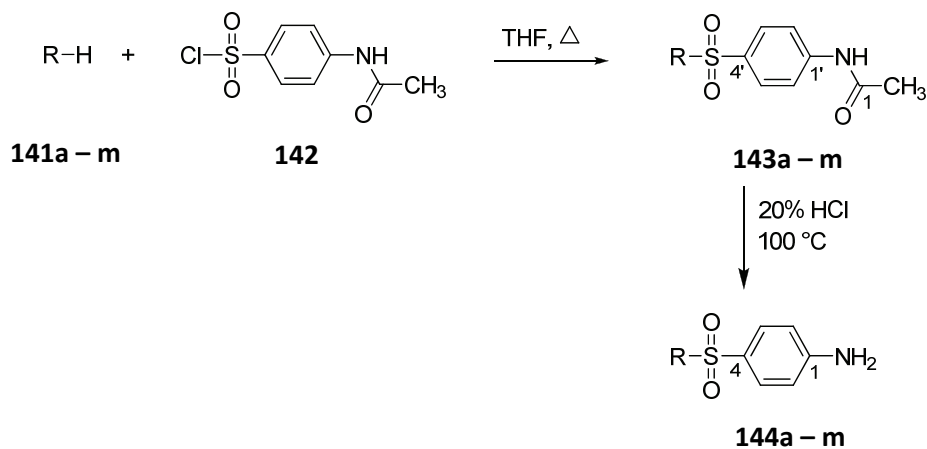


**Figure 3-7.** Structures of **135** analogues for structure-activity studies: Structural differences on **113** and **138** to **135** are highlighted in blue.

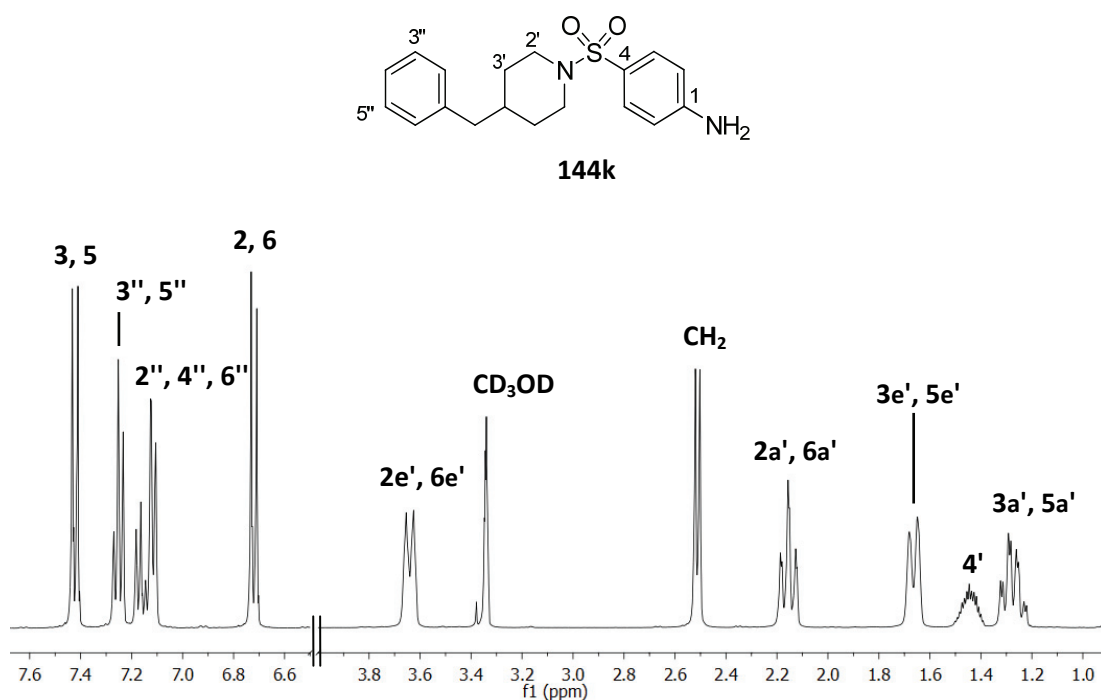
### 3.2.5 Synthesis of sulfonylaniline derivatives

From the preliminary SAR study, the aniline substituent was suggested to be critical for KPR activity while the piperidine portion was more tolerant to changes. As a result, synthesis was focused on optimisation of the amine substitution while maintaining the sulfonylaniline. Scheme 3-1 outlines the synthesis of sulfonylaniline derivatives. The two-step process involved the addition of amine (**141a – m**, 5–10 mol equivalent) to a solution of 4-acetamidobenzene-1-sulfonyl chloride (**142**, 2.14 mmol) in THF, and the solution refluxed. The reaction was worked-up with aqueous acid (1 M HCl) and purified by recrystallisation. The acetylsulfonamide intermediates (**143a – m**) were hydrolysed in aqueous HCl (2 M) at 100 °C and then neutralised. Purification by recrystallisation afforded the desired sulfonylanilines (**144a – m**).

**Scheme 3-1.** Synthetic pathway to sulfonamide analogues (**144a – m**): Refer to Table 3-1 for structures.



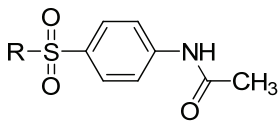
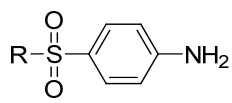
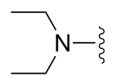
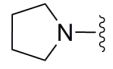
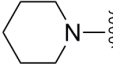
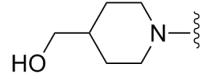
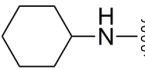
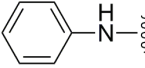
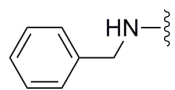
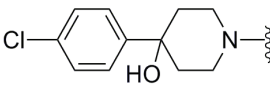
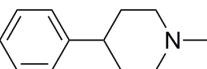
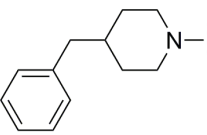
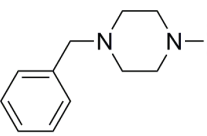
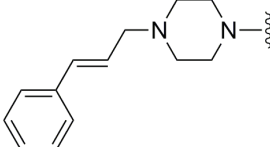
The  $^1\text{H}$  and  $^{13}\text{C}$  NMR spectra showed resonances consistent for all the target compounds (**144a – m**). The  $^1\text{H}$  NMR spectroscopy showed representative peaks for the sulfonylaniline and also supported the incorporation of the functionalised amines. Resonances in the regions  $\delta$  6.71 and 7.42 ppm, each integrating to two protons, are indicative of the aromatic proton sets H2/H6 and H3/H5, respectively. In the  $^1\text{H}$  NMR spectra of compounds containing a monosubstituted piperidine, a characteristic spectral pattern resulting from a chair conformation is observed. The spectra consist of five well separated signals: two for equatorial and three for axial piperidine protons. As an example, the assigned proton resonances of a benzylpiperidine derivative **144k** are summarised and shown in Figure 3-8. The  $^{13}\text{C}$  NMR spectrum showed six methine, three methylene and three different quaternary carbon resonances supporting the  $^1\text{H}$  NMR spectral analysis. Compounds were analysed by reverse phase HPLC using gradient elution conditions and an additional isocratic elution conditions for novel compounds. The chromatogram of **144k** shows a single peak for the analyte and suggests purity of more than 99%, within the limits of detection by absorbance at 254 nm. Table 3-1 shows a summary of yields of the target compounds.



Proton Assignment	<sup>1</sup> H			
	δ (ppm)	Integration	Multiplicity	J (Hz)
CH <sub>2</sub>	2.48	2	d	7
2, 6	6.69	2	d	9
3, 5	7.39	2	d	9
2', 6'	2.12	2	ddd	14, 12, 2
	3.61	2	br d	12
3', 5'	1.24	2	br ddd	16, 13, 4
	1.63	2	br d	13
4'	1.34 – 1.50	1	m	-
2'', 4'', 6''	7.08 – 7.15	3	m	-
3'', 5''	7.22	2	t	7

**Figure 3-8.** Partial <sup>1</sup>H NMR spectrum (400 MHz) of **144k** in CD<sub>3</sub>OD and tabulated <sup>1</sup>H NMR signals

**Table 3-1.** Summary of the yields for the synthesis of sulfonamides

 <b>143a – m</b>		 <b>144a – m</b>	
	R =	Yield (%)	
		143	144
<b>a</b>		72	63
<b>b</b>		85	59
<b>c</b>		63	42
<b>d</b>		90	48
<b>e</b>		85	69
<b>f</b>		54	47
<b>g</b>		43	41
<b>h</b>		79	43
<b>i</b>		34	-
<b>j</b>		92	71
<b>k</b>		55	49
<b>l</b>		58	12
<b>m</b>		48	56

### 3.2.6 Inhibition analysis of sulfonamide analogues

Compounds **144a – m** were designed and synthesised to further investigate the binding of sulfonamides to KPR. The effect of secondary and tertiary amine derivatives were investigated, while the primary amine derivative, **125** has been shown to be ineffective (from the preliminary SAR study). Substitutions of the amine included aliphatic groups such as cycloalkanes of ring sizes 5 and 6 or aryl rings. Since the sulfonylaniline derivatives (**144a – m**) are synthesised *via* the acetamide intermediate (**143a – m**), the acetamides were also included in the testing. The sulfonamide derivatives were tested at a final concentration of 500  $\mu$ M for KPR inhibition and the assays were reported as percentage inhibition (%).

Approximately half of the synthesised sulfonamides displayed limited solubility at 500  $\mu$ M. The insoluble compounds were subsequently prepared at a range of lower concentrations and tested. Generally the derivatives containing the phenyl substituted piperidine/piperazine experienced solubility problems and the sulfonamide containing the cinnamyl moiety was insoluble for testing.

As shown in Table 3-2, the potency is maintained when the sulfonamide derivative is substituted with a phenyl piperidine while the smaller counterparts (with aliphatic substituted amines) lose much of their activity. In the preliminary SAR study, the two acetamide containing compounds (**136** and **140**) displayed enhanced KPR activity. Interestingly, the testing of more acetamides (**143a – m**) did not show such KPR activity, instead very weak KPR inhibition was observed. Generally, the sulfonylaniline derivatives were slightly more potent than the corresponding acetamide analogues (for example **143b**, **143d**, **143e**, **143f**, and **143g**). The SAR is also quite sensitive as

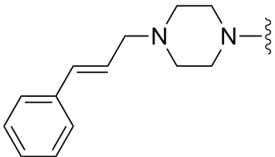
evidenced by the difference in activity between the piperidine **144k** ( $IC_{50}$  53  $\mu$ M) and the corresponding piperazine **144l** (no inhibition). Potentially, the ionisable distal nitrogen of the piperazine is responsible for unfavourable interactions.

In total, 43 sulfonamide analogues (including the original sulfonamide hit and acetamides) were tested against KPR. It is clear that the *para* substituted sulfonylaniline is critical for inhibitory activity. Only 5 analogues demonstrated inhibitory activity with  $IC_{50} < 500$   $\mu$ M and only the benzylpiperidine derivative **144k** showed a modest improvement in potency compared to the lead sulfonamide. However, the improvements are not sufficient for the added heavy atoms to maintain the LE in the desirable range. The benzylpiperidine derivative **144k** showed a value lower than the original sulfonamide hit (**113**, LE 0.36 kcal/mol per HAC) suggesting that the core was not being evolved optimally.

**Table 3-2.** Summary of inhibitory data for the sulfonamides synthesised<sup>2</sup>

		R =		% Inhibition (500 $\mu$ M)		IC <sub>50</sub> ( $\mu$ M)	LE
				143	144	144	
<b>a</b>		9	3	-	-		
<b>b</b>		1	14	-	-		
<b>c</b>		Insoluble	Insoluble	65	0.36		
<b>d</b>		2	6	-	-		
<b>e</b>		8	23	-	-		
<b>f</b>		11	28	-	-		
<b>g</b>		7	17	-	-		
<b>h</b>		18	18	-	-		
<b>i</b>		Insoluble	-	-	-		
<b>j</b>		Insoluble	Insoluble	86	0.25		
<b>k</b>		Insoluble	Insoluble	53	0.25		
<b>l</b>		Insoluble	Insoluble	No inhibition	-		

<sup>2</sup> The data shown were analysed by standard KPR assay conditions: NADPH (**24**, 20  $\mu$ M), ketopantoate (**22**, 1 mM), and KPR (3 nM) in 100 mM HEPES buffer (pH 7.6) with 2% DMSO (vol/vol).

<b>m</b>		Insoluble	Insoluble	Insoluble	-
----------	---	-----------	-----------	-----------	---

### 3.2.7 Summary

The fragments' binding location was investigated using  $^1\text{H}/^{15}\text{N}$ -HSQC NMR wherein most of the sulfonamide analogues exhibited weak and/or scattered CSP. Since the binding location was inconclusive, the information could not be used to determine whether the mode of inhibition is the same between the analogues. Therefore, it is difficult to draw any conclusions. Nevertheless, from investigating the binding of these sulfonamide analogues, a novel binding pocket was suggested. Further kinetic studies confirmed the allosteric site and identified **135** as a non-competitive inhibitor. Non-competitive inhibition can be advantageous since allosteric sites are not subjected to the same evolutionary pressure to accommodate an endogenous ligand therefore greater selectivity may be achieved.<sup>190</sup>

Based on the initial fragment hit **113**, 42 sulfonamide analogues were tested against KPR and 5 compounds demonstrated inhibitory activity with  $\text{IC}_{50} < 500 \mu\text{M}$ . The resulting SAR study illustrated the importance of the sulfonylaniline, and that aromatic substituents on the sulfonylpiperidine were tolerated. However, the LE of these analogues suggests the improvements were not sufficient for the added heavy atoms to maintain the LE in the desirable range.

### 3.3 Thienopyrroles

The thienopyrrole **108** was the top ranked fragment in our preliminary screen, and progress in enhancing this fragment is outlined. Compared to other fragment hits, the thienopyrrole **108** showed significantly greater inhibition and higher LE. Prior to chemical elaboration, **108** was first further characterised for its mode of inhibition and binding location, in order to guide decisions in developing more potent compounds.

#### 3.3.1 Mode of inhibition

To establish whether 4-methyl-4*H*-thieno[3,2-*b*]pyrrole-5-carboxylic acid (**108**) was inhibiting competitively, a determination of  $K_i$  was required. The thienopyrrole **108** was tested at final concentrations of 20, 40, 60 and 80  $\mu\text{M}$  in the reaction containing NADPH (**24**, 10 – 160  $\mu\text{M}$ ), ketopantoate (**22**, 1 mM), and KPR (3 nM) in buffer D (Table 7-5) with 2% DMSO (vol/vol). A full binding curve was measured and the data were fitted to a one-site competition model. Thienopyrrole **108** was found competitive against NADPH (**24**) with  $K_i$  of 21  $\mu\text{M}$  (Figure 3-9).

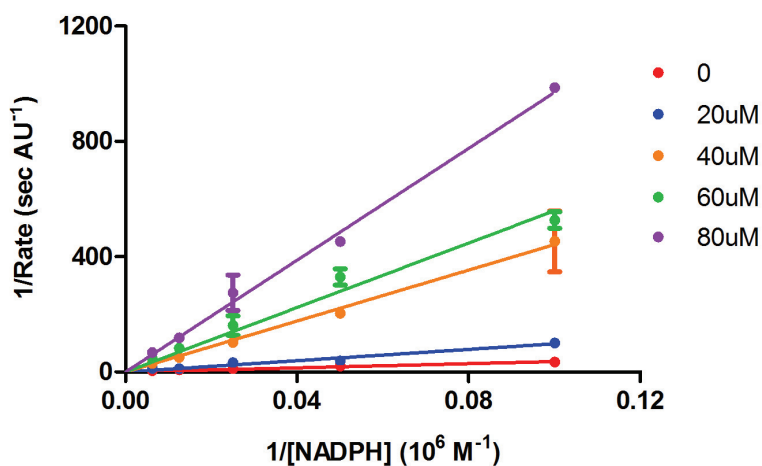


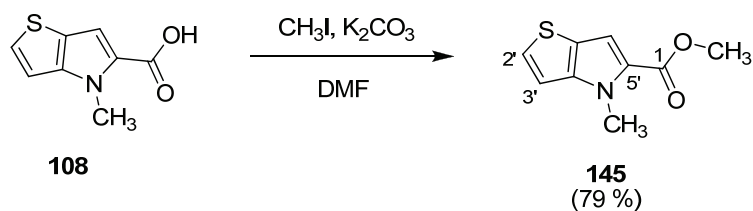
**Figure 3-9** Inhibition analysis: NADPH (**24**) titration of steady state velocity for KPR in the presence of thienopyrrole **108** at varying concentrations. A  $K_i$  of 21  $\mu\text{M}$  was obtained.

### 3.3.2 Preliminary SAR

Although the activity profile of the thienopyrrole **108** is attractive, this interesting scaffold is not well described in the literature. A literature search using the term ‘thieno[3,2-*b*]pyrrole’ only returned 38 references, which was filtered to 9 articles that were appropriate (SciFinder Scholar 2011). Potentially, this may be the result of the thieno[3,2-*b*]pyrrole being challenging to synthesise or that the scaffold is surrounded by patents.<sup>191-193</sup> Similarly, there were only a few analogues from commercial suppliers that would be useful in SAR development. Fortunately there were 3 analogues found in the internal library, as well as one that could be rapidly synthesised and 3 isosteres that could be purchased from a commercial source.

In the case of the synthesised derivative, a small scale (10 mg) reaction was carried out using 4-methyl-4*H*-thieno[3,2-*b*]pyrrole-5-carboxylic acid (**108**). The methyl ester **145** was formed by treating the carboxylic acid **108** with three equivalents of potassium carbonate and methyl iodide in *N,N*-dimethylformamide (DMF) at ambient temperature (Scheme 3-2). The reaction mixture was diluted with ethyl acetate and washed with water. The methyl ester **145** was isolated in good yield (79%) after a column purification (ethyl acetate:hexane; 1:4). The esterification was confirmed by two methyl group resonances ( $\delta$  3.86 ppm and 4.06 ppm) in the <sup>1</sup>H NMR spectrum and the ESI mass spectrum showing molecular ion at *m/z* 196 corresponding to (M + H)<sup>+</sup>.

**Scheme 3-2.** Synthesis of methyl 4-methyl-4*H*-thieno[3,2-*b*]pyrrole-5-carboxylate (**145**)



The thienopyrrole analogues (**145** – **152**) were tested in a single concentration assay. Initial efforts were directed at determining the importance of the carboxylic acid moiety for binding, and whether the heterocyclic core was optimal. To evaluate the carboxylic acid moiety, the corresponding methyl ester **145**, alcohol **147** and methylamine **146** derivatives were tested. The methyl ester **145** showed very poor affinity, while the alcohol **147** and methylamine **146** retained some of the activity (Figure 3-10). Preliminary investigations on the core showed that removing the methyl substituent **150** reduced activity by approximately six-fold and the corresponding indole **152** showed no activity. Details regarding the furo[3,2-*b*]pyrrole analogue **151** were inconclusive due to limited solubility. Thienothiophenes, such as regioisomers **148** and **149** were investigated, and showed improved affinity.

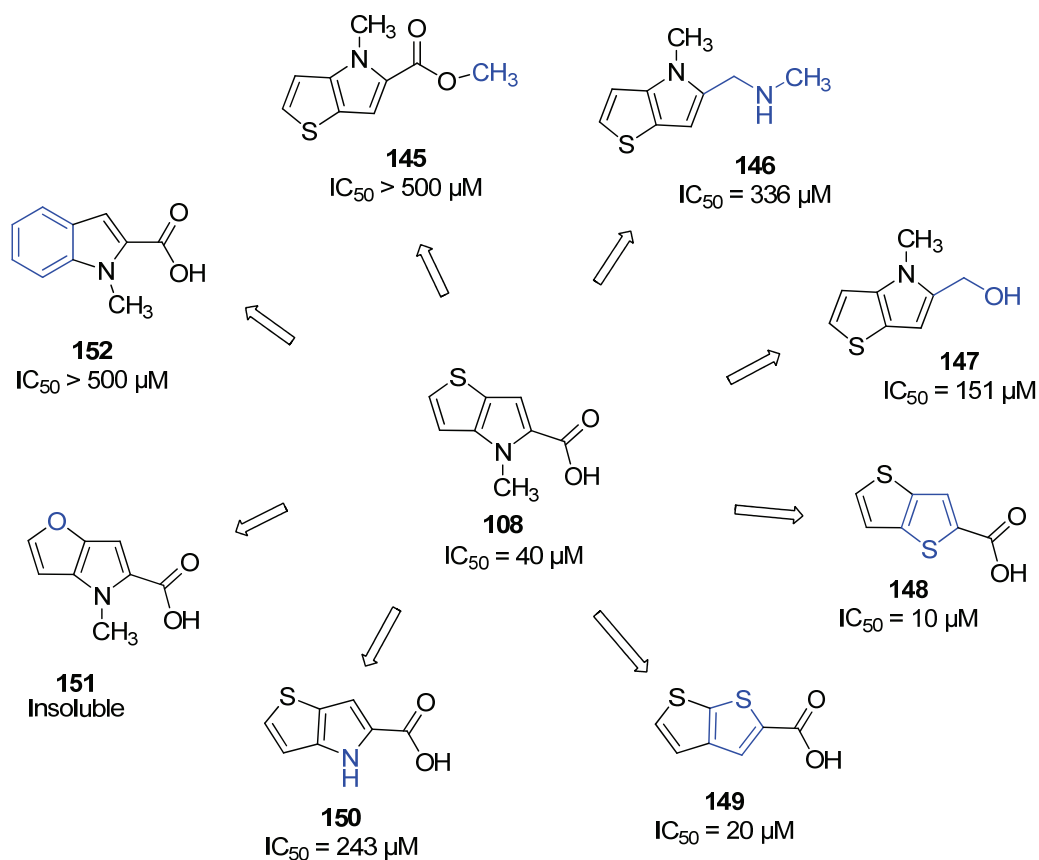


**Figure 3-10.** Chemical structures of thienopyrrole analogues obtained from internal library, synthesised or purchased

### 3.3.3 Chemical shift mapping

The series of thienopyrrole analogues studied in the preliminary SAR were analysed using  $^1\text{H}/^{15}\text{N}$ -HSQC NMR to investigate their binding as described in chapter 2 section 2.5.

The addition of the thienopyrrole **108** to KPR revealed CSPs to residues extending along the NADPH binding site (Figure 3-11). CSPs were also observed for isolated residues away from the catalytic binding cavity. The pattern of perturbations from the thienopyrrole **108** is similar to that observed for the des-methyl thienopyrrole **150** and the methylamine derivative **146** indicating a similar mode of interaction (Figure 3-11). Interestingly, the affected residues Met100 – Glu105 were perturbed for all the thienopyrrole analogues except the methyl ester derivative **145**. However, it is unclear whether the perturbation of the residues (Met100 – Glu105) is due to direct interactions or transferred from nearby interactions since adjacent residues Ile96 – Gly99 of the pantoate-binding pocket could not be unassigned.<sup>92,173</sup> Particularly, for the thienopyrrole **108**, des-methyl thienopyrrole **150** and thieno[3,2-*b*]thiophene analogue **148** the perturbed residues Met100 – Glu105 appeared to be an isolated cluster. Overall, the binding site was difficult to identify since perturbations appeared along the NADPH binding cavity. For the methyl ester derivative **145**, which did not inhibit KPR activity, a different clustering pattern was observed with perturbations localised away from the catalytic binding cavity.

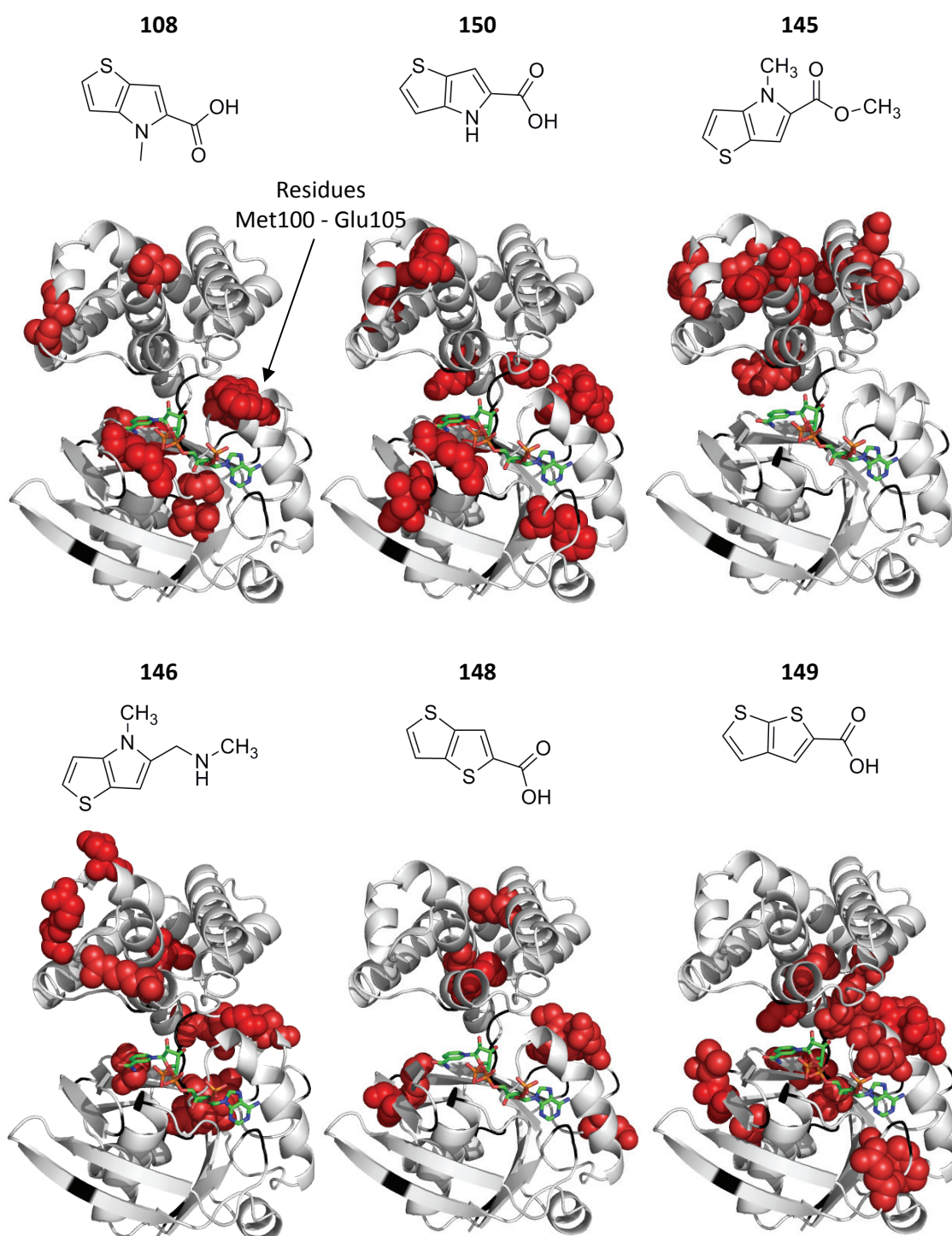


**Figure 3-11.** The residues that were perturbed on addition of fragments **108**, **150**, **145**, **146**, **148** and **149** were mapped onto the crystal structure (PDB ID: 1YJQ): Ribbon representation of KPR and perturbations ( $\Delta\delta > 0.03$  ppm) are shown as red spheres. Unassigned residues are coloured black. NADP<sup>+</sup> shown as green carbons.

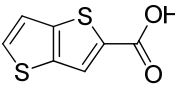
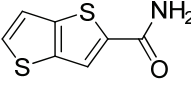
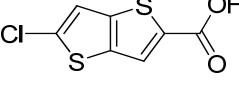
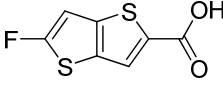
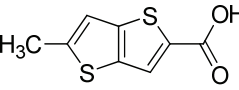
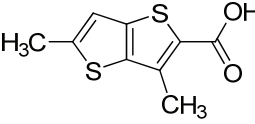
Note: NADP<sup>+</sup> was not included in the actual experiment but is included here to help visualise the binding pocket.

### 3.3.4 Thieno[3,2-*b*]thiophene-2-carboxylic acid

Core optimisation led to the discovery of thieno[3,2-*b*]thiophene-2-carboxylic acid (**148**) with a four-fold improvement in affinity. The  $^1\text{H}/^{15}\text{N}$ -HSQC studies suggested there were similarities in binding position between the thieno[3,2-*b*]thiophene **148** and thienopyrrole **108** derivative with some common residues perturbed. To investigate the inhibition and binding of thieno[3,2-*b*]thiophene **148**, analogues based on the thieno[3,2-*b*]thiophene template were purchased from commercial sources.

The potency of the thieno[3,2-*b*]thiophene analogues (**153 – 157**) are summarised in Table 3-3. Evaluation of the 5-position with substituents such as chlorine and fluorine (**154** and **155**, respectively) demonstrated that electronegative halogens were able to retain some activity. Compound **156** with a methyl substituent at the same position showed loss of activity. On the other side of the scaffold, substituting the carboxylic acid for an amide (compound **153**) retained some of the activity.

**Table 3-3.** IC<sub>50</sub> for thieno[3,2-*b*]thiophene-2-carboxylic acid analogues<sup>3</sup>

	Structure	IC <sub>50</sub> (μM)	LE
148		10	0.62
153		307	0.44
154		33	0.51
155		107	0.45
156		> 500	< 0.38
157		251	0.38

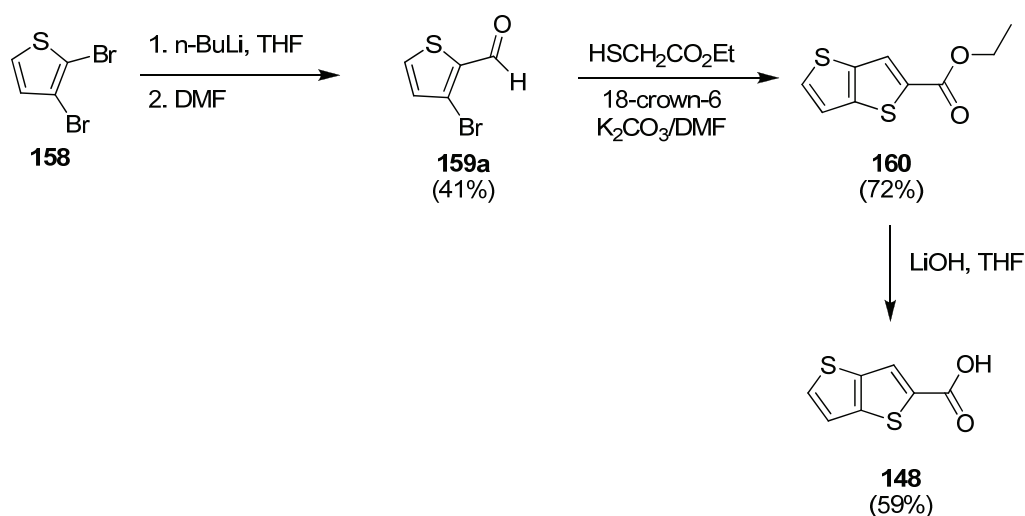
<sup>3</sup> The data shown were analysed by standard KPR assay conditions: NADPH (**24**, 20 μM), ketopantoate (**22**, 1 mM), and KPR (3 nM) in 100 mM HEPES buffer (pH 7.6) with 2% DMSO (vol/vol).

### 3.3.5 Synthesis of thieno[3,2-*b*]thiophenes

#### 3.3.5.1 Thieno[3,2-*b*]thiophene-2-carboxylic acid

Given the preliminary SAR of the thieno[3,2-*b*]thiophenes (although not clear), they were considered worth investigating through synthesis. The synthetic route was investigated to access a range of analogues and identify suitable positions for further elaboration. Effects of functionalisation were examined at the 2-position by amide formation, the 3-position by introduction of methyl and phenyl substituents and the 5-position using Suzuki couplings to bromides to rapidly introduce a range of different substituents. Earlier work describing the preparation of thieno[3,2-*b*]thiophene was reviewed by Litvinov and co-workers (1975).<sup>194-195</sup> However, as attention to the preparation of thieno[3,2-*b*]thiophenes for biological or medicinal purposes has improved, more convenient and reproducible methods have since been reported.<sup>196-199</sup> The synthetic strategy derived from Fuller and co-workers<sup>199</sup> (Scheme 3-3) was employed to investigate the synthesis of **148** derivatives.

**Scheme 3-3.** Synthetic pathway to thieno[3,2-*b*]thiophene-2-carboxylic acid (**148**)



In the first step, formylation of 2,3-dibromothiophene (**158**) was achieved through lithium-halogen metal exchange wherein a solution at  $-20\text{ }^{\circ}\text{C}$  of 2,3-dibromothiophene (**158**) in tetrahydrofuran (THF) was treated with 1.1 equivalents of *n*-butyllithium (*n*-BuLi). The mixture was stirred for 30 mins before re-cooling to  $-78\text{ }^{\circ}\text{C}$  and 2 equivalents of anhydrous DMF were added dropwise. The solution was warmed to room temperature and stirred for a further 2 h prior to quenching with ammonium chloride. The reaction mixture was worked up and purified by flash chromatography (ethyl acetate:petroleum spirit; 5:95) to afford **159a** in 41% yield as a light yellow oil. The  $^1\text{H}$  NMR spectrum of **159a** showed incorporation of the aldehyde substituent by the presence of the resonance at  $\delta$  9.94 ppm (Table 3-4). However, during lithium-halogen metal exchange of 2,3-dibromothiophene, the reaction at  $-78\text{ }^{\circ}\text{C}$  was complicated with deprotonation occurring at both the  $\alpha$ -positions of the thiophene ring affording a mixture of **159a** and a minor by-product 2,5-bis-substituted compound **159b**. The  $^1\text{H}$  NMR spectrum of the by-product showed only two resonances (Table 3-4). The same by-product has been reported in the literature.<sup>199-200</sup>

**Table 3-4.** Tabulated  $^1\text{H}$  NMR signals (300 MHz) of **159a** and **159b** in  $\text{CDCl}_3$

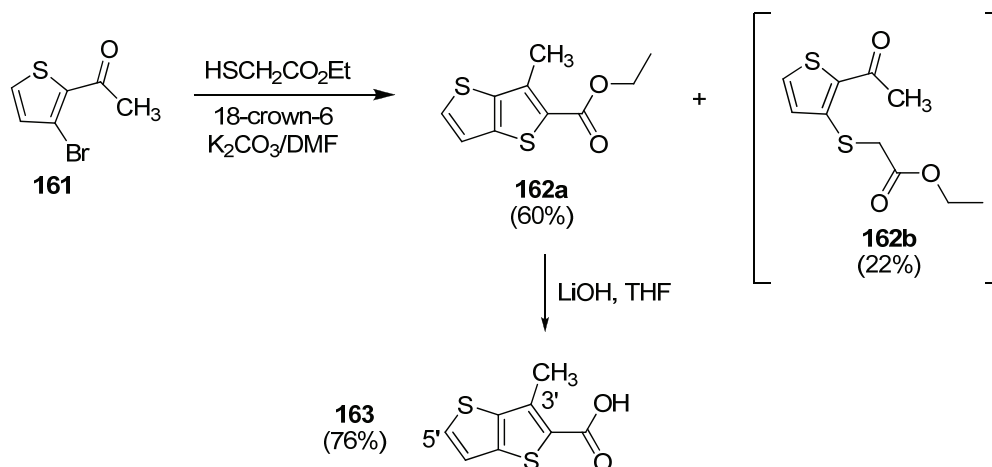
Proton	<b>159a</b>	<b>159b</b>
4', (3')	7.12 ppm, d, $J = 5.1\text{ Hz}$	7.14 ppm, s
5'	7.69 ppm, dd, $J = 5.1, 1.3\text{ Hz}$	-
1	9.94 ppm, d, $J = 1.3\text{ Hz}$	9.82 ppm, s

The second sulfur-containing ring was constructed by reacting 3-bromothiophene-2-carbaldehyde (**159a**) with ethyl 2-sulfanylacetate (1 mmol) in the presence of potassium carbonate (1.4 mmol) and DMF at room temperature for a lengthy reaction time of 72 hours. Following work up and purification using flash chromatography, ethyl thieno[3,2-*b*]thiophene-2-carboxylate (**160**) was obtained in 53% yield as a yellow oil. Using the method reported by He and Zhang,<sup>201</sup> the addition of a catalytic amount of 18-crown-6 ether to help solubilise potassium carbonate and heating the reaction to 60 °C reduced the reaction time from 72 h to 12 h and improved the yield from 53% to 72%. The <sup>1</sup>H NMR spectrum showed resonances of the ethyl ester moiety with a triplet at δ 1.39 ppm (CH<sub>3</sub>) and quartet at δ 4.38 ppm (CH<sub>2</sub>). Three aromatic protons of the thieno[3,2-*b*]thiophene were assigned as H6' (δ 7.27 ppm), H5' (δ 7.57 ppm) and H3' (δ 7.98 ppm). The ESI mass spectrum confirmed the molecular weight of the thieno[3,2-*b*]thiophene-carboxylate **160** (*m/z* 213, (M – H)<sup>+</sup>).

Finally, the hydrolysis of **160** was carried out with aqueous lithium hydroxide (LiOH) in THF. The reaction mixture was heated at reflux for 4 h then cooled to room temperature and concentrated under reduced pressure. Hydrochloric acid (HCl, 1 M) was slowly added resulting in a precipitate which was filtered off to afford the corresponding acid **148** in 59% yield. Hydrolysis was confirmed as the <sup>1</sup>H NMR spectrum showed a broad singlet at δ 13.18 ppm indicative of the OH group from the carboxylic acid and the ESI mass spectrum showed a molecular ion at *m/z* 183 corresponding to M – H<sup>+</sup>.

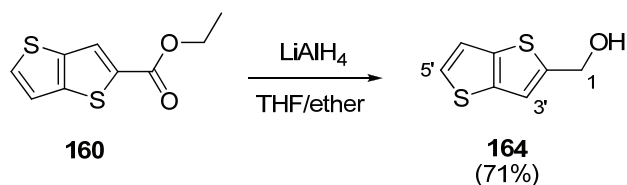
### 3.3.5.2 Modifications at the 3-position of thienothiophene

The preliminary SAR study on thieno[3,2-*b*]thiophene suggested that introducing a methyl group at the 3-position may improve affinity. Therefore, starting with 2-acetyl-3-bromothiophene (**161**), the same method as thieno[3,2-*b*]thiophene-2-carboxylate (**160**) was employed to synthesise ethyl 3-methylthieno[3,2-*b*]thiophene-2-carboxylate (**162a**) as outlined in Scheme 3-4. After heating the reaction at 60 °C for 2 days, work up and purification (ethyl acetate:petroleum spirit; 5:95) afforded **162a** in reasonable yield (60%). Thin layer chromatography (TLC) analysis revealed an additional component with a low retention factor ( $R_f$ ) which was eluted with ethyl acetate. The component was isolated as a yellow oil and confirmed by  $^1\text{H}$  NMR as the reaction intermediate, ethyl 2-[(2-acetylthiophen-3-yl)sulfanyl]acetate (**162b**) suggesting the reaction had not gone to completion (Scheme 3-4). Based on the  $^1\text{H}$  NMR spectra, the key distinguishing feature between the intermediate and the product **162a** was the additional deshielded resonance at  $\delta$  3.70 ppm, appearing as a singlet and integrating to 2 protons, thus corresponding to the  $\text{CH}_2$  between the thiol and ester group. The slower reaction is possibly due to the less reactive ketone compared to the aldehyde during cyclisation. Subsequent conversion of the ester **162a** to the corresponding acid derivative **163** with aqueous LiOH in THF occurred in good yield (76%). The synthesis of the 3-methyl derivative **162a** was not optimised as sufficient acid **163** was obtained for biochemical testing. The  $^1\text{H}$  NMR spectrum supported the formation of 3-methylthieno[3,2-*b*]thiophene-2-carboxylic acid (**163**) with resonances at  $\delta$  2.63 ppm (3H, s,  $\text{CH}_3$ ), 7.49 ppm (1H, d,  $J = 5.1$  Hz, H6') and 7.92 ppm (1H, d,  $J = 5.1$  Hz, H5').

**Scheme 3-4.** Synthetic pathway to 3-methylthieno[3,2-*b*]thiophene-2-carboxylic acid (**163**)

### 3.3.5.3 Modifications at the 2-position of thienothiophene

Reduction of the ester **160** to alcohol **164** was achieved with 1.5 equivalents of lithium aluminium hydride ( $\text{LiAlH}_4$ ) in THF/ether (1:1) as outlined in Scheme 3-5. The resulting mixture was stirred at reflux for 3.5 h then cooled to room temperature and carefully quenched with cold water and enough concentrated HCl to dissolve the inorganic salts. The aqueous layer was extracted with ethyl acetate and the combined organic layers were then washed with sodium hydrogen carbonate and dried to give the desired compound (**164**, 23 mg, 71%) as off-white foam. The  $^1\text{H}$  NMR spectrum was in agreement with reported literature with resonances at  $\delta$  1.83, 4.89, 7.20, 7.24 and 7.36 ppm corresponding to OH,  $\text{CH}_2$ , H3', H6' and H5', respectively.<sup>196</sup>

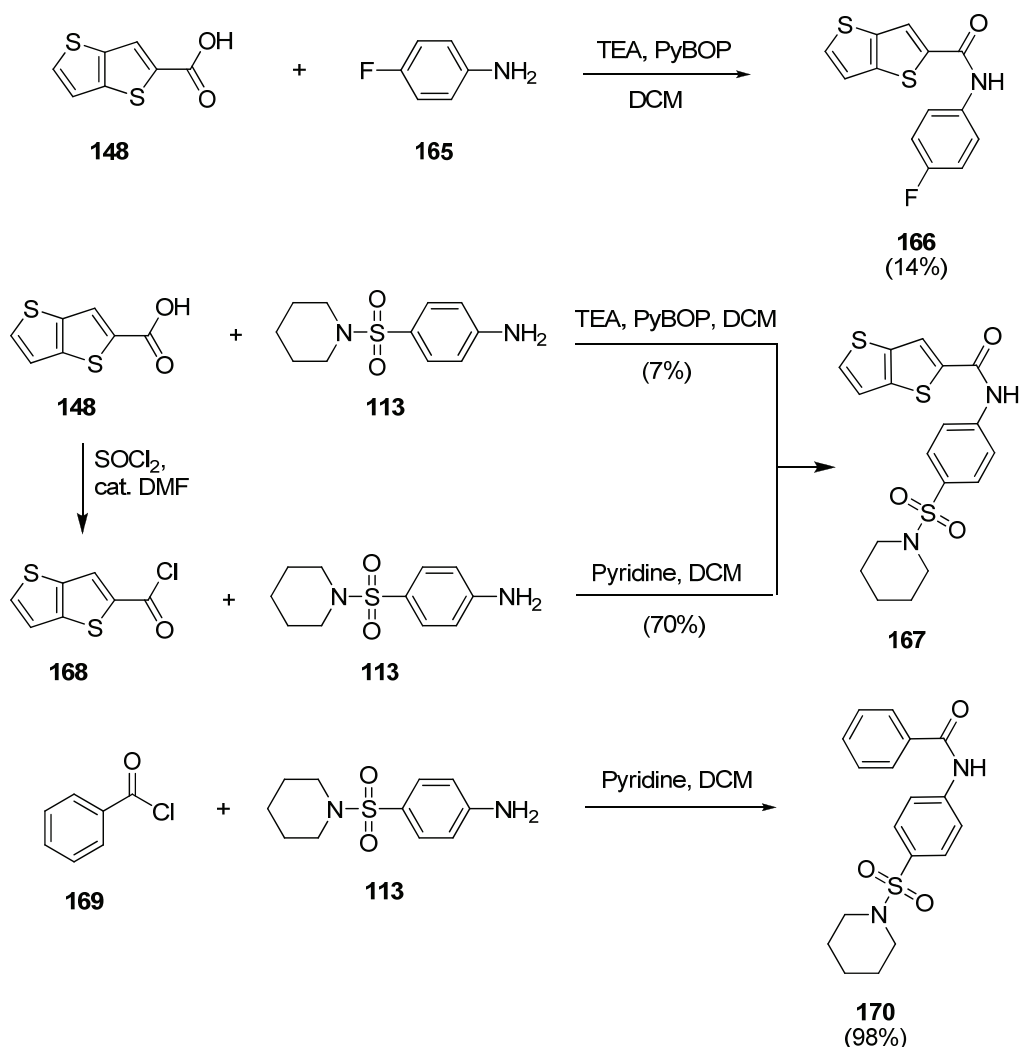
**Scheme 3-5.** Reduction of ethyl thieno[3,2-*b*]thiophene-2-carboxylate (**160**)

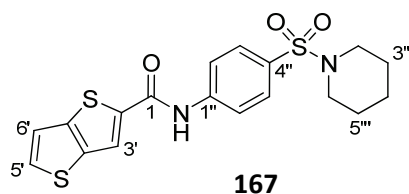
The conversion of the acid substituent at position 2 for an amide group was investigated. Many coupling reagents for amide bond formation *via* activated esters have been described.<sup>202</sup> However, PyBOP ((benzotriazol-1-yloxy)tripyrrolidinophosphonium hexafluorophosphate) was considered since the reagent was readily available and commonly used within the group. As shown in Scheme 3-6, the first attempt involved activation of the acid **148** in the presence of triethylamine (1.1 equivalents) with 1.1 equivalents of PyBOP in dichloromethane (DCM). Then 1.1 equivalents 4-fluoroaniline **165** and another 1.1 equivalents of triethylamine were added. The mixture was left stirring at ambient temperature for 12 h, worked up with an acid/base wash and the residue was purified by flash chromatography. In this manner, the 4-fluorophenyl derivative **166** and linked thienothiophene-sulfonamide derivative **167** were synthesised, however in low yields of 14% and 7%, respectively.

Alternatively, thionyl chloride was employed for the conversion of the acid **148** to the acid chloride **168** in the presence of a catalytic amount of DMF (Scheme 3-6). After stirring for 4 h at ambient temperature the volatiles were removed to provide the product as a yellow crystalline solid. The acid chloride **168** was then reacted with 4-(piperidine-1-sulfonyl)aniline (**113**) to give *N*-[4-(piperidine-1-sulfonyl)phenyl]thieno[3,2-*b*]thiophene-2-carboxamide (**167**) in 70% yield as off-white crystals after recrystallisation from ethyl acetate:hexane (mp 264 – 266 °C). The <sup>1</sup>H NMR spectroscopy showed the characteristic spectral pattern for the piperidine and also supported the incorporation of the thieno[3,2-*b*]thiophene moiety. The assigned proton resonances of the linked thienothiophene-sulfonamide derivative **167** are summarised in Table 3-5. The <sup>13</sup>C NMR spectrum showed five methine, three methylene and six different quaternary carbon resonances supporting the <sup>1</sup>H NMR spectral analysis.

Forming amide bonds *via* the acid chloride intermediate was higher yielding for the thienothiophenes therefore, *via* benzoyl chloride **169**, the *N*-[4-(piperidine-1-sulfonyl)phenyl]benzamide (**170**) was prepared (Scheme 3-6). The yellow precipitate was purified by recrystallisation from ethanol, affording the desired product (71 mg, 98%) as light orange/yellow crystals (mp 120 – 122 °C), confirmed by <sup>1</sup>H NMR spectrum and ESI mass spectrum showing a molecular ion at *m/z* 345 corresponding to *M* + H<sup>+</sup>.

**Scheme 3-6.** Forming amide bonds



**Table 3-5.**  $^1\text{H}$  NMR signals of **167** in  $d_6$ -DMSO

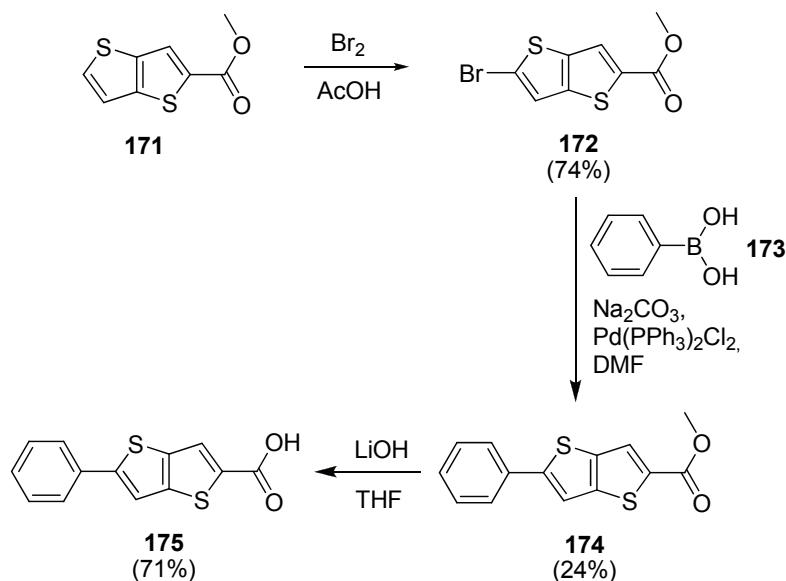
Proton Assignment	$^1\text{H}$			
	$\delta$ (ppm)	Integration	Multiplicity	$J$ (Hz)
NH	10.71	1	bs	-
3'	8.42	1	d	1
5'	7.94	1	d	5
6'	7.55	1	dd	5, 1
2'', 6''	7.73	2	d	9
3'', 5''	8.01	2	d	9
2''', 6'''	2.84 – 2.93	4	m	-
3''', 5'''	1.50 – 1.59	4	m	-
4'''	1.34 – 1.37	2	m	-

### 3.3.5.4 Modifications at the 5-position of thienothiophene

The Suzuki-Miyaura reaction was employed as it is well documented for the cross-coupling of arylboronic acids with aryl and heteroaryl halides.<sup>203-204</sup> To introduce substituents in the 5-position of thieno[3,2-*b*]thiophene, bromination, followed by Suzuki coupling was investigated (Scheme 3-7). Bromination of methyl thieno[3,2-*b*]thiophene-2-carboxylate (**171**) with one equivalent of  $\text{Br}_2$  in acetic acid (AcOH) at room temperature for 12 h produced a mixture of mono- and di-substituted derivatives with the ratio 1:3, respectively. Presumably the  $\text{Br}_2$  was not delivered slowly

enough thus, allowing incorporation of an additional bromine. When the stoichiometry of the starting materials was modified to half an equivalent of Br<sub>2</sub>, the mono-substituted derivative **172** was formed as the major product (in 74% yield). The <sup>1</sup>H NMR spectrum confirmed the mono-substituted bromo derivative with three proton signals corresponding to δ 3.92 ppm (3H, s, CH<sub>3</sub>), 7.30 ppm (1H, s, H6') and 7.88 ppm (1H, s, H3'). The ESI mass spectrum confirmed the presence of the bromine atom by showing isotopic ions at *m/z* 276 (100%) and 278 (98%) corresponding to M[<sup>79</sup>Br]H<sup>+</sup> and M[<sup>81</sup>Br]H<sup>+</sup>, respectively.

Suzuki coupling was used to install a phenyl moiety in the 5-position of thienothiophene (Scheme 3-7). The coupling involved reacting methyl 5-bromothieno[3,2-*b*]thiophene-2-carboxylate (**172**) with 1 equivalent of phenylboronic acid **173** in DMF and aqueous Na<sub>2</sub>CO<sub>3</sub> (1 M) in the presence of dichloro-bis(triphenylphosphine)palladium(II) (0.1% mol) as catalyst. The desired product, methyl 5-phenylthieno[3,2-*b*]thiophene-2-carboxylate (**174**) was obtained in low yield (24%). Hydrolysis of **174** with aqueous LiOH in THF provided 5-phenylthieno[3,2-*b*]thiophene-2-carboxylic acid (**175**) in good yield (71%). The <sup>1</sup>H NMR spectrum of **175** showed incorporation of the phenyl substituent by the presence of additional aromatic resonances at δ 7.28 – 7.34 ppm (1H, m, H4''), 7.37 – 7.45 ppm (2H, m, H3'', H5'') and 7.69 (2H, dd, *J* = 8.4, 1.2 Hz, H2'', H6''), while proton signals at 7.61 and 7.74 ppm corresponded to H6' and H3' of the thieno[3,2-*b*]thiophene core. The <sup>13</sup>C NMR spectrum showed five methine, and six different quaternary carbon resonances supporting the <sup>1</sup>H NMR spectral analysis.

Scheme 3-7. Synthesis of 5-phenylthieno[3,2-*b*]thiophene-2-carboxylic acid (**175**)

### 3.3.6 Inhibition analysis of thienothiophene analogues

The preliminary SAR of the thienothiophene demonstrated that substitutions at the 2- and 5-position were tolerated without abolishing activity. To evaluate the importance of the carboxylic acid moiety, the corresponding ethyl ester **160**, alcohol **164** and amide derivatives **166** and **167** were tested. The ethyl ester **160** showed very poor affinity, while the alcohol **164** displayed a significant 10-fold increase in activity (Table 3-6). Furthermore, the amide derivatives **166** and **167** also maintained inhibitory activity. This suggests a negative charge at the 2-position may not be critical for activity, however, maintaining a hydrogen donor/acceptor at that position is important. An unexpected result was observed for compound **163** with the methyl substitution at the 3-position as potency was eliminated. From earlier investigations of the purchased thienothiophene derivatives, compound **156** (with methyl substitution at the 5-position) showed little activity while compound **157** (with methyl substitutions at 3- and 5-positions) provided an  $\text{IC}_{50}$  of 251  $\mu\text{M}$ . Thus, it was reasoned that eliminating the methyl substituent at the 5-position may improve affinity (unless these compounds were binding in different

locations). Thieno[3,2-*b*]thiophene **175** with the bulky phenyl moiety at the 5-position was reasonably tolerated with some activity retained. The activities of the thienothiophene derivatives are summarised in Table 3-6.

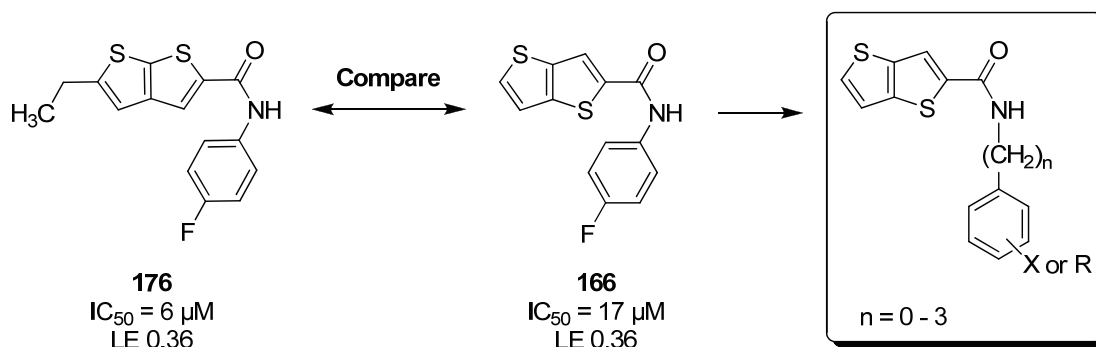
**Table 3-6.** IC<sub>50</sub> for synthesised **148** analogues<sup>4</sup>

	Structure	IC <sub>50</sub> (μM)	LE
<b>160</b>		> 500	< 0.35
<b>164</b>		1	0.82
<b>166</b>		17	0.36
<b>163</b>		> 500	< 0.35
<b>175</b>		47	0.35
<b>167</b>		0.36	0.34

<sup>4</sup> The data shown were analysed by standard KPR assay conditions: NADPH (**24**, 20 μM), ketopantoate (**22**, 1 mM), and KPR (3 nM) in 100 mM HEPES buffer (pH 7.6) with 2% DMSO (vol/vol).

Though the scaffold is based on the thieno[2,3-*b*]thiophene regioisomer, 5-ethyl-*N*-(4-fluorophenyl)thieno[2,3-*b*]thiophene-2-carboxamide (**176**) was purchased from a commercial source and the  $IC_{50}$  at 6  $\mu$ M was 3-fold higher than the starting thieno[2,3-*b*]thiophene (**149**,  $IC_{50}$  20  $\mu$ M). To determine whether the potency would be transferred to the thieno[3,2-*b*]thiophene regioisomer, the compound *N*-(4-fluorophenyl)thieno[3,2-*b*]thiophene-2-carboxamide (**166**) was synthesised and tested. The fluorophenyl analogue **166** displayed good potency with an  $IC_{50}$  of 17  $\mu$ M, despite missing the ethyl moiety at the 5-position. In fact, the LE of **176** and **166** were the same, suggesting the ethyl moiety may not necessarily improve binding for **166**. The progress of **166** prompted the design of further analogues around the template shown in Scheme 3-8.

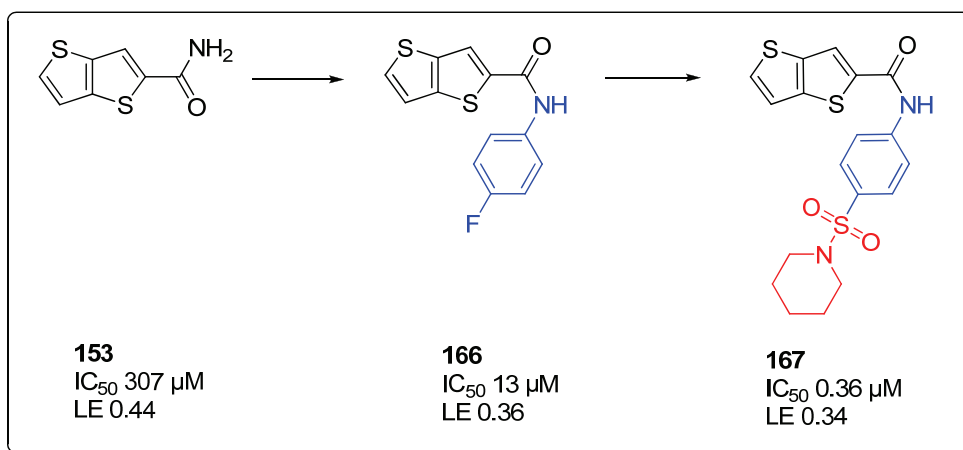
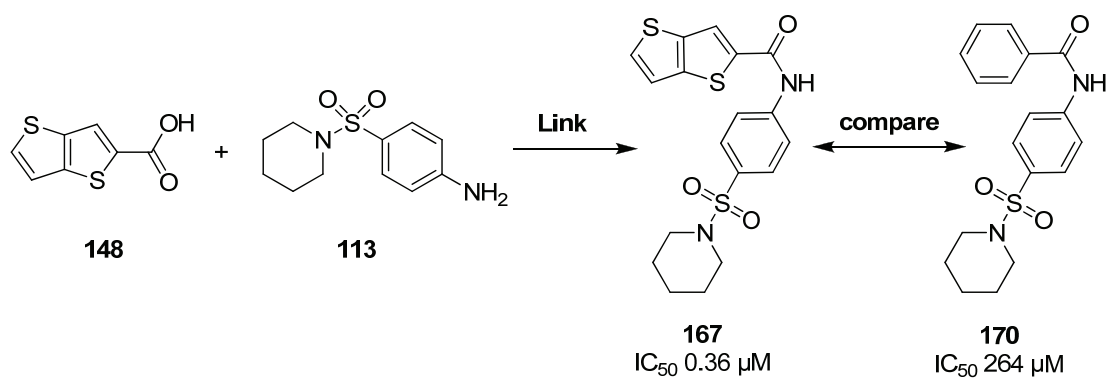
**Scheme 3-8.** Design of further thieno[3,2-*b*]thiophene analogues: The template is shown in the box.



Compound **167** was the product of linking the original sulfonamide hit **113** to thieno[3,2-*b*]thiophene **148**. The KPR inhibition by **167** showed a 30-fold improvement compared to **148** but a remarkable 180-fold to **113** (Scheme 3-9). However, in terms of LE, the linked compound is slightly worse off compared to **148**, yet when compared to **113** the LE values were comparable. To examine the importance of the thieno[3,2-*b*]thiophene in **167**, compound *N*-(4-(piperidin-1-

ylsulfonyl)phenyl)benzamide (**170**) was synthesised and tested. The outcome supported that the thienothiophene scaffold was indeed critical for activity demonstrating almost 100-fold improvement in activity.

**Scheme 3-9.** Thieno[3,2-*b*]thiophene design progression through linking strategy and elaboration



On preparing more analogues of the designed thieno[3,2-*b*]thiophene-2-carboxamide template, a larger amount of thieno[3,2-*b*]thiophene **148** was feasible to purchase from a commercial source at an economical price. Once purchased, **148** was tested in an assay and strangely, no activity was observed for **148** from the new supplier (Peakdale). The recently purchased thieno[3,2-*b*]thiophene was tested again and its activity was compared to **148** from the initial supplier that provided the library collection (Maybridge) and one we had synthesised. Using the same conditions, **148** from Maybridge and the one we synthesised showed inhibitory activity, while the compound from Peakdale resulted in no KPR inhibition (Figure 3-12).

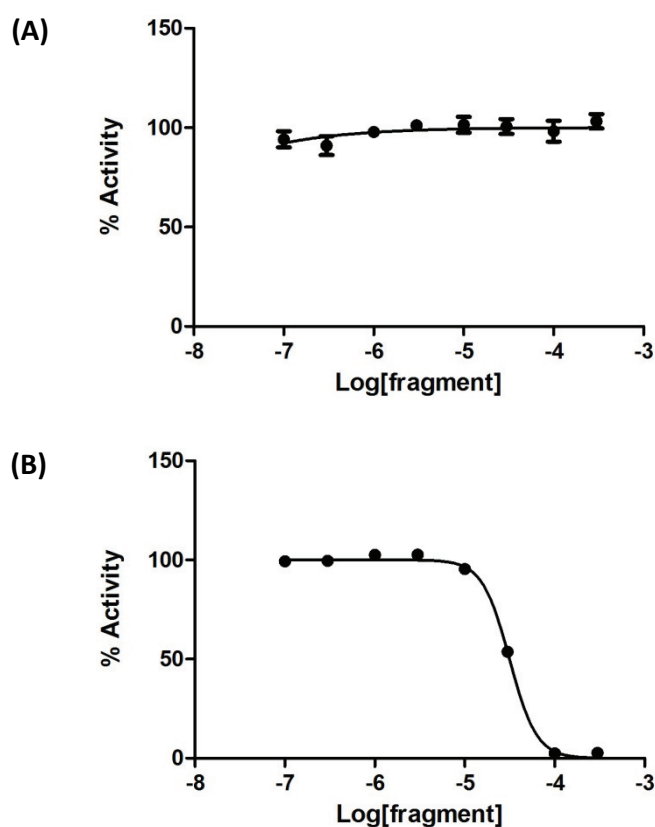


**Figure 3-12.** Thieno[3,2-*b*]thiophene **148** effect on KPR inhibition activity from supplier (A) Peakdale and (B) Maybridge

As a measure of quality control, the thienothiophene from all the different sources were (re-)examined by  $^1\text{H}$  NMR, MS and analytical HPLC. The  $^1\text{H}$  NMR spectra of the different samples (in  $\text{CD}_3\text{OD}$ ) showed aromatic hydrogen resonances consistent with thieno[3,2-*b*]thiophene-2-carboxylic acid. Similarly, the ESI mass spectrum (negative mode) showed the presence of an ion ( $\text{M} - \text{H}$ ) at  $m/z$  183 supporting the NMR data. Thieno[3,2-*b*]thiophene-2-carboxylic acid from the three different sources were then analysed by reverse phase HPLC using gradient elution conditions by absorbance at 214 and 254 nm (Figure 3-13). The chromatogram showed a single peak ( $t_{\text{R}}$  10.89 min) for the compound from Peakdale with purity greater than 99%. The chromatogram belonging to the compound from Maybridge showed a main peak ( $t_{\text{R}}$  11.09 min) with purity at 98% and two tiny peaks at 1% and 0.6%. Likewise, the chromatogram of the synthesised **148** showed a main peak ( $t_{\text{R}}$  10.88 min) with purity greater than 98% and a tiny peak at 0.8%. Notably, a close inspection of the chromatograms between samples from Maybridge and one synthesised show a common small peak in the region  $t_{\text{R}}$  12.04 min. Visually, the compound from Peakdale was crystalline and bright yellow in colour while the synthesised and Maybridge samples were a yellow and brown powder, respectively.

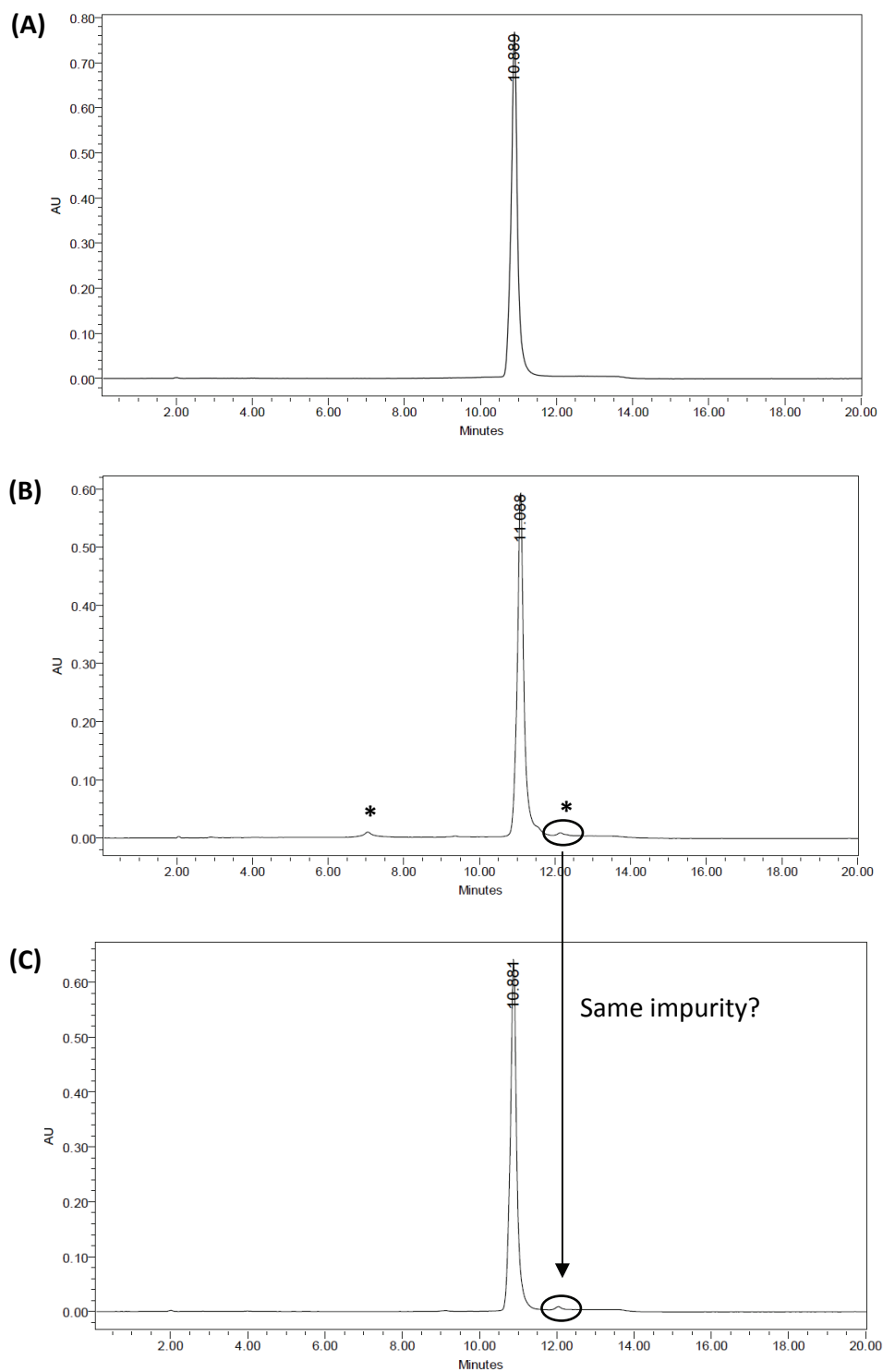


**Figure 3-13.** HPLC chromatogram at absorbance 254 nm from (A) Peakdale, (B) Maybridge and (C) synthesised

The HPLC chromatograms show the samples analysed had purity greater than 98%. Nonetheless, the samples from Maybridge and in-house product indicated the presence of minor peak(s). Therefore, it was important to rule out any possibility of contaminants influencing the biochemical activity. As a result, these samples were purified by preparative HPLC and all fractions collected were tested on KPR. The assay results were reported as percentage inhibition (%). The stock concentration for each fraction was prepared based on the known mass of the main component thieno[3,2-*b*]thiophene **148** isolated after preparative HPLC. Therefore, the determined percentage inhibition values are relative to the isolated thieno[3,2-*b*]thiophene **148**.

From the Maybridge sample, fractions corresponding to the main peak (containing thienothiophene) and the small peak at  $t_R$  7.15 min showed no KPR inhibition. However, the small peak at  $t_R$  12.15 min resulted in 70% inhibition of KPR activity. Consistent with the Maybridge sample, the fraction corresponding to the small peak at  $t_R$  12.15 min from the synthesised sample was the only fraction displaying KPR inhibition.

In an attempt to characterise the small component responsible for inhibiting KPR activity, spectroscopic techniques were used. High-resolution mass spectrometry (HRMS) showed a single peak at  $m/z$  282.3044,  $(M + H)^+$ . Detectable proton signals were observed in the  $^1H$  NMR (Figure 3-14) and COSY (correlation spectroscopy) spectrum on a 600 MHz NMR. The  $^1H$  NMR spectrum suggests there are in fact 2 – 3 components in the sample. The resonances at  $\delta$  0.90, 1.29 and 1.34 ppm are characteristic of a terminal methyl group and a long chain of methylene units. The signal at  $\delta$  5.34 ppm appearing as a triplet may correspond to an alkene proton. Due to the small quantity isolated (< 1 mg), little satisfactory data was obtained by  $^{13}C$  NMR,

HMBC (heteronuclear multiple bond correlation) and HSQC (heteronuclear single quantum correlation). NMR data of samples from Maybridge and one we had synthesised suggests the identity of the minor component is the same. Given the lack of material, and the difficulty in isolating much larger quantities, further investigation into the identity of this component was not considered worthwhile, especially as this component is clearly unrelated to the fragment series under investigation.

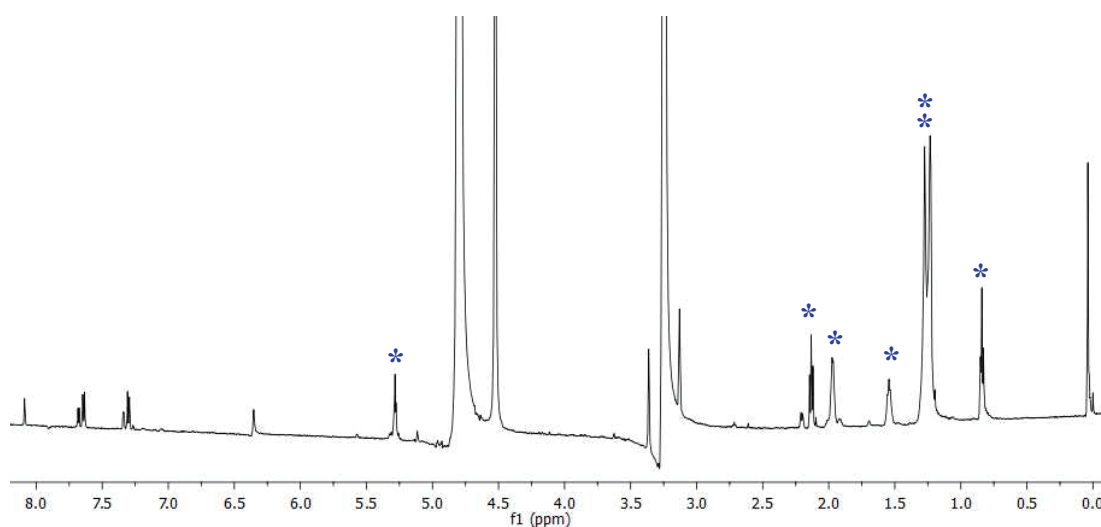


**Figure 3-14.**  $^1\text{H}$  NMR spectrum (600 MHz) of the impurity in  $\text{CD}_3\text{OD}$ : The resonances highlighted by ‘\*’ were shown to be correlated based on the COSY spectrum.

Regardless of the identity of the active minor impurity, these experiments demonstrate that the thienothiophene is inactive, casting doubt on the activity of the whole series.

### 3.3.7 Summary

The binding site for thienopyrrole **108** was difficult to pinpoint as  $^1\text{H}/^{15}\text{N}$ -HSQC NMR analysis show perturbations along the NADPH binding cavity. The pattern of perturbations of the thienopyrrole **108** was analogous to the des-methyl thienopyrrole **150** and methylamine derivative **146** indicating a similar mode of interaction.

During preliminary SAR analysis of thienopyrrole analogues, most derivatives retained some of the activity while the thienothiophenes, **149** and **148** showed improved affinity.  $^1\text{H}/^{15}\text{N}$ -HSQC NMR studies showed thieno[3,2-*b*]thiophene **148** binding to KPR, however, the binding location was not clear. Subsequent thieno[3,2-*b*]thiophene analogues purchased and synthesised were investigated for inhibition. Synthesised amide derivatives **167** and **166** showed promising results ( $\text{IC}_{50}$  0.36  $\mu\text{M}$  and 17  $\mu\text{M}$ , respectively) as the potency was either improved or maintained, leading to the design of elaborated thienothiophene-amide derivatives. However, the synthesis and development was halted as thieno[3,2-*b*]thiophene **148** was shown as not the main active component.

### 3.4 Phenylthiophenes

The fragment hit, (3-(thiophen-2-yl)phenyl)methanol (**71**) has a low affinity ( $IC_{50}$  226  $\mu$ M) compared to the sulfonamide **113** or thienopyrrole **108** with an  $IC_{50}$  of 65  $\mu$ M and 40  $\mu$ M, respectively. However, when the fragment's molecular size (non-hydrogen atoms) was taken into consideration, (3-(thiophen-2-yl)phenyl)methanol (**71**, LE 0.38 kcal/mol per HAC) was actually more ligand efficient than the sulfonamide (**113**, LE 0.36 kcal/mol per HAC).

Among the list of confirmed fragment hits were analogues 2-(thiophen-2-yl)aniline (**73**) and (2-(thiophen-2-yl)phenyl)methanol (**72**) (Figure 3-15). The 2-amino substituted analogue **73** showed high LE (0.39 kcal/mol per HAC), however was missed in the ranking of the top fragment hits (discussed in Chapter 2) because the initial single concentration assay tested the fragments at 1 mM. At 1 mM 2-(thiophen-2-yl)aniline (**73**) showed only 20% inhibition. During follow-up testing of analogues of phenylthiophene **71**, 2-(thiophen-2-yl)aniline (**73**) showed a surprising 81% inhibition at 0.5 mM, while the (2-(thiophen-2-yl)phenyl)methanol (**72**) maintained an inhibition of less than 20% at both 0.5 and 1 mM. The difference in inhibition values of the 2-(thiophen-2-yl)aniline (**73**) is likely due to limited solubility at higher concentration.

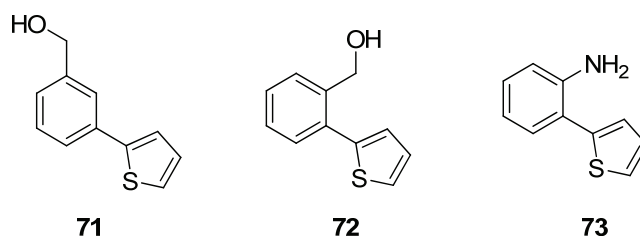


**Figure 3-15.** Identified 2-phenylthiophene KPR binders by  $^1H/^{15}N$ -HSQC NMR experiments

In Chapter 2, the binding of (3-(thiophen-2-yl)phenyl)methanol (**71**) to  $^{15}\text{N}$ -labelled KPR was examined using  $^1\text{H}/^{15}\text{N}$ -HSQC NMR. The (3-(thiophen-2-yl)phenyl)methanol (**71**) showed perturbations with residues Ser77, Ala79, Lys81 adjacent to the hydrophobic pocket (Arg31, Leu6, Leu71, and Gln75) where the adenine portion of NADPH (**24**) binds (Figure 3-16A). An additional cluster of perturbations were also observed above the pantoate-binding pocket suggesting either another binding site or the effect of conformational change. Although the perturbation patterns observed for 2-(thiophen-2-yl)aniline (**73**) and (2-(thiophen-2-yl)phenyl)methanol (**72**) (Figure 3-16B and Figure 3-16C) were different to (3-(thiophen-2-yl)phenyl)methanol (**71**), the clustering of perturbed residues were in and around the same hydrophobic pocket that accommodates the adenine portion of NADPH (**24**). Similarly, an additional cluster of perturbations above the pantoate-binding pocket were also observed, however, the affected residues were different between the analogues.

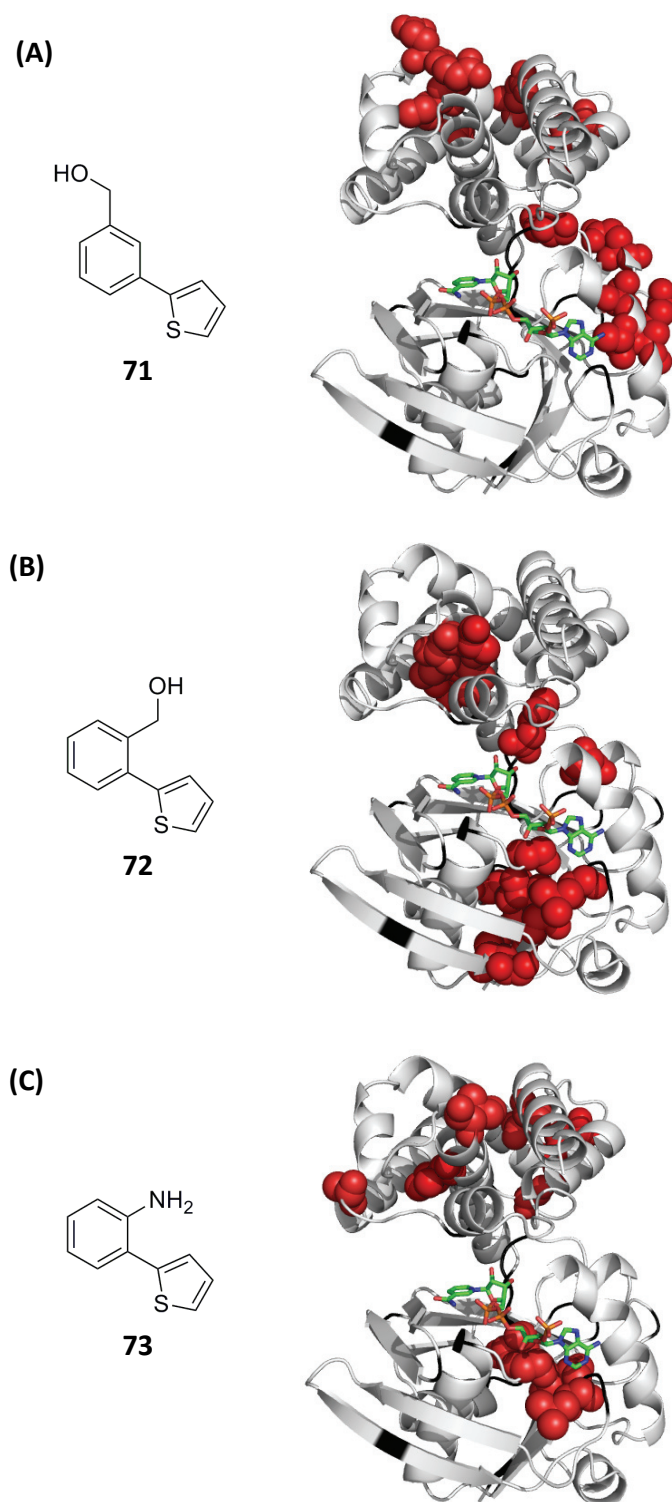


**Figure 3-16.** The residues that were perturbed on addition of (A) **71**, (B) **72** and (C) **73** were mapped onto the crystal structure (PDB ID: 1YJQ): Ribbon representation of KPR is shown and perturbations ( $\Delta\delta > 0.04$  ppm) are shown as red spheres. Unassigned residues are coloured black. NADP<sup>+</sup> shown as green carbons.

Note: NADP<sup>+</sup> was not included in the actual experiment but is included here to help visualise the binding pocket.

The *meta*-hydroxymethyl analogue **71** showed perturbed residues along the side of the hydrophobic pocket and towards the hinge region. The *ortho*-amino and *ortho*-hydroxymethyl analogue (**73** and **72**, respectively) showed perturbations in the hydrophobic pocket and localised around the binding cavity affecting residues Val5, Gly7 and Leu30 as highlighted in Figure 3-17. Presumably the difference in perturbation patterns observed suggests that the *meta*-hydroxymethyl derivative **71** may be binding in a slightly different orientation to the *ortho*-amino **73** and *ortho*-hydroxymethyl derivative **72**.

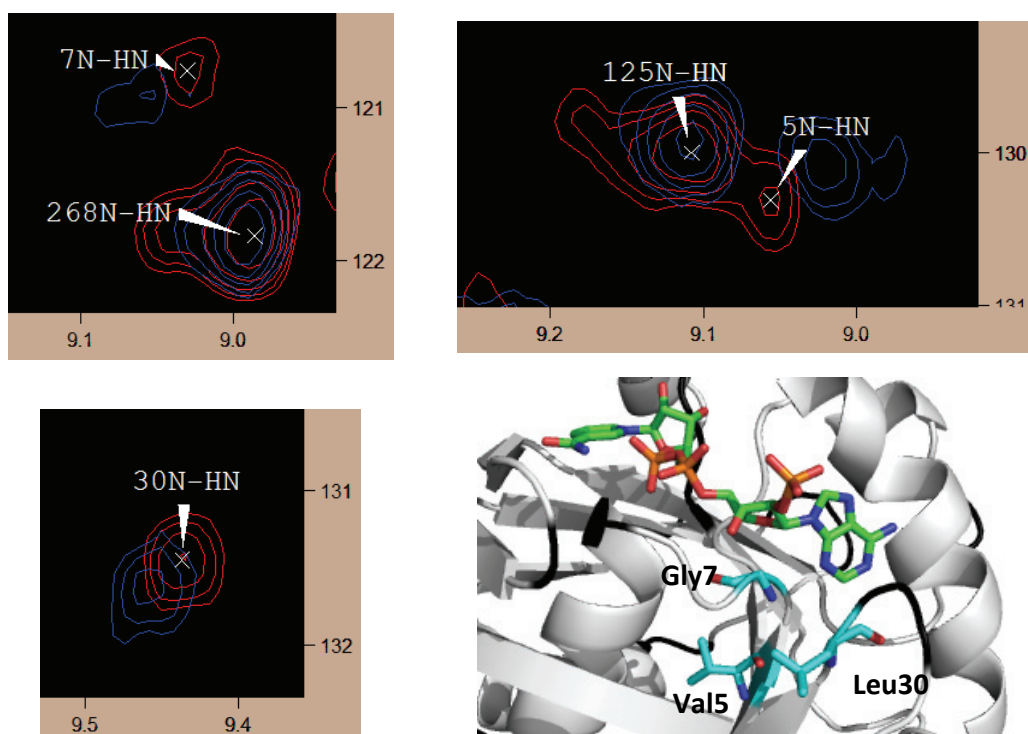


**Figure 3-17.** Portions of the HSQC spectrum of KPR in the absence (blue) and presence (red) of 2-(thiophen-2-yl)aniline (**73**): Ribbon representation of KPR (bottom right) with residues Val5, Gly7 and Leu30 shown as sticks with cyan coloured carbons and NADP<sup>+</sup> shown as green carbons.

Note: NADP<sup>+</sup> was not included in the actual experiment but is included here to help visualise the binding pocket.

### 3.4.1 SAR for phenylthiophenes

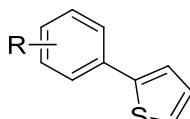
To investigate the importance of the substitution position (*ortho* or *para*) of the amino or hydroxymethyl moiety, its relevance to affinity and binding orientation, more substituted 2-phenylthiophene analogues were tested (**177** – **188**). Most analogues were sourced from commercial sources although the synthesis of 4-(thiophen-2-yl)aniline (**182**) was attempted as below.

The reaction involved coupling 4-iodoaniline in THF with one equivalent of thiophen-2-ylboronic acid and aqueous Na<sub>2</sub>CO<sub>3</sub> (1 M) in the presence of 0.1% mol Pd(PPh<sub>3</sub>)<sub>2</sub>Cl<sub>2</sub> as catalyst. The reaction mixture was heated at 120 °C for 1 h after which it was allowed to cool to room temperature and water was added to it. The aqueous layer was extracted with ethyl acetate and then concentrated. The crude oil was put through flash chromatography (ethyl acetate:hexane; 4:1), however the 4-iodoaniline and the desired product had a very similar *R<sub>f</sub>*, and could not be separated. The crude and partially purified 4-(thiophen-2-yl)aniline (**182**) readily degraded to a dark brown residue, and as a result **182** was not included in the initial round of testing.

To assess the biological activity of the 2-phenylthiophene derivatives, they were tested as outlined earlier (section 3.2.2). Across the series of 2-phenylthiophene derivatives, the substituted carboxylic acid and methylmethanamine derivatives generally had little to no effect on KPR activity (Table 3-7). On the contrary, the hydroxymethyl and methylamine substituted derivatives showed a consistent trend in increasing affinity from *ortho* > *meta* > *para*. The LE of the hydroxymethyl (**71** and **177**) and methylamine (**179** and **180**) substituted at the *meta* or *para* position also showed a consistent pattern

(Table 3-7). The amino derivatives (without the *para*-amino) showed a similar trend whereby affinity improved from *ortho* to *meta*.

**Table 3-7.** The % inhibition at 500  $\mu\text{M}$ ,  $\text{IC}_{50}$  and LE of the 2-phenylthiophene analogues are summarised<sup>5</sup>



R =	R position					
	<i>ortho</i>		<i>meta</i>		<i>para</i>	
	<b>72</b>	7% -	<b>71</b>	82% $\text{IC}_{50}$ 226 $\mu\text{M}$ LE 0.38	<b>177</b>	88% $\text{IC}_{50}$ 101 $\mu\text{M}$ LE 0.42
	<b>178</b>	45% -	<b>179</b>	77% $\text{IC}_{50}$ 260 $\mu\text{M}$ LE 0.38	<b>180</b>	93% $\text{IC}_{50}$ 108 $\mu\text{M}$ LE 0.42
	<b>73</b>	81% $\text{IC}_{50}$ 413 $\mu\text{M}$ LE 0.39	<b>181</b>	71% $\text{IC}_{50}$ 367 $\mu\text{M}$ LE 0.39	<b>182</b>	-
	<b>183</b>	1% -	<b>184</b>	44% -	<b>185</b>	41% -
	<b>186</b>	61% $\text{IC}_{50}$ 252 $\mu\text{M}$ LE 0.35	<b>187</b>	14% -	<b>188</b>	7% -

Another approach used to develop the SAR was to investigate around the 3-phenylthiophene scaffold wherein the hydroxymethyl, methylamine, amino,

<sup>5</sup> The data shown were analysed by standard KPR assay conditions: NADPH (**24**, 20  $\mu\text{M}$ ), ketopantoate (**22**, 1 mM), and KPR (3 nM) in 100 mM HEPES buffer (pH 7.6) with 2% DMSO (vol/vol).

carboxylic acid and methylmethanamine substituents at the *meta* and *para* position were examined. Due to the weak KPR activity observed from the *ortho* substituted 2-phenylthiophene analogues, they were not included. The 3-phenylthiophene analogues (**189** – **198**) studied were all sourced from commercial suppliers, except 4-(thiophen-3-yl)aniline (**194**) was synthesised. The same synthetic conditions as 4-(thiophen-2-yl)aniline (**182**) were used, in which one equivalent of 4-iodoaniline and thiophen-3-ylboronic acid were reacted. After work up, the crude oil was purified by flash chromatography (ethyl acetate:hexane; 1:2) and the desired product was isolated in high purity (> 99% by RP-HPLC). The <sup>1</sup>H NMR spectrum showed resonances of the amino moiety as a broad singlet at  $\delta$  3.71 ppm (NH<sub>2</sub>), the thiophene protons were assigned as H2', H4', H5' ( $\delta$  7.27 – 7.37 ppm) and *p*-substituted phenyl protons were assigned as H2, H6 ( $\delta$  6.72 ppm) and H3, H5 ( $\delta$  7.41 ppm) The ESI mass spectrum confirmed the molecular weight of **194** ( $m/z$  176, (M – H)<sup>+</sup>).

The resulting activity of the 3-phenylthiophene derivatives showed a trend comparable to the 2-phenylthiophene. For example, substitutions with the hydroxymethyl (**189** and **190**) and methylamine (**191** and **192**) moiety showed affinity increasing from *meta* to *para* (Table 3-8). The substituted carboxylic acids (**195** and **196**) showed no KPR activity, while the substituted methylmethanamine (**197** and **198**) and the amino (**193** and **194**) derivatives also showed affinity increasing from *meta* to *para* (Table 3-8). Interestingly, the LE remained constant (0.42 kcal/mol per HAC) for the *para* substituted hydroxymethyl and methylamine of either 2- or 3-phenylthiophene. However, the *para*-amino (**194**) was the most ligand efficient with LE 0.46 kcal/mol per HAC.

**Table 3-8.** The % inhibition, IC<sub>50</sub> and LE of the 3-phenylthiophene analogues are summarised<sup>6</sup>

R =	R position			
	<i>meta</i>		<i>para</i>	
	<b>189</b>	24% -	<b>190</b>	96% IC <sub>50</sub> 103 μM LE 0.42
	<b>191</b>	44% -	<b>192</b>	93% IC <sub>50</sub> 107 μM LE 0.42
	<b>193</b>	69% IC <sub>50</sub> > 500 μM LE ~0.35	<b>194</b>	96% IC <sub>50</sub> 82 μM LE 0.46
	<b>195</b>	2% -	<b>196</b>	3% -
	<b>197</b>	40% -	<b>198</b>	95% IC <sub>50</sub> 192 μM LE 0.36

<sup>6</sup> The data shown were analysed by standard KPR assay conditions: NADPH (**24**, 20 μM), ketopantoate (**22**, 1 mM), and KPR (3 nM) in 100 mM HEPES buffer (pH 7.6) with 2% DMSO (vol/vol).

Up to this point, only changes to the substitution pattern of the six-membered ring have been investigated whilst little has been done to optimise the five-membered heteroaromatic ring. Therefore, keeping the benzylalcohol the same, the thiophene ring was replaced with either furan or thiazole. All the analogues (**71**, **189**, **198** – **200**) were purchased from commercial sources except the 3-furan analogue **200** which was synthesised using synthetic conditions as described for 4-(thiophen-2-yl)aniline (**182**). The reaction involved coupling (3-iodophenyl)methanol and 1.1 equivalents of furan-3-ylboronic acid. After work up, the crude oil was purified by flash chromatography (ethyl acetate:hexane; 1:2) and the desired product was isolated in high purity (> 97% by RP-HPLC). The <sup>1</sup>H NMR spectrum of **200** showed incorporation of the 3-furan ring by the presence of the resonance at δ 6.72 ppm (1H, s, H4"), 7.48 ppm (1H, s, H5") and 7.75 ppm (1H, s, H2"). The ESI mass spectrum confirmed the molecular weight of **200** (*m/z* 157, (M – OH)<sup>+</sup>).

The compounds were tested at 500 μM in a % inhibition assay. The thiazole analogue **201** and 3-thiophene analogue **189** were excluded from more studies as it showed weak KPR inhibition (Table 3-9). Subsequent IC<sub>50</sub> determination for 2-furan **199** and 3-furan **200** derivatives yielded markedly improved affinity by 4- and 11-fold, respectively (Table 3-9).

**Table 3-9.** The % inhibition, IC<sub>50</sub> and LE of the *meta*-benzylalcohol analogues are summarised<sup>7</sup>

	<b>R =</b>	<b>%</b>	<b>IC<sub>50</sub></b>	<b>LE</b>
<b>71</b>		82%	226 μM	0.38
<b>189</b>		24%	-	-
<b>199</b>		82%	20 μM	0.49
<b>200</b>		81%	53 μM	0.45
<b>201</b>		3%	-	-

<sup>7</sup> The data shown were analysed by standard KPR assay conditions: NADPH (**24**, 20 μM), ketopantoate (**22**, 1 mM), and KPR (3 nM) in 100 mM HEPES buffer (pH 7.6) with 2% DMSO (vol/vol).

### 3.4.2 Chemical shift mapping

A number of 2- and 3-phenylthiophene analogues that showed KPR inhibition were further characterised by  $^1\text{H}/^{15}\text{N}$ -HSQC NMR to investigate their binding. Of interest was to determine whether there are any correlations between the substitution position on the phenylthiophene, binding location and affinity. Particularly, for the *para* substituted hydroxymethyl and methylamine substituted 2- and 3-phenylthiophenes which have resulted in higher LE.

The perturbations of (3-(thiophen-2-yl)phenyl)methanol (**71**) and (2-(thiophen-2-yl)phenyl)methanol (**72**) were shown earlier to be in and around the hydrophobic pocket. The subsequent phenylthiophenes studied by  $^1\text{H}/^{15}\text{N}$ -HSQC NMR also shared perturbation patterns generally localised in the hydrophobic pocket (Figure 3-18). With the exception of (2-(thiophen-2-yl)phenyl)methanol (**72**), all the phenylthiophenes in Figure 3-18 showed perturbations of residues (Ser77, Ala79, Lys81) adjacent to the hydrophobic pocket (Arg31, Leu6, Leu71, and Gln75) where the adenine portion of NADPH (**24**) binds. An additional cluster of perturbations were observed above the pantoate-binding pocket only for the *ortho* and *meta* substituted 2-phenylthiophene (**72**, **71**, **179**) in which these clustering were different from each other.

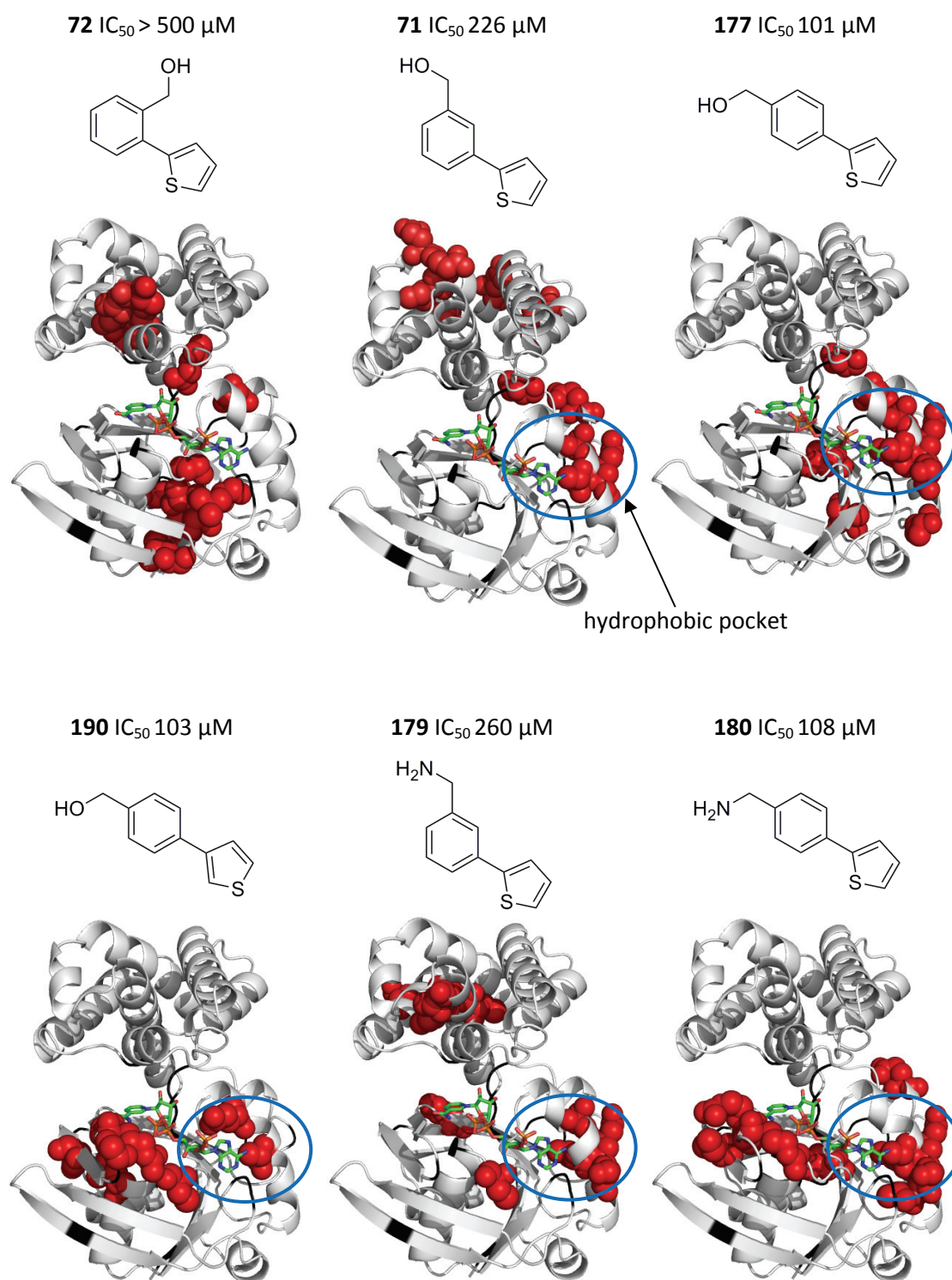


**Figure 3-18.** The residues that were perturbed on addition of fragment are mapped onto the crystal structure (PDB ID: 1YJQ): Ribbon representation of KPR. Perturbations ( $\Delta\delta > 0.04$  ppm) are shown as red spheres. The blue circle highlights perturbed residues in the hydrophobic region. Unassigned residues are coloured black. NAD<sup>+</sup> shown as green carbons.

Note: NAD<sup>+</sup> was not included in the actual experiment but is included here to help visualise the binding pocket.

The SAR study of the five-membered heteroaromatic ring, identified the 2-furan derivative **199** as 11-fold more potent than the initial fragment hit (3-(thiophen-2-yl)phenyl)methanol, **71**). Therefore, the CSPs for the (3-(furan-2-yl)phenyl)methanol (**199**) were determined and its binding location investigated. Analysis of the residues affected in the presence of the 2-phenylfuran **199** showed a large cluster of perturbed residues (Leu71, Gln75, Ala79 – Lys81) localised in the hydrophobic pocket (Figure 3-19). Away from the large clustering were also perturbed distal residues presumably affected by local conformational changes.

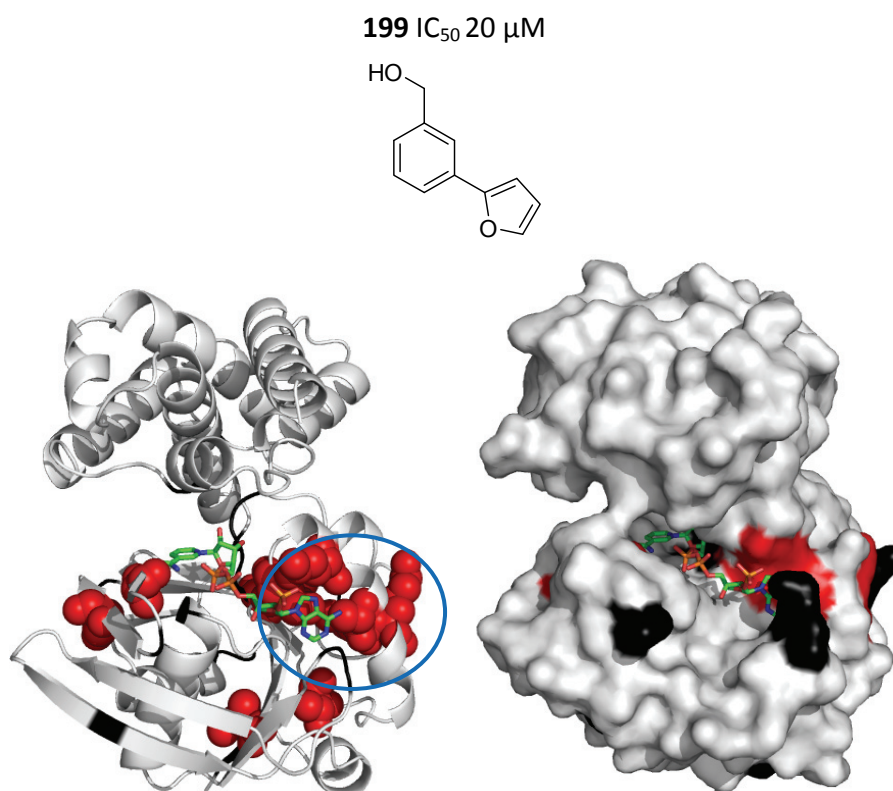
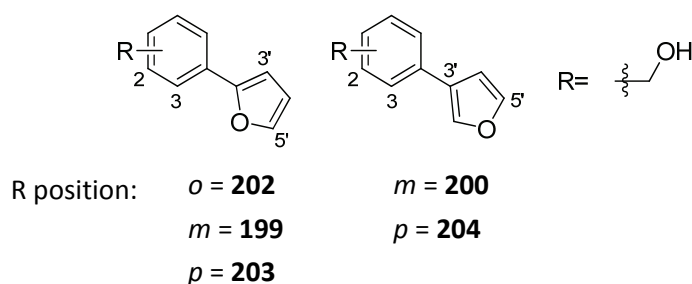


**Figure 3-19.** The residues that were perturbed on addition of **199** are mapped onto the crystal structure (PDB ID: 1YJQ): Ribbon (left) and surface (right) representation of KPR. Perturbations ( $\Delta\delta > 0.04$  ppm) are shown as red spheres. The blue circle highlights perturbed residues in the hydrophobic region. Unassigned residues are coloured black. NADP<sup>+</sup> shown as green carbons.

Note: NADP<sup>+</sup> was not included in the actual experiment but is included here to help visualise the binding pocket.

### 3.4.3 SAR for phenylfurans

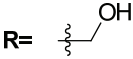
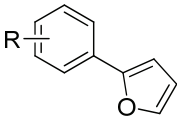
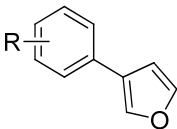
The 2-phenylfuran **199** showed CSPs in the same hydrophobic pocket as the phenylthiophene, yet there was a significant improvement in KPR activity by the 2- and 3-phenylfuran derivatives (**199** and **200**), which prompted investigations into the scaffold. A similar approach to the phenylthiophene SAR study was used. To begin with, the optimal substitution position of the hydroxymethyl moiety on the phenylfuran (reflected in high LE) was investigated. The study was undertaken for both 2- and 3-phenylfuran derivatives (Figure 3-20). The 2-phenylfuran derivatives (**199**, **202** – **203**) were sourced from commercial suppliers and the 3-phenylfuran derivatives (**200** and **204**) were synthesised using the Suzuki reaction as described for the synthesis of 4-(thiophen-2-yl)aniline (**182**). The coupling reaction for **204** was analysed by  $^1\text{H}$  NMR. Resonances of the hydroxyl methyl group at  $\delta$  1.67 ppm (1H, br s, OH) and 4.70 ppm (2H, s,  $\text{CH}_2$ ). Aromatic protons of the 3-phenylfuran were assigned with resonances at  $\delta$  6.70 ppm (1H, dd,  $J = 0.9, 1.8$  Hz,  $\text{H}4''$ ), 7.38 ppm (2H, app d,  $J = 8.5$  Hz,  $\text{H}2'$ ,  $\text{H}6'$ ), 7.47 – 7.51 ppm (3H, m,  $\text{H}5''$ ,  $\text{H}3'$ ,  $\text{H}5'$ ), 7.74 ppm (1H, dd,  $J = 1.0, 1.4$  Hz,  $\text{H}2''$ ) in the  $^1\text{H}$  NMR spectrum. The ESI mass spectrum confirmed the molecular weight of **204** ( $m/z$  157,  $(\text{M} - \text{OH})^+$ ).



**Figure 3-20.** Hydroxymethyl substitutions on 2- and 3-phenylfuran

To assess the biological activity of the 2- and 3-phenylfuran derivatives, they were tested as outlined earlier (section 3.2.2). In Table 3-10, the *meta*-hydroxymethyl analogue **199** of the 2-phenylfuran derivatives was by far the most active with an  $IC_{50}$  20  $\mu$ M. For the 3-phenylfuran derivatives, both the *meta* (**200**) and *para* (**204**) substituted hydroxymethyls achieved high affinity with an  $IC_{50}$  of 53  $\mu$ M and 65  $\mu$ M, respectively. However, the (3-(furan-2-yl)phenyl)methanol (**199**) was still the most potent and ligand efficient.

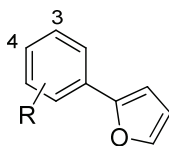
**Table 3-10.** The effects of hydroxymethyl substituted 2- and 3-phenylfuran analogues on KPR activity: The % inhibition,  $IC_{50}$  and LE are summarised.<sup>8</sup>

	R= 					
	<i>ortho</i>		<i>meta</i>		<i>para</i>	
	<b>202</b>	2% -	<b>199</b>	82% $IC_{50}$ 20 $\mu$ M LE 0.49	<b>203</b>	26% -
	<b>NA</b>		<b>200</b>	81% $IC_{50}$ 53 $\mu$ M LE 0.45	<b>204</b>	89% $IC_{50}$ 65 $\mu$ M LE 0.44

<sup>8</sup> The data shown were analysed by standard KPR assay conditions: NADPH (**24**, 20  $\mu$ M), ketopantoate (**22**, 1 mM), and KPR (3 nM) in 100 mM HEPES buffer (pH 7.6) with 2% DMSO (vol/vol).

A broader SAR around the 2-phenylfuran template was analysed by substituting the hydroxymethyl with the corresponding methylamino, amino, carboxylic acid and methylmethanamine at the *meta* and *para* position (**205** – **212**). Noticeably in Table 3-11, only the *para* substituted methylamine **206** and amino **208** analogues showed significant KPR activity with an IC<sub>50</sub> of 14 μM and 29 μM, respectively. Both compounds (**206** and **208**) were slightly more ligand efficient than the initial *meta*-hydroxymethyl analogue **199**. The carboxylic acid (**184** and **185**) and the methylmethanamine (**187** and **188**) substituted analogues showed weak KPR activity, following a similar trend to that observed in the phenylthiophene derivatives.

The SAR of the 2-phenylfuran shows that across the substituted hydroxymethyl derivatives, the *meta* position was clearly preferred, however substitutions with either methylamino or amino derivatives show the *para* position was preferred. At this stage, the reasons for this different substitution preference are not clear, however potentially the hydroxymethyl substituted derivatives are binding in a different orientation with different interactions.

**Table 3-11.** Effects on KPR activity from varying substituents on the 2-phenylfuran scaffold: The % inhibition, IC<sub>50</sub> and LE are summarised.<sup>9</sup>

R =	R position			
	<i>meta</i>		<i>para</i>	
	<b>205</b>	30%	<b>206</b>	99% IC <sub>50</sub> 14 μM LE 0.51
	<b>207</b>	6%	<b>208</b>	89% IC <sub>50</sub> 29 μM LE 0.52
	<b>209</b>	32%	<b>210</b>	10%
	<b>211</b>	5%	<b>212</b>	4%

To examine substitutions at the *para* position on the 2- and 3-phenylfuran, substituents such as dimethylamine, acetamide and amide were prepared (**213** – **218**). The phenylfurans were synthesised using a Suzuki-Miyaura reaction as described for the synthesis of 4-(thiophen-2-yl)aniline (**182**). A range of arylhalides were coupled to the furanyl boronic acid using a single set of reaction conditions. The yields from the Pd-catalysed couplings ranged from 27 to 75%, obtaining adequate amounts of the desired products for biochemical evaluation (Table 3-12).

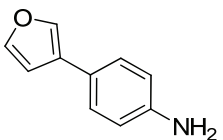
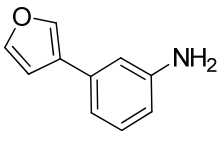
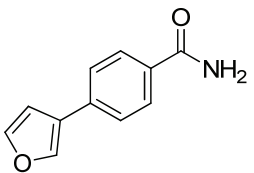
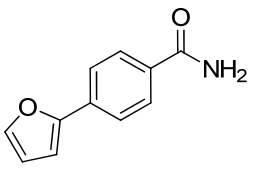
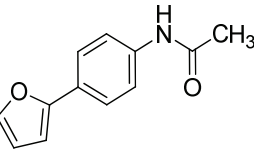
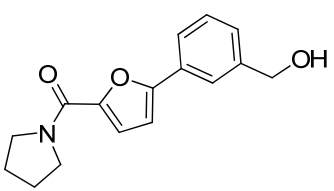
<sup>9</sup> The data shown were analysed by standard KPR assay conditions: NADPH (**24**, 20 μM), ketopantoate (**22**, 1 mM), and KPR (3 nM) in 100 mM HEPES buffer (pH 7.6) with 2% DMSO (vol/vol).

The synthesised 2- and 3-phenylfuran analogues were evaluated in the biochemical assay and their potency measured. The resulting activity of the *para* substituted 2-phenylfuran analogues suggested the acetamide **218** and dimethylamine **217** retained some of the activity ( $IC_{50}$  350  $\mu$ M and 367  $\mu$ M, respectively) while the amide **216** showed weak KPR inhibition (Table 3-12). The amide substituted on the 3-phenylfuran **215** also showed relatively weak KPR inhibition. The *meta* and *para* substituted amino group on the 3-phenylfuran (**214** and **213**) showed weak KPR inhibition with 21% and 45%, respectively. The weak activity of the *para* substituted amino **213** was unexpected as previous testing suggested the corresponding 2-phenylfuran (i.e. 4-(furan-2-yl)aniline **208**) was approximately 35-fold more active.

To begin to examine substitution on the furan, (3-(furan-2-yl)phenyl)methanol (**199**) with a pyrrolidine carboxamide **219** was purchased and tested. The compound showed low solubility at 500  $\mu$ M; however once tested at lower concentrations, the activity looked promising with an  $IC_{50}$  of 44  $\mu$ M. Although, the pyrrolidine carboxamide **219** showed a modest decrease in LE compared to the starting (3-(furan-2-yl)phenyl)methanol (**199**), it remains above the desirable limit of 0.3.

Overall, the activities for the furan derivatives were unexpected, particularly for the *para* substituted 2-phenylfuran analogues. The synthesised derivatives were far less active (by up to 35-fold) compared to the *para*-methyl amine **206** or *para*-amino **208** analogues.

**Table 3-12.** The % inhibition and IC<sub>50</sub> of synthesised 2- and 3-phenylfuran analogues are summarised<sup>10</sup>

	Structure	Inhibition (%)	IC <sub>50</sub> (μM)
213		45	-
214		21	-
215		37	-
216		17	-
217		-	367
218		-	350
219		-	44

<sup>10</sup> The data shown were analysed by standard KPR assay conditions: NADPH (**24**, 20 μM), ketopantoate (**22**, 1 mM), and KPR (3 nM) in 100 mM HEPES buffer (pH 7.6) with 2% DMSO (vol/vol).

### 3.4.4 Summary

Clear SAR trends are emerging for the 2- and 3-phenylthiophenes strongly suggesting substitutions of the hydroxymethyl and methylamine at the *para*-position was preferred, resulting in higher LE. Higher affinities for substitutions at the *para* position were more pronounced among the 3-phenylthiophene derivatives investigated. Undoubtedly, the negative charge of the carboxylic acid derivatives was detrimental for KPR inhibition, while a neutral or positive charge were equally favourable for KPR activity. The methylmethanamine derivatives generally showed weak KPR activity.

All the phenylthiophenes studied by  $^1\text{H}/^{15}\text{N}$ -HSQC NMR shared perturbation patterns generally localised around the hydrophobic pocket. With exceptions to the *ortho* substituted analogues (**73** and **72**), the phenylthiophenes showed perturbations of residues (Ser77, Ala79, Lys81) adjacent to the hydrophobic pocket (Arg31, Leu6, Leu71, and Gln75). Similarly, the residues affected in the presence of the 2-phenylfuran **199** were localised in the hydrophobic pocket (Leu71, Gln75, Ala79 – Lys81).

The significant improvement in KPR activity by the 2- and 3-phenylfuran derivatives (**199** and **200**) led to further investigations into the scaffold. The SAR around (3-(furan-2-yl)phenyl)methanol (**199**) summarised in Figure 3-21 suggested the scaffold was optimal as a starting point and identifying the pyrrolidine carboxamide **219** highlighted the potential for elaboration at the 5-position on the furan to increase potency. At this point in time, a decision to pursue either the phenylfuran or phenylthiophene series was required; however, given the similar levels of activity between the two series, it was not obvious which was preferable. As will become apparent in Chapter 4, this decision became less important.

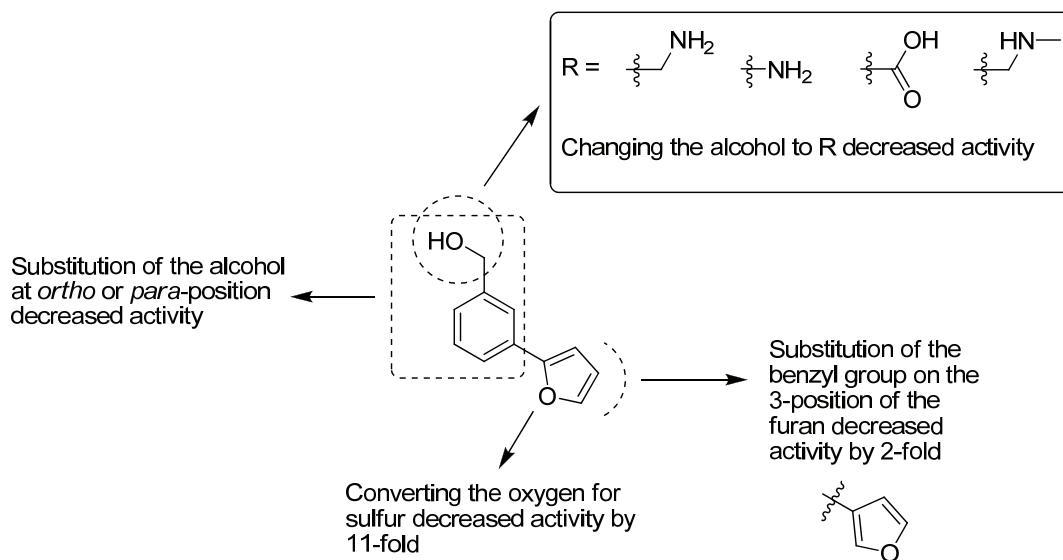


**Figure 3-21.** SAR study of the phenylfuran

### 3.5 Conclusions

Efforts at initial hit development for selected fragments sulfonamide **113**, thienopyrrole **108** and phenylthiophene **71** have been described. An iterative approach was adopted, in which preliminary SAR was quickly obtained by testing obvious analogues from readily available commercial suppliers or otherwise synthesised. The binding location of the compounds on KPR was evaluated by  $^1\text{H}/^{15}\text{N}$ -HSQC NMR, and their potency and LE tracked. The preliminary SAR was subsequently used to judge whether the scaffold was worth pursuing and direct further synthesis of analogues or larger molecules to optimise binding and improve the potency.

After two iterations of testing involving 43 sulfonamide analogues, only 5 compounds demonstrated inhibitory activity with  $\text{IC}_{50} < 500 \mu\text{M}$  and just one showing a modest improvement in potency compared to the lead sulfonamide **113**. In this case, the chemical modifications of the compounds caused only small changes in the biological activity suggestive of a ‘flat SAR’.<sup>205</sup> Furthermore, the relationship was unclear between the compounds that showed KPR activity and those that did not.

The preliminary SAR analysis of the thienopyrrole analogues showed most derivatives retained some of the activity; however the isostere thienothiophene **148** showed a 4-fold improvement in affinity. During the synthesis and SAR development of thieno[3,2-*b*]thiophene analogues, it was discovered that the main component was actually inactive and in fact an unidentified tiny impurity was responsible for all the KPR inhibition.

For the phenylthiophenes, an apparent SAR was observed and the testing of phenylfuran derivatives showed some improvement in KPR activity. However, the decision to pursue elaboration based on the phenylfuran scaffold or go back to the phenylthiophene scaffold was pending until further analysis.

The flat SAR of the sulfonamide and identifying the lead thienothiophene as false positive raised concerns about the fragment hits. The next chapter describes efforts to assess the fragment hits in relation to the possibility that they may be false positives.

# Chapter 4

---

## Screening evaluation and optimisation

## 4 Screening evaluation and optimisation

### 4.1 Introduction

Efforts to improve fragment hits raised the prospect that some or all of these hits may be false positives. False positives arise from compounds that are for example reactive, aggregators or interfere with the screen/assay signal and consequently affect the target protein or the detection method. Screening of compound libraries at 0.1 to 1 mM has been reported to increase the number false-positives due to aggregation.<sup>206-207</sup>

#### 4.1.1 What is aggregation?

At micromolar concentrations, many organic small molecules form aggregates of ~30 – 1000 nm in diameter in aqueous solution.<sup>208</sup> It is estimated that each aggregate contains approximately  $10^8$  small-molecule monomers which are densely packed.<sup>207</sup> When aggregates are formed, they can bind to many sites on proteins and non-specifically inhibit their activity. These molecular aggregates have steep dose-response curves, show little relationship between structure and activity, and non-specifically inhibit enzyme targets.<sup>209</sup> Such compounds have been known for some time among pharmaceutical companies but the mechanism and properties of these aggregation-based inhibitions were obscure.<sup>208</sup>

When high-throughput methods slowly became more tractable in academic laboratories,<sup>210</sup> McGovern and co-worker's<sup>209</sup> published a controversial report suggesting many compounds in HTS collections actually form aggregates at screening concentrations in buffer and that these aggregates can interact with enzyme targets to produce false-positive hits. Shoichet<sup>208</sup> described their frustration and confusion at trying

to understand these aggregates, initially speculating the compounds to be covalent inhibitors or denaturants. To this day, exactly how the aggregates cause inhibition remains poorly understood.<sup>211</sup>

#### **4.1.2 Proposed mechanism of aggregation-based inhibition**

Although the exact mechanism of aggregation-based inhibition remains unknown, the general understanding of the characteristics of aggregates have improved since McGovern and co-worker's first report in 2002.<sup>209</sup> The mechanism of aggregation-based inhibition was initially thought to proceed *via* complete denaturation of the target enzyme however, several studies have suggested otherwise.<sup>209,212</sup> Firstly, an enzyme could rapidly refold into its active state upon addition of detergent, which seems unlikely if it has been denatured. Secondly, a test study using green fluorescent protein showed its ability to retain fluorescence while bound to an aggregate.<sup>212</sup> Finally, the addition of denaturants such as guanidinium or urea did not correspond to an increase of inhibition by aggregates.<sup>209</sup>

To understand the mechanism of action of aggregation-based inhibition, Coan *et al.*<sup>211</sup> used hydrogen-deuterium exchange mass spectroscopy (HDX MS). This technique is commonly employed to measure changes in solvent accessibility, particularly for protein folding/unfolding or protein-protein interactions. HDX MS relies on the different exchange rates of backbone amide protons in a deuterated solvent. A change in mass is observed when deuterium replaces hydrogen. Coan *et al.*<sup>211</sup> found an increase of deuterium exchange affecting 41% of the backbone amide protons in the presence of all the aggregators. The increase in proton accessibility upon aggregate binding is consistent with partial protein unfolding. Additionally, as partially unfolded protein is

more susceptible to protease degradation, they observed significant digestion for the  $\beta$ -lactamase-aggregate complexes in the presence of trypsin, compared to non-aggregate enzyme complexes.

### 4.1.3 Characteristics of aggregation-based inhibition

False positive aggregation-based inhibition generally shows sensitivity to changes in enzyme concentrations. For example increasing an enzyme concentration 10-fold, increases the  $IC_{50}$  values or eliminates the observed inhibition.<sup>209</sup> This is an unusual phenomenon considering the inhibitor is present at concentrations 1,000- to 1,000,000-fold higher than that of the enzyme. However, a study has shown that the aggregates themselves are present only in the mid-femtomolar ( $10^{-15}$ ) range. Since the stoichiometry of binding is about 10,000 enzyme molecules per aggregate particle (Figure 4-1), the low concentration of the aggregates explains their sensitivity to changes in enzyme concentration.<sup>207</sup>

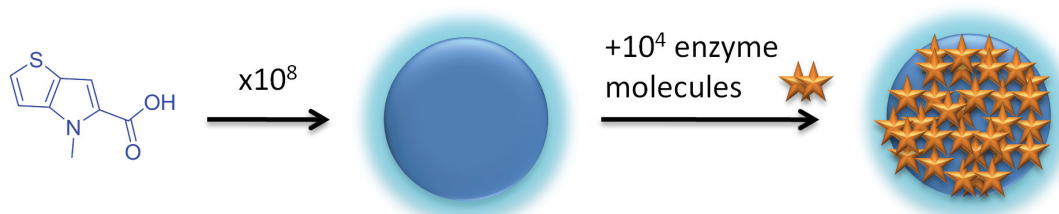


**Figure 4-1.** Model of aggregate structure and enzyme binding.<sup>207</sup> Structure shown in blue, thienopyrrole **108** is an example that can form aggregates in aqueous media. The aggregate particles then inhibit enzyme with approximately  $10^4$  enzyme molecules per aggregate.

Steep dose-response curves are another common characteristic of aggregation-based inhibition suggesting multisite binding. For such compounds, the dose-response curves show inhibition occurs in a narrow concentration range.<sup>206,213-214</sup> For example, in Figure 4-2, aggregation-based inhibition is apparent for the black slope when a rapid decline in the % activity was observed as the inhibitor concentration was approaching 1  $\mu\text{M}$ . For this inhibitor, aggregates form at approximately 1  $\mu\text{M}$  and subsequently bind to multiple enzymes preventing any catalytic turn-over. Classical, single-site inhibition generally increases from 10% to 90% inhibition over approximately a 2 log unit concentration range, as shown in the red curve in Figure 2.<sup>213-214</sup>

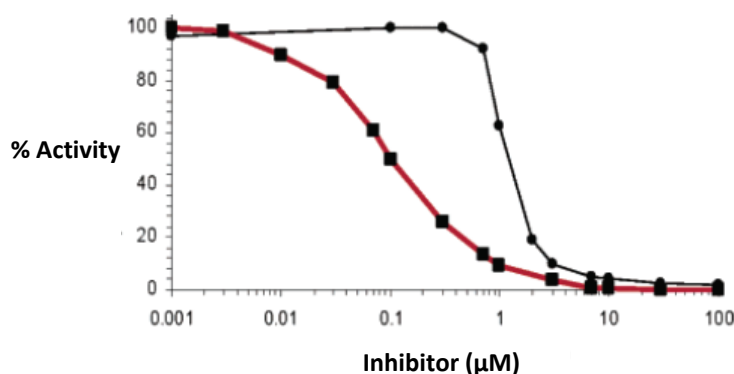


**Figure 4-2.** Dose-response curves of a classical inhibitor (■) and aggregation-based inhibitor (●) Reprinted with permission from (*J. Med. Chem.* 2006, 49 (25), 7274-7277).<sup>213</sup> Copyright (2012) American Chemical Society

Another way to identify aggregation-based inhibition is to add BSA to the enzyme assay. BSA has the unique ability to bind to many different classes of compounds but has also been found to attenuate non-specific inhibition of aggregates.<sup>209,215-218</sup> The addition of milligram per millilitre concentrations of BSA prior to the addition of the target enzyme have shown to prevent aggregation based inhibition of the enzyme turnover.<sup>216,218</sup> The action of BSA can be explained through two possible mechanisms, either (a) the addition of BSA binds to and saturates the aggregate preventing the

aggregates binding to target enzyme or (b) BSA disrupts the formation of aggregates. A study using dynamic light scattering (DLS) has shown a relatively unchanged number of aggregates in the presence of BSA suggesting inhibition is prevented by saturating the aggregates.<sup>217</sup>

However to establish the existence of aggregates in solutions, DLS measurements have been used.<sup>207,212</sup> Aggregates are ~30 – 1000 nm in diameter in aqueous solution which is within the DLS detectable range (0.3 nm - 10 microns). DLS measures the Brownian motion (the random movement of particles suspended in a fluid) and relates this to the size of the particle. Therefore, as a beam of light passes through a colloidal dispersion, the particles scatter light and the fluctuation in scattering intensity based on the speed of movement is measured and used to calculate the particle size (Figure 4-3). Large amounts of movement where the particle positions are quite different correspond to smaller particles and higher frequency in scattering intensity; however when there has been only small movements and the particle positions are very similar, then the particles in the sample will be large corresponding to lower frequency in scattering intensity.

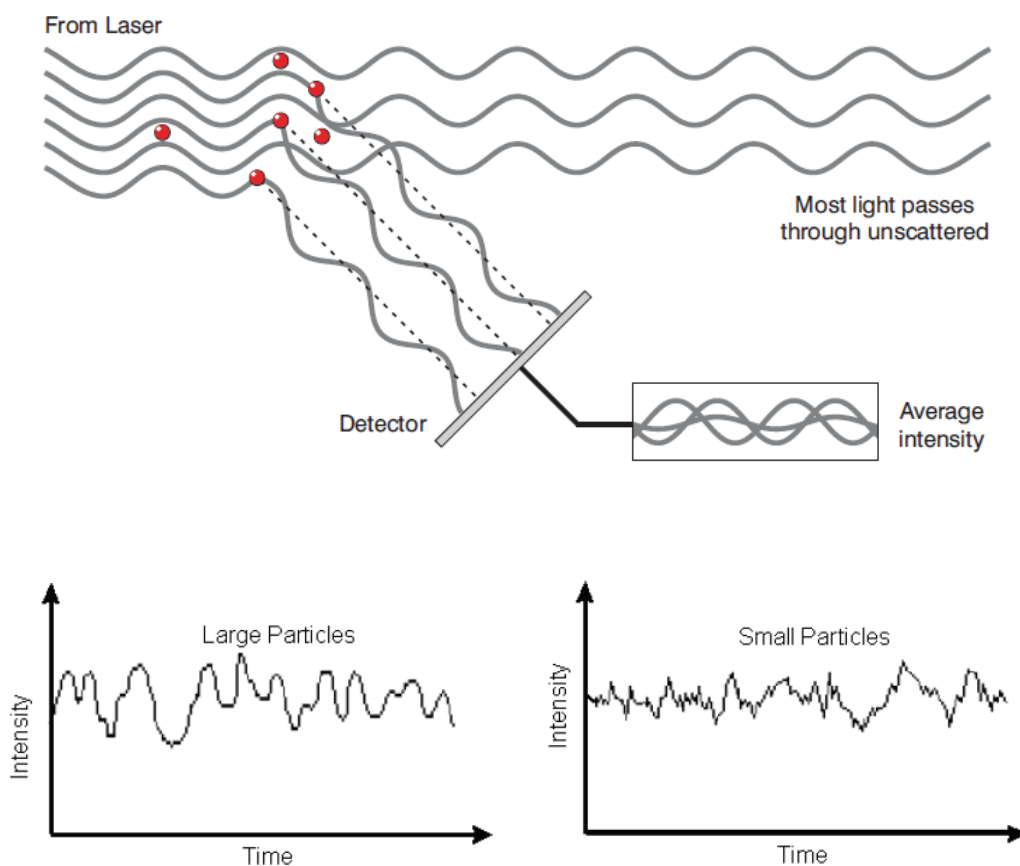


**Figure 4-3.** Top: A schematic diagram of scattered light falling on the detector; Bottom: the fluctuation in the intensity of scattered light as a function of time.

(<http://www.malvern.com/common/downloads/campaign/MRK656-01.pdf>)

In this chapter, common characteristics of aggregation-based inhibition such as steep dose-response curves, binding to unrelated proteins and sensitivity to the presence of detergent were used to assess whether the fragment hits thienopyrrole **108**, sulfonamide **113** and phenylfuran **199** are false positives acting through aggregation. Also described is the optimisation of the STD-NMR screen and enzyme assay to allow for better identification of specific binders to reduce false-positives.

## 4.2 Characterisation of aggregation-based false positives

### 4.2.1 Steep dose-response curves: Sulfonamide series

The fragment hit 4-(piperidin-1-ylsulfonyl)aniline (**113**) was confirmed by  $^1\text{H}/^{15}\text{N}$ -HSQC NMR to bind to KPR and also showed reasonable inhibitory activity. Therefore, more sulfonamide analogues were tested and interestingly a large proportion of these analogues were less potent. A closer inspection of their dose-response curves (**113** and **124** shown as an example in Figure 4-4) for the sulfonamide series showed close resemblance to those reported by Shoichet indicating inhibition may be through non-classical binding.<sup>213</sup>

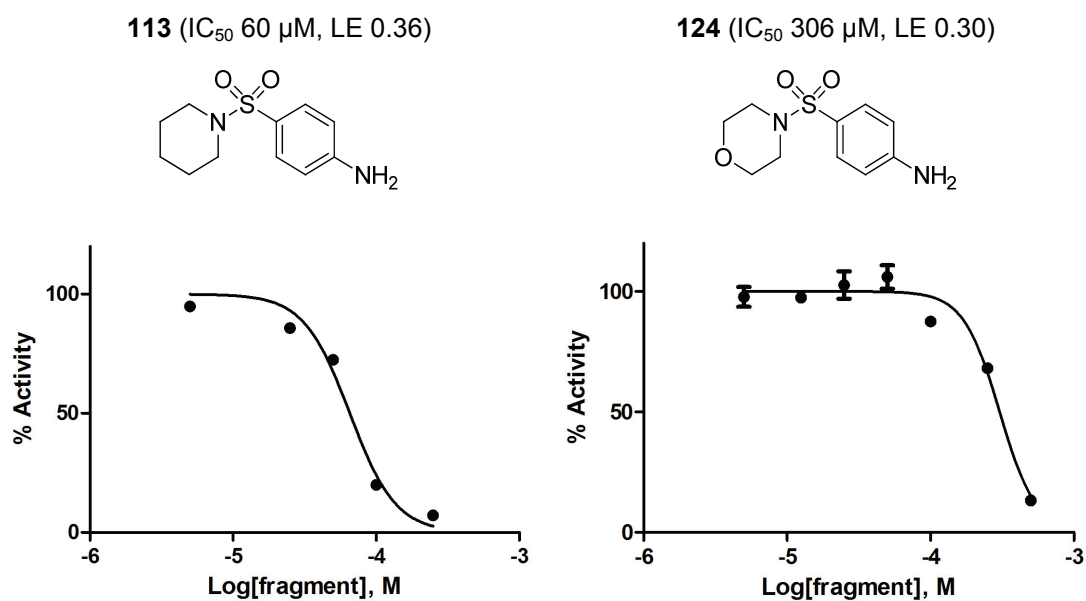


Figure 4-4. Dose-response curves of sulfonamide analogues

#### 4.2.2 Non-specific interactions: bovine serum albumin

The fragments thienopyrrole **108**, sulfonamide **113** and phenylfuran **199** were tested for their ability to inhibit KPR in the presence of BSA and examine whether introducing BSA would interfere with the enzyme assay. Therefore control experiments were initially performed with three concentrations of BSA, 0.1, 0.5 and 1 mg/mL. No change in KPR activity was observed, therefore, the thienopyrrole **108**, sulfonamide **113** and phenylfuran **199** were tested at 100  $\mu$ M using standard UV-based enzyme assay conditions in the presence and absence of BSA.

The testing revealed a similar pattern for all three hit compounds in the presence and absence of BSA (Figure 4-5). When BSA is present at 0.1, 0.5 or 1 mg/mL, no inhibition of KPR activity was observed. On the other hand, the fragments show complete KPR inhibition in the absence of BSA.

The results are suggestive that the thienopyrrole **108**, sulfonamide **113** and phenylfuran **199** are binding to KPR non-specifically. Even when the stoichiometry of binding is about 10,000 enzyme molecules per aggregate particle, BSA's relatively non-specific binding site is taken into consideration, or that the fragments may coincidentally bind more strongly to BSA than KPR, the concentration of fragments is several fold higher than that of both proteins present in the assay. Therefore, if any of these fragments were genuine inhibitors then some inhibition should have been observed in the presence of BSA.

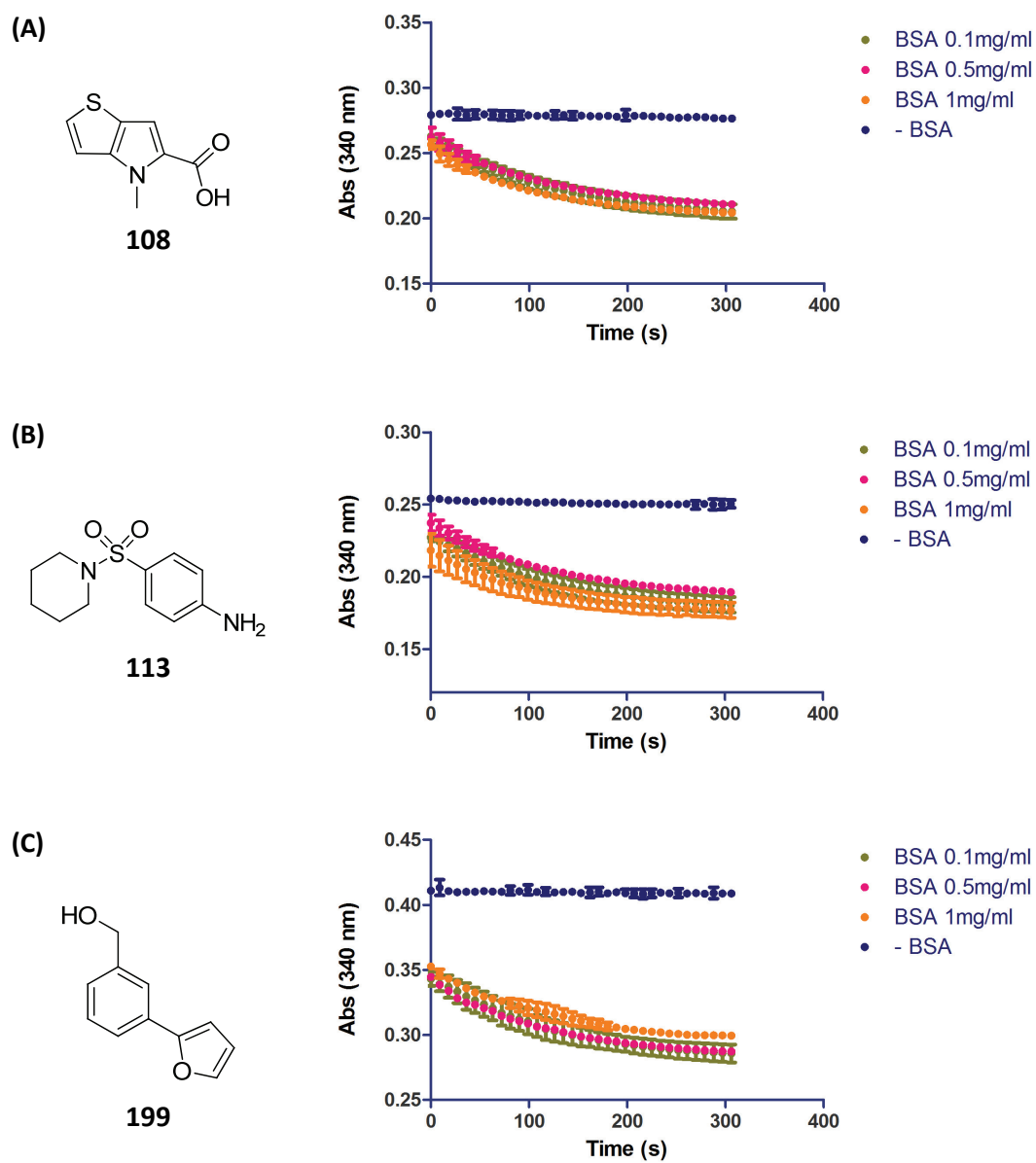


**Figure 4-5.** Measure of KPR activity in the presence of BSA for (A) thienopyrrole **108** (B) sulfonamide **113**, and (C) phenylfuran **199**

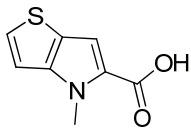
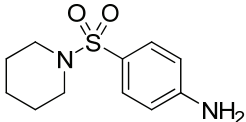
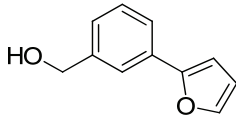
### 4.2.3 Dynamic light scattering

DLS was employed to determine the presence of aggregates and measure their particle size. Using the same buffer conditions as the enzyme assay, the three fragments **108**, **113** and **199** were examined at 500  $\mu\text{M}$ . Fragment concentrations of 50 and 100  $\mu\text{M}$  were also investigated to determine whether at concentrations close to their  $\text{IC}_{50}$  values, they were inhibiting *via* aggregation in the enzyme assay.

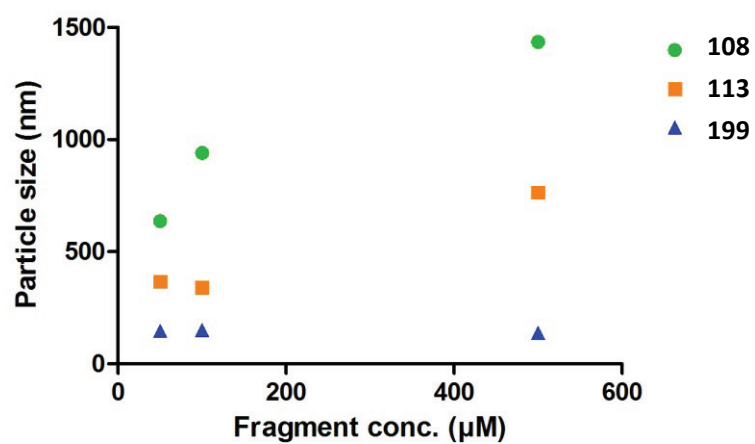
DLS experiments for each of these fragments yielded scattering intensities consistent with the presence of particles (Table 4-1A). The diameter of the particles varied depending on the nature and concentration of the fragments. Of the three fragments, the thienopyrrole **108** formed the largest aggregates with particle diameters ranging from 640 – 1440 nm. Second was the sulfonamide **113** with particle diameters 370 – 760 nm and the smallest, was the phenylfuran **199**, with diameters 140 – 150 nm. The addition of non-ionic detergent 0.01% Triton X-100 eliminated detectable aggregates in solution (Table 4-1B).

Interestingly, the thienopyrrole **108** formed the largest particles across all concentrations and a plot comparing particle sizes and concentrations revealed aggregates of the thienopyrrole **108** grew with increasing concentration (Figure 4-6). On the other hand, the particle size for the phenylfuran **199** was smaller (~150 nm) and was maintained with increasing concentrations.

**Table 4-1.** The observed particle sizes for **108**, **113** and **199** in aqueous buffer determined by DLS (A) in the absence of Triton X-100 and (B) in the presence of 0.01% Triton X-100

Sample	Conc. ( $\mu\text{M}$ )	Diameter (nm)	
		(A)	(B)
Buffer + DMSO (2%)		0.8	12.6
 <b>108</b>	500	1435.8	1001.5
	100	940.1	13.0
	50	636.8	13.3
 <b>113</b>	500	764.5	14.4
	100	341.0	nd
	50	366.3	nd
 <b>199</b>	500	137.9	12.4
	100	150.8	nd
	50	146.3	nd

nd = not determined

**Figure 4-6.** A graph of particle size versus fragment concentration

Although DLS is a more direct method to identify the presence of aggregates, there are several challenges associated with this technique. The aggregate form is a phase between soluble, free small molecule and precipitate. One of the challenges is that the precipitate can also lead to light scattering, however does not typically inhibit enzymes. Therefore, DLS cannot be the only method used to determine the presence of aggregates. DLS can also be time-consuming as it is necessary to equilibrate samples for a sufficient period to allow the aggregates in solution to be homogenous; otherwise the varying particle sizes can lead to results that are hard to interpret.

Using known characteristics of aggregation-based inhibition such as steep dose-response curves, BSA to identify non-specific binding and DLS to detect the presence of particles all suggest that the fragment hits thienopyrrole **108**, sulfonamide **113** and phenylfuran **199** are false positives. Therefore, the optimisation of the enzyme assay is crucial to allow for better identification of specific binders leading to reduced false-positives.

### **4.3 UV-Vis assay**

The inclusion of detergent in enzyme assays has been shown to be a reliable method to remove promiscuous aggregation.<sup>218-221</sup> The protocol for the detergent-based enzyme assay was adapted from Feng *et al.*<sup>218</sup> with slight modifications. Firstly, the detergent properties were compared and their potential effects on KPR activity were investigated.

### 4.3.1 Detergent selection

Three detergents (Triton X-100, Tween-20 and CHAPS at concentrations 0.001, 0.01 and 0.1%) were included in the assay and the catalytic activity was measured (Figure 4-7). The inclusion of 0.001% Tween-20 and CHAPS increased the enzyme catalytic activity possibly by reducing non-specific protein binding onto the plastic plates. The enzyme activity profiles of the three detergents demonstrate that, at 0.01% concentration, there were no observed affect on the native function of KPR.

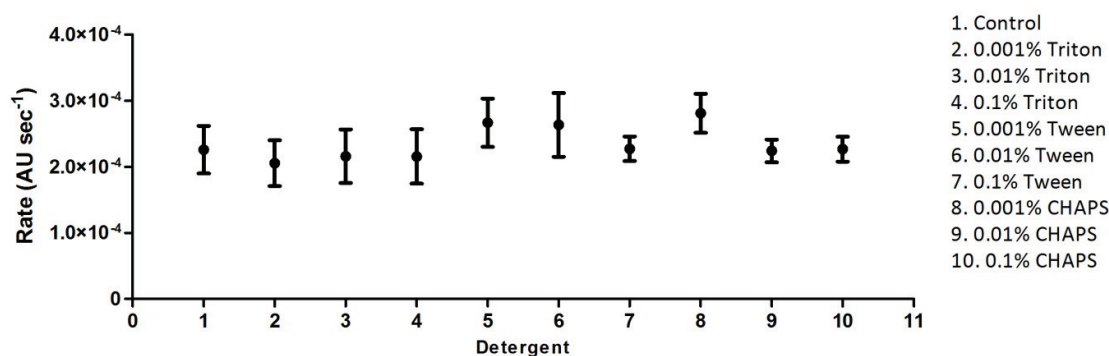
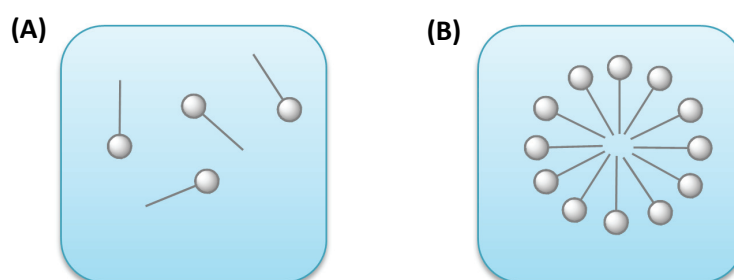


Figure 4-7. Measured activity of KPR in the presence of detergents

#### 4.3.1.1 Critical micelle concentration

Another important factor to consider when selecting detergents is the critical micelle concentration (CMC). CMC is defined by the lowest concentration at which detergent monomers cluster to form micelles or the highest concentration of the detergent monomer (Figure 4-8). The CMC for the selected detergents and the concentrations used in the assay are summarised in Table 4-2. None of the three detergents tested had a negative impact on KPR activity. Tween-20 was preferred due to its lower CMC profile requiring only a small amount to reach CMC.



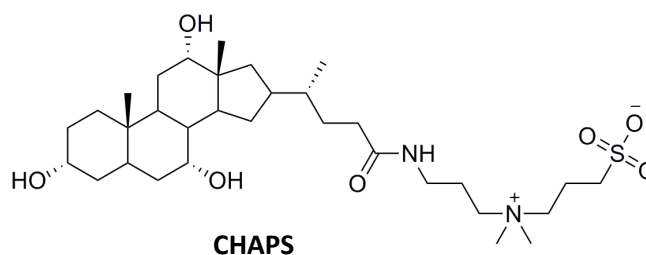
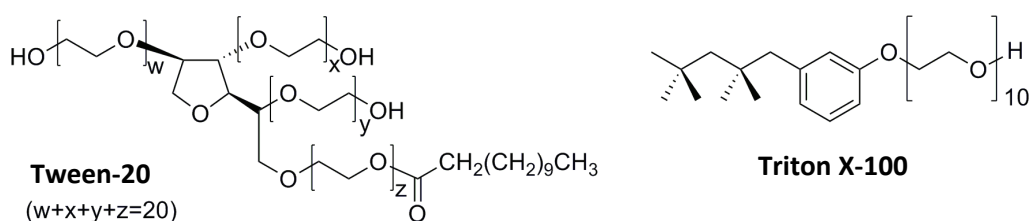
**Figure 4-8.** (A) Detergent monomer at low concentrations, (B) at CMC detergent monomers form a micelle in which the hydrophobic portions are oriented within the cluster and the hydrophilic portions are exposed to the water

**Table 4-2.** Detergent CMC and concentrations used in the assay: Detergent structures shown below

	<b>Tween-20</b> CMC 0.06 mM	<b>Triton X-100</b> CMC 0.2 – 0.9 mM	<b>CHAPS</b> CMC 6 mM
<b>Amount (%)</b>	(mM)	(mM)	(mM)
<b>0.001</b>	0.009	0.017	0.016
<b>0.01</b>	0.089	0.171	0.163
<b>0.1</b>	0.893	1.712	1.626

Values of CMC are from the Sigma-Aldrich website

([http://www.sigmaaldrich.com/img/assets/15402/Detergent\\_Selection\\_Table.pdf](http://www.sigmaaldrich.com/img/assets/15402/Detergent_Selection_Table.pdf))



According to a study by Ryan *et al.*<sup>220</sup> it is important to be working close to or at the detergent's CMC. Ryan *et al.*<sup>220</sup> demonstrated that aggregation-based inhibition was observed below the CMC while exploring the inhibition profile of a known aggregation-based inhibitor with increasing concentrations of CHAPS (Figure 4-9). However, consideration of potential negative effects of micelles on compounds is also important. Ouellet *et al.*<sup>221</sup> reported that above the CMC they observed  $IC_{50}$  values for certain inhibitors increase (less potent) linearly with detergent concentration. Ouellet *et al.*<sup>221</sup> suggested that certain compounds diffuse into micelles and are prevented from binding to the target protein. In their study, 3 of 10 inhibitors displayed this type of profile. Therefore, alternative complementary techniques are imperative to validate fragment hits.

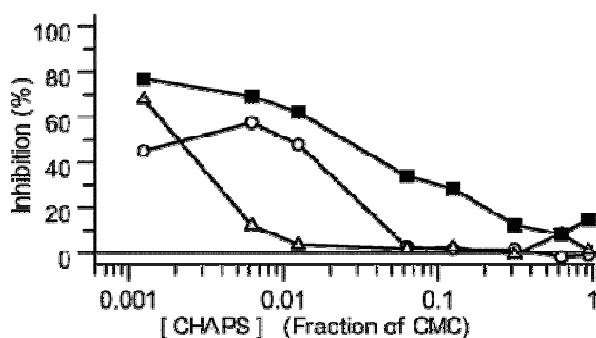


**Figure 4-9.** The effect of detergent (CHAPS) concentration on the inhibition profile of three known aggregation-based inhibitors of  $\beta$ -lactamase

Reprinted with permission from (*J. Med. Chem.* 2003, 46 (16), 3448-3451).<sup>220</sup> Copyright (2012) American Chemical Society

### 4.3.2 NADPH and NADH

Using the assay conditions (described in Chapter 2 and 3) adapted from Ciulli *et al.*<sup>42</sup> the VersaMax Microplate reader was used to monitor the enzymatic reactions. However, though the concentration of NADPH (**24**) (20  $\mu\text{M}$ ) used allowed reasonable absorbance readings at 340 nm, an improved sensitivity was desirable. Low NADPH (**24**) concentrations may increase the risk of interfering noise levels in the absorbance reading and compromise analysis of results. An alternative was to use the structurally similar dinucleotide NADH (**29**), which lacks the 2'-phosphate. A significantly poorer substrate with literature  $K_{\text{m(NADH)}} = 750 \mu\text{M}$ ,<sup>42</sup> allowed higher substrate concentrations in the assay to improve the signal to noise levels without saturating the enzyme.

Initially, a dose-response curve for NADH (**29**) was tested to confirm that it is a suitable substrate replacement of NADPH (**24**). However, the experimentally determined  $K_{\text{m(NADH)}}$  (200  $\mu\text{M}$ ) was more than 3-fold lower compared to the literature value ( $K_{\text{m(NADH)}} = 750 \mu\text{M}$ ).<sup>42</sup> A study carried out by Mr Geqing Wang (MIPS, Monash University) determined that high concentrations of NADH ( $> 500 \mu\text{M}$ ) had reached detection limits of the instrument and the absorbance was no longer within the linearity range. Mr Geqing Wang found that the absorbance of NADH at high concentrations (4 mM) can be accurately measured at 395 nm ( $\epsilon_{340 \text{ nm}}$  for NADH =  $175 \text{ M}^{-1} \text{ cm}^{-1}$ ) to give good signal-to-noise ratio. Therefore, after measuring KPR activity with varying concentrations of NADH at 395 nm, the  $K_{\text{m(NADH)}}$  was determined to be  $637 \pm 100 \mu\text{M}$ , which is consistent with the literature value 750  $\mu\text{M}$ . At low concentrations of NADH ( $\sim 25 \mu\text{M}$ , typically used in inhibition assays) the absorbance is measured at 340 nm. The dose-response of NADH (**29**) was also monitored in the presence and absence of 0.01 – 0.1% Tween-20 vol/vol. KPR activity was enhanced in the presence of Tween-20

presumably due to the detergent causing a reduction in nonspecific protein binding to the walls of the plastic well plates.

### 4.3.3 Test case

The original 14 fragment hits that had been confirmed as binding to KPR by  $^1\text{H}/^{15}\text{N}$ -HSQC NMR studies from Chapter 2 (Figure 4-10) were selected to investigate the detergent-based enzyme assay. Fragments in the test set were prepared in neat DMSO and tested at a final concentration of 1 mM. Inhibition of KPR catalysis was measured in the presence and absence of 0.01% Tween-20 (Figure 4-11)

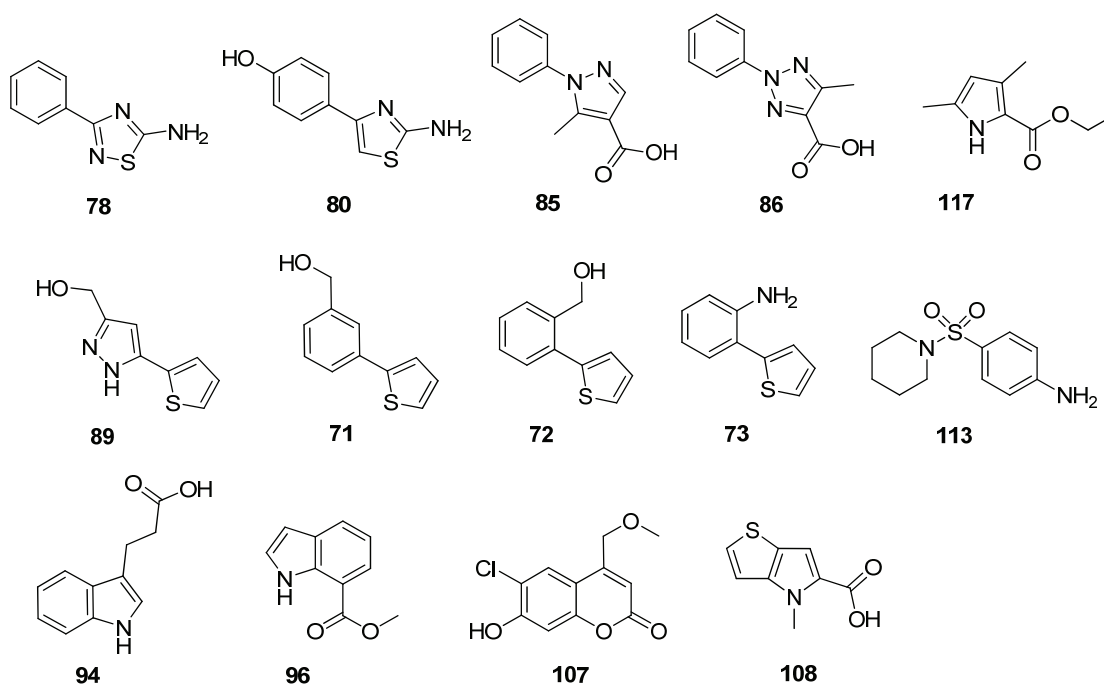


**Figure 4-10.** Structure of fragments in the test set, confirmed binders against KPR by  $^1\text{H}/^{15}\text{N}$ -HSQC

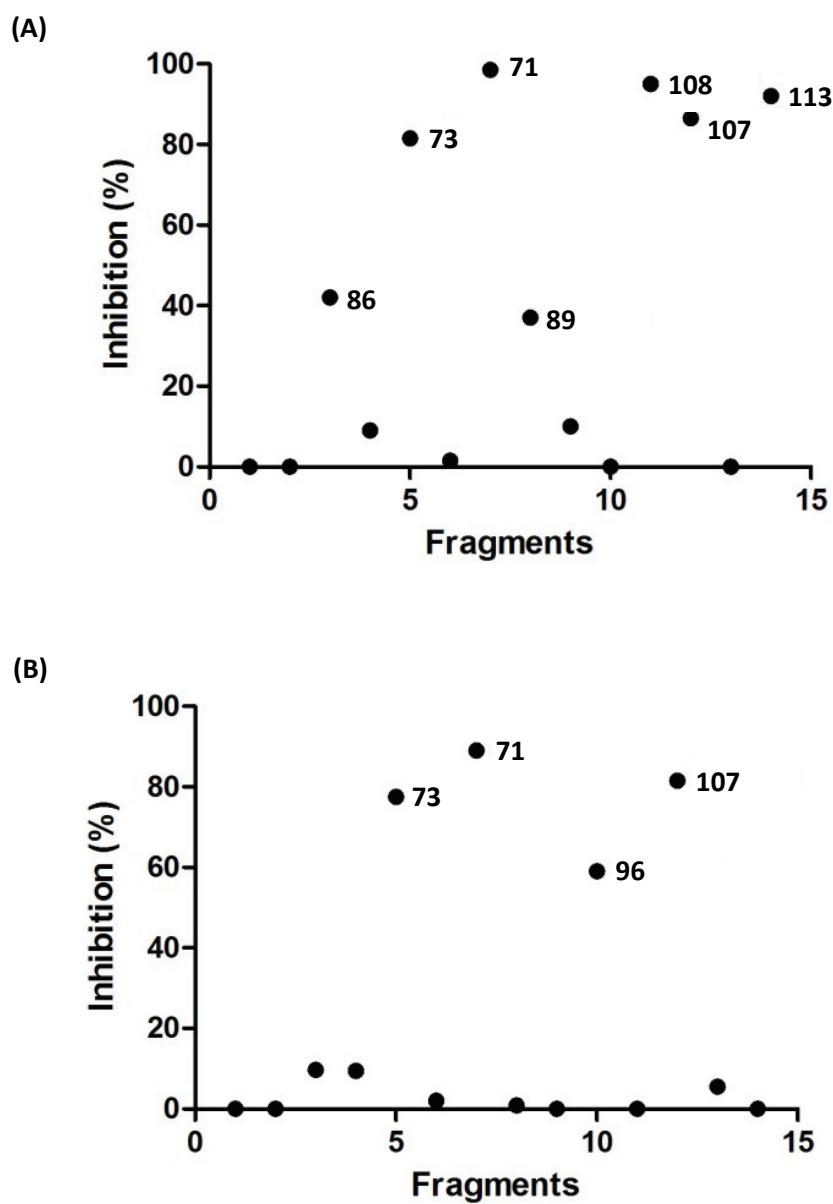


**Figure 4-11.** Summary of the % inhibition assay results using test set fragments (A) in the absence of Tween-20, (B) in the presence of Tween-20

Not surprisingly, the thienopyrrole **108** and sulfonamide **113** displayed strong inhibition (> 80%) in the absence of Tween-20, while inhibition was abolished in the presence of detergent. This demonstrates that the detergent-based enzyme assay is effective in removing aggregate false positives. The (3-(thiophen-2-yl)phenyl)methanol (**71**), coumarin **107** and 2-(thiophen-2-yl)aniline (**73**) were the only fragments that maintained inhibition of KPR activity upon addition of detergent. An interesting inhibition profile was observed for the indole carboxylate **96**. Contrary to what has been observed with aggregation-based inhibitors, the indole carboxylate **96** did not inhibit KPR activity in the absence of Tween-20 but instead in the presence of detergent. The mechanism of this unusual inhibition is unknown.

Fragments which showed KPR inhibitory activity in the % inhibition assay were followed-up with an IC<sub>50</sub> determination revealing some unexpected results. Only the (3-(thiophen-2-yl)phenyl)methanol (**71**) displayed a classical dose-response curve characteristic of single-site inhibition with an IC<sub>50</sub> of 292 μM (Figure 4-12). On the other hand, the coumarin **107** displayed a fairly steep dose-response curve and points in the lower concentration were not consistent with single site binding. At low concentrations (30 – 100 μM) of the coumarin **107**, the points were above 100% suggesting that the rate was enhanced. The dose-response curve for 2-(thiophen-2-yl)aniline (**73**) could not be fitted to the line of best fit as the points were scattered.

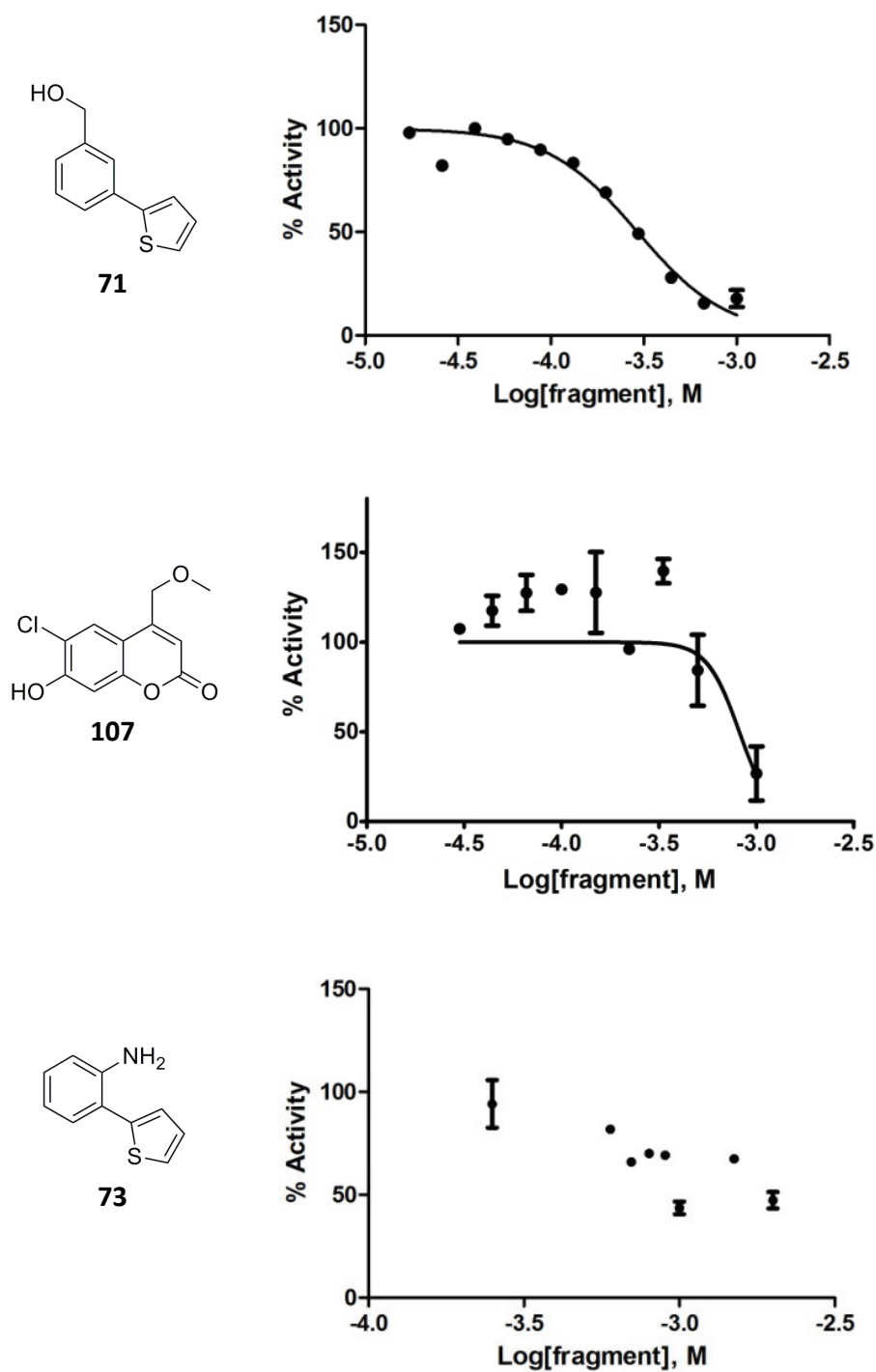


Figure 4-12. IC<sub>50</sub> binding curve for fragments 71, 107 and 73

## 4.4 STD-NMR optimisation

The prevalence of false positives in STD-NMR is common, although the mechanism by which they occur is less understood. The question is: can we reduce the number of false positives at an earlier stage in our experimental approach (described in Chapter 2) such as in an STD screen? If the inclusion of detergent in enzyme assays is a reliable control for aggregation-based false positives,<sup>218</sup> is it the same for STD-NMR? It would be advantageous to be able to reduce the number of false positives as early in the process as possible saving time and cost. To investigate these questions, detergent was incorporated into the STD-NMR. The initial process, prior to screening progression, involved finding a suitable detergent and examining its potential side effects using a small test set of fragments.

### 4.4.1 Detergent selection

The non-ionic detergents Tween-20 and Triton X-100 were investigated for their suitability and potential interference with the NMR experiment. Firstly, a <sup>1</sup>H-spectrum of both Tween-20 and Triton X-100 were acquired and their proton signals compared. Two important factors considered were: (1) that the detergent proton signals were not close to  $\delta$  0 ppm where STD-NMR 'on-resonance' irradiation frequency is set ( $\delta$  -2 to 0 ppm) and (2) that no interfering proton signals were present which may overlap with fragment proton signals complicating the analysis/deconvolution for STD-NMR fragment hits. Tween-20 proton signals were all localised in the aliphatic region,  $\delta$  1.0 – 2.5, 4.23 ppm. Triton X-100 proton signals were found in both aliphatic and aromatic regions ( $\delta$  0.5 – 2, 3.5 – 4 and 6.5 – 7.5 ppm). Based on these considerations, Tween-20 was more appropriate for the STD-NMR screen as it has no aromatic protons, whereas most fragments in the library have at least one aromatic proton signal.

#### 4.4.2 Test case

A small set of fragments were used to investigate potential detergent interference effects and also evaluate the detergents effectiveness in reducing the number of false positives in an STD-NMR screen. The original 14 fragment hits from  $^1\text{H}/^{15}\text{N}$ -HSQC NMR were selected (Figure 4-10). High (1 mM) and low (0.3 mM) fragment concentrations were also examined to determine whether lower fragment concentrations would aid in reducing the number of false positives in an STD-NMR screen.

The 14 fragments were prepared from stock solutions in DMSO of 100 mM and diluted to final concentrations of 1 mM and 0.3 mM. The test set were screened for binding against KPR in the presence and absence of 0.01% Tween-20 vol/vol making a total of 56 samples.

A comparison of the resulting STD spectra (off-resonance) in the presence and absence of 0.01% Tween-20 vol/vol revealed for some fragments, that their proton signals have shifted between the two conditions (Figure 4-13). The chemical shifts appear to be affected by the addition of detergent, which may result from encapsulation (and the corresponding different environment) within detergent micelles.

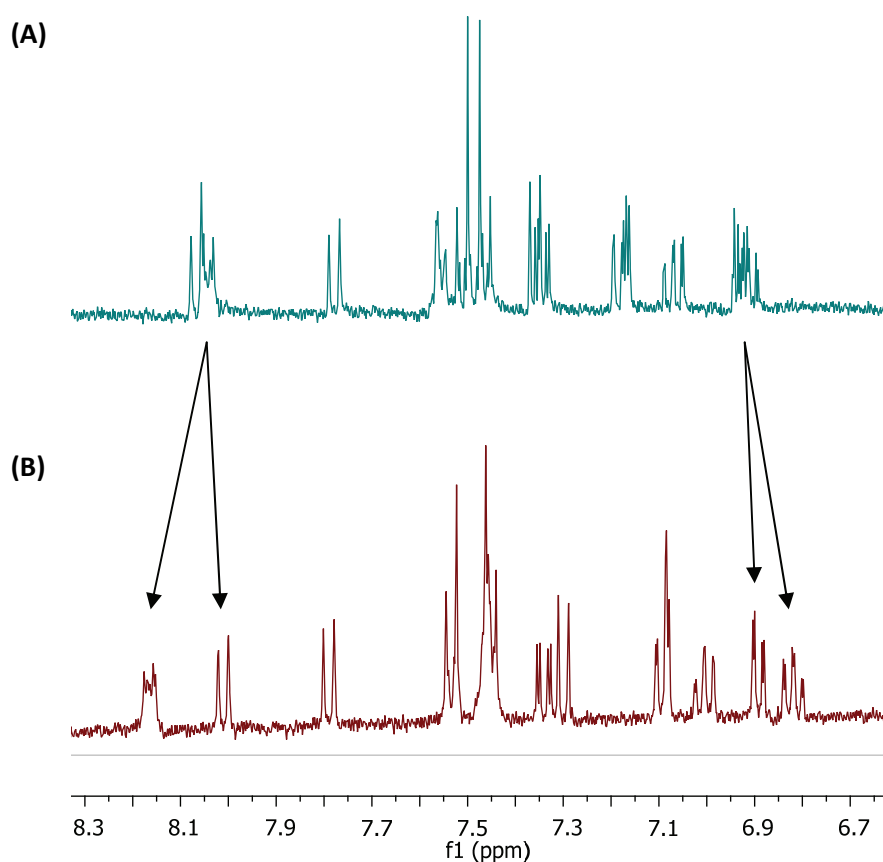


**Figure 4-13.** The 1D  $^1\text{H}$  NMR spectrum (aromatic region) of a fragment cocktail in  $\text{D}_2\text{O}$  (A) absence of Tween-20 and (B) in the presence of 0.01% Tween-20 vol/vol

Interestingly, for some fragments positive STD signals were observed in the absence of KPR. For the fragments involved, they will increase the hit-rate and consequently the number of false positives in an STD-NMR screen. The exact mechanism of this STD false positive is not clear.

To separate genuine fragment hits from ones affected by Tween-20, a comparison of the test set fragments screened in the presence and absence of KPR was performed. Fragments that gave a positive STD signal in the initial screen (Tween-20 + KPR) and negative signal in the latter screen (Tween-20 only) were taken to be genuine KPR binders. However, a positive signal may also be observed for both screens, in these

cases, the intensity of the STD signal was compared. If the signal intensity was at least two-fold higher for the screen in the presence of KPR, then the fragment was considered to be a hit.

#### **4.4.3 Analysis of ligand binding**

A similar approach described in Chapter 2 was employed to analyse the STD-NMR data to determine fragment hits. From Figure 4-14, spectrum B (STD + KPR) shows STD signals indicating a few fragments binding. However, spectrum C (STD - KPR) also has similar resonances present in the STD experiment. To determine whether a fragment is binding to KPR and not the detergent, a comparison of the signal intensities are made between spectrum B and C. The signals highlighted by the dotted lines correspond to a single fragment (spectrum A). In spectrum B, this fragment has a two-fold greater intensity over spectrum C, thus demonstrating that it is binding to KPR. On the other hand, the signals highlighted by the asterisks show similar signal intensities between spectrum B and C, and therefore these fragments were removed from further analysis. In this manner the test set was analysed and the STD results are summarised in Table 4-3.

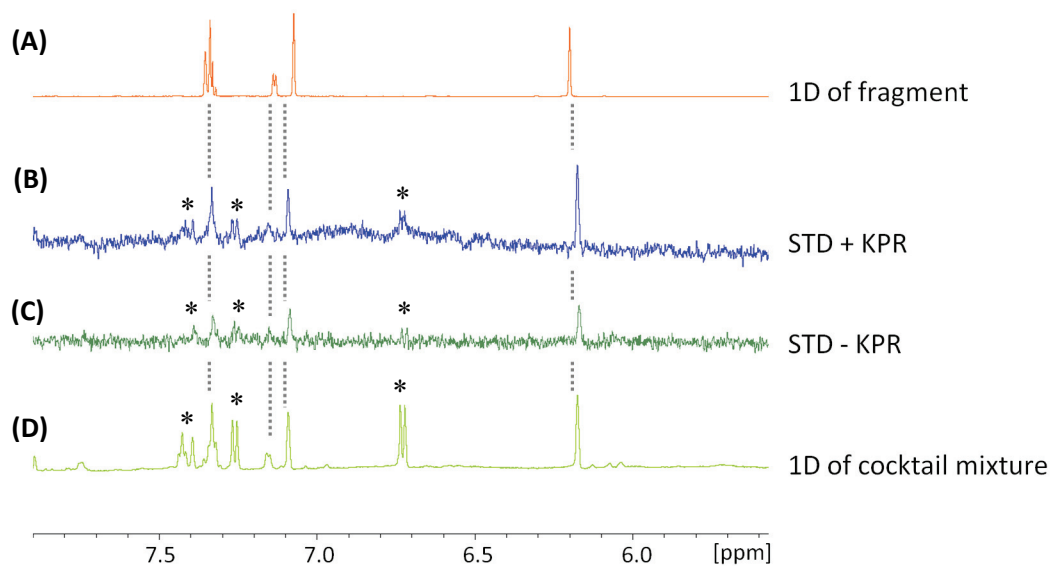


**Figure 4-14.** Detection of ligand binding to KPR using STD-NMR: The dotted lines indicate the resonances from the fragment with a positive STD signal and binds to KPR. The asterisks indicate the resonances from fragments that do not bind to KPR.

To reduce aggregation and the number of false positives, two factors were explored in this STD-NMR study: non-ionic detergent and lower fragment concentration. Given that the detergent-based enzyme assay of the test set suggested (3-(thiophen-2-yl)phenyl)methanol (**71**), coumarin **107** and 2-(thiophen-2-yl)aniline (**73**) were the only genuine fragments inhibiting KPR activity, the optimised STD-NMR showed a similar trend in the reduced number of fragment hits. The 14 fragments re-examined were reduced to 4 fragments. Positive STD signals were observed for the (3-(thiophen-2-yl)phenyl)methanol (**71**) and the coumarin **107**, however, a positive STD signal for the 2-(thiophen-2-yl)aniline (**73**) was only observed in the absence of Tween-20.

Interestingly, the difference in the number of false positives was reduced by 30 - 43% when each factor (presence of detergent and fragment concentration) was considered individually. However, the combination of having 0.01% Tween-20 vol/vol present and

lowering the fragment concentration from 1 mM to 0.3 mM showed significant reduction in the number of false positives (> 70%).

**Table 4-3.** A summary of the STD results using fragments in test set: (+) represents a positive STD hit, (-) is not a STD hit. Highlighted fragments were taken for follow-up studies.

Fragment	(-) Tween-20		(+) Tween-20	
	[1 mM]	[0.3 mM]	[1 mM]	[0.3 mM]
<b>71</b>	+	+	+	+
<b>72</b>	+	+	+	-
<b>73</b>	+	+	-	-
<b>78</b>	+	-	-	-
<b>80</b>	+	+	+	+
<b>85</b>	+	-	-	-
<b>86</b>	+	-	+	-
<b>89</b>	+	+	+	-
<b>94</b>	+	-	+	-
<b>96</b>	+	+	+	-
<b>107</b>	+	+	+	+
<b>108</b>	+	-	-	-
<b>113</b>	+	+	+	+
<b>117</b>	+	-	+	-

#### 4.4.4 Rescreen

The positive outcome from the test set warranted the library of 500 fragments to be rescreened in the optimised STD-NMR conditions. The 500 fragments were screened in groups of 5 (100 mixtures) at a final concentration of 300  $\mu\text{M}$  each. Fragment mixtures were added to KPR (15  $\mu\text{M}$ ) in buffer with Tween-20 (0.01%) and  $\text{D}_2\text{O}$  (10%) in a final volume of 560  $\mu\text{L}$  for screening. Two sets of samples were prepared that is in the presence and absence of KPR giving a total of 200 samples.

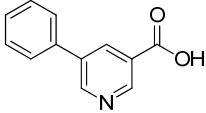
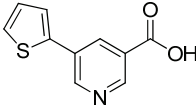
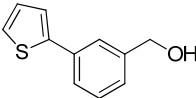
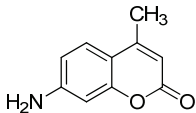
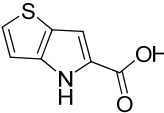
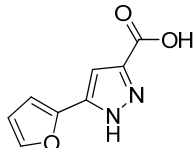
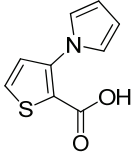
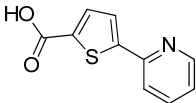
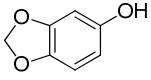
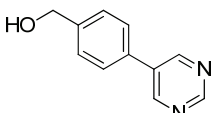
Using the analysis method described in section 4.4.3 the 500 fragments rescreened were analysed in this manner. In Chapter 2 (section 2.4), fragments were prioritised based on their STD signal strength (strong, medium or weak) and only fragments with stronger STD signals were followed-up with further analysis. Unlike Chapter 2, the rescreened fragment STD-NMR hits were all followed-up by an enzyme assay and  $^1\text{H}/^{15}\text{N}$ -HSQC-NMR. The rescreen using optimised STD-NMR conditions resulted in 71 out of 500 (14%) fragment hits (Appendix II), compared to the initial screen in the absence of Tween-20, which resulted in 196 out of 500 (39%) fragments (all STD-NMR hits: strong, medium and weak).

The new STD results demonstrate that we can reduce the number of false positives at an earlier stage in our experimental approach (described in Chapter 2). A simple and effective method to reduce post-STD hit follow-up burden is the inclusion of a suitable detergent and the use of an appropriate fragment concentration.

## 4.5 Detergent-based enzyme assay

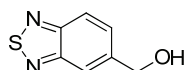
The resulting 71 fragment hits (Appendix II) from the 500 fragments rescreened using the optimised STD-NMR condition (section 4.4.4) were followed-up by the new detergent-based enzyme assay. The fragment hits were initially tested at a final concentration of 1 mM in a % inhibition assay. Based on the 40% inhibition cut-off, the number of fragment hits were reduced to 11 fragments (**71**, **220** – **229**) and their IC<sub>50</sub> values determined (Table 4-4). The assay revealed some exciting results, for example, the three most potent fragment inhibitors were structurally closely related. Fragments phenylnicotinic acid **220**, thiophenylnicotinic acid **221** and (3-(thiophen-2-yl)phenyl)methanol (**71**) had IC<sub>50</sub> of 13 μM, 6 μM and 292 μM, respectively. Both the phenylnicotinic acid **220** and thiophenylnicotinic acid **221** have a nicotinic acid core substituted at the *meta*-position with an aryl group. On the other hand, (3-(thiophen-2-yl)phenyl)methanol (**71**) has a phenyl-methanol core but also substituted at the *meta*-position with an aryl group. The coumarin **222** with an IC<sub>50</sub> of 664 μM is an analogue of **107** in the test set, and also showed a steep dose-response curve, so was not further investigated. The rest of the fragments tested had IC<sub>50</sub> values greater than 1 mM.

**Table 4-4.** Summary of fragment hits with greater than 40% inhibition at 1 mM and their IC<sub>50</sub> values<sup>11</sup>

	Structure	Inhibition (%)	IC <sub>50</sub> (μM)
220		69	13
221		76	6
71		89	292
222		63	664
150		45	> 1000
90		44	> 1000
223		66	> 1000
224		42	> 1000
110		44	> 1000
225		73	> 1000

<sup>11</sup> The data shown were analysed by optimised detergent-based conditions: NADH (**29**, 25 μM), ketopantoate (**22**, 1 mM), and KPR (3 nM) in 100 mM HEPES buffer (pH 7.6) with 0.01% Tween-20 and 2% DMSO (vol/vol).

226



51

&gt; 1000

#### 4.6 Fragment binding evaluation and mapping

Emphasised throughout the chapter is the importance of using independent and complementary biophysical techniques to validate screening hits.  $^1\text{H}/^{15}\text{N}$ -HSQC is superior to STD-NMR due to its lower incidence of false positives. The  $^1\text{H}/^{15}\text{N}$ -HSQC technique and analysis used in this section is the same as that described in Chapter 2. The resulting 71 fragment hits from the 500 fragments rescreened using the optimised STD-NMR condition were followed-up by  $^1\text{H}/^{15}\text{N}$ -HSQC (Appendix II).

The  $^1\text{H}/^{15}\text{N}$ -HSQC spectrum for each fragment (1 mM) was compared to the *apo*-KPR spectrum. From the 71 fragments, 24 did not show any change in the overlaid spectra of fragment-KPR and *apo*-KPR. These were excluded from further analyses. For the 47 fragments that had detectable changes in the amide chemical shifts the  $^1\text{H}/^{15}\text{N}$ -HSQC spectra were mapped onto the structure of KPR and the location of the fragment binding site identified. Details of the binding location for phenylnicotinic acid **220**, thiophenylnicotinic acid **221** and (3-(thiophen-2-yl)phenyl)methanol (**71**) will be discussed in greater detail in the following chapter.

## 4.7 Conclusions

While fragment-based approaches are now fast establishing in academia,<sup>161</sup> we were one of the first academic laboratories in Australia to do so. In this chapter, the dangers of aggregation in fragment-based identification of KPR inhibitors are described. The fragments thienopyrrole **108**, sulfonamide **113** and phenylfuran **199** were shown to be aggregation-based inhibitors. Firstly, any sulfonamide analogue that did exhibit reasonable inhibitory KPR activity also showed steep dose-response curves similar to ones described for aggregation-based inhibition. Secondly, the inhibition of these compounds was abolished in the presence of BSA or detergent and finally, DLS experiments found detectable particle formation indicating that these fragments are inhibiting *via* aggregation.

We have developed an NMR-based fragment screening approach together with an optimised detergent-based enzyme assay. A number of observations suggest that the fragment hits of the rescreen are directly binding to KPR and are also not aggregates. First, a comparison of STD screen in the presence and absence of KPR was performed to remove fragments which were affected by Tween-20; second, there is a range of potencies observed in the enzyme inhibition studies; and thirdly, inhibition is saturable and a Hill slope of 1 is observed, as expected for a competitive single site inhibitor, strongly suggesting a stoichiometric interaction. Fourth, addition of the fragment STD-NMR hits resulted in chemical shift perturbations in  $^1\text{H}/^{15}\text{N}$ -HSQC. In Chapter 5 the newly identified and structurally related fragment hits phenylnicotinic acid **220** and thiophenylnicotinic acid **221** are investigated by examining their binding location and KPR activity.

# Chapter 5

---

## Fragment hit development

## 5 Fragment hit development

### 5.1 Introduction

Three of the most potent fragment hits resulting from the optimised screen shared the same *meta* substituted heterobiaryl scaffold (Figure 5-1). The substituted nicotinic acids (**220** and **221**) had greater affinity and LE than the (3-(thiophen-2-yl)phenyl)methanol (**71**) (Figure 5-1). The (3-(thiophen-2-yl)phenyl)methanol (**71**) was a fragment hit identified from the original screen described earlier (Chapter 3, section 3.4). Notably, the  $IC_{50}$  of (3-(thiophen-2-yl)phenyl)methanol (**71**) was previously determined as 226  $\mu$ M and in the presence of Tween-20 had increased marginally to 292  $\mu$ M. However, the analogues in Chapter 3 that were used to develop the SAR for (3-(thiophen-2-yl)phenyl)methanol (**71**) have not been tested in the optimised assay conditions. Therefore, this chapter will only cover SAR development around the nicotinic acids (**220** and **221**).

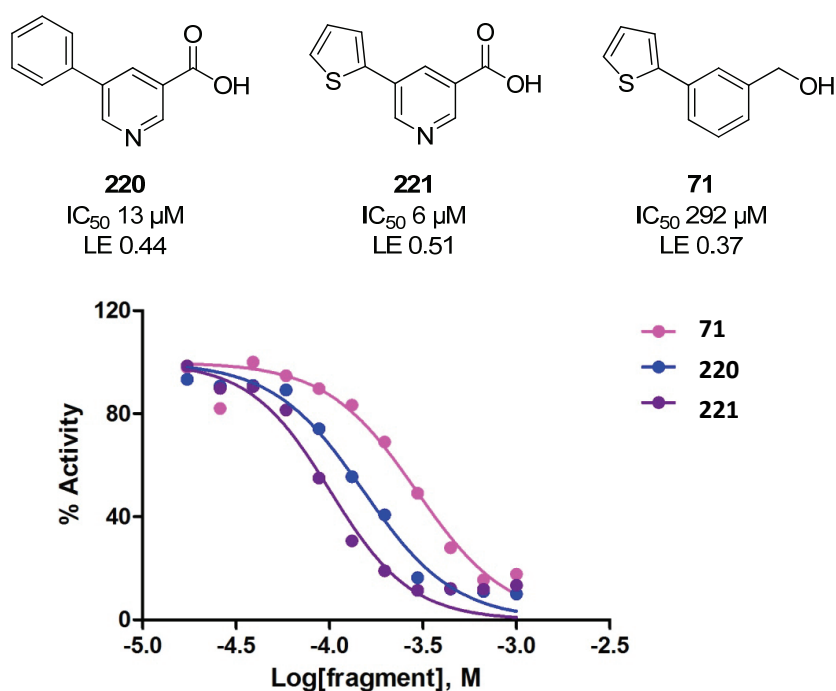


Figure 5-1. Identified fragment KPR binders by  $^1H/^{15}N$ -HSQC studies

### 5.1.1 Mode of inhibition of the nicotinic acid derivatives

The mode of inhibition by the nicotinic acid derivatives (**220** and **221**) against KPR activity was examined by Mr Tony Wang (Monash University). The enzyme assay was carried using the optimised conditions determined in Chapter 4. The mode of inhibition suggested these compounds were competitive inhibitors and the determined  $K_i$  for 5-phenylnicotinic acid (**220**) and 5-(thiophen-2-yl)nicotinic acid (**221**) were 14  $\mu\text{M}$  and 6  $\mu\text{M}$ , respectively.

### 5.1.2 Chemical shift mapping

The CSP mapping of fragments binding to KPR revealed very exciting results. The well-defined clustering observed for the rescreened fragment hits was indicative that the optimised STD-NMR is finding fragment hits with genuine binding. The CSP of (3-(thiophen-2-yl)phenyl)methanol (**71**) were shown earlier (Chapter 3, section 3.4) to be clustered around the hydrophobic pocket where the adenine portion of the NADPH binds.

Mapping of chemical shift changes induced by 5-phenylnicotinic acid (**220**) and 5-(thiophen-2-yl)nicotinic acid (**221**) confirmed that they both bind in a similar location on KPR (Figure 5-2). Distinct clusters of perturbations were observed along the nicotinamide portion of  $\text{NADP}^+$ . Additionally, the same cluster of perturbations was observed above the pantoate binding pocket, presumably due to local conformational change. The nicotinic acids (**220** and **221**) were binding in KPR's active site distinct from the (3-(thiophen-2-yl)phenyl)methanol (**71**) (Figure 5-2).

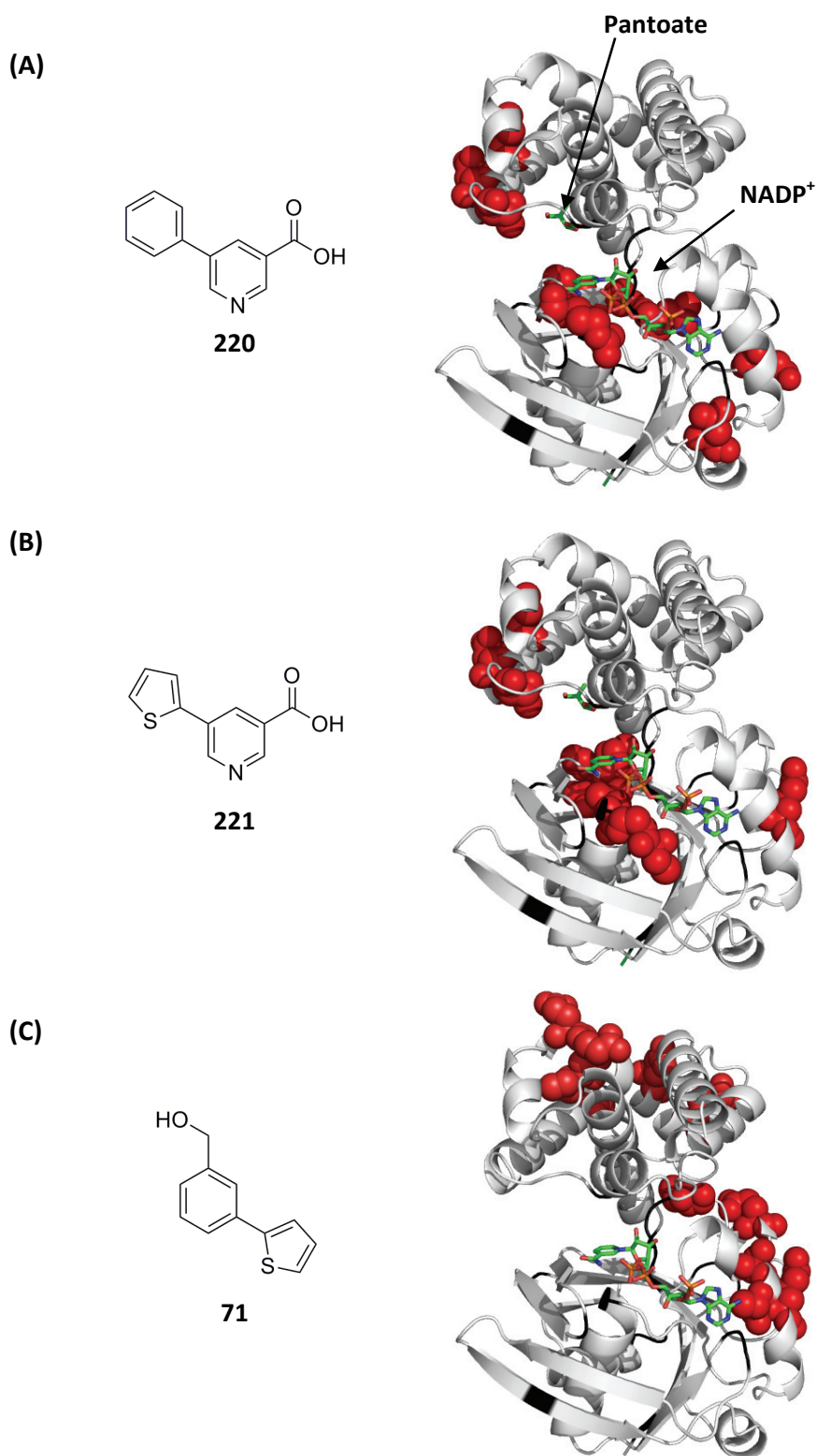


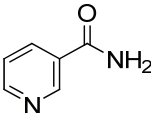
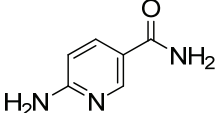
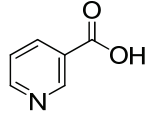
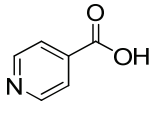
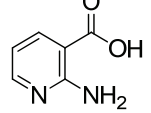
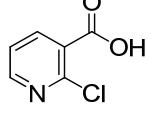
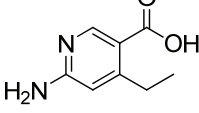
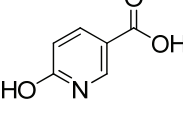
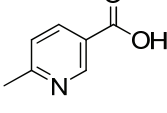
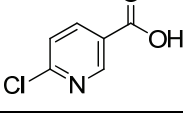
**Figure 5-2.**  $^1\text{H}/^{15}\text{N}$ -HSQC NMR analysis of fragment binding to KPR: Left: structures for (A) **220**, (B) **221** and (C) **71**. Right: Ribbon representation of their binding locations against KPR. NADP<sup>+</sup> and pantoate shown as green carbons (not included in actual experiment). Perturbations are shown as red spheres. Unassigned residues are coloured black ribbons.

### 5.1.3 Preliminary SAR for nicotinic acids

The resemblance of the nicotinic acid to the nicotinamide of NADPH generated interest in the importance of the nicotinic acids of **220** and **221** for KPR activity. Therefore, 2 nicotinamides (**227** – **228**) and the nicotinic acid (**229**) and its analogues (**230** – **236**) were tested in a percentage inhibition assay (1 mM). The results are summarised in Table 5-1.

The weak activity (less than 20%) demonstrated by these compounds may suggest that the nicotinic acid core in **220** and **221** is not critical for activity. However these nicotinic acids and nicotinamides may not have been complex enough to bind with sufficient potency to permit detection.<sup>222</sup> Similar observations were described by Ciulli and co-workers<sup>42</sup> on deconstructing NADPH in which no binding or inhibition was detected for the nicotinamide fragment (**227**) based on NMR, isothermal titration calorimetry (ITC) and UV-based kinetic analysis even when tested at higher concentrations (0% at 5 – 10 mM concentration).

**Table 5-1.** Summary of inhibitory data for the nicotinic acid analogues<sup>12</sup>

	Structure	Inhibition (%) at 1 mM
227		18
228		4
229		6
230		10
231		8
232		3
233		2
234		6
235		6
236		16

<sup>12</sup> The data shown were analysed by optimised detergent-based conditions: NADH (**29**, 25  $\mu$ M), ketopantoate (**22**, 1 mM), and KPR (3 nM) in 100 mM HEPES buffer (pH 7.6) with 0.01% Tween-20 and 2% DMSO (vol/vol).

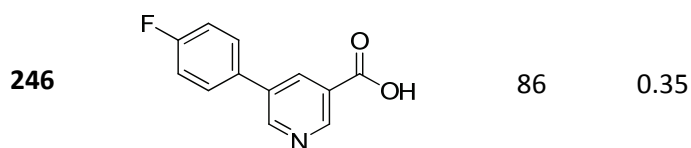
Subsequently, a series of biaryl analogues selected by a similarity search on the substituted nicotinic acid (**237** – **248**) with a threshold of 0.7 (where 0 is completely dissimilar and 1 is identical) were purchased from commercial suppliers. The compounds were initially tested at a single concentration of 0.5 mM. Of the 12 compounds purchased, two compounds (6-morpholinonicotinic acid (**247**) and *N*-methyl-1-(3-(pyridin-3-yl)phenyl)methanamine) (**248**) showed very weak KPR activity (19% and 10%, respectively) and were not investigated further. The 5-phenylpicolinic acid **237** and 2-(pyridin-3-yl)benzoic acid **238**, were selected to examine the importance of the position of the acid group, however showed poor solubility and were not able to be assayed. The remaining compounds (**239** – **246**) had their IC<sub>50</sub> determined as shown in Table 5-2.

The resulting IC<sub>50</sub> values suggest that the 6-phenyl substituent (**241**, IC<sub>50</sub> 4 μM, LE 0.49) was more favourable and ligand efficient than the 5-phenyl substituent (**220**, IC<sub>50</sub> 13 μM, LE 0.44). Moreover, the fluorine and methoxy substitution on the phenyl ring (**243** – **246**) decreased potency, particularly at the *meta* position as the activity trend *meta* < *para* < *ortho* was observed. Though given that substitution is tolerated, there might be the possibility of elaborating at these positions. The 4-(pyridin-3-yl)benzoic acid (**239**) and 3-(pyridin-4-yl)benzoic acid (**242**) with the same LE as the initial fragment hit (5-phenylnicotinic acid (**220**)) suggest that the position of the pyridine ring may not be critical for activity.

**Table 5-2.** Summary of inhibitory data for the nicotinic acid analogues<sup>13</sup>

	Structure	IC <sub>50</sub> (μM)	LE
237		-	-
238		-	-
239		20	0.43
240		222	0.33
241		4	0.49
242		15	0.44
243		40	0.35
244		14	0.41
245		137	0.33

<sup>13</sup> The data shown were analysed by optimised detergent-based conditions: NADH (**29**, 25 μM), ketopantoate (**22**, 1 mM), and KPR (3 nM) in 100 mM HEPES buffer (pH 7.6) with 0.01% Tween-20 and 2% DMSO (vol/vol).



#### 5.1.4 Conclusions

The optimised detergent-based STD-NMR screen has identified fragment hits which have shown well-defined clustering through  $^1\text{H}/^{15}\text{N}$ -HSQC NMR CSP mapping and the ability to inhibit KPR in the new detergent-based assay. The structurally related fragment hits 5-phenylnicotinic acid (**220**) and 5-(thiophen-2-yl)nicotinic acid (**221**) were identified to bind in a similar location on KPR.

The observation of some SAR around the nicotinic acids is reassuring for this series, as it suggests further development is possible. However, assessing these compounds using  $^1\text{H}/^{15}\text{N}$ -HSQC NMR or crystallography to determine the binding position would be a key step forward to progress this series in the future.

# Chapter 6

---

## Conclusions and future directions

---

## 6 Conclusions and future directions

Since the biosynthetic pathway for pantothenate is present only in bacteria and plants and inhibitors of enzymes of this pathway have been proposed as potential antibiotics, we have chosen to target KPR, the second enzyme of the biosynthetic pathway. A FBLD approach was used to identify small molecule inhibitors of KPR. Despite extensive structural and mechanistic information being available, no inhibitors of KPR have been reported in the literature to date. The benefits of finding a small molecule inhibitor for the pantothenate pathway include using these compounds to investigate the role of KPR in the development of antimicrobials.

The work presented in chapter 2 investigated the high-level expression of unlabelled and  $^{15}\text{N}$ -labelled KPR and optimised yields of 122 mg/L and 53 mg/L, respectively were obtained. The fragment-based approach involved using a broad range of techniques such as STD-NMR,  $^1\text{H}/^{15}\text{N}$ -HSQC, UV-based enzyme assay and initially computational modelling to assess binding and inhibition. The primary screen of 500 fragments by STD-NMR identified 47 hits and the validation step by  $^1\text{H}/^{15}\text{N}$ -HSQC narrowed down the hits to 14 fragments correlating to a 2.8% hit rate, which were subsequently evaluated by UV-based assay for KPR activity. Glide docking for KPR was investigated and docking was able to predict binding modes for larger ligands, however performed less well for small fragments.

The process of hit development for the sulfonamide **113**, thienopyrrole **108** and phenylthiophene **71** were described in chapter 3. In developing the sulfonamide **113**, 43

sulfonamide analogues were tested against KPR and only 5 compounds showed  $IC_{50} < 500 \mu\text{M}$ . The activity of the sulfonamides was unusual since small structural modifications seem to abolish or reduce activity. The investigation also revealed a novel binding pocket where further kinetic studies suggested an allosteric site and identified 3-(piperidin-1-ylsulfonyl)aniline (**135**) as a non-competitive inhibitor. Core hopping from the thienopyrrole **108** to the isostere thienothiophene **148** initially appeared to show a 4-fold improvement in affinity; however the KPR inhibitory activity was discovered to be due to an unidentified tiny impurity responsible. For the phenylthiophene **71**, an apparent SAR was observed that was complemented by consistent binding location among the analogues. Identifying the lead thienothiophene as false positive and the flat SAR of the sulfonamides raised concerns about the fragment hits.

In chapter 4, the risks of false positives in fragment-based identification of KPR inhibitors are described. The chapter highlights that although the purity of the fragments can be controlled; it is difficult to account for residual impurities (1 – 2%). Furthermore, predicting fragments that may form aggregates in aqueous solution is currently impossible. Thus, the importance of follow-up strategies or the use of orthogonal methods to screen and confirm the hits is emphasised. An optimised STD-NMR fragment screen together with an optimised assay incorporating detergent was developed to overcome many of the challenges posed by false positives. With the methods fine-tuned, the fragment-based screen with KPR is able to considerably filter the total number of hits into potentially productive binders. Using the optimised screen and assay a total of 47 validated inhibitors were identified from the library of 500 fragments. The number of fragment hits was reduced to 11 fragments (based on 40% inhibition cut-off at 1 mM) and the three most potent fragment inhibitors were phenylnicotinic acid **220**,

thiophenenicotinic acid **221** and phenylthiophene **71** with  $IC_{50}$  of 13  $\mu$ M, 6  $\mu$ M and 292  $\mu$ M, respectively. Additionally, the well-defined clustering of chemical shift perturbations in the  $^{15}N$ - $^1H$  HSQC spectra for the rescreened fragment hits suggests that the optimised methods are finding fragment hits with genuine binding.

In chapter 5, the structurally related fragment hits 5-phenylnicotinic acid (**220**) and 5-(thiophen-2-yl)nicotinic acid (**221**) were identified to bind in a similar location on KPR in a highly ligand efficient manner with LE of 0.51 and 0.44, respectively. Preliminary testing of some nicotinic acid analogues is promising; however, information on the binding location is required for interpreting the SAR, and further developing these compounds.

Some of the major challenges we have experienced in fragment-based lead discovery of KPR inhibitors have been prioritising novel fragment hits without knowledge of the binding mode amongst a very large number of possible design ideas. It is apparent that the majority of advanced applications in the fragment-based approach have used extensive structural biology.<sup>154,223</sup> The ability to crystallise complexes of KPR with fragments would be valuable, and attempts to do this are currently in progress, in collaboration with Professor James Whisstock and co-workers (Monash University). Another challenge is that fragments are weak binders. Therefore, high concentrations of fragments were used which at times caused limited solubility in the enzyme assay and in particular NMR experiments leading to potential false negatives. However, testing the fragments in high concentrations has also resulted in false positives due to aggregators thus emphasising the value of following up hits with multiple complementary biophysical and biochemical techniques.

For future investigations, there is scope for chemistry to develop the nicotinic acid series into more potent inhibitors of KPR as well as screening further fragments to identify other series of inhibitors since having multiple series of active compounds is important in progressing leads.<sup>224</sup> Potent KPR inhibitors could be tested for their effects on *E. coli* for example, in disc diffusion assays to provide cell-based activity.<sup>225</sup> Importantly, this study allows us to determine whether these compounds are specific for KPR. Therefore, the effect of the *E. coli ilvC* mutant, the *panE* mutant, *ilvC* and *panE* double mutant, and wild type *E. coli* to KPR inhibitors are compared.

Additionally, it would be interesting to retest the thienothiophene series with the optimised detergent-based enzyme assay. Particularly for compounds **166**, **167** and **176**, which were shown to be quite active (based on the initial enzyme assay). To determine whether the thienothiophene series are worth pursuing, there are two important issues that need to be addressed. The first is to establish that inhibition is not aggregation based and second is to determine that the inhibition is not due to the presence of the minor active impurity.

# Chapter 7

---

## Experimental

# 7 Experimental

## 7.1 Biochemistry

### 7.1.1 Materials

#### 7.1.1.1 Chemicals

The following chemicals were purchased from Sigma-Aldrich (Castle Hill, NSW, Australia): tetramethylethylenediamine (TEMED), sodium dodecyl sulfate (SDS), imidazole, tris(hydroxymethyl)aminomethane hydrochloride (Tris-HCl), 2-[4-(2-hydroxyethyl)piperazin-1-yl]ethanesulfonic acid (HEPES), sodium phosphate dibasic ( $\text{Na}_2\text{HPO}_4$ ), potassium phosphate monobasic ( $\text{KH}_2\text{PO}_4$ ), ammonium chloride ( $\text{NH}_4\text{Cl}$ ), potassium chloride (KCl), magnesium sulfate ( $\text{MgSO}_4$ ), sodium sulfate ( $\text{Na}_2\text{SO}_4$ ), glucose,  $\alpha$ -lactose, ferric chloride ( $\text{FeCl}_3$ ), calcium chloride ( $\text{CaCl}_2$ ), zinc chloride ( $\text{ZnCl}_2$ ), thiamine, sodium azide ( $\text{NaN}_3$ ), isopropyl  $\beta$ -D-1-thiogalactopyranoside (IPTG), dithiothreitol (DTT), ampicillin (Amp), polyoxyethylene (20) sorbitan monolaurate (Tween-20), polyethylene glycol *p*-(1,1,3,3-tetramethylbutyl)-phenyl ether (Triton-X-100) and dihydro-4,4-dimethyl-2,3-furandione. The following chemicals were purchased from Merck Chemicals (Kilsyth, VIC, Australia): glycerol, ethylenediaminetetraacetic acid (EDTA) and 3-[(3-cholamidopropyl)dimethylammonio]-1-propanesulfonate (CHAPS). The following chemicals were purchased from Proscience (Blackburn, VIC, Australia): acetic acid, ammonium persulfate, sodium chloride ( $\text{NaCl}$ ), and bacteriological agar. Acrylamide solution and Bradford reagents were purchased from Bio-Rad (Regents Park, NSW, Australia). Deuterated solvents,  $^{15}\text{NH}_4\text{Cl}$  and deuterium oxide ( $\text{D}_2\text{O}$ ) were purchased from Cambridge Isotopes Laboratories (Novachem Pty Ltd, Collingwood, VIC, Australia). Tryptone and yeast extract were purchased from Oxoid (Adelaide, SA,

Australia). The expression plasmid pRSETA containing *panE* (gene for KPR) was provided by Prof. Chris Abell (University of Cambridge, Cambridge, UK). Chemically competent *E. coli* strain C41(DE3) cells were purchased from Lucigen (Astral Scientific Pty. Ltd. Caringbah, NSW, Australia).

#### 7.1.1.1.1 Fragment library

The fragment library used in the screen was composed of 500 structurally diverse compounds and was purchased from Maybridge (Trevillet, Cornwall, UK). The fragments have an average molecular weight of 208 Da and are ‘Rule of three’ physicochemical parameters compliant.<sup>127</sup> The library has also been filtered removing inappropriate functionality such as acid chloride, sulfonyl chlorides, aldehydes, cyclopropanes substituted with either oxygen, nitrogen or sulfur, carbonates, nitriles, pyridine thiols and others not listed.<sup>123,125</sup> Chemical cores included benzene, thiophene, furan, pyrimidine, pyridine, pyrazole, isoxazole, oxazole, thiazole, indole, benzimidazole, indazole, benzofuran, benzothiophene, pteridine, quinoline, naphthalene, quinazoline, isoquinoline, piperidine, and cyclohexane. The library included chemical cores with 1 – 3 substituents attached with at least one polar substituent such as an amine, acid or hydroxyl.

The compounds were provided as solids or oils in 25 mg quantities which were dissolved in neat DMSO to generate a concentrated stock solution and stored at 4 °C. All compounds were assessed individually for purity and solubility by 1D <sup>1</sup>H NMR. Those that were < 90% pure, of questionable identity or not soluble (based on the chemical shifts, coupling and intensity of peaks in the 1D <sup>1</sup>H NMR spectra) were noted and removed from analysis. Purity of compound hits for follow up was analysed on an

Agilent 1200 Series LCMS system, incorporating a photodiode array detector (214/254 nm) coupled directly to an electrospray ionisation source and a single quadrupole mass analyser (Agilent 6120 Quadrupole MS). A Phenomenex column (Luna 5 $\mu$ m C8 (2), 50  $\times$  4.60 mm ID) was employed. Each sample was analysed in a total run time of 10 min with a flow rate of 0.5 mL/min and 0 – 80% acetonitrile gradient in the presence of 0.1% formic acid. RP-HPLC was carried out at 30 °C and also employing a Phenomenex column (Luna 5 $\mu$ m C8 (2), 50  $\times$  4.60 mm ID). The following buffers were used; buffer A (99.9% H<sub>2</sub>O, 0.1% formic acid) and buffer B (99.9% CH<sub>3</sub>CN, 0.1% formic acid). The following gradient was used with a flow rate of 0.5 mL/min and total run time of 12 min; from 95% buffer A and 5% buffer B over 0 – 4 min to 0% buffer A and 100% buffer B over 4 – 7 min, and then to 95% buffer A and 5% buffer B over 7 – 12 min. Mass spectra were acquired in positive and negative ion mode with a scan range of 0 – 1000 m/z at 5V. All compounds were of  $\geq$  95% purity.

Fragments selected as positive hits from the screen and used in follow-up experiments were purchased from Sigma-Aldrich (Castle Hill, NSW, Australia), Maybridge (Trevillet, Cornwall, UK), Specs (HT Delft, Netherlands), Apollo Scientific (Bredbury, Stockport, UK), Peakdale Molecular (Chapel-en-le-Frith, High Peak, UK) and AMRI Albany (Albany, New York, USA).

#### **7.1.1.2 Proteins**

BSA used in the Bradford protein assay was purchased from Sigma-Aldrich (Castle Hill, NSW, Australia). BSA used in the enzyme assay was purchased from Promega (Hawthorn, VIC, Australia).

### 7.1.1.3 Columns

Columns used for protein purification included a 5 mL HisTrap (nickel affinity column), a desalting column (HiPrep 26/10) and a gel filtration column (Superdex 75 HR 10/30), which were purchased from GE Healthcare (Rydalmere, NSW, Australia). Protein purifications were undertaken on ÄKTA basic and ÄKTA purifier systems (GE Healthcare). Molecular weight cut-off concentrators (5 kDa) were purchased from Millipore (North Ryde, NSW, Australia).

## 7.1.2 Molecular methods

### 7.1.2.1 Buffer and media preparation

All nutrient media used in protein expression were autoclaved at 121 °C for 20 min and stored at 4 °C prior to use. Heat labile additives were sterile-filtered prior to inoculation. The compositions of different nutrient media are shown in Table 7-1 – Table 7-3. All buffers were filtered using 0.22 µm nitrocellulose membrane filters (Millipore, North Ryde, NSW, Australia) and degassed prior to use. Buffers and solutions used are as stated in Table 7-4 and Table 7-5.

### 7.1.2.2 Transformation of *E. coli*

The *panE* gene encoding KPR, cloned into the pRSETA plasmid was used to transform competent cells of *E. coli* strain C41(DE3). The initial transformation step involved the addition of the cloned plasmid (1 µL) to competent cells (100 µL) which were then incubated on ice for 30 min. The cells were heat shocked for 45 sec at 42 °C and allowed to recover on ice for at least 2 min. Super optimal broth with catabolite repression (SOC medium, 900 µL) was added to the cells and incubated for 1h at 37 °C. The cell culture suspension (70 µL) was then plated on LB agar containing Amp (100 µg/mL) and

incubated for 16 hr at 37 °C. The composition of nutrients used in the transformation is given in Table 7-1.

**Table 7-1.** Composition of media used in transformation

LB agar was prepared with all the components (except for Amp) in MilliQ water and then autoclaved. Amp was added once the mixture had cooled to approximately 50 °C. Shortly after adding the Amp, the warm mixture was poured into sterile culture plates. After setting, the plates were incubated overnight at 37 °C to test for contamination. Plates which showed no bacterial and/or fungal growth were stored at 4 °C until use. All nutrients except MgCl<sub>2</sub>, D-glucose, and Amp in SOC media were autoclaved. MgCl<sub>2</sub>, D-glucose, and Amp were 0.22 µm filter sterilised.

<b>Component</b>	<b>LB agar</b>	<b>SOC media</b>
Tryptone	2 g	3 g
NaCl	1 g	0.075 g
Yeast extract	1 g	0.75 g
Agar	2 g	
KCl		0.028 g
MgCl <sub>4</sub>		1.5 mL
D-glucose (1 M)		3 mL
Amp (100 mg/mL)	0.2 mL	1 mL
MilliQ H <sub>2</sub> O	made up to 200 mL	made up to 150 mL

### 7.1.2.3 Plasmid purification

Plasmid DNA was purified from *E. coli* cultures using a Qiagen Plasmid Maxikit from Qiagen Pty Ltd (Doncaster, VIC, Australia) according to the manufacturer's instructions.

### 7.1.2.4 Protein expression

#### 7.1.2.4.1 Expression of unlabeled *E. coli* KPR

Single colonies of freshly transformed *E. coli* strain C41(DE3) cells were selected to inoculate starter cultures in LB broth containing Amp (100 µg/mL) and incubated overnight with shaking (260 rpm) at 37 °C. Overnight cultures from a single colony were pelleted by centrifugation at 3,500 rpm for 15 min (4 °C), resuspended in fresh media (~2 mL) and subsequently transferred into 2 × 500 mL LB/Amp. The cells were grown at 28 °C to an OD<sub>600</sub> of 0.6 when they were induced with 1 mM IPTG. Growth continued for an additional 9 hr at 28 °C before harvesting (10,000 rpm, 15 min, and 4 °C). The supernatant was discarded and the cell pellet was frozen at -20 °C until further purification.

Alternatively, KPR expression was performed by transferring the overnight culture to auto-induction media (2 × 500 mL) using a method described by Studier.<sup>169</sup> The composition of nutrients used in the auto-induction media is given in Table 7-2. Auto-induction media was prepared using ZY which is LB in the absence of NaCl, 1 M MgSO<sub>4</sub>, 20 × NPS and 50 × 5052 mixtures with antibiotic Amp (100 µg/mL). The cells were incubated for 24 hr with shaking (260 rpm) at 28 °C and harvested (10,000 rpm, 15 min, and 4 °C). The supernatant was discarded and the cell pellet was frozen at -20 °C until further purification.

**Table 7-2.** Composition of the nutrients used in the auto-induction media

The composition of the different nutrient mixtures is listed in (A). The salts (20 × NPS) and ZY broth were autoclaved at 121 °C for 20 min, while the carbon source (50 × 5052), Amp and MgSO<sub>4</sub> were filter sterilised. When the autoclaved ZY and 20 × NPS salts had cooled to approximately 50 °C, all the ingredients were added together in the order listed in (B).

<b>(A) ZY</b>	
Tryptone	10 g
Yeast extract	5 g
MilliQ H <sub>2</sub> O	925 mL

<b>20 × NPS</b>	
(NH <sub>4</sub> ) <sub>2</sub> SO <sub>4</sub>	5.4 g
KH <sub>2</sub> PO <sub>4</sub>	13.6 g
Na <sub>2</sub> HPO <sub>4</sub>	14.2 g
MilliQ H <sub>2</sub> O	90 mL

<b>50 × 5052 (0.22 µm filtered)</b>	
Glycerol	25 g
α-Lactose	10 g
D-Glucose	2.5 g
MilliQ H <sub>2</sub> O	73 mL

MgSO <sub>4</sub> (1 M) (250 mg/mL)	1 mL
Amp (100 mg/mL)	1 mL

<b>(B) Auto-induction media</b>	
1. ZY	925 mL
2. 20 × NPS	50 mL
3. 50 × 5052	20 mL
4. MgSO <sub>4</sub>	1 mL
5. Amp	1 mL

#### 7.1.2.4.2 Expression of labelled *E. coli* KPR

Expression of  $^{15}\text{N}$  isotope-labelled KPR was carried out according to the method described by Marley *et al.*<sup>170</sup> Single colonies of freshly transformed *E. coli* strain C41(DE3) competent cells were selected to inoculate starter cultures in LB broth containing Amp (100  $\mu\text{g}/\text{mL}$ ) and incubated overnight with shaking (260 rpm) at 37 °C. The overnight cultures were pelleted at 3,500 rpm for 15 min (4 °C) and subsequently transferred to 8  $\times$  500 mL LB/Amp. The large cultures were incubated at 37 °C with shaking (260 rpm) until the cell density reached log phase with  $\text{OD}_{600}$  of 0.6. The culture was centrifuged (3,500 rpm, 4 °C, 15 min) and the cell pellets were resuspended in one quarter of the volume of defined, labelled minimal media (2  $\times$  500 mL) where  $^{15}\text{NH}_4\text{Cl}$  was employed for nitrogen labelling (Table 7-3). The *E. coli* cells were incubated at 28 °C, 260 rpm until growth recovery and unlabeled metabolite clearance ( $\text{OD}_{600} \sim 2.4$ , approximately 1.5 hr) prior to induction with 1 mM IPTG. Once the cell density plateaued, typically 5 – 6 h post-induction, the cells were collected by centrifugation at 10,000 rpm, 4 °C for 10 min. The supernatant was discarded and the cell pellet was frozen at -20 °C until further purification.

**Table 7-3.** Composition of the nutrients used in minimal media

The combination of nutrients for 5 × M9 salts is listed in (A). The salts and LB broth were autoclaved at 121 °C for 20 min, while heat labile additives such as D-glucose, thiamine and Amp were filter sterilised. Once the autoclaved 5 × M9 salts mixture cooled to approximately 50 °C, the ingredients listed in (B) were added and made up to 1 L.

<b>(A) 5 × M9 salts (autoclaved)</b>		<b>(B) Minimal growth medium (1 L)</b>	
KH <sub>2</sub> PO <sub>4</sub> ·2H <sub>2</sub> O	3.8 g	5 × M9 salts	200 mL
Na <sub>2</sub> HPO <sub>4</sub> ·2H <sub>2</sub> O	6.8 g	D-Glucose (20 g/100 mL)	20 mL
NaCl	0.5 g	Thiamine (2 mg/mL)	5 mL
<sup>15</sup> NH <sub>4</sub> Cl (pH adjusted to 7.2)	1 g	MgSO <sub>4</sub> (1 M)	2 mL
MilliQ H <sub>2</sub> O	200 mL	CaCl <sub>2</sub> (1 M)	2 mL
		FeCl <sub>3</sub> (10 mg/mL)	0.2 mL
		ZnCl <sub>2</sub> (34 mg/mL)	0.2 mL
		Amp (100 mg/mL)	1 mL
		MilliQ H <sub>2</sub> O	770 mL

#### 7.1.2.5 Purification of KPR

Frozen cell pellets (from a 1 L cell culture) were thawed and resuspended in 2 × 30 mL buffer A (10 mM KH<sub>2</sub>PO<sub>4</sub>, 300 mM NaCl, 10 mM imidazole, pH 8.0) containing 1 tablet of EDTA-free protease inhibitor cocktail (Roche, NSW, Australia). The cells were disrupted by sonication for 10 × 30 seconds on ice (with a cooling period of 30 secs between each cycle). The resulting cell debris was removed by centrifugation (25,000 rpm, 4 °C, 15 min). The supernatant was carefully separated from the pellet avoiding any disturbance and retained to be purified.

An ÄKTA basic and ÄKTA purifier (GE Healthcare) were used for the purification of KPR. Purification for His<sub>6</sub>-KPR was typically a three-step process, in which it was first applied to a nickel affinity column then a desalting column and a size exclusion column. The different column conditions are described below:

#### *7.1.2.5.1 Nickel affinity column*

The purification process involved binding of His<sub>6</sub>-KPR proteins to Ni-NTA silica in 100% buffer A (Table 7-4). The majority of cellular proteins are unable to bind to this support and are contained in the column flow-through. After a wash step over 1 column volume in buffer A, purified His<sub>6</sub>-KPR was eluted by gradually increasing the concentration of imidazole in the running buffer. Purified His<sub>6</sub>-KPR was eluted at a gradient of 0 – 100% buffer B (Table 7-4) over 1 column volume (Figure 7-1).

**Table 7-4.** Buffer eluent for purification using nickel affinity column

Buffer	Component
A	10 mM KH <sub>2</sub> PO <sub>4</sub> , 300 mM NaCl, 10 mM Imidazole, pH 8.0
B	10 mM KH <sub>2</sub> PO <sub>4</sub> , 300 mM NaCl, 500 mM Imidazole, pH 8.0

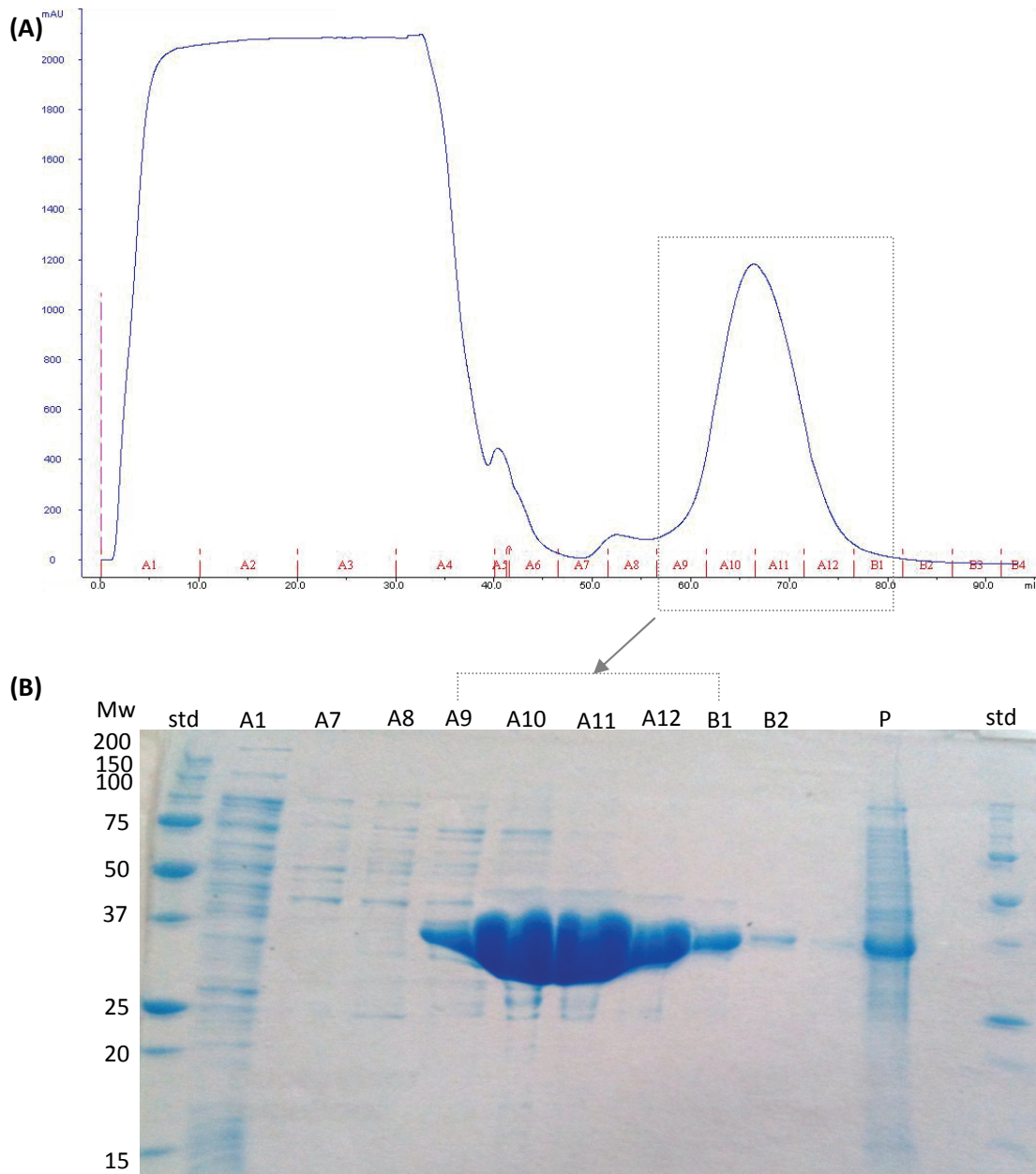


**Figure 7-1.** (A) A chromatogram of KPR purification using nickel affinity column: The blue line represents the  $A_{280}$  and the numbers shown in red correspond to fractions collected. (B) Fractions were run on the SDS gel (15%) stained with Coomassie blue. Lane denoted 'std' has the molecular weight marker and the weights are indicated on the left (kDa). Fraction A1 was flow-through, fractions A9 – B1 contain purified KPR as indicated by the band at 35 kDa and the fraction denoted 'P' represents the cell pellet.

### 7.1.2.5.2 Desalting and size exclusion column

Fractions containing His<sub>6</sub>-KPR from HisTrap affinity column, as assessed by SDS-PAGE were pooled, and imidazole was removed using the desalting column. A size exclusion column was then used to separate protein impurities from His<sub>6</sub>-KPR (Figure 7-2). An isocratic elution in buffer C or D was used (for both columns) depending on the requirements of subsequent experiments (NMR, assays).

**Table 7-5.** Buffer eluent for purification using size exclusion or desalt column

Buffer	Component
C	100 mM HEPES, 150 mM NaCl, 1 mM DTT, 1 mM EDTA, pH 8.0
D	100 mM HEPES, 100 mM NaCl, 1 mM DTT, 1 mM EDTA, pH 7.6

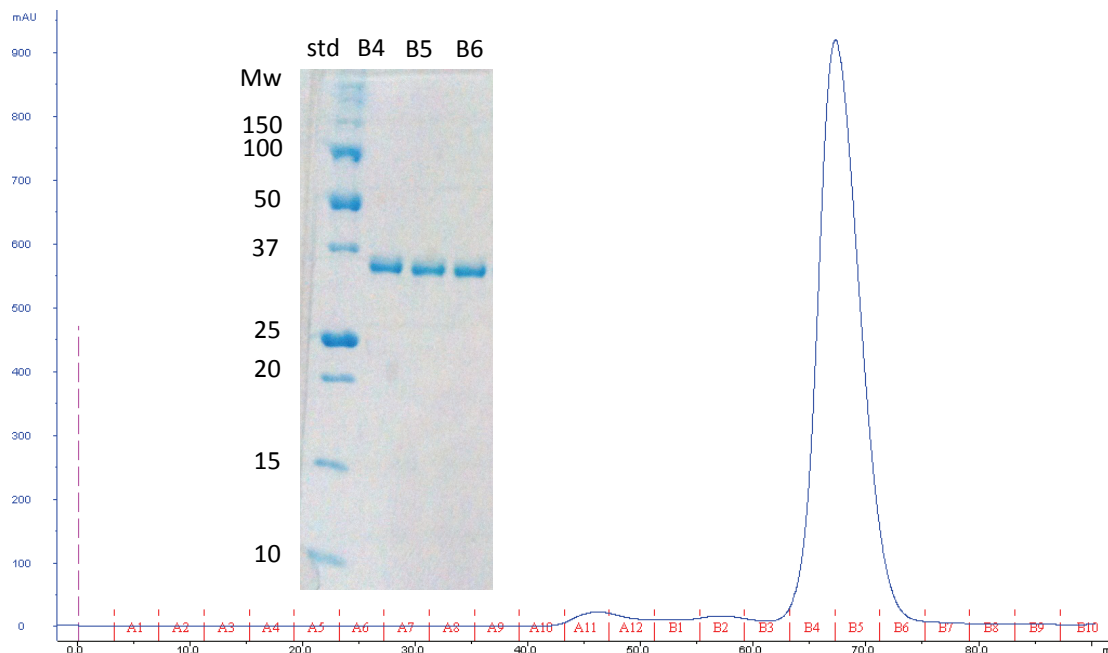


**Figure 7-2.** A chromatogram of KPR purification using size exclusion column and SDS gel (15%) of selected fractions: Fractions were run on the SDS gel (15%) stained with Coomassie blue. Lane denoted 'std' has the molecular weight marker and the weights are indicated on the left (kDa). Fractions B4 – B6 contain purified KPR as indicated by the band at 35 kDa.

### 7.1.2.5.3 Summary

Stage	Ni-NTA	Desalting	Size Exclusion
Column	HisTrap HP 5 ml	HiPrep 26/10	HiLoad Superdex 75 HR 16/60
Buffer/s	A and B	C or D	C or D
Equilibrate (Column Volume)	5 CV	2 CV	5 CV
Flow Rate	2 mL/min	10 mL/min	1 mL/min
Injection Size	10 – 30 mL	10 mL	1 – 4.8 mL
Gradient	0 – 100% B in 1 CV		

### 7.1.2.6 Analysis of KPR expression

#### 7.1.2.6.1 SDS-PAGE

Polyacrylamide gels were made using the Biorad mini-PROTEAN 3 gel casting set (Biorad Laboratories Inc., NSW, Australia). The 5% stacking gel was prepared with 1.0 M Tris/HCl buffer pH 6.8 and a 15% polyacrylamide resolving gel was prepared with 1.5 M Tris/HCl buffer pH 8.8. Sample wells in the gels were produced by the well dividers, which were placed into the stacking gel prior to polymerisation. The gel was positioned upright with separate reservoirs filled with running buffer (25 mM Tris/HCl, 0.19 M glycine and 1% SDS, pH 8.3).

Equal volume (1:1) of sample and Laemmli buffer (50 mM Tris/HCl pH 6.8, 10% glycerol, 2.0% SDS and 0.01% w/v bromophenol blue) were heated at 100 °C for 10 min and loaded onto a 15% polyacrylamide gel. The sample loading volume was typically between 5 – 10 µL. Molecular weights were estimated by comparison to a set

of known molecular weight standards (Biorad Laboratories Inc., NSW, Australia). The gel was run at 100 V until the dye reached the bottom of the stacking gel. Then the voltage was increased to 250 V and continued to run until the dye band reached the bottom of the gel. The gel was stained by incubating in Coomassie blue staining solution (Coomassie blue 1 g/L, acetic acid 100 mL/L, and ethanol 300 mL/L in MilliQ water) for 20 min then destained with destaining solution (30% methanol and 10% acetic acid in MilliQ water) to visualise the protein bands.

Alternatively, the gels were silver stained by soaking the gel in fixing solution (40% methanol, 13.5% formalin in MilliQ water) for 10 min followed by two successive water washes of 5 min each. The gel was soaked in  $\text{Na}_2\text{S}_2\text{O}_3$  for 1 min and then two water washes for 20 sec each. Next, the gel was soaked in 0.1%  $\text{AgNO}_3$  in MilliQ water for 10 min and rinsed with water. A small volume of developing solution (3% sodium carbonate, 0.05% formalin, 0.000016%  $\text{Na}_2\text{S}_2\text{O}_3$  in MilliQ water) was added and the gel was soaked until the band intensities were determined to be adequate as judged visually (1 – 3 min) before the reaction was quenched with 2.3 M citric acid with shaking for a further 10 min. Finally, the gel was washed in water and soaked in water for 30 min before drying.

#### 7.1.2.6.2 *Estimation of protein concentration*

Total protein concentration was quantified using a Cary 50 UV-Vis spectrophotometer (Agilent Technologies, Forest Hill, VIC, Australia) operated by version 4.1 Cary WinUV software or a NanoVue spectrophotometer (GE Healthcare, NSW, Australia). Absorption at 280 nm and an extinction coefficient of  $62650 \text{ M}^{-1} \text{ cm}^{-1}$  were used.<sup>91</sup> Bradford assays were performed using BioRad kit according to the manufacturer's instructions.

#### 7.1.2.6.3 *Mass spectrometry*

Samples of purified protein were analysed using Agilent Technologies 6510 Q-TOF LC/MS. MS data were analysed and deconvoluted using Mass Hunter (Agilent Technologies, Forest Hill, VIC, Australia). Purified soluble protein samples were injected directly onto the MS. Samples containing high salt concentration were applied to a C8 guard column, which was then washed for 2 min in 0.1% formic acid before being eluted onto the MS with a 10 min 0 – 80% acetonitrile gradient in the presence of 0.1% formic acid, all at 0.25 mL/min. The mass spectrum of purified KPR gave an ES-MS value of 35790.21 Da (Figure 7-3), which was consistent to the calculated amino acid sequence of His<sub>6</sub>-KPR (35791.90 Da) using the ExPASy site (<http://web.expasy.org/protparam/>).

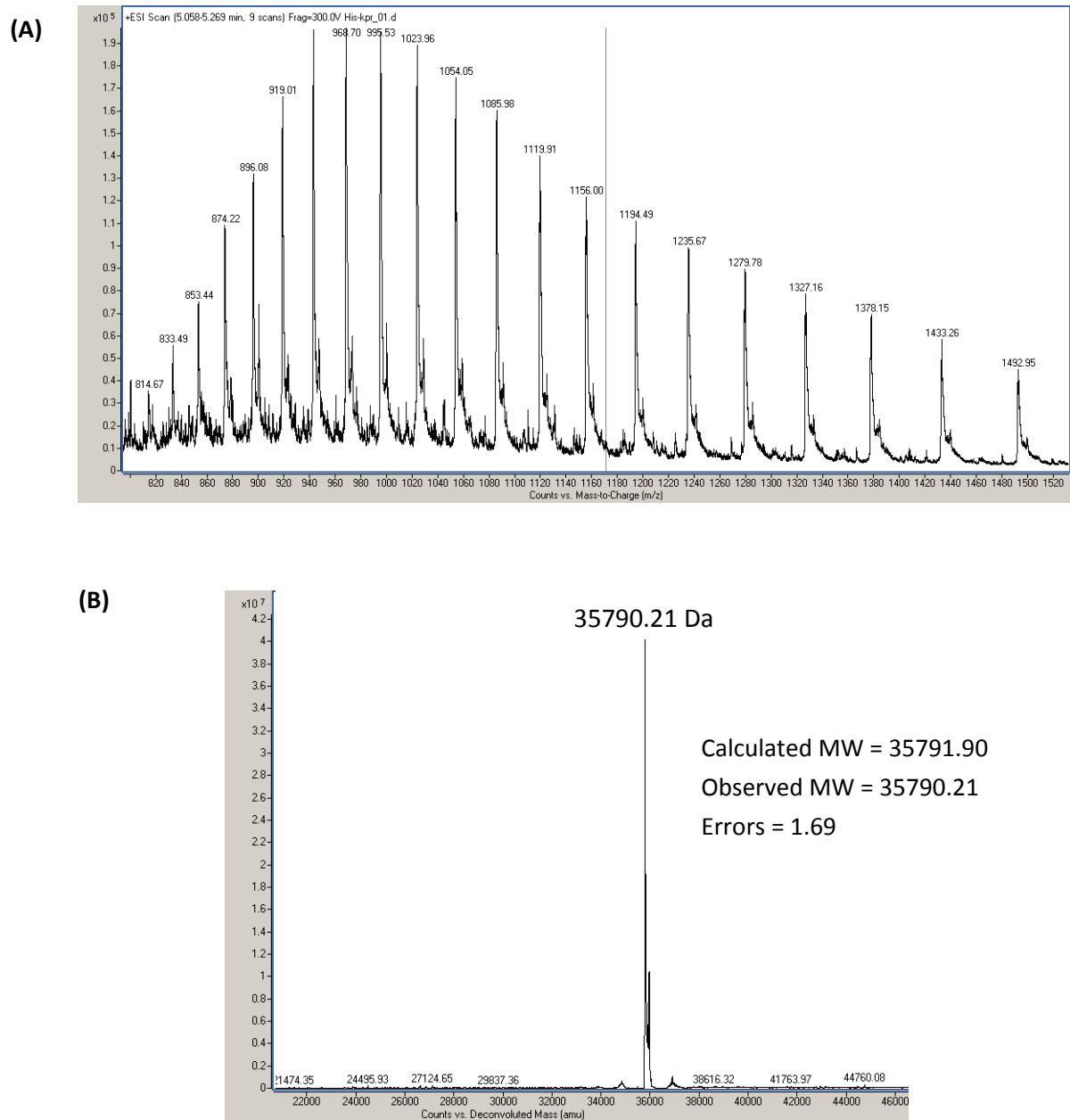


**Figure 7-3.** (A) Electrospray mass spectrum of purified KPR, (B) Deconvoluted mass spectrum

### 7.1.3 Functional assay

#### 7.1.3.1 Kinetics and inhibition assay

The standard KPR assay was adapted from the procedure reported by Ciulli *et al.*<sup>42</sup> KPR activity was assayed by following the decrease in absorbance resulting from converting NADPH to NADP<sup>+</sup> ( $\epsilon_{340 \text{ nm}}$  for NADPH = 6220 M<sup>-1</sup> cm<sup>-1</sup>) at 340 nm with temperature regulated at 30 °C. The assays were carried out on a VERSAmax micro plate reader (Molecular Devices Corporation, Sunnyvale, California, USA) operated by version 4.7 SoftMax Pro software. For measurement of inhibition, fragment compounds in 4  $\mu$ L volumes were added to each well of a 96-well plate (Greiner Bio-One, Frickenhausen, Germany), followed by 176  $\mu$ L of master mix (NADPH and KPR in buffer). The reaction was initiated with the addition of 20  $\mu$ L ketopantoate. The final concentrations and volumes used in a typical inhibition assay are given in Table 7-6. The reactions were carried out in 100 mM HEPES buffer (pH 7.6) in a final volume of 200  $\mu$ L. No more than 2% DMSO was present in any assay. A 2% DMSO control containing no fragment was run on each plate. Measurements were obtained in at least duplicates. Data were fitted to the appropriate rate equation using GraphPad Prism (version 5.00 for Windows, GraphPad Software, San Diego, California USA, [www.graphpad.com](http://www.graphpad.com)).<sup>226</sup>

**Table 7-6.** Reagent concentrations and volumes used in a typical inhibition assay

	[Stock], $\mu$ M	[Final], $\mu$ M	Volume, $\mu$ L
KPR	0.15	0.003	4
NADPH	200	20	20
Ketopantoate	10,000	1,000	20
DMSO			4
Buffer			152

### 7.1.3.1.1 Inhibition determination

The UV-based kinetics assay was used to assess KPR inhibition by the fragments. Initially their inhibitory activity was evaluated and the results were presented as percent inhibition at 0.5 or 1 mM concentration. Based on a given cut-off (30 – 50%), the half maximal inhibitory concentration ( $IC_{50}$ ), that was calculated using non-linear regression of log(antagonist) vs response model. Further characterisation involved obtaining the inhibition constant of the inhibitor ( $K_i$ ). The data were analysed using non-linear regression with a competitive inhibition model based on the Cheng-Prusoff equation:

#### Equation 7-1

$$K_i = \frac{IC_{50}}{1 + [S]/K_m}$$

where:  $K_i$  = inhibition constant  
 $IC_{50}$  = inhibitor concentration at 50% inhibition  
[S] = substrate concentration  
 $K_m$  = Michaelis-Menten constant (for Substrate S)

### 7.1.3.2 Non-specific interaction, bovine serine albumin test

A control experiment was performed with three concentrations of BSA, 0.1, 0.5 and 1 mg/mL in the absence of any test compound to establish whether BSA may interfere with the enzyme assay. The standard KPR assay protocol was adapted and was carried out on a VERSAmax micro plate reader. BSA (0.1 – 1 mg/mL) was added to the buffer before the addition of KPR.

### 7.1.3.3 Optimised detergent-based enzyme assay

In the optimised assay, NADH was used instead of NADPH and detergent was added to the reaction mixture. The assays were carried out on a VERSAmax micro plate reader. To each well of a 96-well plate, compounds were added in 4  $\mu\text{L}$  volumes. Tween-20 was mixed with the buffer (100 mM HEPES buffer (pH 7.6)) first and then NADH and KPR were added to form the master mix. The master mix (176  $\mu\text{L}$ ) was then added to each well and the reaction was initiated by the addition of 20  $\mu\text{L}$  ketopantoate. The final concentrations and volumes used in the reaction for % inhibition or  $\text{IC}_{50}$  are summarised in Table 7-7.

**Table 7-7.** Reagent concentrations and volumes used in a typical inhibition assay

	[Stock], $\mu\text{M}$	[Final], $\mu\text{M}$	Volume, $\mu\text{L}$
KPR	0.15	0.003	4
NADH	250	25	20
Ketopantoate	10,000	1,000	20
DMSO			4
Buffer			152
Tween-20			0.02

### 7.1.3.4 $\text{IC}_{50}$ and ligand efficiency

The quality of fragment hits was assessed through LE to ensure the best fragment hits were selected for optimisation. Given that we did not have any  $K_d$  values,  $\text{IC}_{50}$  values were used as an approximation. LE was calculated using two equations, first by converting the  $\text{IC}_{50}$  into the free energy of binding (Equation 7-2) where  $R$  is the gas constant (1.9872 kcal/mol; 1 kcal  $\approx$  4.184 kJ) and  $T$  is the temperature (303 K) of the experiment and  $\text{IC}_{50}$  is the half maximal inhibition concentration for the compound.

Subsequently, the  $\Delta G$  free energy of binding (kcal/mol) from Equation 7-2 is divided by  $N$  the number of heavy atoms (non-hydrogen atoms) in the compound (Equation 7-3).

**Equation 7-2.**

$$\Delta G = -RT \cdot \ln (IC_{50})$$

**Equation 7-3.**

$$LE = -\Delta G / N_{\text{non-hydrogen atoms}}$$

#### 7.1.4 Dynamic light scattering

The buffer (100 mM HEPES, 100 mM NaCl, pH 7.6) used in compound dilutions was filtered first using 0.22  $\mu\text{m}$  nitrocellulose membrane filters to remove dust prior to DLS measurements. The polystyrene cuvettes were washed with milliQ water and dried prior to use. Compounds were tested at final concentrations of 50, 100 and 500  $\mu\text{M}$ , with (and without) 0.01% Triton X-100 (vol/vol) and 2% DMSO (vol/vol) in a final volume of 1 mL. Each sample was prepared in at least duplicate to check reproducibility. For negative controls, 2% DMSO was added to the buffer in the presence (and absence) of 0.01% Triton X-100 (vol/vol). Samples were assessed using a Malvern Zetasizer Nano S, (Malvern Instruments, Worcestershire, U.K.) with a 4 mW He-Ne laser ( $\lambda$ ) 632.8 nm with detection at  $173^\circ$  and a thermostated sample chamber set to  $25^\circ\text{C}$  was used. Size information was obtained from the correlation function by two mean values on the Zetasizer Nano DS using the software package DTS Nano version 5.10.

## 7.1.5 NMR methods

### 7.1.5.1 STD-NMR

Unless otherwise indicated, the NMR buffer for all KPR samples consisted of HEPES 100 mM, NaCl 150 mM, DTT 1 mM and EDTA 1 mM in H<sub>2</sub>O with 10% D<sub>2</sub>O (vol/vol), adjusted to pH 8.0. All 1D <sup>1</sup>H NMR reference spectra for individual library fragments were acquired on a Brüker AvanceII 800 Spectrometer (Brüker BioSpin, Billerica, MA, USA) at 800.13 MHz equipped with a cryo-cooled probe in 10% D<sub>2</sub>O and buffer (20 mM KH<sub>2</sub>PO<sub>4</sub>, 80 mM NaCl pH 7.4), using the WATERGATE<sup>227</sup> sequence for water suppression. <sup>1</sup>H NMR reference spectra also served as a quality check for purity and correct fragment identity.

#### 7.1.5.1.1 Standard STD-NMR

For primary screening, samples were prepared using 25 µM unlabelled KPR in buffer (535 µL) with mixtures of 5 fragments (5 µL) at a final concentration of 1 mM each and 10% D<sub>2</sub>O (60 µL). Each sample was immediately transferred into a 5 mm NMR tube with a final volume of 600 µL. The STD measurements were acquired on an 800 MHz Brüker AvanceII spectrometer, employing a triple-resonance 5 mm TXI cryoprobe equipped with single-axis gradients and an autosampler. Standard pulse sequences were used for 1D and STD data acquisition and water suppression was achieved using the WATERGATE scheme. STD-NMR experiments were carried out at 10 °C. The 3s irradiation period consisted of a train of 50 ms Gaussian pulses separated by a 1 ms delay. A 35 ms T<sub>2</sub> filter was used to suppress residual protein signals. STD data sets were obtained in 128 scans. NMR data were processed in TOPSPIN version 3.1 (Bruker Biospin).

To begin with, the STD analysis involved comparing 10 STD spectra at a time and those that displayed stronger signals were selected for further investigation. For an individual analysis of the STD an example is shown in Figure 7-4. The 1D  $^1\text{H}$  NMR spectra of five different fragments in solution (A – E) are shown for reference. The 1D  $^1\text{H}$  NMR spectrum of a mix of the five fragments in the presence of KPR (red spectrum) is compared with the STD (blue spectrum). The resonance signals observed in the STD spectrum are indicative of a fragment binding. In the example shown, fragment (C) is a KPR fragment binder.

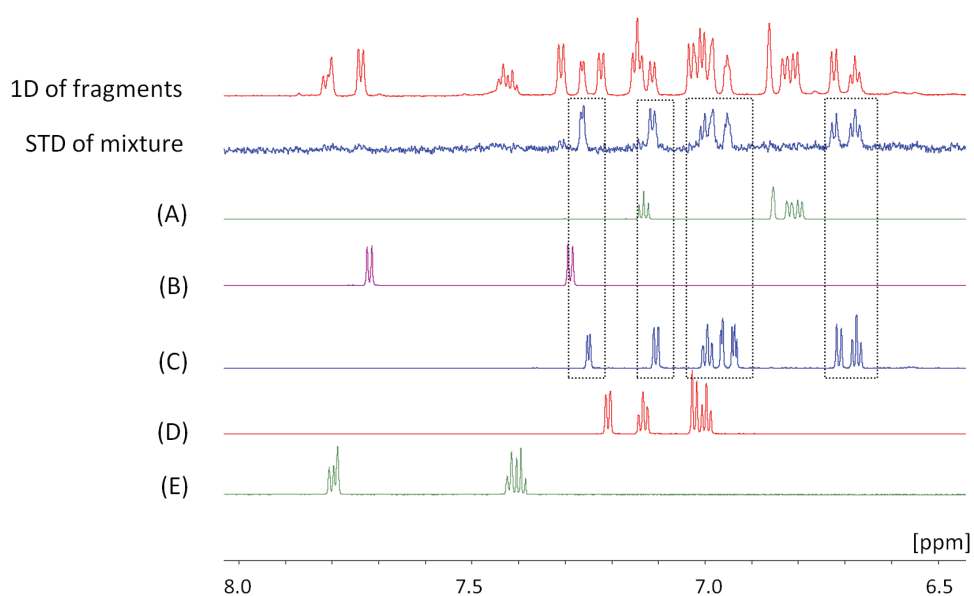


**Figure 7-4.** Detection of ligand binding to KPR using STD-NMR: The box highlights fragment C proton signals matching those observed in the STD spectrum indicating fragment C is binding to KPR.

#### 7.1.5.1.2 Optimised detergent-based STD-NMR

The samples were prepared as cocktails of 5 fragments at a final concentration of 300  $\mu\text{M}$  each. Tween-20 (0.01%) was mixed with buffer (495  $\mu\text{L}$ ) prior to the addition of 5  $\mu\text{L}$  of KPR (at final concentration of 15  $\mu\text{M}$ ) and 10%  $\text{D}_2\text{O}$  (55  $\mu\text{L}$ ). The KPR mixture was added to the fragment cocktail (5  $\mu\text{L}$ ) to give a final volume of 560  $\mu\text{L}$ . Mixed gently in a microcentrifuge tube, the sample was then transferred to a standard NMR tube. Control samples without KPR were also prepared and analysed. The method used to process the NMR data was the same as that described for standard STD-NMR.

Since some fragments display a positive STD signal in the absence of KPR a comparison of the signal intensities was made between STD in the presence of KPR (Tween-20 + KPR) and absence of KPR (Tween-20 only). A fragment was designated binding to KPR and not the detergent when it showed at least a two-fold greater intensity of STD signal in the presence of KPR.

#### 7.1.5.2 $^1\text{H}/^{15}\text{N}$ -HSQC NMR

$^1\text{H}/^{15}\text{N}$ -HSQC spectra were acquired on a Varian Unity Inova 600 spectrometer at 599.76 MHz equipped with a single axis gradient triple resonance cryogenic probe with 32 scans and 64  $t_1$  increments or on a Bruker Avance 800 spectrometer with 8 scans and 160  $t_1$  increments. Typical acquisition time was 30 min for each  $^1\text{H}/^{15}\text{N}$ -HSQC experiment and the standard pulse sequence was used for data acquisition.

Samples were prepared with 100  $\mu\text{M}$  uniformly  $^{15}\text{N}$ -labelled KPR in 100 mM HEPES buffer (pH 8.0), containing 150 mM NaCl and 10%  $\text{D}_2\text{O}$  in the presence and absence of added compound. Compounds were tested at 1 mM (0.2% DMSO) using Shigemi tubes

(Hachioji-City, Tokyo, Japan) in a final volume of 300  $\mu$ L. The  $^1\text{H}/^{15}\text{N}$ -HSQC spectra were processed with TOPSPIN version 3.1 (Bruker Biospin) and analysed using Sparky.<sup>228</sup> Binding was analysed by monitoring the weighted average of the  $^1\text{H}$  and  $^{15}\text{N}$  chemical shift changes.

### 7.1.5.3 Chemical shift mapping

Ligand binding to a target protein affects the chemical shifts of both the ligand and the protein nuclei resonance signals.  $^1\text{H}/^{15}\text{N}$ -HSQC spectra were acquired in the presence and absence of the fragments. Binding was analysed using the weighted combined  $^1\text{H}$  and  $^{15}\text{N}$  amide shifts ( $\Delta\delta$ ) using Equation 7-4.

#### Equation 7-4

$$\Delta\delta = \sqrt{(\delta H_{\text{bound}} \text{KPR} - \delta H_{\text{free}} \text{KPR})^2 + 0.154 (\delta N_{\text{bound}} \text{KPR} - \delta N_{\text{free}} \text{KPR})^2}$$

Residues that experience the greatest changes in chemical shift were mapped onto the crystal structure of KPR (PDB ID: 1YJQ).<sup>91</sup> The CSP were categorised as strong ( $\Delta\delta > 0.04$  ppm), medium ( $0.04 > \Delta\delta > 0.01$  ppm) or weak ( $\Delta\delta > 0.01$  ppm). PyMOL molecular viewer (DeLano Scientific LLC, USA) was used for visualisation of the CSP mapped onto the KPR structure.<sup>229</sup>

## 7.1.6 Computational docking

### 7.1.6.1 Analysis of water molecules in the binding site

KPR crystal structures were retrieved from the Protein Data Bank (PDB ID: 1YON, 2OFP, 1YJQ, 1KS9) and converted into 2D plots using the program LIGPLOT.<sup>95</sup> Water molecules involved in hydrogen bonds between the protein and the ligand are listed (Table 7-8). The crystal structures were then superimposed to identify any waters that were structurally conserved (Chapter 1, Figure 1-5).

**Table 7-8.** The hydrogen bond interactions for the different water molecules

H <sub>2</sub> O-#	Hydrogen bond Interactions
1	Gly7 or Gly9, Gly12 (conserved <sup>7</sup> GCGALG <sup>12</sup> glycine-rich loop), Thr70 and cofactor pyrophosphate group
2	Cys8 and the cofactor adenine nitrogen
3	Gln75 and cofactor 2'-phosphate group (all except PDB ID: 1YON) For 1YON: Gln75 and cofactor pyrophosphate group
4	Arg124 and cofactor pyrophosphate group

### 7.1.6.2 Ligand preparation

The library of 500 fragments from Maybridge used in the docking experiment was converted from 2D to 3D structures using the program SYBYL (Tripos, St. Louis, MO, USA, 1999) with the aid of scripting written by Dr David Chalmers (MIPS, Monash University). Other ligands such as NADPH and its analogues were constructed in SYBYL. The ligands were assigned Gasteiger-Marsili charges and energy minimised prior to docking.

### 7.1.6.3 Protein preparation

The protein was prepared with the standard options of the Protein Preparation Wizard protocol in Maestro (version 8.0; Schrödinger). Hydrogen additions and the adjustment of protonation and tautomerization states of binding site residues were carried out at pH 7.4. Only water molecules involved in protein-cofactor interactions were retained during the preparation of the system. Some residues containing structural errors were fixed manually.

### 7.1.6.4 Glide docking

In Glide (version 5.0; Schrödinger) the protein was assigned Macromodel/OPLS charges and atom types. The co-crystallised NADP<sup>+</sup> was used to define a centroid for the docking grid and the enclosing box length was set to 10 Å in X, Y and Z directions. Default parameters were used for van der Waals (vdW) radii scaling factor (0.8), per-atom vdW radius and charge scaling values (cut-off of 0.25). Distance-dependent dielectric constant was defined as 2.0 and maximum number of steps was set to 500 during the conjugate gradient minimization cycles for the energy minimization stages for selected poses.

Two modes of Glide processing were examined. The standard-precision (SP) allows docking with high speed, though relatively moderate accuracy and restricted conformational sampling. The extra-precision (XP) mode requires more CPU time as it combines the sampling protocol with the use of a custom scoring function designed to identify ligand poses that would be expected to have favourable energies. The GlideScore scoring function (Equation 7-5) was used to select up to 20 poses for each ligand.

**Equation 7-5:**

$$\text{GlideScore} = A \times \text{vdW} + B \times \text{Coul} + \text{Lipo} + \text{Hbond} + \text{Metal} + \text{BuryP} + \text{RotB} + \text{Site}$$

Where:

vdW = van der Waals energy

Coul = Coulomb energy

Lipo = Lipophilic contact term

HBond = Hydrogen-bonding term

Metal = Metal-binding term

BuryP = Penalty for buried polar groups

RotB = Penalty for freezing rotatable bonds

Site = Polar interactions in the active site

## 7.2 Chemistry

### 7.2.1 General experimental

$^1\text{H}$  NMR spectra were recorded on a Brüker Avance DPX 300 or 400 spectrometer at 300.13 or 400.13 MHz respectively or on a Varian Unity Inova 600 spectrometer at 599.76 MHz. Data was acquired using TOPSPIN/ICONNMR (Brüker) and plotting was managed using MestReNova 6.0.2 software. Chemical shifts ( $\delta$ ) for all  $^1\text{H}$  are reported in parts per million (ppm) and were referenced to residual proteo-solvent residual peaks, such as  $\delta$  7.26 for deuterated chloroform ( $\text{CDCl}_3$ ),  $\delta$  2.50 for  $d_6$ -dimethyl sulfoxide ( $d_6$ -DMSO), or  $\delta$  3.31 for  $d_4$ -methanol ( $\text{CD}_3\text{OD}$ ).<sup>230</sup> Each proton resonance was assigned according to the following convention: chemical shift ( $\delta$ ), number of protons, multiplicity, coupling constant(s) ( $J$  Hz) and proton assignment. Multiplicities are denoted as: s, singlet; d, doublet; t, triplet; q, quartet; p, pentet; m, multiplet; br, broad and app, apparent. Proton-fluorine  $^{19}\text{F}$  coupling constants are reported as  $^3J_{\text{HF}}$  and recorded to the nearest 0.5 Hz.

$^{13}\text{C}$  NMR spectra were recorded on a Brüker Avance DPX 400 spectrometer at 100.61 MHz, or on a Varian Unity Inova 600 spectrometer at 150.83 MHz. Data was acquired using TOPSPIN/ICONNMR (Brüker) and plotting was managed using MestReNova 6.0.2 software. Chemical shifts ( $\delta$ ) for all  $^{13}\text{C}$  NMR spectra are reported in parts per million (ppm), referenced to the relevant solvent signals:  $\delta$  77.16 for  $\text{CDCl}_3$ ;  $\delta$  39.52 for  $d_6$ -DMSO; and  $\delta$  49.00 for  $\text{CD}_3\text{OD}$ .<sup>230</sup> Carbon signals are assigned as:  $\text{C}_q$ , quaternary; CH, methine carbon;  $\text{CH}_2$ , methylene carbon; and  $\text{CH}_3$ , methyl carbon. Coupling to fluorine  $^{19}\text{F}$  is reported as  $J_{\text{CF}}$  coupling and recorded to the nearest Hz. Homonuclear ( $^1\text{H}$ - $^1\text{H}$ ) correlation spectroscopy (gradient COSY), and HSQC spectra were obtained using the standard Brüker pulse sequence for structural assignment of some compounds.

High Resolution Mass Spectra (HRMS) were collected on a Waters Micromass LCT Premier XE time-of-flight (TOF) mass spectrometer fitted with an electrospray ion source and controlled with MassLynx software version 4.5. Low resolution mass spectra (LRMS) were recorded using electrospray ionisation (ESI) on a Micromass Platform II Single Quadrupole Mass Spectrometer. The principle ion peaks ( $m/z$ ) are reported. Sample management was facilitated by an Agilent 1100 series HPLC system and the instrument was controlled using MassLynx software version 3.5.

Target compounds were analysed using analytical reverse-phase High Performance Liquid Chromatography (HPLC) conducted on a Waters 2690 Separation Module with a Waters 996 Photodiode Array detector on a Phenomenex Luna C8 (2) 100Å (150 × 4.60 mm, 5 µm) column. The following buffers were used; buffer A: 99.9% H<sub>2</sub>O, 0.1% TFA and buffer B: 80% CH<sub>3</sub>CN (or CH<sub>3</sub>OH), 19.9% H<sub>2</sub>O, 0.1% TFA. The following eluent systems were used with a flow rate of 1 mL/min and total run time of 20 min; eluent A (gradient) 0-11 mins, 20% buffer A and 80% buffer B, 11-20 mins 80% buffer A and 20% buffer B. Novel compounds were further analysed using specified conditions (Appendix III) of isocratic buffer A and B over 20 min. All compounds were of ≥ 95% purity. Analytical Thin Layer Chromatography (TLC) was carried out on silica gel 60 F<sub>254</sub> pre-coated plates (0.25 mm, Merck) and visualised by the use of UV light and iodine or vanillin. Flash column chromatography was carried out according to the method described by Still *et al.*,<sup>231</sup> using Davisil<sup>®</sup> LC60A 40 – 63 µm silica gel. Melting points were determined with a Mettler Toledo MP50 melting point apparatus and are uncorrected.

Hexane refers to the hydrocarbon fraction boiling at 60 – 80 °C and petroleum spirit refers to the hydrocarbon fraction boiling at 40 – 60 °C. Hexane, petroleum spirit and ethyl acetate were distilled before use. HPLC-grade DCM, THF and DMF were dried using MBraun solvent purification system (SPS-800) according to manufacturer's instructions. All other solvents were reagent grade and used as received. All commercially available chemicals were purchased from Aldrich/Fluka, Merck or Matrix and used without purification, unless otherwise indicated.

## 7.2.2 Synthesis of sulfonamides

### 7.2.2.1 Preparation of *N*-(4-sulfonylphenyl)acetamide

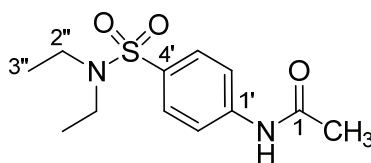
#### *General procedure A:*

To a stirred solution of 4-acetamidobenzene-1-sulfonyl chloride (**142**) (500 mg, 2.14 mmol) in THF (10 mL) was added amine (**141a – m**, 5 – 10 mol equivalent) at ambient temperature. The reaction mixture was heated at reflux for 1 h after which it was concentrated under reduced pressure. The resulting residue was dissolved in aqueous HCl (1 M, 30 mL) to which ethyl acetate (30 mL) was added. The layers were separated, the aqueous phase was extracted with ethyl acetate (3 × 30 mL) and the combined organic fractions were washed with water, brine, dried over anhydrous magnesium sulfate and dried *in vacuo* to give the required crude product (**143a – m**).

### 7.2.2.2 Preparation of 4-aminobenzenesulfonamide

#### *General procedure B:*

The subsequent *N*-(4-sulfamoylphenyl)acetamide product (**143a – m**, 50 – 200 mg) of general procedure B was mixed in aqueous HCl (2 M) and stirred at 100 °C for 1 h. The reaction mixture was then neutralised at 0 °C with sodium hydroxide (2 M). The crude solid thus obtained was filtered, washed with cold water and dried. Purification of the title compound (**144a – m**) was achieved by recrystallisation using the solvent(s) specified.

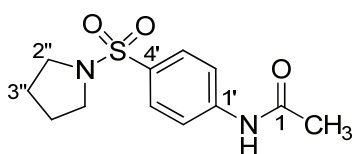
***N*-[4-(Diethylsulfonyl)phenyl]acetamide (143a)**

Diethylamine **141a** (783 mg, 10.70 mmol) was added to 4-acetamidobenzene-1-sulfonyl chloride (**142**) (500 mg, 2.14 mmol) in THF (10 mL) as described in general procedure A. Recrystallisation from ethyl acetate-hexane afforded the desired product **143a** (415 mg, 72%) as white crystals, mp 72 – 74 °C (lit. 71 – 73 °C) with spectroscopic data in agreement with literature data.<sup>232</sup>

**<sup>1</sup>H NMR** (300 MHz, *d*<sub>6</sub>-DMSO) δ: 1.02 (6H, t, *J* = 7.2 Hz, H3''), 2.08 (3H, s, H2), 3.13 (4H, q, *J* = 7.2 Hz, H2''), 7.71 – 7.80 (4H, m, H2', H3', H5', H6'), 10.32 (1H, s, NH).

**LRMS** (ESI) *m/z* 271 (M + H)<sup>+</sup>.

**RP-HPLC**: *t*<sub>R</sub> 8.85 min, 99% (gradient).

***N*-[4-(Pyrrolidine-1-sulfonyl)phenyl]acetamide (143b)**

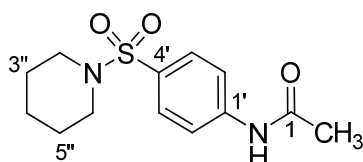
Pyrrolidine **141b** (760 mg, 10.7 mmol) was added to 4-acetamidobenzene-1-sulfonyl chloride (**142**) (500 mg, 2.14 mmol) in THF (10 mL) as described in general procedure A. Recrystallisation from ethyl acetate-hexane afforded *N*-[4-pyrrolidine-1-sulfonyl]phenyl]acetamide **143b** (489 mg, 85%) as white long needles, mp 180 – 182 °C (lit. 183 – 185 °C) with spectroscopic data in agreement with reported literature data.<sup>233</sup>

**<sup>1</sup>H NMR** (300 MHz, CD<sub>3</sub>OD) δ: 1.71 – 1.76 (4H, m, H3'', H4''), 2.16 (3H, s, H2), 3.19 – 3.24 (4H, m, H2'', H5''), 7.74 – 7.81 (4H, m, H2', H3', H5', H6').

**LRMS** (ESI):  $m/z$  269 (85%, (M + H)<sup>+</sup>), 537 (100%, (2M + H)<sup>+</sup>).

**RP-HPLC**:  $t_R$  8.18 min, >99% (gradient).

***N*-[4-(Piperidine-1-sulfonyl)phenyl]acetamide (143c)**



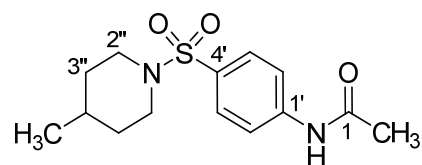
Piperidine **141c** (360 mg, 4.23 mmol) was added to 4-acetamidobenzene-1-sulfonyl chloride (**142**) (100 mg, 0.42 mmol) in THF (10 mL) as described in general procedure A. Recrystallisation from ethyl acetate-hexane afforded the desired product **143c** (75 mg, 63%) as white micro-crystals, mp 160 – 161 °C (lit. 137 – 139 °C) with spectroscopic data in agreement with literature data.<sup>233</sup>

**<sup>1</sup>H NMR** (300 MHz, CD<sub>3</sub>OD)  $\delta$ : 1.41 – 1.47 (2H, m, H4''), 1.62 (4H, app p,  $J$  = 5.7 Hz, H3'', H5''), 2.17 (3H, s, H2), 2.95 (4H, dd,  $J$  = 5.4, 5.4 Hz, H2'', H6''), 6.69 (2H, app d,  $J$  = 9.0 Hz, H2', H6'), 7.81 (2H, app d,  $J$  = 8.7 Hz, H3', H5').

**LRMS** (ESI)  $m/z$  283 (M + H)<sup>+</sup>.

**RP-HPLC**:  $t_R$  9.13 min, >99% (gradient).

***N*-[4-(4-Methylpiperidine-1-sulfonyl)phenyl]acetamide (143d)**



4-Methylpiperidine **141d** (1.06 g, 10.70 mmol) was added to 4-acetamidobenzene-1-sulfonyl chloride (**142**) (500 mg, 2.14 mmol) in THF (10 mL) as described in general procedure A. Recrystallisation from ethyl acetate-hexane afforded the desired product

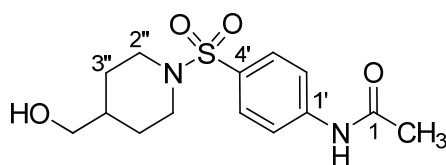
**143d** (571 mg, 90%) as light orange-yellow crystals, mp 152 – 154 °C (lit. 140 – 142 °C) with spectroscopic data in agreement with literature data.<sup>234</sup>

<sup>1</sup>H NMR (400 MHz, CD<sub>3</sub>OD) δ: 0.90 (3H, d, *J* = 6.2 Hz, 4"-CH<sub>3</sub>), 1.16 – 1.35 (3H, m, H<sub>3a</sub>", H<sub>5a</sub>", H<sub>4</sub>"'), 1.69 (2H, br dd, *J* = 12.4, 2.4 Hz, H<sub>3e</sub>", H<sub>5e</sub>"'), 2.16 (3H, s, H<sub>2</sub>), 2.25 (2H, ddd, *J* = 14.2, 11.8, 2.4 Hz, H<sub>2a</sub>"', H<sub>6a</sub>"'), 3.69 (2H, br d, *J* = 12.0 Hz, H<sub>2e</sub>"', H<sub>6e</sub>"'), 7.69 (2H, app d, *J* = 8.9 Hz, H<sub>2</sub>'', H<sub>6</sub>''), 7.79 (2H, app d, *J* = 8.9 Hz, H<sub>3</sub>'', H<sub>5</sub>'').

LRMS (ESI) *m/z* 297 (M + H)<sup>+</sup>.

RP-HPLC: *t<sub>R</sub>* 9.91 min, >99% (gradient).

#### *N*-{4-[4-(Hydroxymethyl)piperidine-1-sulfonyl]phenyl}acetamide (**143e**)



Piperidin-4-ylmethanol **141e** (1.23 g, 10.70 mmol) was added to 4-acetamidobenzene-1-sulfonyl chloride (**142**) (0.50 g, 2.14 mmol) in THF (10 mL) as described in general procedure A. Recrystallisation from ethyl acetate-hexane afforded the desired product **143e** as white micro-crystals (0.57 g, 85%), mp 207 – 208 °C.

<sup>1</sup>H NMR (400 MHz, *d*<sub>6</sub>-DMSO) δ: 1.13 (2H, br ddd, *J* = 16.1, 12.3, 3.7 Hz, H<sub>3a</sub>"', H<sub>5a</sub>"'), 1.20 – 1.35 (1H, m, H<sub>4</sub>"'), 1.68 (2H, dd, *J* = 12.8, 2.1 Hz, H<sub>3e</sub>"', H<sub>5e</sub>"'), 2.09 (3H, s, H<sub>2</sub>), 2.15 (2H, ddd, *J* = 14.0, 11.8, 2.2 Hz, H<sub>2a</sub>"', H<sub>6a</sub>"'), 3.19 (2H, t, *J* = 5.7 Hz, CH<sub>2</sub>OH), 3.60 (2H, br d, *J* = 11.6 Hz, H<sub>2e</sub>"', H<sub>6e</sub>"'), 4.48 (1H, t, *J* = 5.3 Hz, OH), 7.65 (2H, app d, *J* = 8.8 Hz, H<sub>2</sub>'', H<sub>6</sub>''), 7.80 (2H, app d, *J* = 8.9 Hz, H<sub>3</sub>'', H<sub>5</sub>''), 10.36 (1H, s, NH).

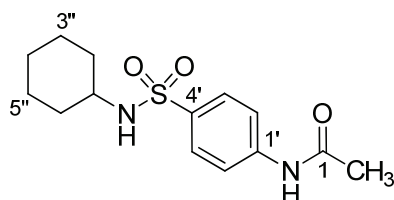
<sup>13</sup>C NMR (101 MHz, *d*<sub>6</sub>-DMSO) δ: 24.2 (CH<sub>3</sub>), 27.8 (CH<sub>2</sub>), 37.3 (CH), 45.9 (CH<sub>2</sub>), 65.2 (CH<sub>2</sub>), 118.7 (CH), 128.7 (CH), 129.1 (C<sub>q</sub>), 143.3 (C<sub>q</sub>), 169.0 (C<sub>q</sub>).

LRMS (ESI) *m/z* 313 (M + H)<sup>+</sup>.

**HRMS** (ESI) calcd for  $C_{14}H_{20}N_2O_4S$  ( $M + H$ )<sup>+</sup> 313.1217, found: ( $M + H$ )<sup>+</sup> 313.1227.

**RP-HPLC**:  $t_R$  4.01 min, >99% (isocratic),  $t_R$  7.51 min, >99% (gradient).

***N*-[4-(Cyclohexylsulfamoyl)phenyl]acetamide (143f)**

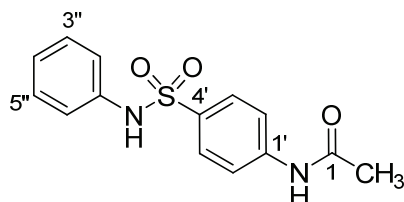


Cyclohexylamine **141f** (419 mg, 4.23 mmol) was added to 4-acetamidobenzene-1-sulfonyl chloride (**142**) (100 mg, 0.42 mmol) in THF (10 mL) as described in general procedure A. Recrystallisation from ethyl acetate-hexane afforded the desired product **143f** (68 mg, 54%) as white prism-like crystals, mp 221 – 222 °C (lit. 197 – 200 °C) with spectroscopic data in agreement with literature data.<sup>233</sup>

**<sup>1</sup>H NMR** (400 MHz,  $d_6$ -DMSO)  $\delta$ : 0.99 – 1.15 (5H, m, H2<sub>a</sub>'', H3<sub>a</sub>'', H4<sub>a</sub>'', H5<sub>a</sub>'', H6<sub>a</sub>''), 1.42 – 1.56 (5H, m, H2<sub>e</sub>'', H3<sub>e</sub>'', H4<sub>e</sub>'', H5<sub>e</sub>'', H6<sub>e</sub>''), 2.08 (3H, s, H2), 2.83 – 2.93 (1H, m, H1''), 7.48 (1H, d,  $J = 7.4$  Hz, NHSO<sub>2</sub>), 7.70 – 7.75 (4H, m, H2', H3', H5', H6'), 10.28 (1H, s, NHCO).

**LRMS** (ESI)  $m/z$  297 ( $M + H$ )<sup>+</sup>.

**RP-HPLC**:  $t_R$  9.49 min, >99% (gradient).

***N*-[4-(Phenylsulfamoyl)phenyl]acetamide (143g)**

Aniline **141g** (498 mg, 5.35 mmol) was added to a stirred solution of 4-acetamidobenzene-1-sulfonyl chloride (**142**) (250 mg, 1.07 mmol) in THF (10 mL) as described in general procedure A. Recrystallisation from ethyl acetate-hexane afforded the desired product **143g** as a white solid (135 mg, 43%), mp 210 – 211 °C.

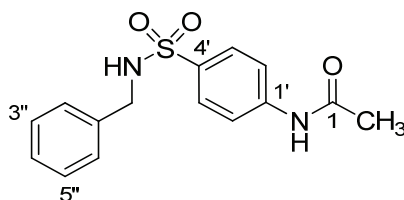
**<sup>1</sup>H NMR** (400 MHz, *d*<sub>6</sub>-DMSO) δ: 2.05 (3H, s, H<sub>2</sub>), 6.97 – 7.03 (1H, m, H<sub>4''</sub>), 7.04 – 7.09 (2H, m, H<sub>2''</sub>, H<sub>6''</sub>), 7.17 – 7.24 (2H, m, H<sub>3''</sub>, H<sub>5''</sub>), 7.64 – 7.72 (4H, m, H<sub>2'</sub>, H<sub>3'</sub>, H<sub>5'</sub>, H<sub>6'</sub>), 10.15 (1H, s, NHSO<sub>2</sub>), 10.29 (1H, s, NHCO).

**<sup>13</sup>C NMR** (101 MHz, *d*<sub>6</sub>-DMSO) δ: 24.1 (CH<sub>3</sub>), 118.6 (CH), 120.1 (CH), 124.0 (CH), 128.0 (CH), 129.2 (CH), 133.1 (C<sub>q</sub>), 137.9 (C<sub>q</sub>), 143.1 (C<sub>q</sub>), 169.1 (C<sub>q</sub>).

**LRMS** (ESI) *m/z* 291 (M + H)<sup>+</sup>, 581 (2M + H)<sup>+</sup>.

**HRMS** (ESI) calcd for C<sub>14</sub>H<sub>14</sub>N<sub>2</sub>O<sub>3</sub>S (M + H)<sup>+</sup> 291.0798, found: (M + H)<sup>+</sup> 291.0808.

**RP-HPLC**: *t*<sub>R</sub> 6.03 min, >99% (isocratic), *t*<sub>R</sub> 8.54 min, >99% (gradient).

***N*-[4-(Benzylsulfamoyl)phenyl]acetamide (143h)**

Benzylamine **141h** (1.15 g, 10.70 mmol) was added to 4-acetamidobenzene-1-sulfonyl chloride (**142**) (0.50 g, 2.14 mmol) in THF (10 mL) as described in general procedure A. Recrystallisation from ethyl acetate-hexane afforded the desired product **143h** (0.52 g,

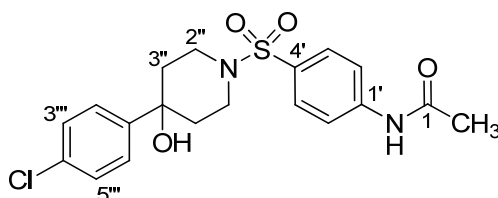
79%) as off-white crystals, mp 160 – 161 °C (lit. 171 – 172 °C) with spectroscopic data in agreement with literature data.<sup>233</sup>

<sup>1</sup>H NMR (300 MHz, CD<sub>3</sub>OD) δ: 2.15 (3H, s, H<sub>2</sub>), 4.04 (2H, s, CH<sub>2</sub>), 7.17 – 7.26 (5H, m, H<sub>2</sub>'', H<sub>3</sub>'', H<sub>4</sub>'', H<sub>5</sub>'', H<sub>6</sub>''), 7.69 – 7.77 (4H, m, H<sub>2</sub>', H<sub>3</sub>', H<sub>5</sub>', H<sub>6</sub>').

LRMS (ESI) *m/z* 305 (M + H)<sup>+</sup>.

RP-HPLC: *t<sub>R</sub>* 9.19 min, >99% (gradient).

***N*-{4-[4-(4-Chlorophenyl)-4-hydroxypiperidine-1-sulfonyl]phenyl}acetamide (143i)**



4-(4-Chlorophenyl)piperidin-4-ol **141i** (452 mg, 2.14 mmol) was added to 4-acetamidobenzene-1-sulfonyl chloride (**142**) (250 mg, 1.07 mmol) in THF (10 mL) as described in general procedure A. Recrystallisation from ethyl acetate-hexane afforded the desired product **143i** as white micro-crystals (147 mg, 34%), mp 216 – 218 °C.

<sup>1</sup>H NMR (400 MHz, *d*<sub>6</sub>-DMSO) δ: 1.62 (2H, br d, *J* = 12.7 Hz, H<sub>3e</sub>'', H<sub>5e</sub>''), 1.95 (2H, ddd, *J* = 17.2, 13.1, 4.4 Hz, H<sub>3a</sub>'', H<sub>5a</sub>''), 2.10 (3H, s, H<sub>2</sub>), 2.57 (2H, app t, *J* = 10.9 Hz, H<sub>2a</sub>'', H<sub>6a</sub>''), 3.47 – 3.57 (2H, m, H<sub>2e</sub>'', H<sub>6e</sub>''), 5.05 (1H, s, OH), 7.35 (2H, app d, *J* = 8.7 Hz, H<sub>3</sub>'', H<sub>5</sub>''), 7.45 (2H, app d, *J* = 8.7 Hz, H<sub>2</sub>'', H<sub>6</sub>''), 7.71 (2H, app d, *J* = 8.9 Hz, H<sub>2</sub>', H<sub>6</sub>'), 7.84 (2H, app d, *J* = 8.9 Hz, H<sub>3</sub>', H<sub>5</sub>'), 10.40 (1H, s, NH).

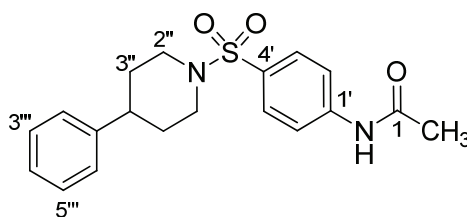
<sup>13</sup>C NMR (101 MHz, *d*<sub>6</sub>-DMSO) δ: 24.2 (CH<sub>3</sub>), 36.7 (CH<sub>2</sub>), 42.2 (CH<sub>2</sub>), 68.7 (C<sub>q</sub>), 118.7 (CH), 126.8 (CH), 127.9 (CH), 128.7 (C<sub>q</sub>), 128.8 (CH), 131.2 (C<sub>q</sub>), 143.5 (C<sub>q</sub>), 148.0 (C<sub>q</sub>), 169.2 (C<sub>q</sub>).

LRMS (ESI) *m/z* 409 (M [<sup>35</sup>Cl] + H)<sup>+</sup>.

**HRMS** (ESI) calcd for  $C_{19}H_{21}ClN_2O_4S$  ( $M + H$ )<sup>+</sup> 409.0983, found: ( $M + H$ )<sup>+</sup> 409.0991.

**RP-HPLC**:  $t_R$  4.85 min, >99% (isocratic),  $t_R$  10.38 min, >99% (gradient).

***N*-[4-(4-Phenylpiperidine-1-sulfonyl)phenyl]acetamide (143j)**



4-Phenylpiperidine **141j** (987 mg, 6.12 mmol) was added to 4-acetamidobenzene-1-sulfonyl chloride (**142**) (500 mg, 2.14 mmol) in THF (10 mL) as described in general procedure A. Recrystallisation from ethyl acetate-hexane afforded the desired product **143j** as light orange small needle-like crystals (703 mg, 92%), mp 191 – 192 °C.

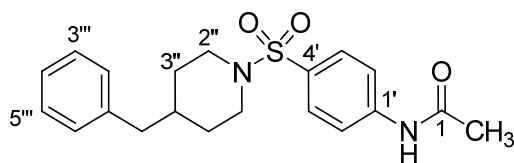
**<sup>1</sup>H NMR** (400 MHz, *d*<sub>6</sub>-DMSO)  $\delta$ : 1.64 (2H, br ddd,  $J = 16.2, 12.5, 3.7$  Hz, H3<sub>a</sub>'', H5<sub>a</sub>''), 1.75 – 1.82 (2H, m, H3<sub>e</sub>'', H5<sub>e</sub>''), 2.10 (3H, s, H2), 2.21 – 2.31 (2H, m, H2<sub>a</sub>'', H6<sub>a</sub>''), 2.44 (1H, tt,  $J = 12.0, 3.3$  Hz, H4''), 3.73 (2H, br d,  $J = 11.6$  Hz, H2<sub>e</sub>'', H6<sub>e</sub>''), 7.13 – 7.21 (3H, m, H2''', H4''', H6'''), 7.22 – 7.30 (2H, m, H3''', H5'''), 7.70 (2H, app d,  $J = 8.8$  Hz, H2', H6'), 7.84 (2H, app d,  $J = 8.9$  Hz, H3', H5'), 10.39 (1H, s, NH).

**<sup>13</sup>C NMR** (101 MHz, *d*<sub>6</sub>-DMSO)  $\delta$ : 24.2 (CH<sub>3</sub>), 32.0 (CH<sub>2</sub>), 40.6 (CH), 46.6 (CH<sub>2</sub>), 118.7 (CH), 126.3 (CH), 126.7 (CH), 128.4 (CH), 128.8 (CH), 128.8 (C<sub>q</sub>), 143.4 (C<sub>q</sub>), 145.2 (C<sub>q</sub>), 169.2 (C<sub>q</sub>).

**LRMS** (ESI)  $m/z$  359 ( $M + H$ )<sup>+</sup>.

**HRMS** (ESI) calcd for  $C_{19}H_{22}N_2O_3S$  ( $M + H$ )<sup>+</sup> 359.1424, found: ( $M + H$ )<sup>+</sup> 359.1438.

**RP-HPLC**:  $t_R$  3.95 min, >99% (isocratic),  $t_R$  11.19 min, >99% (gradient).

***N*-[4-(4-Benzylpiperidine-1-sulfonyl)phenyl]acetamide (143k)**

4-Benzylpiperidine **141k** (1.88 g, 10.70 mmol) was added to 4-acetamidobenzene-1-sulfonyl chloride (**142**) (0.50 g, 2.14 mmol) in THF (10 mL) as described in general procedure A. Recrystallisation from ethyl acetate-hexane afforded the desired product **143k** as off-white solid (0.45 g, 55%), mp 149 – 150 °C.

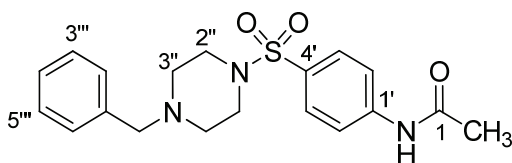
**<sup>1</sup>H NMR** (400 MHz, CD<sub>3</sub>OD) δ: 1.22 (2H, br ddd, *J* = 15.9, 12.4, 3.9 Hz, H3<sub>a</sub>'', H5<sub>a</sub>''), 1.33 – 1.45 (1H, m, H4''), 1.62 (2H, br d, *J* = 12.4 Hz, H3<sub>e</sub>'', H5<sub>e</sub>''), 2.06 – 2.22 (5H, m, H2<sub>a</sub>'', H6<sub>a</sub>'', H2), 2.46 (2H, d, *J* = 6.8 Hz, CH<sub>2</sub>), 3.66 (2H, br d, *J* = 12.0 Hz, H2<sub>e</sub>'', H6<sub>e</sub>''), 7.06 (2H, d, *J* = 7.2 Hz, H2''', H6'''), 7.12 (1H, t, *J* = 7.3 Hz, H4'''), 7.21 (2H, t, *J* = 7.3 Hz, H3''', H5'''), 7.64 (2H, d, *J* = 8.8 Hz, H2', H6'), 7.77 (2H, d, *J* = 8.7 Hz, H3', H5').

**<sup>13</sup>C NMR** (101 MHz, CD<sub>3</sub>OD) δ: 24.1 (CH<sub>3</sub>), 32.4 (CH<sub>2</sub>), 38.5 (CH), 43.5 (CH<sub>2</sub>), 47.7 (CH<sub>2</sub>), 120.4 (CH), 127.0 (CH), 129.3 (CH), 129.8 (CH), 130.1 (CH), 131.6 (C<sub>q</sub>), 141.1 (C<sub>q</sub>), 144.3 (C<sub>q</sub>), 172.0 (C<sub>q</sub>).

**LRMS** (ESI) *m/z* 373 (M + H)<sup>+</sup>.

**HRMS** (ESI) calcd for C<sub>20</sub>H<sub>24</sub>N<sub>2</sub>O<sub>3</sub>S (M + H)<sup>+</sup> 373.1580, found: (M + H)<sup>+</sup> 373.1599.

**RP-HPLC**: *t*<sub>R</sub> 4.61 min, >99% (isocratic), *t*<sub>R</sub> 11.37 min, >99% (gradient).

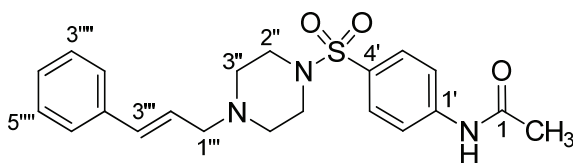
***N*-[4-(4-Benzylpiperazine-1-sulfonyl)phenyl]acetamide (**143I**)**

1-Benzylpiperazine **143I** (1.89 g, 10.70 mmol) was added to 4-acetamidobenzene-1-sulfonyl chloride (**142**) (0.50 g, 2.14 mmol) in THF (10 mL) as described in general procedure A. Recrystallisation from ethyl acetate-hexane afforded the desired product **143I** (0.46 g, 58%) as light yellow micro-crystals, mp 179 – 180 °C with spectroscopic data in agreement with literature data.<sup>235</sup>

<sup>1</sup>H NMR (300 MHz, CD<sub>3</sub>OD)  $\delta$ : 2.16 (3H, s, H<sub>2</sub>), 2.47 – 2.51 (4H, m, H<sub>3''</sub>, H<sub>5''</sub>), 2.98 – 3.01 (4H, m, H<sub>2''</sub>, H<sub>6''</sub>), 3.49 (2H, s, CH<sub>2</sub>), 7.19 – 7.31 (5H, m, H<sub>2'''</sub>, H<sub>3'''</sub>, H<sub>4'''</sub>, H<sub>5'''</sub>, H<sub>6'''</sub>), 7.69 (2H, app d,  $J = 9.0$  Hz, H<sub>2'</sub>, H<sub>6'</sub>), 7.80 (2H, app d,  $J = 9.0$  Hz, H<sub>3'</sub>, H<sub>5'</sub>).

LRMS (ESI)  $m/z$  374 (M + H)<sup>+</sup>.

RP-HPLC:  $t_R$  7.32 min, >99% (gradient).

***N*-[4-(4-Cinnamylpiperazine-1-sulfonyl)phenyl]acetamide (**143m**)**

1-Cinnamylpiperazine **141m** (432 mg, 2.14 mmol) was added to a stirred solution of 4-acetamidobenzene-1-sulfonyl chloride (**142**) (250 mg, 1.07 mmol) in THF (10 mL) as described in general procedure A. Recrystallisation from ethyl acetate-hexane afforded the desired product **143m** as orange crystals (209 mg, 48%), mp 115 – 118 °C.

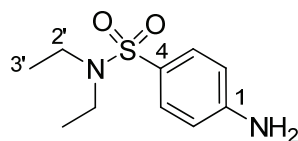
**<sup>1</sup>H NMR** (400 MHz, *d*<sub>6</sub>-DMSO) δ: 2.10 (3H, s, H<sub>2</sub>), 2.40 – 2.48 (4H, m, H<sub>3''</sub>, H<sub>5''</sub>), 2.80 – 2.94 (4H, m, H<sub>2''</sub>, H<sub>6''</sub>), 3.07 (2H, d, *J* = 6.3 Hz, H<sub>1'''</sub>), 6.18 (1H, dt, *J* = 15.9, 6.5 Hz, H<sub>2'''</sub>), 6.49 (1H, d, *J* = 16.0 Hz, H<sub>3'''</sub>), 7.17 – 7.25 (1H, m, H<sub>4'''</sub>), 7.25 – 7.34 (2H, m, H<sub>3'''</sub>, H<sub>5'''</sub>), 7.36 – 7.41 (2H, m, H<sub>2'''</sub>, H<sub>6'''</sub>), 7.65 (2H, app d, *J* = 8.9 Hz, H<sub>2'</sub>, H<sub>6'</sub>), 7.82 (2H, app d, *J* = 8.9 Hz, H<sub>3'</sub>, H<sub>5'</sub>), 10.40 (1H, s, NH).

**<sup>13</sup>C NMR** (101 MHz, *d*<sub>6</sub>-DMSO) δ: 24.2 (CH<sub>3</sub>), 46.0 (CH<sub>2</sub>), 51.5 (CH<sub>2</sub>), 59.5 (CH<sub>2</sub>), 118.7 (CH), 126.2 (CH), 126.5 (CH), 127.5 (CH), 128.2 (C<sub>q</sub>), 128.6 (CH), 128.9 (CH), 132.3 (CH), 136.6 (C<sub>q</sub>), 143.5 (C<sub>q</sub>), 169.2 (C<sub>q</sub>).

**LRMS** (ESI) *m/z* 400 (M + H)<sup>+</sup>.

**HRMS** (ESI) calcd for C<sub>21</sub>H<sub>25</sub>N<sub>3</sub>O<sub>3</sub>S (M + H)<sup>+</sup> 400.1689, found: (M + H)<sup>+</sup> 400.1695.

**RP-HPLC**: *t*<sub>R</sub> 6.93 min, >99% (isocratic), *t*<sub>R</sub> 8.39 min, 99% (gradient).

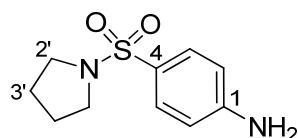
**4-Amino-*N,N*-diethylbenzene-1-sulfonamide (144a)**

Acetamide **143a** (100 mg, 370  $\mu\text{mol}$ ) was treated with aqueous HCl (2 M, 5 mL) as described in general procedure B. Recrystallisation from methanol-ether afforded the desired product **144a** (53 mg, 63%) as white solid, mp 104 – 106  $^{\circ}\text{C}$  (lit. 105 – 106  $^{\circ}\text{C}$ ) with spectroscopic data in agreement with literature data.<sup>236</sup>

$^1\text{H NMR}$  (300 MHz,  $d_6$ -DMSO)  $\delta$ : 1.01 (6H, t,  $J = 7.1$  Hz, H3'), 3.06 (4H, q,  $J = 7.1$  Hz, H2'), 5.93 (2H, br s, NH<sub>2</sub>), 6.61 (2H, app d,  $J = 8.7$  Hz, H2, H6), 7.38 (2H, app d,  $J = 8.7$  Hz, H3, H5).

**LRMS** (ESI)  $m/z$  229 (M + H)<sup>+</sup>.

**RP-HPLC**:  $t_R$  10.82 min, >99% (gradient).

**4-(Pyrrolidine-1-sulfonyl)aniline (144b)**

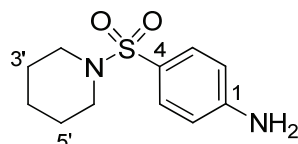
Acetamide **143b** (100 mg, 372  $\mu\text{mol}$ ) was treated with aqueous HCl (2 M, 5 mL) as described in general procedure B. Recrystallisation from methanol-ether afforded the desired product **144b** (50 mg, 59%) as white crystals, mp 168 – 169  $^{\circ}\text{C}$  (lit.<sup>237</sup> 167 – 168  $^{\circ}\text{C}$  and lit.<sup>233</sup> 172 – 173  $^{\circ}\text{C}$ ) with spectroscopic data in agreement with literature data.<sup>237</sup>

$^1\text{H NMR}$  (400 MHz, CD<sub>3</sub>OD)  $\delta$ : 1.71 – 1.74 (4H, m, H3', H4'), 3.14 – 3.18 (4H, m, H2', H5'), 6.72 (2H, app d,  $J = 8.9$  Hz, H2, H6), 7.50 (2H, app d,  $J = 8.9$  Hz, H3, H5).

LRMS (ESI)  $m/z$  227 ( $M + H$ )<sup>+</sup>.

RP-HPLC:  $t_R$  8.78 min, >99% (gradient).

#### 4-(Piperidine-1-sulfonyl)aniline (**113**)



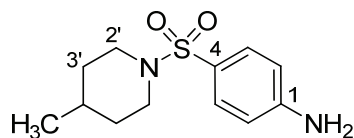
Acetamide **143c** (50 mg, 177  $\mu$ mol) was treated with aqueous HCl (2 M, 5 mL) as described in general procedure B. Recrystallisation from methanol-ether afforded the desired product **113** (18 mg, 42%) as white prism-like crystals, mp 167 – 169 °C (lit. 190 – 192 °C) with spectroscopic data in agreement with literature data.<sup>233</sup>

<sup>1</sup>H NMR (300 MHz, CD<sub>3</sub>OD)  $\delta$ : 1.40 – 1.46 (2H, m, H4'), 1.61 (4H, app p,  $J = 5.7$  Hz, H3', H5'), 2.91 (4H, dd,  $J = 5.4, 5.4$  Hz, H2', H6'), 6.71 (2H, app d,  $J = 8.7$  Hz, H2, H6), 7.42 (2H, app d,  $J = 8.7$  Hz, H3, H5).

LRMS (ESI)  $m/z$  241 ( $M + H$ )<sup>+</sup>.

RP-HPLC:  $t_R$  8.61 min, >99% (gradient).

#### 4-(4-Methylpiperidine-1-sulfonyl)aniline (**144d**)



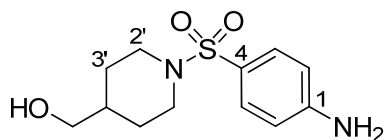
Acetamide **143d** (200 mg, 647  $\mu$ mol) was treated with aqueous HCl (2 M, 5 mL) as described in general procedure B. Recrystallisation from methanol-ether afforded the desired product **144d** (78 mg, 48%) as off-white crystals, mp 104 – 106 °C (lit. 140 – 142 °C) with spectroscopic data in agreement with literature data.<sup>234</sup>

**<sup>1</sup>H NMR** (400 MHz, CD<sub>3</sub>OD)  $\delta$ : 0.91 (3H, d,  $J$  = 6.2 Hz, piperidine-CH<sub>3</sub>), 1.19 – 1.35 (3H, m, H<sub>3a'</sub>, H<sub>5a'</sub>, H<sub>4'</sub>), 1.68 (2H, dd,  $J$  = 12.4, 2.3 Hz, H<sub>3e'</sub>, H<sub>5e'</sub>), 2.23 (2H, ddd,  $J$  = 14.0, 11.7, 2.4 Hz, H<sub>2a'</sub>, H<sub>6a'</sub>), 3.64 (2H, br d,  $J$  = 12.0 Hz, H<sub>2e'</sub>, H<sub>6e'</sub>), 6.81 (2H, app d,  $J$  = 8.9 Hz, H<sub>2</sub>, H<sub>6</sub>), 7.48 (2H, app d,  $J$  = 8.9 Hz, H<sub>3</sub>, H<sub>5</sub>).

**LRMS** (ESI)  $m/z$  255 (M + H)<sup>+</sup>.

**RP-HPLC**:  $t_R$  9.60 min, >99% (gradient).

**{1-[(4-Aminobenzene)sulfonyl]piperidin-4-yl}methanol (144e)**



Acetamide **143e** (100 mg, 320  $\mu$ mol) was treated with aqueous HCl (2 M, 5 mL) as described in general procedure B. The product **144e** was recrystallised from methanol-ether affording white crystals (60 mg, 69%), mp 211 – 212 °C.

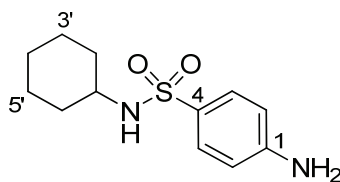
**<sup>1</sup>H NMR** (400 MHz, *d*<sub>6</sub>-DMSO)  $\delta$ : 1.12 (2H, ddd,  $J$  = 15.8, 12.3, 4.0 Hz, H<sub>3a'</sub>, H<sub>5a'</sub>), 1.19 – 1.37 (1H, m, H<sub>4'</sub>), 1.68 (2H, dd,  $J$  = 12.7, 2.4 Hz, H<sub>3e'</sub>, H<sub>5e'</sub>), 2.09 (2H, ddd,  $J$  = 11.8, 11.7, 2.3 Hz, H<sub>2a'</sub>, H<sub>6a'</sub>), 3.20 (2H, d,  $J$  = 6.2 Hz, CH<sub>2</sub>), 3.53 (2H, br d,  $J$  = 11.6 Hz, H<sub>2e'</sub>, H<sub>6e'</sub>), 6.30 (2H, br s, NH<sub>2</sub>), 6.65 (2H, app d,  $J$  = 8.7 Hz, H<sub>2</sub>, H<sub>6</sub>), 7.34 (2H, app d,  $J$  = 8.8 Hz, H<sub>3</sub>, H<sub>5</sub>).

**<sup>13</sup>C NMR** (101 MHz, *d*<sub>6</sub>-DMSO)  $\delta$ : 27.9 (CH<sub>2</sub>), 37.4 (CH), 45.9(CH<sub>2</sub>), 65.3 (CH<sub>2</sub>), 113.0 (CH), 120.5 (C<sub>q</sub>), 129.4 (CH), 152.7 (C<sub>q</sub>).

**LRMS** (ESI)  $m/z$  271 (M + H)<sup>+</sup>.

**HRMS** (ESI) calcd for C<sub>12</sub>H<sub>18</sub>N<sub>2</sub>O<sub>3</sub>S (M + H)<sup>+</sup> 271.1111, found: (M + H)<sup>+</sup> 271.1118.

**RP-HPLC**:  $t_R$  2.47 min, >99% (isocratic),  $t_R$  6.13 min, >99% (gradient).

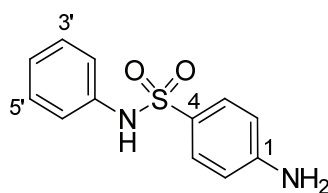
**4-Amino-N-cyclohexylbenzenesulfonamide (144f)**

Acetamide **143f** (50 mg, 168  $\mu\text{mol}$ ) was treated with aqueous HCl (2 M, 5 mL) as described in general procedure B. Recrystallisation from methanol-ether afforded the desired product **144f** as off-white precipitate (20 mg, 47%), with spectroscopic data in agreement with literature data.<sup>233</sup>

<sup>1</sup>H NMR (400 MHz, CDCl<sub>3</sub>)  $\delta$ : 1.04 – 1.29 (5H, m, H<sub>2a'</sub>, H<sub>3a'</sub>, H<sub>4a'</sub>, H<sub>5a'</sub>, H<sub>6a'</sub>), 1.45 – 1.80 (5H, m, H<sub>2e'</sub>, H<sub>3e'</sub>, H<sub>4e'</sub>, H<sub>5e'</sub>, H<sub>6e'</sub>), 3.07 (1H, tdt,  $J = 11.3, 7.7, 3.9$  Hz, H<sub>1'</sub>), 4.10 (2H, br s, NH<sub>2</sub>), 4.34 (1H, d,  $J = 7.4$  Hz, NHSO<sub>2</sub>), 6.67 (2H, app d,  $J = 8.7$  Hz, H<sub>2</sub>, H<sub>6</sub>), 7.65 (2H, app d,  $J = 8.7$  Hz, H<sub>3</sub>, H<sub>5</sub>).

LRMS (ESI)  $m/z$  255 (M + H)<sup>+</sup>.

RP-HPLC:  $t_R$  8.16 min, >99% (gradient).

**4-Amino-N-phenylbenzene-1-sulfonamide (144g)**

Acetamide **143g** (100 mg, 344  $\mu\text{mol}$ ) was treated with aqueous HCl (2 M, 5 mL) as described in general procedure B. The product **144g** was recrystallised from methanol-ether affording white micro-crystals (35 mg, 41%), mp 194 – 196 °C.

$^1\text{H NMR}$  (400 MHz,  $d_6$ -DMSO)  $\delta$ : 5.96 (2H, br s,  $\text{NH}_2$ ), 6.52 (2H, d,  $J = 8.6$  Hz, H2, H6), 6.96 (1H, t,  $J = 7.3$  Hz, H4'), 7.06 (2H, d,  $J = 7.8$  Hz, H2', H6'), 7.19 (2H, t,  $J = 7.8$  Hz, H3', H5'), 7.19 (2H, d,  $J = 8.6$  Hz, H3, H5), 9.86 (1H, br s, NH).

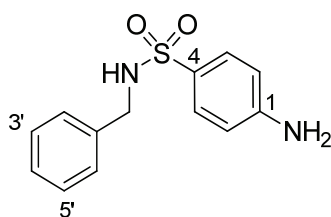
$^{13}\text{C NMR}$  (101 MHz,  $d_6$ -DMSO)  $\delta$ : 112.6 (CH), 119.5 (CH), 123.4 (CH), 124.5 ( $\text{C}_q$ ), 128.7 (CH), 129.0 (CH), 138.6 ( $\text{C}_q$ ), 152.9 ( $\text{C}_q$ ).

LRMS (ESI)  $m/z$  249 ( $\text{M} + \text{H}$ ) $^+$ .

HRMS (ESI) calcd for  $\text{C}_{12}\text{H}_{12}\text{N}_2\text{O}_2\text{S}$  ( $\text{M} + \text{H}$ ) $^+$  249.0692, found: ( $\text{M} + \text{H}$ ) $^+$  249.0702.

RP-HPLC:  $t_R$  4.32 min, >99% (isocratic),  $t_R$  8.98 min, >99% (gradient).

#### 4-Amino-*N*-benzylbenzene-1-sulfonamide (**144h**)

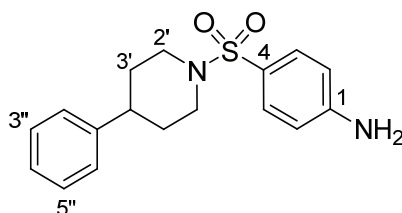


Acetamide **143h** (100 mg, 328  $\mu\text{mol}$ ) was treated with aqueous HCl (2 M, 5 mL) as described in general procedure B. Recrystallisation from methanol-ether afforded the desired product **144h** (37 mg, 43%) as off-white/light yellow crystals, mp 118 – 119  $^{\circ}\text{C}$  (lit. 200 – 201  $^{\circ}\text{C}$ ) with spectroscopic data in agreement with literature data.<sup>233</sup>

$^1\text{H NMR}$  (400 MHz,  $\text{CD}_3\text{OD}$ )  $\delta$ : 3.97 (2H, s,  $\text{CH}_2$ ), 6.69 (2H, app d,  $J = 8.7$  Hz, H2, H6), 7.17 – 7.32 (5H, m, H2'', H3'', H4'', H5'', H6''), 7.53 (2H, app d,  $J = 8.7$  Hz, H3, H5).

LRMS (ESI)  $m/z$  263 ( $\text{M} + \text{H}$ ) $^+$ .

RP-HPLC:  $t_R$  8.58 min, >99% (gradient).

**4-(4-Phenylpiperidine-1-sulfonyl)aniline (144j)**

Acetamide **143j** (100 mg, 278  $\mu\text{mol}$ ) was treated with aqueous HCl (2 M, 5 mL) as described in general procedure B. The product **144j** was recrystallised from methanol-ether affording off-white needle-like crystals (63 mg, 71%), mp 198 – 200 °C.

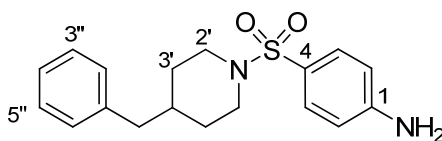
**$^1\text{H}$  NMR** (400 MHz,  $d_6$ -DMSO)  $\delta$ : 1.64 (2H, br ddd,  $J = 16.2, 12.5, 3.7$  Hz,  $\text{H}_{3\text{a}'}, \text{H}_{5\text{a}'}$ ), 1.74 – 1.82 (2H, m,  $\text{H}_{3\text{e}'}, \text{H}_{5\text{e}'}$ ), 2.21 (2H, ddd,  $J = 14.1, 11.9, 2.2$  Hz,  $\text{H}_{2\text{a}'}, \text{H}_{6\text{a}'}$ ), 2.43 (1H, tt,  $J = 12.0, 3.4$  Hz,  $\text{H}_{4'}$ ), 3.67 (2H, br d,  $J = 11.5$  Hz,  $\text{H}_{2\text{e}'}, \text{H}_{6\text{e}'}$ ), 6.06 (2H, s,  $\text{NH}_2$ ), 6.67 (2H, app d,  $J = 8.8$  Hz, H2, H6), 7.14 – 7.22 (3H, m,  $\text{H}_{2'''}, \text{H}_{4'''}, \text{H}_{6''}$ ), 7.23 – 7.30 (2H, m,  $\text{H}_{3'''}, \text{H}_{5''}$ ), 7.38 (2H, app d,  $J = 8.8$  Hz, H3, H5).

**$^{13}\text{C}$  NMR** (101 MHz,  $d_6$ -DMSO)  $\delta$  32.0 ( $\text{CH}_2$ ), 40.7 (CH), 46.6 ( $\text{CH}_2$ ), 112.8 (CH), 119.9 ( $\text{C}_q$ ), 126.3 (CH), 126.7 (CH), 128.4 (CH), 129.5 (CH), 145.4 ( $\text{C}_q$ ), 153.2 ( $\text{C}_q$ ).

**LRMS** (ESI)  $m/z$  317 ( $\text{M} + \text{H}$ ) $^+$ .

**HRMS** (ESI) calcd for  $\text{C}_{17}\text{H}_{20}\text{N}_2\text{O}_2\text{S}$  ( $\text{M} + \text{H}$ ) $^+$  317.1318, found: ( $\text{M} + \text{H}$ ) $^+$  317.1331.

**RP-HPLC**:  $t_{\text{R}}$  7.11 min, >99% (isocratic),  $t_{\text{R}}$  11.05 min, >99% (gradient).

**4-(4-Benzylpiperidine-1-sulfonyl)aniline (144k)**

Acetamide **143k** (100 mg, 268  $\mu\text{mol}$ ) was treated with aqueous HCl (2 M, 5 mL) as described in general procedure B. The product **144k** was recrystallised from methanol-ether affording orange needle-like crystals (44 mg, 49%), mp 146 – 147 °C.

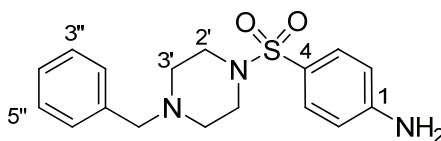
$^1\text{H NMR}$  (400 MHz,  $\text{CD}_3\text{OD}$ )  $\delta$ : 1.24 (2H, br ddd,  $J = 15.8, 12.6, 3.8$  Hz,  $\text{H}_{3\text{a}}', \text{H}_{5\text{a}}'$ ), 1.34 – 1.50 (1H, m,  $\text{H}_{4}'$ ), 1.63 (2H, br d,  $J = 12.8$  Hz,  $\text{H}_{3\text{e}}', \text{H}_{5\text{e}}'$ ), 2.12 (2H, ddd,  $J = 14.0, 12.0, 2.4$  Hz,  $\text{H}_{2\text{a}}', \text{H}_{6\text{a}}'$ ), 2.48 (2H, d,  $J = 7.1$  Hz,  $\text{CH}_2$ ), 3.61 (2H, br d,  $J = 11.7$  Hz,  $\text{H}_{2\text{e}}', \text{H}_{6\text{e}}'$ ), 6.69 (2H, app d,  $J = 8.8$  Hz, H2, H6), 7.08 – 7.15 (3H, m,  $\text{H}_{2''}, \text{H}_{4''}, \text{H}_{6''}$ ), 7.22 (2H, t,  $J = 7.3$  Hz,  $\text{H}_{3''}, \text{H}_{5''}$ ), 7.39 (2H, app d,  $J = 8.8$  Hz, H3, H5).

$^{13}\text{C NMR}$  (101 MHz,  $\text{CD}_3\text{OD}$ )  $\delta$ : 32.5 ( $\text{CH}_2$ ), 38.6 (CH), 43.6 ( $\text{CH}_2$ ), 47.7 ( $\text{CH}_2$ ), 114.4 (CH), 122.8 ( $\text{C}_q$ ), 127.0 (CH), 129.3 (CH), 130.1 (CH), 130.8 (CH), 141.3 ( $\text{C}_q$ ), 154.4 ( $\text{C}_q$ ).

**LRMS** (ESI)  $m/z$  331 ( $\text{M} + \text{H}$ ) $^+$ .

**HRMS** (ESI) calcd for  $\text{C}_{18}\text{H}_{22}\text{N}_2\text{O}_2\text{S}$  ( $\text{M} + \text{H}$ ) $^+$  331.1475, found: ( $\text{M} + \text{H}$ ) $^+$  331.1489.

**RP-HPLC**:  $t_{\text{R}}$  8.69 min, >99% (isocratic),  $t_{\text{R}}$  11.25 min, >99% (gradient).

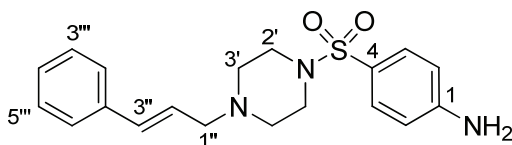
**4-(4-Benzylpiperazine-1-sulfonyl)aniline (144I)**

Acetamide **143I** (100 mg, 267  $\mu\text{mol}$ ) was treated with aqueous HCl (2 M, 5 mL) as described in general procedure B. Recrystallisation from methanol-ether afforded the desired product **144I** (10 mg, 12%) as white micro-crystals, mp 239 – 241  $^{\circ}\text{C}$  with spectroscopic data in agreement with literature data.<sup>235</sup>

$^1\text{H NMR}$  (400 MHz,  $d_6$ -DMSO)  $\delta$ : 2.40 (4H, br t,  $J = 4.5$  Hz, H3', H5'), 2.75 – 2.83 (4H, m, H2', H6'), 3.44 (2H, s, CH<sub>2</sub>), 6.09 (2H, br s, NH<sub>2</sub>), 6.64 (2H, app d,  $J = 8.7$  Hz, H2, H6), 7.19 – 7.25 (3H, m, H2'', H4'', H6''), 7.25 – 7.30 (2H, m, H3'', H5''), 7.33 (2H, app d,  $J = 8.7$  Hz, H3, H5).

**LRMS** (ESI)  $m/z$  332 (M + H)<sup>+</sup>.

**RP-HPLC**:  $t_R$  6.95 min, >99% (gradient).

**4-(4-Cinnamylpiperazine-1-sulfonyl)aniline (144m)**

Acetamide **143m** (50 mg, 125  $\mu$ mol) was treated with aqueous HCl (2 M, 5 mL) as described in general procedure B. The product **144m** was recrystallised from methanol-ether affording light orange prism-like crystals (25 mg, 56%), mp 125 – 126 °C.

$^1\text{H NMR}$  (400 MHz,  $d_6$ -DMSO)  $\delta$ : 2.42 – 2.48 (4H, m, H3', H5'), 2.75 – 2.88 (4H, m, H2', H6'), 3.08 (2H, d,  $J$  = 6.1 Hz, H1''), 6.08 (2H, s, NH<sub>2</sub>), 6.19 (1H, dt,  $J$  = 15.9, 6.5 Hz, H2''), 6.50 (1H, d,  $J$  = 16.0 Hz, H3'''), 6.65 (2H, app d,  $J$  = 8.8 Hz, H2, H6), 7.20-7.24 (1H, m, H4'''), 7.26 – 7.37 (4H, m, H3, H5, H3''', H5'''), 7.37 – 7.45 (2H, m, H2''', H6''').

$^{13}\text{C NMR}$  (101 MHz,  $d_6$ -DMSO)  $\delta$ : 45.9 (CH<sub>2</sub>), 51.5 (CH<sub>2</sub>), 59.5 (CH<sub>2</sub>), 112.6 (CH), 119.1 (C<sub>q</sub>), 126.2 (CH), 126.6 (CH), 127.4 (CH), 128.5 (CH), 129.6 (CH), 132.2 (CH), 136.5 (C<sub>q</sub>), 152.3 (C<sub>q</sub>).

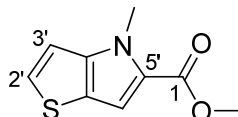
**LRMS** (ESI)  $m/z$  358 (M + H)<sup>+</sup>.

**HRMS** (ESI) calcd for C<sub>19</sub>H<sub>23</sub>N<sub>3</sub>O<sub>2</sub>S (M + H)<sup>+</sup> 358.1584, found: (M + H)<sup>+</sup> 358.1584.

**RP-HPLC**:  $t_R$  3.26 min, >99% (isocratic),  $t_R$  8.19 min, 99% (gradient).

### 7.2.3 Synthesis of thieno-thiophene/pyrrole analogues

#### Methyl 4-methyl-4*H*-thieno[3,2-*b*]pyrrole-5-carboxylate (**145**)

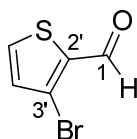


To a solution of 4-methyl-4*H*-thieno[3,2-*b*]pyrrole-5-carboxylic acid **108** (10 mg, 55  $\mu\text{mol}$ ) and potassium carbonate (23 mg, 166  $\mu\text{mol}$ ) in DMF (500  $\mu\text{L}$ ), was added methyl iodide (10  $\mu\text{L}$ , 166  $\mu\text{mol}$ ) and the mixture was stirred at 25  $^{\circ}\text{C}$  for 12 h. The reaction mixture was diluted with ethyl acetate (25 mL) and washed with water (25 mL). The water layer was extracted with ethyl acetate (3  $\times$  25 mL), and the organic layers were combined, washed with brine then dried over anhydrous magnesium sulfate, filtered and evaporated to dryness *in vacuo*. Purification by flash chromatography (ethyl acetate:hexane; 1:4) afforded *methyl 4-methyl-4H-thieno[3,2-*b*]pyrrole-5-carboxylate* **145** (8.5 mg, 79%) as off-white foam, with spectroscopic data in agreement with literature data.<sup>238</sup>

**$^1\text{H}$  NMR** (300 MHz,  $\text{CDCl}_3$ )  $\delta$ : 3.86 (3H, s,  $\text{CH}_3$ ), 4.06 (3H, s,  $\text{CH}_3$ ), 6.93 (1H, d,  $J = 5.4$  Hz, H3'), 7.17 (1H, s, H6'), 7.33 (1H, d,  $J = 5.4$  Hz, H2').

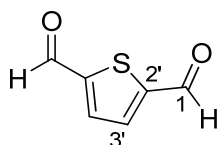
**LRMS** (ESI)  $m/z$  196 ( $\text{M} + \text{H}$ )<sup>+</sup>.

**RP-HPLC**:  $t_{\text{R}}$  10.06 min, >99% (gradient).

**3-Bromothiophene-2-carbaldehyde (159a)**

To an ice/sodium chloride cooled solution of 2,3-dibromothiophene **158** (1 g, 4.1 mmol) in THF (50 mL), *n*-butyllithium dissolved in hexane (1.6 M, 2.9 mL, 4.6 mmol) was added dropwise with stirring. The mixture was stirred for 30 mins before cooling to -78 °C and DMF (639  $\mu$ L, 8.3 mmol) was added dropwise. The solution was warmed to room temperature followed by stirring for a further 2 h then quenched with ammonium chloride (100 mL). The aqueous phase was extracted with ethyl acetate (3  $\times$  40 mL) and the combined organic layers were washed with brine then dried over anhydrous magnesium sulfate, filtered and evaporated to dryness *in vacuo*. The light yellow residue was purified by flash chromatography (ethyl acetate:petroleum spirit; 5:95) to give *3-bromothiophene-2-carbaldehyde* **159a** (323 mg, 41%) as a light yellow oil, with spectroscopic data in agreement with literature data.<sup>199</sup>

<sup>1</sup>H NMR (300 MHz, CDCl<sub>3</sub>)  $\delta$ : 7.12 (1H, d,  $J$  = 5.1 Hz, H4'), 7.69 (1H, dd,  $J$  = 5.1, 1.3 Hz, H5'), 9.94 (1H, d,  $J$  = 1.3 Hz, H1).

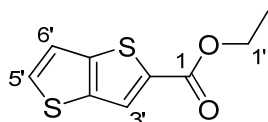
**Thiophene-2,5-dicarbaldehyde (159b)**

Thiophene-2,5-dicarbaldehyde **159b** was prepared according to the method for 3-bromothiophene-2-carbaldehyde **159a**. The light yellow residue was purified by flash chromatography (ethyl acetate:petroleum spirit; 5:95) to give *thiophene-2,5-*

*dicarbaldehyde (159b)* (53 mg, 7%) as an off-white foam, with spectroscopic data in agreement with literature data.<sup>199-200</sup>

<sup>1</sup>H NMR (300 MHz, CDCl<sub>3</sub>) δ: 7.14 (2H, s, H3', H4'), 9.82 (2H, s, formyl-H).

#### Ethyl thieno[3,2-*b*]thiophene-2-carboxylate (**160**)

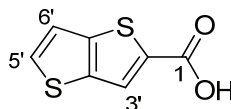


To a stirred mixture of ethyl 2-sulfanylacetate (126 mg, 1 mmol) and potassium carbonate (195 mg, 1.4 mmol) in DMF (5 mL) was added 3-bromothiophene-2-carbaldehyde **159a** (200 mg, 1 mmol) followed by a catalytic amount of 18-crown-6-ether. The resulting mixture was heated at 60 °C for 12 h then cooled to room temperature and poured into water (50 mL). After separation, the water layer was extracted with DCM (3 × 50 mL) and the organic layers were combined, washed with brine (50 mL) and dried over anhydrous magnesium sulfate. The solvent was removed *in vacuo* and the crude oil was purified by flash chromatography (ethyl acetate:petroleum spirit; 5:95). Evaporation of the appropriate fractions afforded *ethyl thieno[3,2-*b*]thiophene-2-carboxylate* **160** (160 mg, 72%) as a yellow oil, with spectroscopic data in agreement with literature data.<sup>199</sup>

<sup>1</sup>H NMR (300 MHz, CDCl<sub>3</sub>) δ: 1.39 (3H, t, *J* = 7.1 Hz, CH<sub>3</sub>), 4.38 (2H, q, *J* = 7.1 Hz, CH<sub>2</sub>), 7.27 (1H, dd, *J* = 5.3, 0.7 Hz, H6'), 7.57 (1H, d, *J* = 5.3 Hz, H5'), 7.98 (1H, d, *J* = 0.7 Hz, H3').

LRMS (ESI) *m/z* 213 (M + H)<sup>+</sup>.

RP-HPLC: *t*<sub>R</sub> 10.81 min, 95% (gradient).

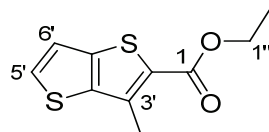
**Thieno[3,2-*b*]thiophene-2-carboxylic acid (148)**

Thieno[3,2-*b*]thiophene-2-carboxylic acid **148** was synthesised according to the procedure of Fuller *et al.*<sup>199</sup> with slight modifications. Thieno[3,2-*b*]thiophene carboxylate **160** (100 mg, 472  $\mu\text{mol}$ ) was added to a stirred mixture of aqueous LiOH (251 mg, 6 mmol) and THF (12 mL). The reaction mixture was heated under reflux for 4 h then cooled to room temperature and concentrated under reduced pressure. HCl (1 M, 10 mL) was slowly added to the residue resulting in precipitation which was filtered off, washed with water and dried *in vacuo* to give the acid **148** (51 mg, 59%) as a yellow precipitate, with spectroscopic data in agreement with literature data.<sup>199</sup>

**<sup>1</sup>H NMR** (300 MHz, *d*<sub>6</sub>-DMSO)  $\delta$ : 7.51 (1H, dd,  $J = 5.2, 0.4$  Hz, H6'), 7.92 (1H, d,  $J = 5.3$  Hz, H5'), 8.11 (1H, d,  $J = 0.4$  Hz, H3'), 13.18 (1H, br s, OH).

**LRMS** (ESI)  $m/z$  183 ( $M - H$ )<sup>+</sup>.

**RP-HPLC**:  $t_R$  10.88 min, >99% (gradient).

**Ethyl 3-methylthieno[3,2-*b*]thiophene-2-carboxylate (162a)**

Ethyl 3-methylthieno[3,2-*b*]thiophene-2-carboxylate **162a** was prepared according to the method of He *et al.*<sup>201</sup> with slight modifications. To a stirred mixture of 2-acetyl-3-bromothiophene **161** (50 mg, 243  $\mu\text{mol}$ ) and potassium carbonate (44 mg, 317  $\mu\text{mol}$ ) in DMF (5 mL) was added ethyl 2-sulfanylacetate (27  $\mu\text{L}$ , 243  $\mu\text{mol}$ ) dropwise followed by a catalytic amount of 18-crown-6-ether. The resulting mixture was heated at 60  $^{\circ}\text{C}$  for 2 days then cooled to room temperature and poured into water (30 mL). After separation, the water layer was extracted with DCM (3  $\times$  30 mL) and the organic layers were combined, washed with brine (30 mL) and dried over anhydrous magnesium sulfate. The solvent was removed *in vacuo* and the crude oil was purified by flash chromatography (ethyl acetate:petroleum spirit; 5:95). Evaporation of the appropriate fractions afforded the title compound (33 mg, 60%) as a yellow oil, with spectroscopic data in agreement with literature data.<sup>201</sup>

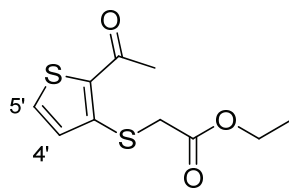
**<sup>1</sup>H NMR** (400 MHz, *d*<sub>6</sub>-DMSO)  $\delta$ : 1.31 (3H, t,  $J = 7.1$  Hz,  $\text{CH}_2\text{CH}_3$ ), 2.63 (3H, s,  $\text{CH}_3$ ), 4.30 (2H, q,  $J = 7.1$  Hz,  $\text{CH}_2$ ), 7.50 (1H, d,  $J = 5.2$  Hz, H6'), 7.95 (1H, d,  $J = 5.2$  Hz, H5').

**<sup>13</sup>C NMR** (101 MHz, *d*<sub>6</sub>-DMSO)  $\delta$ : 14.2 ( $\text{CH}_3$ ), 14.9 ( $\text{CH}_3$ ), 60.8 ( $\text{CH}_2$ ), 120.8 ( $\text{C}_q$ ), 120.9 (CH), 132.5 ( $\text{C}_q$ ), 132.6 (CH), 137.5 ( $\text{C}_q$ ), 140.2 ( $\text{C}_q$ ), 162.5 ( $\text{C}_q$ ).

**LRMS** (ESI)  $m/z$  227 ( $\text{M} + \text{H}$ )<sup>+</sup>.

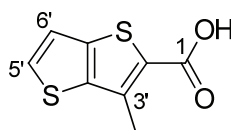
**HRMS** (ESI) calcd for  $\text{C}_{10}\text{H}_{10}\text{O}_2\text{S}_2$  ( $\text{M} + \text{H}$ )<sup>+</sup> 227.0195, found: ( $\text{M} + \text{H}$ )<sup>+</sup> 227.0205.

**RP-HPLC**:  $t_R$  6.59 min, >99% (isocratic),  $t_R$  12.16 min, >99% (gradient).

**Ethyl 2-[(2-acetylthiophen-3-yl)sulfanyl]acetate (162b)**

Purified by flash column chromatography (ethyl acetate) and the product evaporated to dryness as a yellow oil (13 mg, 22%).

$^1\text{H NMR}$  (300 MHz,  $\text{CDCl}_3$ )  $\delta$ : 1.23 (3H, t,  $J = 7.1$  Hz,  $\text{CH}_2\text{CH}_3$ ), 2.50 (3H, s,  $\text{CH}_3$ ), 3.70 (2H, s,  $\text{SCH}_2$ ), 4.17 (2H, q,  $J = 7.1$  Hz,  $\text{CH}_2\text{CH}_3$ ), 7.13 (1H, d,  $J = 5.2$  Hz,  $\text{H}5'$ ), 7.51 (1H, d,  $J = 5.2$  Hz,  $\text{H}4'$ ).

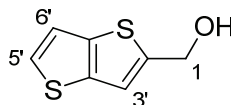
**3-Methylthieno[3,2-*b*]thiophene-2-carboxylic acid (163)**

3-Methylthieno[3,2-*b*]thiophene-2-carboxylic acid **163** was prepared according to the method for thieno[3,2-*b*]thiophene-2-carboxylic acid **148**. Purification by flash chromatography (ethyl acetate:petroleum spirit; 5:95) afforded the title compound (33 mg, 76%) as white micro-crystals, mp 211 – 213 °C with spectroscopic data in agreement with literature data.<sup>195</sup>

$^1\text{H NMR}$  (300 MHz,  $\text{CD}_3\text{OD}$ )  $\delta$ : 2.63 (3H, s,  $\text{CH}_3$ ), 7.49 (1H, d,  $J = 5.1$  Hz,  $\text{H}6'$ ), 7.92 (1H, d,  $J = 5.1$  Hz,  $\text{H}5'$ ).

**LRMS** (ESI)  $m/z$  199 ( $\text{M} + \text{H}$ )<sup>+</sup>.

**RP-HPLC**:  $t_R$  9.55 min, 95% (gradient).

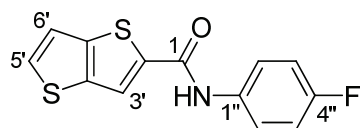
**Thieno[3,2-*b*]thiophen-2-ylmethanol (164)**

Thieno[3,2-*b*]thiophen-2-ylmethanol **164** was prepared according to the procedure of Carpino *et al.*<sup>239</sup> A solution of thieno[3,2-*b*]thiophene carboxylate **160** (41 mg, 192  $\mu\text{mol}$ ) in 10 mL of anhydrous THF/ether (1:1) was added under  $\text{N}_2$  to a suspension of lithium aluminium hydride (11 mg, 288  $\mu\text{mol}$ ) in 5 mL of anhydrous THF/ether (1:1). The resulting mixture was stirred at reflux for 3.5 h then cooled to room temperature and carefully quenched with cold water (15 mL) and enough concentrated HCl to dissolve the inorganic salts. The aqueous layer was extracted with ethyl acetate ( $3 \times 20$  mL) where the combined organic layers were washed with sodium hydrogen carbonate (20 mL) and brine (20 mL), dried over anhydrous magnesium sulfate and filtered. The solvent was removed *in vacuo* to give the title compound (23 mg, 71%) as off-white foam, with spectroscopic data in agreement with literature data.<sup>196</sup>

**$^1\text{H}$  NMR** (300 MHz,  $\text{CDCl}_3$ )  $\delta$ : 1.83 (1H, t,  $J = 5.9$  Hz, OH), 4.89 (2H, d,  $J = 5.4$  Hz,  $\text{CH}_2$ ), 7.20 (1H, d,  $J = 0.4$  Hz, H3'), 7.24 (1H, d,  $J = 5.3$  Hz, H6'), 7.36 (1H, d,  $J = 5.2$  Hz, H5').

**LRMS** (ESI)  $m/z$  153 ( $\text{M} - \text{OH}$ )<sup>+</sup>.

**RP-HPLC**:  $t_{\text{R}}$  9.27 min, >99% (gradient).

***N*-(4-Fluorophenyl)thieno[3,2-*b*]thiophene-2-carboxamide (166)**

To a stirred solution of thieno[3,2-*b*]thiophene-2-carboxylic acid **148** (50 mg, 271  $\mu\text{mol}$ ) in DCM (5 mL) was added triethylamine (42  $\mu\text{L}$ , 298  $\mu\text{mol}$ ). To this, PyBOP (154 mg, 298  $\mu\text{mol}$ ) is added followed by 4-fluoroaniline **165** (28  $\mu\text{L}$ , 298  $\mu\text{mol}$ ) and triethylamine (42  $\mu\text{L}$ , 298  $\mu\text{mol}$ ). The mixture was left stirring at ambient temperature for 12 h then diluted with DCM (40 mL). The organic layer was washed with HCl (2 M, 3  $\times$  20 mL), sodium hydrogen carbonate (3  $\times$  20 mL), sodium chloride (20 mL) and brine (20 mL). The organic layer was dried over magnesium sulfate, filtered and the solvent removed *in vacuo*. The dark brown residue was purified by flash chromatography (ethyl acetate:petroleum spirit; 35:65). Evaporation of the appropriate fractions afforded the title compound **166** (11 mg, 14%) as white micro-crystals (mp 194 – 196  $^{\circ}\text{C}$ ).

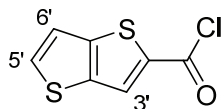
**$^1\text{H}$  NMR** (400 MHz,  $d_6$ -DMSO)  $\delta$ : 7.21 (2H, app t,  $^3J_{\text{HF}} = 9.0$  Hz, H3'', H5''), 7.54 (1H, dd,  $J = 5.3, 0.6$  Hz, H6'), 7.75 (2H, app dd,  $J = 9.2, 5.0$  Hz, H2'', H6''), 7.90 (1H, d,  $J = 5.3$  Hz, H5'), 8.34 (1H, d,  $J = 0.6$  Hz, H3'), 10.40 (1H, br s, NH).

**$^{13}\text{C}$  NMR** (101 MHz,  $d_6$ -DMSO)  $\delta$ : 115.3 (d,  $^2J_{\text{CF}} = 22.3$  Hz, CH), 120.4 (CH), 121.8 (CH), 122.1 (d,  $^3J_{\text{CF}} = 7.9$  Hz, CH), 132.0 (CH), 135.0 (C<sub>q</sub>), 138.4 (C<sub>q</sub>), 141.0 (C<sub>q</sub>), 142.1 (C<sub>q</sub>), 158.3 (d,  $^1J_{\text{CF}} = 240.5$  Hz, C<sub>q</sub>), 160.2 (C<sub>q</sub>).

**LRMS** (ESI)  $m/z$  278 (M + H)<sup>+</sup>.

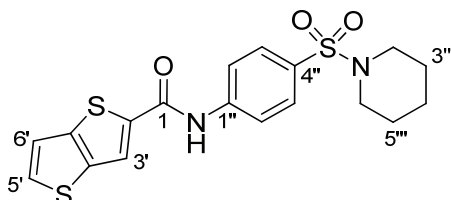
**HRMS** (ESI) calcd for C<sub>13</sub>H<sub>8</sub>FNOS<sub>2</sub> (M + H)<sup>+</sup> 278.0104, found: (M + H)<sup>+</sup> 278.0117.

**RP-HPLC**:  $t_{\text{R}}$  4.24 min, >99% (isocratic),  $t_{\text{R}}$  10.98 min, >99% (gradient).

**Thieno[3,2-*b*]thiophene-2-carbonyl chloride (168)**

Under anhydrous conditions thieno[3,2-*b*]thiophene-2-carboxylic acid **148** (100 mg, 542  $\mu\text{mol}$ ) was taken up in neat thionyl chloride (5 mL). Two drops of dry DMF was added to the reaction mixture which stirred for a further 4 h at ambient temperature. The volatiles were removed *in vacuo* to provide the product as a yellow crystalline solid. The product was reacted on without further purification.

$^1\text{H NMR}$  (300 MHz,  $d_6$ -DMSO)  $\delta$ : 7.50 (1H, d,  $J = 5.4$  Hz, H6'), 7.91 (1H, d,  $J = 5.1$  Hz, H5'), 8.10 (1H, s, H3').

***N*-[4-(Piperidine-1-sulfonyl)phenyl]thieno[3,2-*b*]thiophene-2-carboxamide (167)**

To a stirred solution of 4-(piperidine-1-sulfonyl)aniline **113** (130 mg, 540  $\mu\text{mol}$ ) in DCM (2.5 mL) was slowly added dropwise thieno[3,2-*b*]thiophene-2-carbonyl chloride **168** (100 mg, 490  $\mu\text{mol}$ ) and pyridine (79  $\mu\text{L}$ , 980  $\mu\text{mol}$ ) in DCM (5 mL) at ambient temperature. The resulting mixture was stirred for a further 12 h then diluted with DCM (30 mL) and washed successively with HCl (2 M, 3  $\times$  30 mL), sodium hydrogen carbonate (3  $\times$  30 mL) and brine (20 mL). The organic layer was dried over magnesium sulfate, filtered and the solvent removed *in vacuo*. The crude solid, *N*-[4-(piperidine-1-sulfonyl)phenyl]thieno[3,2-*b*]thiophene-2-carboxamide **167** thus obtained was

recrystallised from ethyl acetate:hexane giving the desired product (138 mg, 70%) as off-white crystals, mp 264 – 266 °C.

$^1\text{H NMR}$  (400 MHz,  $d_6$ -DMSO)  $\delta$ : 1.34 – 1.37 (2H, m, H4'''), 1.50 – 1.59 (4H, m, H3''', H5'''), 2.84 – 2.93 (4H, m, H2''', H6'''), 7.55 (1H, dd,  $J$  = 5.3, 0.7 Hz, H6'), 7.73 (2H, d,  $J$  = 8.8 Hz, H2'', H6''), 7.94 (1H, d,  $J$  = 5.3 Hz, H5'), 8.01 (2H, d,  $J$  = 8.8 Hz, H3'', H5''), 8.42 (1H, d,  $J$  = 0.7 Hz, H3'), 10.71 (1H, br s, NH).

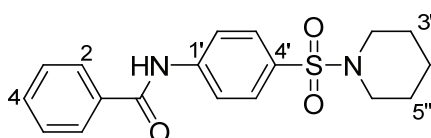
$^{13}\text{C NMR}$  (101 MHz,  $d_6$ -DMSO)  $\delta$ : 22.9 (CH<sub>2</sub>), 24.7 (CH<sub>2</sub>), 46.6 (CH<sub>2</sub>), 119.8 (CH), 120.5 (CH), 122.7 (CH), 128.6 (CH), 129.7 (C<sub>q</sub>), 132.6 (CH), 138.5 (C<sub>q</sub>), 140.5 (C<sub>q</sub>), 142.9 (C<sub>q</sub>), 151.1 (C<sub>q</sub>), 160.7 (C<sub>q</sub>).

**LRMS** (ESI)  $m/z$  407 (M + H)<sup>+</sup>.

**HRMS** (ESI) calcd for C<sub>18</sub>H<sub>18</sub>N<sub>2</sub>O<sub>3</sub>S<sub>3</sub> (M + H)<sup>+</sup> 407.0552, found: (M + H)<sup>+</sup> 407.0572.

**RP-HPLC**:  $t_R$  5.79 min, 96% (isocratic),  $t_R$  12.67 min, 96% (gradient).

#### ***N*-[4-(Piperidine-1-sulfonyl)phenyl]benzamide (170)**



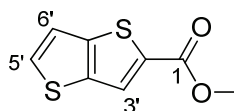
The *N*-[4-(piperidine-1-sulfonyl)phenyl]benzamide **170** was prepared according to the method for the linked thienothiophene-sulfonamide **167**, however, . To a stirred solution of 4-(piperidine-1-sulfonyl)aniline (**113**) (50 mg, 208  $\mu\text{mol}$ ) in DCM (5 mL) was slowly added dropwise benzoyl chloride (**169**) (48  $\mu\text{L}$ , 416  $\mu\text{mol}$ ) and pyridine (34  $\mu\text{L}$ , 416  $\mu\text{mol}$ ) in DCM (5 mL) at ambient temperature. The yellow precipitate was purified by recrystallisation from ethanol that afforded the desired product (71 mg, 98%) as light orange/yellow crystals, mp 120 – 122 °C with spectroscopic data in agreement with literature data.<sup>240</sup>

**<sup>1</sup>H NMR** (300 MHz, CDCl<sub>3</sub>) δ: 1.36 – 1.47 (2H, m, H4''), 1.58 – 1.71 (4H, m, H3'', H5''), 2.95 – 3.03 (4H, m, H2'', H6''), 7.50 (2H, dd, *J* = 15.7, 7.9 Hz, H3, H5), 7.61 (1H, dd, *J* = 15.3, 7.8 Hz, H4), 7.79 (2H, dd, *J* = 25.9, 8.5 Hz, H2', H6'), 7.90 (2H, d, *J* = 7.5 Hz, H3', H5'), 8.13 (2H, d, *J* = 7.6 Hz, H2, H6).

**LRMS** (ESI) *m/z* 345 (M + H)<sup>+</sup>.

**RP-HPLC**: *t<sub>R</sub>* 13.00 min, >99% (gradient).

### Methyl thieno[3,2-*b*]thiophene-2-carboxylate (**171**)

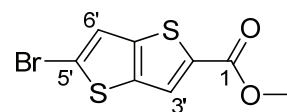


Methyl thieno[3,2-*b*]thiophene-2-carboxylate **171** was prepared according to the method for the thieno[3,2-*b*]pyrrole carboxylate **145**. Purification by flash chromatography (ethyl acetate:hexane; 1:5) afforded the title compound **171** (984 mg, 92%) as yellow long needle-like crystals mp 95 – 97 °C, with spectroscopic data in agreement with literature data.<sup>194,196</sup>

**<sup>1</sup>H NMR** (400 MHz, CDCl<sub>3</sub>) δ: 3.92 (3H, s, CH<sub>3</sub>), 7.29 (1H, dd, *J* = 5.3, 0.8 Hz, H6'), 7.59 (1H, d, *J* = 5.3 Hz, H5'), 8.00 (1H, d, *J* = 0.8 Hz, H3').

**LRMS** (ESI) *m/z* 199 (M + H)<sup>+</sup>.

**RP-HPLC**: *t<sub>R</sub>* 12.59 min, 95% (gradient).

**Methyl 5-bromothieno[3,2-*b*]thiophene-2-carboxylate (172)**

To a solution of methyl thieno[3,2-*b*]thiophene-2-carboxylate **171** (50 mg, 252  $\mu\text{mol}$ ) in acetic acid (10 mL), bromine (20 mg, 126  $\mu\text{mol}$ ) was added dropwise with stirring, and the resulting mixture was left at room temperature for 12 h. After that time, water (5 mL) was added to the mixture causing white precipitation then stirred for a further 2 h. The precipitate was filtered off and taken up in ethyl acetate, washed with 5% aqueous sodium thiosulfate (3  $\times$  20 mL) and dried over anhydrous magnesium sulfate. The solvent was removed *in vacuo* affording the title compound **172** (52 mg, 74%) as white precipitate.

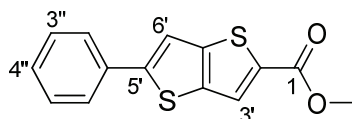
$^1\text{H NMR}$  (300 MHz,  $\text{CDCl}_3$ )  $\delta$ : 3.92 (3H, s,  $\text{CH}_3$ ), 7.30 (1H, s,  $\text{H}_{6'}$ ), 7.88 (1H, s,  $\text{H}_{3'}$ ).

$^{13}\text{C NMR}$  (101 MHz,  $d_6$ -DMSO)  $\delta$ : 52.5 ( $\text{CH}_3$ ), 118.5 ( $\text{C}_q$ ), 123.5 (CH), 126.6 (CH), 133.0 ( $\text{C}_q$ ), 138.9 ( $\text{C}_q$ ), 142.5 ( $\text{C}_q$ ), 162.3 ( $\text{C}_q$ ).

**LRMS** (ESI)  $m/z$  276 (100%)  $\text{M}^{[79}\text{Br}]\text{H}^+$  and 278 (95%)  $\text{M}^{[81}\text{Br}]\text{H}^+$ .

**HRMS** (ESI) calcd for  $\text{C}_8\text{H}_5\text{BrO}_2\text{S}_2$  ( $\text{M} + \text{H}$ ) $^+$  276.8695, found: ( $\text{M} + \text{H}$ ) $^+$  276.8698.

**RP-HPLC**:  $t_R$  4.90 min, 99% (isocratic),  $t_R$  13.17 min, 95% (gradient).

**Methyl 5-phenylthieno[3,2-*b*]thiophene-2-carboxylate (174)**

To a solution of the brominated thieno[3,2-*b*]thiophene **172** (100 mg, 360  $\mu\text{mol}$ ) in DMF (10 mL) were added phenylboronic acid **173** (44 mg, 360  $\mu\text{mol}$ ) and aqueous  $\text{Na}_2\text{CO}_3$  (1 M, 1 mL). The resulting suspension was degassed with  $\text{N}_2$  for 60 mins and dichloro-

bis(triphenylphosphine)palladium(II) (0.1% mol) was added at once. The resulting mixture was heated at 100 °C for 1 h then cooled to room temperature and poured into water (20 mL). After separation, the water layer was extracted with ethyl acetate (3 × 20 mL) and the organic layers were combined, washed with brine (20 mL) and dried over anhydrous magnesium sulfate. The solvent was removed *in vacuo* and the crude oil was purified by flash chromatography (ethyl acetate:hexane; 1:1). Evaporation of the appropriate fractions afforded *methyl 5-phenylthieno[3,2-b]thiophene-2-carboxylate* **174** (24 mg, 24%) as an orange precipitate.

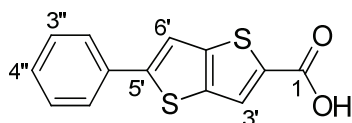
**<sup>1</sup>H NMR** (400 MHz, *d*<sub>6</sub>-DMSO) δ: 3.87 (3H, s, CH<sub>3</sub>), 7.40 (1H, t, *J* = 7.4 Hz, H4''), 7.49 (2H, t, *J* = 7.5 Hz, H3'', H5''), 7.74 (2H, d, *J* = 7.3 Hz, H2'', H6''), 7.98 (1H, s, H6'), 8.22 (1H, s, H3').

**<sup>13</sup>C NMR** (101 MHz, *d*<sub>6</sub>-DMSO) δ: 52.4 (CH<sub>3</sub>), 116.6 (CH), 125.8 (CH), 127.0 (CH), 128.9 (CH), 129.4 (CH), 133.1 (C<sub>q</sub>), 133.5 (C<sub>q</sub>), 137.6 (C<sub>q</sub>), 144.4 (C<sub>q</sub>), 150.0 (C<sub>q</sub>), 162.2 (C<sub>q</sub>).

**LRMS** (ESI) *m/z* 275 (M + H)<sup>+</sup>.

**HRMS** (ESI) calcd for C<sub>14</sub>H<sub>10</sub>O<sub>2</sub>S<sub>2</sub> (M + H)<sup>+</sup> 275.0195, found: (M + H)<sup>+</sup> 275.0206.

**RP-HPLC**: *t*<sub>R</sub> 7.17 min, 99% (isocratic), *t*<sub>R</sub> 12.33 min, >99% (gradient).

**5-Phenylthieno[3,2-*b*]thiophene-2-carboxylic acid (175)**

5-Phenylthieno[3,2-*b*]thiophene-2-carboxylic acid **175** was prepared according to the method for thieno[3,2-*b*]thiophene-2-carboxylic acid **148**. The resulting precipitate was filtered off, washed with water and dried *in vacuo* affording the title compound (12 mg, 71%) as a light brown precipitate.

**<sup>1</sup>H NMR** (400 MHz, CD<sub>3</sub>OD)  $\delta$ : 7.28 – 7.34 (1H, m, H4''), 7.37 – 7.45 (2H, m, H3'', H5''), 7.61 (1H, d,  $J = 0.6$  Hz, H6') 7.69 (2H, dd,  $J = 8.4, 1.2$  Hz, H2'', H6''), 7.74 (1H, d,  $J = 0.7$  Hz, H3').

**<sup>13</sup>C NMR** (101 MHz, CD<sub>3</sub>OD)  $\delta$ : 116.9 (CH), 123.4 (CH), 126.8 (CH), 129.1 (CH), 130.1 (CH), 136.0 (C<sub>q</sub>), 139.0 (C<sub>q</sub>), 141.2 (C<sub>q</sub>), 144.4 (C<sub>q</sub>), 149.1 (C<sub>q</sub>), 169.7 (C<sub>q</sub>).

**LRMS** (ESI)  $m/z$  261 (M + H)<sup>+</sup>.

**HRMS** (ESI) calcd for C<sub>13</sub>H<sub>8</sub>O<sub>2</sub>S<sub>2</sub> (M + H)<sup>+</sup> 258.9893, found: (M + H)<sup>+</sup> 258.9884.

**RP-HPLC**:  $t_R$  4.67 min, >99% (isocratic),  $t_R$  11.35 min, >99% (gradient).

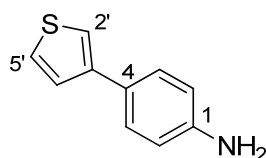
## 7.2.4 Synthesis of phenyl-furan/thiophene analogues

### 7.2.4.1 Suzuki coupling reaction

*General procedure C:*

To a solution of thiophene/furan boronic acid (1 mol equiv.) in THF (3 mL) was added substituted aryl halide (1.5 mol equiv.) and aqueous Na<sub>2</sub>CO<sub>3</sub> (2 M, 1 mL). The resulting suspension was degassed with N<sub>2</sub> for 30 mins and dichlorobis(triphenylphosphine)palladium(II) (0.1% mol) was added in one portion. The reaction mixture was heated at 120 °C for 1 h after which it was allowed to cool to room temperature and water (20 mL) was added to it. The aqueous layer was extracted with ethyl acetate (3 × 20 mL) where the combined organic fractions were washed with brine, dried over anhydrous magnesium sulfate and dried *in vacuo* to give the required crude product. The crude oil was purified by flash chromatography.

#### 4-(Thiophen-3-yl)aniline (194)



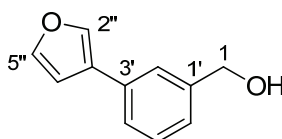
Prepared according to general procedure C with 4-iodoaniline (171 mg, 782 μmol) in THF (3 mL), thiophen-3-ylboronic acid (100 mg, 782 μmol), aqueous Na<sub>2</sub>CO<sub>3</sub> (2 M, 1 mL) and dichlorobis(triphenylphosphine)palladium(II) (0.1% mol). The crude oil was purified by flash chromatography (ethyl acetate:hexane; 1:2). Evaporation of the appropriate fractions afforded 4-(thiophen-3-yl)aniline **194** (34 mg, 25%) as a colourless oil, with spectroscopic data in agreement with literature data.<sup>241</sup>

$^1\text{H NMR}$  (300 MHz,  $\text{CDCl}_3$ )  $\delta$ : 3.71 (2H, br s,  $\text{NH}_2$ ), 6.72 (2H, d,  $J = 7.0$  Hz, H2, H6), 7.27 – 7.37 (3H, m, H2', H4', H5'), 7.41 (2H, d,  $J = 7.0$  Hz, H3, H5).

**LRMS** (ESI)  $m/z$  176 ( $\text{M} + \text{H}$ ) $^+$ .

**RP-HPLC**:  $t_R$  6.86 min, >99% (gradient).

### [3-(Furan-3-yl)phenyl]methanol (**200**)

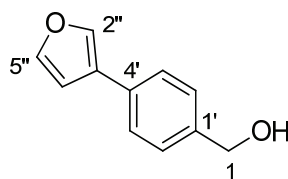


Prepared according to general procedure C with (3-iodophenyl)methanol (170 mg, 726  $\mu\text{mol}$ ) in THF (3 mL), furan-3-ylboronic acid (89 mg, 799  $\mu\text{mol}$ ), aqueous  $\text{Na}_2\text{CO}_3$  (2 M, 1 mL) and dichlorobis(triphenylphosphine)palladium(II) (0.1% mol). The crude oil was purified *via* flash chromatography (ethyl acetate:hexane; 1:2) and evaporation of the appropriate fractions afforded [3-(furan-3-yl)phenyl]methanol **200** (41 mg, 32%) as a colourless oil.

$^1\text{H NMR}$  (600 MHz,  $\text{CDCl}_3$ )  $\delta$ : 1.70 (1H, br s, OH), 4.73 (2H, s,  $\text{CH}_2$ ), 6.72 (1H, s, H4''), 7.24 – 7.28 (1H, m, H4'), 7.37 (1H, t,  $J = 7.4$  Hz, H5'), 7.42 (1H, d,  $J = 7.0$  Hz, H6'), 7.48 (1H, s, H5''), 7.51 (1H, s, H2'), 7.75 (1H, s, H2'').

**LRMS** (ESI)  $m/z$  157 ( $\text{M} - \text{OH}$ ) $^+$ .

**RP-HPLC**:  $t_R$  9.71 min, 96% (gradient).

**[4-(Furan-3-yl)phenyl]methanol (204)**

Prepared according to general procedure C with (4-iodophenyl)methanol (209 mg, 894  $\mu\text{mol}$ ) in THF (3 mL), furan-3-ylboronic acid (100 mg, 894  $\mu\text{mol}$ ), aqueous  $\text{Na}_2\text{CO}_3$  (2 M, 1 mL) and dichlorobis(triphenylphosphine)palladium(II) (0.1% mol). The crude oil was purified *via* flash chromatography (ethyl acetate:hexane; 1:2) and evaporation of the appropriate fractions afforded [4-(furan-3-yl)phenyl]methanol **204** (51 mg, 33%) as white foam.

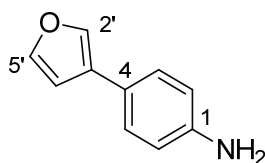
$^1\text{H NMR}$  (400 MHz,  $\text{CDCl}_3$ )  $\delta$ : 1.67 (1H, br s, OH), 4.70 (2H, s,  $\text{CH}_2$ ), 6.70 (1H, dd,  $J = 0.9, 1.8$  Hz,  $\text{H}4''$ ), 7.38 (2H, app d,  $J = 8.5$  Hz,  $\text{H}2', \text{H}6'$ ), 7.47 – 7.51 (3H, m,  $\text{H}5'', \text{H}3', \text{H}5'$ ), 7.74 (1H, dd,  $J = 1.0, 1.4$  Hz,  $\text{H}2''$ ).

$^{13}\text{C NMR}$  (101 MHz,  $\text{CDCl}_3$ )  $\delta$ : 65.3 ( $\text{CH}_2$ ), 109.0 (CH), 126.2 (CH), 126.3 ( $\text{C}_q$ ), 127.7 (CH), 132.0 ( $\text{C}_q$ ), 138.7 (CH), 139.7 ( $\text{C}_q$ ), 143.9 (CH).

**LRMS** (ESI)  $m/z$  157 ( $\text{M} - \text{OH}$ ) $^+$ .

**HRMS** (ESI) calcd for  $\text{C}_{11}\text{H}_{10}\text{O}_2$  ( $\text{M} - \text{OH}$ ) $^+$  157.0653, found: ( $\text{M} - \text{OH}$ ) $^+$  157.0645.

**RP-HPLC**:  $t_R$  4.02 min, >99% (isocratic),  $t_R$  8.83 min, >99% (gradient).

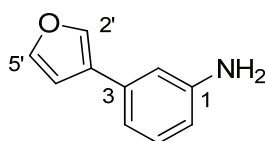
**4-(Furan-3-yl)aniline (213)**

Prepared according to general procedure C with 4-iodoaniline (196 mg, 894  $\mu\text{mol}$ ) in THF (3 mL), furan-3-ylboronic acid (100 mg, 894  $\mu\text{mol}$ ), aqueous  $\text{Na}_2\text{CO}_3$  (2 M, 1 mL) and dichlorobis(triphenylphosphine)palladium(II) (0.1% mol). The crude oil was purified *via* flash chromatography (ethyl acetate:hexane; 1:5) and evaporation of the appropriate fractions afforded 4-(furan-3-yl)aniline **213** (38 mg, 27%) as yellow precipitate, with spectroscopic data in agreement with literature data.<sup>242</sup>

**$^1\text{H}$  NMR** (300 MHz,  $\text{CDCl}_3$ )  $\delta$ : 3.68 (2H, br s,  $\text{NH}_2$ ), 6.63 (1H, s,  $\text{H}_4'$ ), 6.71 (2H, d,  $J = 7.0$ ,  $\text{H}_2$ ,  $\text{H}_6$ ), 7.30 (2H, d,  $J = 7.1$  Hz,  $\text{H}_3$ ,  $\text{H}_5$ ), 7.44 (1H, s,  $\text{H}_5'$ ), 7.63 (1H, s,  $\text{H}_2'$ ).

**LRMS** (ESI)  $m/z$  160 ( $\text{M} + \text{H}$ )<sup>+</sup>.

**RP-HPLC**:  $t_{\text{R}}$  6.06 min, >99% (gradient).

**3-(Furan-3-yl)aniline (214)**

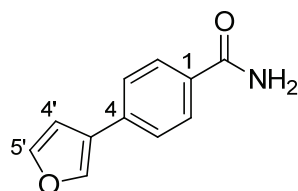
Prepared according to general procedure C with 3-bromoaniline (154 mg, 894  $\mu\text{mol}$ ) in THF (3 mL), furan-3-ylboronic acid (100 mg, 894  $\mu\text{mol}$ ), aqueous  $\text{Na}_2\text{CO}_3$  (2 M, 1 mL) and dichlorobis(triphenylphosphine)palladium(II) (0.1% mol). The crude oil was purified *via* flash chromatography (ethyl acetate:hexane; 1:5) and evaporation of the appropriate fractions afforded 3-(furan-3-yl)aniline **214** (72 mg, 51%) as an off-white precipitate, with spectroscopic data in agreement with reported literature data.<sup>242</sup>

$^1\text{H NMR}$  (300 MHz,  $\text{CDCl}_3$ )  $\delta$ : 3.70 (2H, br s,  $\text{NH}_2$ ), 6.61 (1H, d,  $J = 7.4$  Hz, H6), 6.67 (1H, s, H2), 6.82 (1H, d,  $J = 1.0$  Hz, H4'), 6.90 (1H, d,  $J = 7.6$  Hz, H4), 7.16 (1H, t,  $J = 7.6$  Hz, H5), 7.46 (1H, d,  $J = 1.1$  Hz, H5'), 7.69 (1H, s, H2').

**LRMS** (ESI)  $m/z$  160 ( $\text{M} + \text{H}$ ) $^+$ .

**RP-HPLC**:  $t_R$  7.03 min, >99% (gradient).

#### 4-(Furan-3-yl)benzamide (**215**)



Prepared according to general procedure C with 4-iodobenzamide (55 mg, 223  $\mu\text{mol}$ ) in THF (3 mL), furan-3-ylboronic acid (50 mg, 445  $\mu\text{mol}$ ), aqueous  $\text{Na}_2\text{CO}_3$  (2 M, 1 mL) and dichlorobis(triphenylphosphine)palladium(II) (0.1% mol). The yellow-brownish crude product was purified *via* flash chromatography (ethyl acetate:chloroform:triethylamine; 1:1:0.01) and evaporation of the appropriate fractions afforded 4-(furan-3-yl)benzamide **215** (21 mg, 49%) as a white precipitate.

$^1\text{H NMR}$  (400 MHz,  $d_6$ -DMSO)  $\delta$ : 7.04 (1H, d,  $J = 0.9$  Hz, H4'), 7.34 (1H, br s, NH), 7.70 (2H, d,  $J = 8.3$  Hz, H3, H5), 7.77 (1H, t,  $J = 1.5$  Hz, H5'), 7.89 (2H, d,  $J = 8.3$  Hz, H2, H6), 7.97 (1H, br s, NH), 8.29 (1H, s, H2').

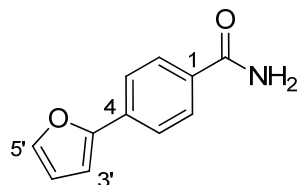
$^{13}\text{C NMR}$  (101 MHz,  $d_6$ -DMSO)  $\delta$ : 108.6 (CH), 125.1 (CH), 128.0 (CH), 132.4 ( $\text{C}_q$ ), 132.4 ( $\text{C}_q$ ), 134.7 ( $\text{C}_q$ ), 140.2 (CH), 144.5 (CH), 167.4 ( $\text{C}_q$ ).

**LRMS** (ESI)  $m/z$  188 ( $\text{M} + \text{H}$ ) $^+$ .

**HRMS** (ESI) calcd for  $\text{C}_{11}\text{H}_9\text{NO}_2$  ( $\text{M} + \text{H}$ ) $^+$  188.0706, found: ( $\text{M} + \text{H}$ ) $^+$  188.0706.

**RP-HPLC:**  $t_R$  3.43 min, >99% (isocratic),  $t_R$  7.86 min, 99% (gradient).

**4-(Furan-2-yl)benzamide (216)**



Prepared according to general procedure C with 4-iodobenzamide (60 mg, 243  $\mu$ mol) in THF (3 mL), furan-2-ylboronic acid (54 mg, 486  $\mu$ mol), aqueous  $\text{Na}_2\text{CO}_3$  (2 M, 1 mL) and dichlorobis(triphenylphosphine)palladium(II) (0.1% mol). The yellow-brownish crude product was purified *via* flash chromatography (ethyl acetate:chloroform:triethylamine; 1:1:0.01) and evaporation of the appropriate fractions afforded 4-(furan-2-yl)benzamide **216** (34 mg, 75%) as white foam.

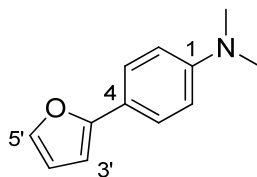
**$^1\text{H}$  NMR** (400 MHz,  $d_6$ -DMSO)  $\delta$ : 6.67 (1H, dd,  $J$  = 1.7, 3.2 Hz, H4'), 7.13 (1H, d,  $J$  = 3.3 Hz, H3'), 7.41 (1H, s, NH), 7.81 (2H, d,  $J$  = 8.4 Hz, H3, H5), 7.84 (1H, d,  $J$  = 1 Hz, H5'), 7.97 (2H, d,  $J$  = 8.4 Hz, H2, H6), 8.03 (1H, s, NH).

**$^{13}\text{C}$  NMR** (101 MHz,  $d_6$ -DMSO)  $\delta$ : 107.4 (CH), 112.3 (CH), 122.9 (CH), 128.2 (CH), 132.6 ( $\text{C}_q$ ), 132.7 ( $\text{C}_q$ ), 143.7 (CH), 152.3 ( $\text{C}_q$ ), 167.3 ( $\text{C}_q$ ).

**LRMS** (ESI)  $m/z$  188 ( $\text{M} + \text{H}$ ) $^+$ .

**HRMS** (ESI) calcd for  $\text{C}_{11}\text{H}_9\text{NO}_2$  ( $\text{M} + \text{H}$ ) $^+$  188.0706, found: ( $\text{M} + \text{H}$ ) $^+$  188.0707.

**RP-HPLC:**  $t_R$  3.70 min, >99% (isocratic),  $t_R$  8.16 min, >99% (gradient).

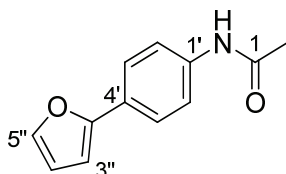
**4-(Furan-2-yl)-*N,N*-dimethylaniline (217)**

Prepared according to general procedure C with 4-bromo-*N,N*-dimethylaniline (100 mg, 0.5 mmol) in THF (3 mL), furan-2-ylboronic acid (112 mg, 1 mmol), aqueous Na<sub>2</sub>CO<sub>3</sub> (2 M, 1 mL) and dichlorobis(triphenylphosphine)palladium(II) (0.1% mol). The crude oil was purified *via* flash chromatography (DCM:hexane; 1:2) and evaporation of the appropriate fractions afforded 4-(furan-2-yl)-*N,N*-dimethylaniline **217** (40 mg, 43%) as a white solid, with spectroscopic data in agreement with literature data.<sup>243</sup>

<sup>1</sup>H NMR (600 MHz, CDCl<sub>3</sub>) δ: 2.99 (6H, s, (CH<sub>3</sub>)<sub>2</sub>), 6.41 – 6.44 (2H, m, H3', H4'), 6.72 – 6.76 (2H, m, H2, H6), 7.37 – 7.42 (1H, m, H5'), 7.56 – 7.54 (2H, m, H3, H5).

LRMS (ESI) *m/z* 188 (M + H)<sup>+</sup>.

RP-HPLC: *t*<sub>R</sub> 8.75 min, >99% (gradient).

***N*-[4-(Furan-2-yl)phenyl]acetamide (218)**

Prepared according to general procedure C with *N*-(4-bromophenyl)acetamide (105 mg, 491 μmol) in THF (3 mL), furan-2-ylboronic acid (100 mg, 892 μmol), aqueous Na<sub>2</sub>CO<sub>3</sub> (2 M, 1 mL) and dichlorobis(triphenylphosphine)palladium(II) (0.1% mol). The crude oil was purified *via* flash chromatography (ethyl acetate:hexane; 1:2) and evaporation of

the appropriate fractions afforded N-[4-(furan-2-yl)phenyl]acetamide **218** (56 mg, 62%) as a white solid, with spectroscopic data in agreement with literature data.<sup>244</sup>

**<sup>1</sup>H NMR** (600 MHz, CDCl<sub>3</sub>)  $\delta$ : 2.19 (3H, s, CH<sub>3</sub>), 6.46 (1H, s, H3''), 6.58 (1H, s, H4''), 7.18 (1H, br s, NH), 7.44 (1H, s, H5''), 7.53 (2H, d,  $J = 7.5$  Hz, H3', H5'), 7.62 (2H, d,  $J = 7.5$  Hz, H2', H6').

**LRMS** (ESI)  $m/z$  202 (M + H)<sup>+</sup>.

**RP-HPLC**:  $t_R$  9.40 min, 95% (gradient).

# References

---

---

## References

1. Gilbert, D. N.; Guidos, R. J.; Boucher, H. W.; Talbot, G. H.; Spellberg, B.; Edwards, J. E.; Scheld, W. M.; Bradley, J. S.; Bartlett, J. G.; Infect Dis Soc, A., The 10 x '20 initiative: Pursuing a global commitment to develop 10 new antibacterial drugs by 2020. *Clin. Infect. Dis.* **2010**, *50* (8), 1081-1083.
2. Spellberg, B., Infections, antibiotics and antibiotic resistance. In *Rising plague: the global threat from deadly bacteria and our dwindling arsenal to fight them*, Prometheus Books: Amherst, N.Y., 2009; pp 33-48.
3. Boucher, H. W.; Talbot, G. H.; Bradley, J. S.; Edwards, J. E.; Gilbert, D.; Rice, L. B.; Scheld, M.; Spellberg, B.; Bartlett, J., Bad bugs, no drugs: no ESCAPE! An update from the Infectious Diseases Society of America. *Clin. Infect. Dis.* **2009**, *48* (1), 1-12.
4. Chastre, J., Evolving problems with resistant pathogens. *Clin. Microbiol. Infect.* **2008**, *14 Suppl 3*, 3-14.
5. French, G. L., Clinical impact and relevance of antibiotic resistance. *Adv. Drug Deliv. Rev.* **2005**, *57* (10), 1514-1527.
6. Mulvey, M. R.; Simor, A. E., Antimicrobial resistance in hospitals: how concerned should we be? *CMAJ* **2009**, *180* (4), 408-415.
7. Klevens, R. M.; Edwards, J. R.; Richards, C. L., Jr.; Horan, T. C.; Gaynes, R. P.; Pollock, D. A.; Cardo, D. M., Estimating health care-associated infections and deaths in U.S. hospitals, 2002. *Public Health Rep.* **2007**, *122* (2), 160-166.
8. Jarvis, W. R., Handwashing--the Semmelweis lesson forgotten? *Lancet* **1994**, *344* (8933), 1311-1312.
9. Barrett, J. F., Can biotech deliver new antibiotics? *Curr. Opin. Microbiol.* **2005**, *8* (5), 498-503.
10. Payne, D. J.; Gwynn, M. N.; Holmes, D. J.; Pompliano, D. L., Drugs for bad bugs: confronting the challenges of antibacterial discovery. *Nat. Rev. Drug Discov.* **2007**, *6* (1), 29-40.
11. Charles, P. G.; Grayson, M. L., The dearth of new antibiotic development: why we should be worried and what we can do about it. *Med. J. Aust.* **2004**, *181* (10), 549-553.
12. Projan, S. J., Why is big Pharma getting out of antibacterial drug discovery? *Curr. Opin. Microbiol.* **2003**, *6* (5), 427-430.
13. Wise, R., Antimicrobial resistance: priorities for action. *J. Antimicrob. Chemother.* **2002**, *49* (4), 585-586.
14. Hamad, B., The antibiotics market. *Nat. Rev. Drug Discov.* **2010**, *9* (9), 675-676.
15. Torres, C., Up against the wall. *Nat. Med.* **2010**, *16* (6), 628-631.

16. Kohanski, M. A.; Dwyer, D. J.; Collins, J. J., How antibiotics kill bacteria: from targets to networks. *Nat. Rev. Microbiol.* **2010**, *8* (6), 423-435.
17. Livermore, D. M.; Woodford, N., The beta-lactamase threat in *Enterobacteriaceae*, *Pseudomonas* and *Acinetobacter*. *Trends Microbiol.* **2006**, *14* (9), 413-420.
18. Davies, J.; Gorini, L.; Davis, B. D., Misreading of RNA codewords induced by aminoglycoside antibiotics. *Mol. Pharmacol.* **1965**, *1* (1), 93-106.
19. Misumi, M.; Nishimura, T.; Komai, T.; Tanaka, N., Interaction of kanamycin and related antibiotics with the large subunit of ribosomes and the inhibition of translocation. *Biochem. Biophys. Res. Commun.* **1978**, *84* (2), 358-365.
20. Cabanas, M. J.; Vazquez, D.; Modolell, J., Inhibition of ribosomal translocation by aminoglycoside antibiotics. *Biochem. Biophys. Res. Commun.* **1978**, *83* (3), 991-997.
21. Hirokawa, G.; Kiel, M. C.; Muto, A.; Selmer, M.; Raj, V. S.; Liljas, A.; Igarashi, K.; Kaji, H.; Kaji, A., Post-termination complex disassembly by ribosome recycling factor, a functional tRNA mimic. *EMBO J.* **2002**, *21* (9), 2272-2281.
22. Bermingham, A.; Derrick, J. P., The folic acid biosynthesis pathway in bacteria: evaluation of potential for antibacterial drug discovery. *Bioessays* **2002**, *24* (7), 637-648.
23. Kompis, I. M.; Islam, K.; Then, R. L., DNA and RNA synthesis: antifolates. *Chem. Rev.* **2005**, *105* (2), 593-620.
24. Drlica, K.; Malik, M.; Kerns, R. J.; Zhao, X., Quinolone-mediated bacterial death. *Antimicrob. Agents. Chemother.* **2008**, *52* (2), 385-392.
25. Floss, H. G.; Yu, T. W., Rifamycin-mode of action, resistance, and biosynthesis. *Chem. Rev.* **2005**, *105* (2), 621-632.
26. Campbell, E. A.; Korzheva, N.; Mustaev, A.; Murakami, K.; Nair, S.; Goldfarb, A.; Darst, S. A., Structural mechanism for rifampicin inhibition of bacterial RNA polymerase. *Cell* **2001**, *104* (6), 901-912.
27. Martinez, J. L.; Baquero, F.; Andersson, D. I., Predicting antibiotic resistance. *Nat. Rev. Microbiol.* **2007**, *5* (12), 958-965.
28. McManus, M. C., Mechanisms of bacterial resistance to antimicrobial agents. *Am. J. Health Syst. Pharm.* **1997**, *54* (12), 1420-1433; quiz 1444-1426.
29. Tenover, F. C., Mechanisms of antimicrobial resistance in bacteria. *Am. J. Infect. Control* **2006**, *34* (5 Suppl 1), S3-10; discussion S64-73.
30. Neu, H. C., The crisis in antibiotic resistance. *Science* **1992**, *257* (5073), 1064-1073.
31. Clatworthy, A. E.; Pierson, E.; Hung, D. T., Targeting virulence: a new paradigm for antimicrobial therapy. *Nat. Chem. Biol.* **2007**, *3* (9), 541-548.
32. Drawz, S. M.; Bonomo, R. A., Three decades of beta-lactamase inhibitors. *Clin. Microbiol. Rev.* **2010**, *23* (1), 160-201.

33. Livermore, D. M., Of *Pseudomonas*, porins, pumps and carbapenems. *J. Antimicrob. Chemother.* **2001**, *47* (3), 247-250.
34. Jacoby, G. A.; Mills, D. M.; Chow, N., Role of beta-lactamases and porins in resistance to ertapenem and other beta-lactams in *Klebsiella pneumoniae*. *Antimicrob. Agents Chemother.* **2004**, *48* (8), 3203-3206.
35. Laible, G.; Spratt, B. G.; Hakenbeck, R., Interspecies recombinational events during the evolution of altered PBP 2x genes in penicillin-resistant clinical isolates of *Streptococcus pneumoniae*. *Mol. Microbiol.* **1991**, *5* (8), 1993-2002.
36. Poole, K., Efflux-mediated multiresistance in Gram-negative bacteria. *Clin. Microbiol. Infect.* **2004**, *10* (1), 12-26.
37. Mingeot-Leclercq, M. P.; Glupczynski, Y.; Tulkens, P. M., Aminoglycosides: activity and resistance. *Antimicrob. Agents Chemother.* **1999**, *43* (4), 727-737.
38. Magnet, S.; Blanchard, J. S., Molecular insights into aminoglycoside action and resistance. *Chem. Rev.* **2005**, *105* (2), 477-498.
39. Weisblum, B., Macrolide resistance. *Drug Resist. Updat.* **1998**, *1* (1), 29-41.
40. Piddock, L. J., Mechanisms of fluoroquinolone resistance: an update 1994-1998. *Drugs* **1999**, *58 Suppl 2*, 11-18.
41. Webb, M. E.; Smith, A. G.; Abell, C., Biosynthesis of pantothenate. *Nat. Prod. Rep.* **2004**, *21* (6), 695-721.
42. Ciulli, A.; Williams, G.; Smith, A. G.; Blundell, T. L.; Abell, C., Probing hot spots at protein-ligand binding sites: a fragment-based approach using biophysical methods. *J. Med. Chem.* **2006**, *49* (16), 4992-5000.
43. Kleinkauf, H., The role of 4'-phosphopantetheine in the biosynthesis of fatty acids, polyketides and peptides. *Biofactors* **2000**, *11* (1-2), 91-92.
44. Williams, R. J.; Lyman, C. M.; Goodyear, G. H.; Truesdail, J. H.; Holaday, D., "Pantothenic acid," a growth determinant of universal biological occurrence. *J. Am. Chem. Soc.* **1933**, *55*, 2912-2927.
45. Williams, R. J.; Saunders, D. H., The effects of inositol, crystalline vitamin B(1) and "pantothenic acid" on the growth of different strains of yeast. *Biochem. J.* **1934**, *28* (5), 1887-1893.
46. Williams, R. J.; Major, R. T., The structure of pantothenic acid. *Science* **1940**, *91* (2358), 246.
47. Vandamme, E. J., Production of vitamins, coenzymes and related biochemicals by biotechnological processes. *J. Chem. Technol. Biotechnol.* **1992**, *53* (4), 313-327.
48. Raman, S. B.; Rathinasabapathi, B., Pantothenate synthesis in plants. *Plant Sci.* **2004**, *167* (5), 961-968.

49. Coxon, K. M.; Chakauya, E.; Ottenhof, H. H.; Whitney, H. M.; Blundell, T. L.; Abell, C.; Smith, A. G., Pantothenate biosynthesis in higher plants. *Biochem. Soc. Trans.* **2005**, *33* (Pt 4), 743-746.
50. Chakauya, E.; Coxon, K. M.; Wei, M.; Macdonald, M. V.; Barsby, T.; Abell, C.; Smith, A. G., Towards engineering increased pantothenate (vitamin B5) levels in plants. *Plant Mol. Biol.* **2008**, *68* (4-5), 493-503.
51. Ottenhof, H. H.; Ashurst, J. L.; Whitney, H. M.; Saldanha, S. A.; Schmitzberger, F.; Gweon, H. S.; Blundell, T. L.; Abell, C.; Smith, A. G., Organisation of the pantothenate (vitamin B5) biosynthesis pathway in higher plants. *Plant J.* **2004**, *37* (1), 61-72.
52. Chakauya, E.; Coxon, K. M.; Whitney, H. M.; Ashurst, J. L.; Abell, C.; Smith, A. G., Pantothenate biosynthesis in higher plants: advances and challenges. *Physiol. Plant.* **2006**, *126* (3), 319-329.
53. Cronan, J. E., Jr.; Littel, K. J.; Jackowski, S., Genetic and biochemical analyses of pantothenate biosynthesis in *Escherichia coli* and *Salmonella typhimurium*. *J. Bacteriol.* **1982**, *149* (3), 916-922.
54. Lobley, C. M.; Schmitzberger, F.; Kilkenny, M. L.; Whitney, H.; Ottenhof, H. H.; Chakauya, E.; Webb, M. E.; Birch, L. M.; Tuck, K. L.; Abell, C.; Smith, A. G.; Blundell, T. L., Structural insights into the evolution of the pantothenate-biosynthesis pathway. *Biochem. Soc. Trans.* **2003**, *31* (Pt 3), 563-571.
55. Powers, S. G.; Snell, E. E., Ketopantoate hydroxymethyltransferase. II. Physical, catalytic, and regulatory properties. *J. Biol. Chem.* **1976**, *251* (12), 3786-3793.
56. Frodyma, M. E.; Downs, D., The panE gene, encoding ketopantoate reductase, maps at 10 minutes and is allelic to apbA in *Salmonella typhimurium*. *J. Bacteriol.* **1998**, *180* (17), 4757-4759.
57. Cronan, J. E., Jr., Beta-alanine synthesis in *Escherichia coli*. *J. Bacteriol.* **1980**, *141* (3), 1291-1297.
58. von Delft, F.; Inoue, T.; Saldanha, S. A.; Ottenhof, H. H.; Schmitzberger, F.; Birch, L. M.; Dhanaraj, V.; Witty, M.; Smith, A. G.; Blundell, T. L.; Abell, C., Structure of *E. coli* ketopantoate hydroxymethyl transferase complexed with ketopantoate and Mg<sup>2+</sup>, solved by locating 160 selenomethionine sites. *Structure* **2003**, *11* (8), 985-996.
59. Matak-Vinkovic, D.; Vinkovic, M.; Saldanha, S. A.; Ashurst, J. L.; von Delft, F.; Inoue, T.; Miguel, R. N.; Smith, A. G.; Blundell, T. L.; Abell, C., Crystal structure of *Escherichia coli* ketopantoate reductase at 1.7 Å resolution and insight into the enzyme mechanism. *Biochemistry* **2001**, *40* (48), 14493-14500.
60. Albert, A.; Dhanaraj, V.; Genschel, U.; Khan, G.; Ramjee, M. K.; Pulido, R.; Sibanda, B. L.; von Delft, F.; Witty, M.; Blundell, T. L.; Smith, A. G.; Abell, C., Crystal structure of aspartate decarboxylase at 2.2 Å resolution provides evidence for an ester in protein self-processing. *Nat. Struct. Biol.* **1998**, *5* (4), 289-293.

61. von Delft, F.; Lewendon, A.; Dhanaraj, V.; Blundell, T. L.; Abell, C.; Smith, A. G., The crystal structure of *E. coli* pantothenate synthetase confirms it as a member of the cytidylyltransferase superfamily. *Structure* **2001**, *9* (5), 439-450.
62. Mdluli, K.; Spigelman, M., Novel targets for *tuberculosis* drug discovery. *Curr. Opin. Pharmacol.* **2006**, *6* (5), 459-467.
63. Murphy, D. J.; Brown, J. R., Identification of gene targets against dormant phase *Mycobacterium tuberculosis* infections. *BMC Infect. Dis.* **2007**, *7*, 84.
64. Gerdes, S. Y.; Scholle, M. D.; D'Souza, M.; Bernal, A.; Baev, M. V.; Farrell, M.; Kurnasov, O. V.; Daugherty, M. D.; Mseeh, F.; Polanuyer, B. M.; Campbell, J. W.; Anantha, S.; Shatalin, K. Y.; Chowdhury, S. A.; Fonstein, M. Y.; Osterman, A. L., From genetic footprinting to antimicrobial drug targets: examples in cofactor biosynthetic pathways. *J. Bacteriol.* **2002**, *184* (16), 4555-4572.
65. Saliba, K. J.; Kirk, K., H<sup>+</sup>-coupled pantothenate transport in the intracellular malaria parasite. *J. Biol. Chem.* **2001**, *276* (21), 18115-18121.
66. Jackowski, S.; Alix, J. H., Cloning, sequence, and expression of the pantothenate permease (*panF*) gene of *Escherichia coli*. *J. Bacteriol.* **1990**, *172* (7), 3842-3848.
67. Sambandamurthy, V. K.; Wang, X.; Chen, B.; Russell, R. G.; Derrick, S.; Collins, F. M.; Morris, S. L.; Jacobs, W. R., Jr., A pantothenate auxotroph of *Mycobacterium tuberculosis* is highly attenuated and protects mice against *tuberculosis*. *Nat. Med.* **2002**, *8* (10), 1171-1174.
68. Sambandamurthy, V. K.; Derrick, S. C.; Hsu, T.; Chen, B.; Larsen, M. H.; Jalapathy, K. V.; Chen, M.; Kim, J.; Porcelli, S. A.; Chan, J.; Morris, S. L.; Jacobs, W. R., Jr., *Mycobacterium tuberculosis* DeltaRD1 DeltapanCD: a safe and limited replicating mutant strain that protects immunocompetent and immunocompromised mice against experimental *tuberculosis*. *Vaccine* **2006**, *24* (37-39), 6309-6320.
69. Sambandamurthy, V. K.; Derrick, S. C.; Jalapathy, K. V.; Chen, B.; Russell, R. G.; Morris, S. L.; Jacobs, W. R., Jr., Long-term protection against *tuberculosis* following vaccination with a severely attenuated double lysine and pantothenate auxotroph of *Mycobacterium tuberculosis*. *Infect. Immun.* **2005**, *73* (2), 1196-1203.
70. Cheldelin, V. H.; Schink, C. A., Pantothenic acid studies; growth effect of pantoic acid analogs. *J. Am. Chem. Soc.* **1947**, *69* (11), 2625-2628.
71. Baillie, A. C.; Cornell, C. L.; Wright, B. J.; Wright, K., Synthesis of potential inhibitors of the enzyme pantothenate synthetase. *Tetrahedron Lett.* **1992**, *33* (35), 5133-5136.
72. Miyatake, K.; Nakano, Y.; Kitaoka, S., Enzymological properties of pantothenate synthetase from *Escherichia-Coli-B*. *J. Nutr. Sci. Vitaminol.* **1978**, *24* (3), 243-253.
73. Miyatake, K.; Nakano, Y.; Kitaoka, S., [41] Pantothenate synthetase from *Escherichia coli* [D-pantoate:  $\beta$ -alanine ligase (AMP-forming), EC 6.3.2.1]. *Methods Enzymol.* **1979**, *62*, 215-219.
74. White, E. L.; Southworth, K.; Ross, L.; Cooley, S.; Gill, R. B.; Sosa, M. I.; Manouvakhova, A.; Rasmussen, L.; Goulding, C.; Eisenberg, D.; Fletcher, T. M.,

- 3rd, A novel inhibitor of *Mycobacterium tuberculosis* pantothenate synthetase. *J. Biomol. Screen.* **2007**, *12* (1), 100-105.
75. Tuck, K. L.; Saldanha, S. A.; Birch, L. M.; Smith, A. G.; Abell, C., The design and synthesis of inhibitors of pantothenate synthetase. *Org. Biomol. Chem.* **2006**, *4* (19), 3598-3610.
76. Ciulli, A.; Scott, D. E.; Ando, M.; Reyes, F.; Saldanha, S. A.; Tuck, K. L.; Chirgadze, D. Y.; Blundell, T. L.; Abell, C., Inhibition of *Mycobacterium tuberculosis* pantothenate synthetase by analogues of the reaction intermediate. *ChemBioChem* **2008**, *9* (16), 2606-2611.
77. Hung, A. W.; Silvestre, H. L.; Wen, S. J.; Ciulli, A.; Blundell, T. L.; Abell, C., Application of fragment growing and fragment linking to the discovery of inhibitors of *Mycobacterium tuberculosis* pantothenate synthetase. *Angew. Chem. Int. Ed.* **2009**, *48* (45), 8452-8456.
78. Sledz, P.; Silvestre, H. L.; Hung, A. W.; Ciulli, A.; Blundell, T. L.; Abell, C., Optimization of the interligand overhauser effect for fragment linking: application to inhibitor discovery against *Mycobacterium tuberculosis* pantothenate synthetase. *J. Am. Chem. Soc.* **2010**, *132* (13), 4544-4545.
79. Scott, D. E.; Dawes, G. J.; Ando, M.; Abell, C.; Ciulli, A., A fragment-based approach to probing adenosine recognition sites by using dynamic combinatorial chemistry. *ChemBioChem* **2009**, *10* (17), 2772-2779.
80. Lee, B. I.; Suh, S. W., Crystal structure of the schiff base intermediate prior to decarboxylation in the catalytic cycle of aspartate alpha-decarboxylase. *J. Mol. Biol.* **2004**, *340* (1), 1-7.
81. Gopalan, G.; Chopra, S.; Ranganathan, A.; Swaminathan, K., Crystal structure of uncleaved L-aspartate- $\alpha$ -decarboxylase from *Mycobacterium tuberculosis*. *Proteins* **2006**, *65* (4), 796-802.
82. Shive, W.; Macow, J., Biochemical transformations as determined by competitive analogue-metabolite growth inhibitions; some transformations involving aspartic acid. *J. Biol. Chem.* **1946**, *162*, 451-462.
83. Ravel, J. M.; Shive, W., Biochemical transformations as determined by competitive analogue-metabolite growth inhibitions; prevention of pantothenic acid synthesis by cysteic acid. *J. Biol. Chem.* **1946**, *166* (2), 407-415.
84. Maas, W. K.; Davis, B. D., Pantothenate studies. I. Interference by D-serine and L-aspartic acid with pantothenate synthesis in *Escherichia coli*. *J. Bacteriol.* **1950**, *60* (6), 733-745.
85. Williamson, J. M.; Brown, G. M., Purification and properties of L-aspartate- $\alpha$ -decarboxylase, an enzyme that catalyzes the formation of  $\beta$ -alanine in *Escherichia coli*. *J. Biol. Chem.* **1979**, *254* (16), 8074-8082.
86. Webb, M. E.; Stephens, E.; Smith, A. G.; Abell, C., Rapid screening by MALDI-TOF mass spectrometry to probe binding specificity at enzyme active sites. *Chem. Commun.* **2003**, (19), 2416-2417.

- 
87. de Villiers, J.; Koekemoer, L.; Strauss, E., 3-Fluoroaspartate and pyruvoyl-dependant aspartate decarboxylase: exploiting the unique characteristics of fluorine to probe reactivity and binding. *Chem. Eur. J.* **2010**, *16* (33), 10030-10041.
88. Zheng, R.; Blanchard, J. S., Kinetic and mechanistic analysis of the *E. coli panE*-encoded ketopantoate reductase. *Biochemistry* **2000**, *39* (13), 3708-3717.
89. Zheng, R.; Blanchard, J. S., Identification of active site residues in *E. coli* ketopantoate reductase by mutagenesis and chemical rescue. *Biochemistry* **2000**, *39* (51), 16244-16251.
90. Zheng, R.; Blanchard, J. S., Substrate specificity and kinetic isotope effect analysis of the *Escherichia coli* ketopantoate reductase. *Biochemistry* **2003**, *42* (38), 11289-11296.
91. Lobley, C. M.; Ciulli, A.; Whitney, H. M.; Williams, G.; Smith, A. G.; Abell, C.; Blundell, T. L., The crystal structure of *Escherichia coli* ketopantoate reductase with NADP<sup>+</sup> bound. *Biochemistry* **2005**, *44* (25), 8930-8939.
92. Ciulli, A.; Chirgadze, D. Y.; Smith, A. G.; Blundell, T. L.; Abell, C., Crystal structure of *Escherichia coli* ketopantoate reductase in a ternary complex with NADP<sup>+</sup> and pantoate bound: substrate recognition, conformational change, and cooperativity. *J. Biol. Chem.* **2007**, *282* (11), 8487-8497.
93. Murzin, A. G.; Brenner, S. E.; Hubbard, T.; Chothia, C., SCOP: a structural classification of proteins database for the investigation of sequences and structures. *J. Mol. Biol.* **1995**, *247* (4), 536-540.
94. Ciulli, A.; Lobley, C. M.; Tuck, K. L.; Smith, A. G.; Blundell, T. L.; Abell, C., pH-tuneable binding of 2'-phospho-ADP-ribose to ketopantoate reductase: a structural and calorimetric study. *Acta Crystallogr. D Biol. Crystallogr.* **2007**, *63* (Pt 2), 171-178.
95. Wallace, A. C.; Laskowski, R. A.; Thornton, J. M., LIGPLOT: a program to generate schematic diagrams of protein-ligand interactions. *Protein Eng.* **1995**, *8* (2), 127-134.
96. Downs, D. M.; Petersen, L., *apbA*, a new genetic locus involved in thiamine biosynthesis in *Salmonella typhimurium*. *J. Bacteriol.* **1994**, *176* (16), 4858-4864.
97. Frodyma, M. E.; Downs, D., ApbA, the ketopantoate reductase enzyme of *Salmonella typhimurium* is required for the synthesis of thiamine via the alternative pyrimidine biosynthetic pathway. *J. Biol. Chem.* **1998**, *273* (10), 5572-5576.
98. Primerano, D. A.; Burns, R. O., Role of acetohydroxy acid isomeroreductase in biosynthesis of pantothenic acid in *Salmonella typhimurium*. *J. Bacteriol.* **1983**, *153* (1), 259-269.
99. Shimizu, S.; Kataoka, M.; Chung, M. C.; Yamada, H., Ketopantoic acid reductase of *Pseudomonas maltophilia* 845. Purification, characterization, and role in pantothenate biosynthesis. *J. Biol. Chem.* **1988**, *263* (24), 12077-12084.

- 
100. Baigori, M.; Grau, R.; Morbidoni, H. R.; de Mendoza, D., Isolation and characterization of *Bacillus subtilis* mutants blocked in the synthesis of pantothenic acid. *J. Bacteriol.* **1991**, *173* (13), 4240-4242.
101. Elischewski, F.; Puhler, A.; Kalinowski, J., Pantothenate production in *Escherichia coli* K12 by enhanced expression of the *panE* gene encoding ketopantoate reductase. *J. Biotechnol.* **1999**, *75* (2-3), 135-146.
102. Merkamm, M.; Chassagnole, C.; Lindley, N. D.; Guyonvarch, A., Ketopantoate reductase activity is only encoded by *ilvC* in *Corynebacterium glutamicum*. *J. Biotechnol.* **2003**, *104* (1-3), 253-260.
103. DiMasi, J. A.; Faden, L. B., Competitiveness in follow-on drug R&D: a race or imitation? *Nat. Rev. Drug Discov.* **2011**, *10* (1), 23-27.
104. Newman, D. J.; Cragg, G. M., Natural products as sources of new drugs over the last 25 years. *J. Nat. Prod.* **2007**, *70* (3), 461-477.
105. Breinbauer, R.; Mentel, M., Combinatorial chemistry and the synthesis of compound libraries. *Methods Mol. Biol.* **2009**, *572*, 73-80.
106. Gribbon, P.; Sewing, A., High-throughput drug discovery: what can we expect from HTS? *Drug Discov. Today* **2005**, *10* (1), 17-22.
107. Mestres, J.; Veeneman, G. H., Identification of "latent hits" in compound screening collections. *J. Med. Chem.* **2003**, *46* (16), 3441-3444.
108. Erlanson, D. A.; McDowell, R. S.; O'Brien, T., Fragment-based drug discovery. *J. Med. Chem.* **2004**, *47* (14), 3463-3482.
109. Erlanson, D. A., Fragment-based lead discovery: a chemical update. *Curr. Opin. Biotechnol.* **2006**, *17* (6), 643-652.
110. Jencks, W. P., On the attribution and additivity of binding energies. *Proc. Natl. Acad. Sci. U.S.A.* **1981**, *78* (7), 4046-4050.
111. Shuker, S. B.; Hajduk, P. J.; Meadows, R. P.; Fesik, S. W., Discovering high-affinity ligands for proteins: SAR by NMR. *Science* **1996**, *274* (5292), 1531-1534.
112. Martin, Y. C., Challenges and prospects for computational aids to molecular diversity. *Perspect. Drug Discov. Des.* **1997**, *7-8* (1), 159-172.
113. Fink, T.; Bruggesser, H.; Reymond, J. L., Virtual exploration of the small-molecule chemical universe below 160 Daltons. *Angew. Chem. Int. Ed.* **2005**, *44* (10), 1504-1508.
114. Fink, T.; Reymond, J. L., Virtual exploration of the chemical universe up to 11 atoms of C, N, O, F: assembly of 26.4 million structures (110.9 million stereoisomers) and analysis for new ring systems, stereochemistry, physicochemical properties, compound classes, and drug discovery. *J. Chem. Inf. Model* **2007**, *47* (2), 342-353.
115. Zartler, E. R.; Shapiro, M. J., Fragonomics: fragment-based drug discovery. *Curr. Opin. Chem. Biol.* **2005**, *9* (4), 366-370.

- 
116. Carr, R. A.; Congreve, M.; Murray, C. W.; Rees, D. C., Fragment-based lead discovery: leads by design. *Drug Discov. Today* **2005**, *10* (14), 987-992.
117. Hann, M. M.; Leach, A. R.; Harper, G., Molecular complexity and its impact on the probability of finding leads for drug discovery. *J. Chem. Inf. Comput. Sci.* **2001**, *41* (3), 856-864.
118. Hopkins, A. L.; Groom, C. R.; Alex, A., Ligand efficiency: a useful metric for lead selection. *Drug Discov. Today* **2004**, *9* (10), 430-431.
119. Hajduk, P. J., Fragment-based drug design: how big is too big? *J. Med. Chem.* **2006**, *49* (24), 6972-6976.
120. Fejzo, J.; Lepre, C. A.; Peng, J. W.; Bemis, G. W.; Ajay; Murcko, M. A.; Moore, J. M., The SHAPES strategy: an NMR-based approach for lead generation in drug discovery. *Chem. Biol.* **1999**, *6* (10), 755-769.
121. Lewell, X. Q.; Judd, D. B.; Watson, S. P.; Hann, M. M., RECAP--retrosynthetic combinatorial analysis procedure: a powerful new technique for identifying privileged molecular fragments with useful applications in combinatorial chemistry. *J. Chem. Inf. Comput. Sci.* **1998**, *38* (3), 511-522.
122. Hajduk, P. J.; Bures, M.; Praestgaard, J.; Fesik, S. W., Privileged molecules for protein binding identified from NMR-based screening. *J. Med. Chem.* **2000**, *43* (18), 3443-3447.
123. Chen, I.; Hubbard, R., Lessons for fragment library design: analysis of output from multiple screening campaigns. *J. Comput. Aided Mol. Des.* **2009**, *23* (8), 603-620.
124. Schulz, M. N.; Landstrom, J.; Bright, K.; Hubbard, R. E., Design of a fragment library that maximally represents available chemical space. *J. Comput. Aided Mol. Des.* **2011**, *25* (7), 611-620.
125. Blomberg, N.; Cosgrove, D.; Kenny, P. W.; Kolmodin, K., Design of compound libraries for fragment screening. *J. Comput. Aided Mol. Des.* **2009**, *23* (8), 513-525.
126. Lipinski, C. A.; Lombardo, F.; Dominy, B. W.; Feeney, P. J., Experimental and computational approaches to estimate solubility and permeability in drug discovery and development settings. *Adv. Drug Deliv. Rev.* **2001**, *46* (1-3), 3-26.
127. Congreve, M.; Carr, R.; Murray, C.; Jhoti, H., A 'rule of three' for fragment-based lead discovery? *Drug Discov. Today* **2003**, *8* (19), 876-877.
128. Boettcher, A.; Ruedisser, S.; Erbel, P.; Vinzenz, D.; Schiering, N.; Hassiepen, U.; Rigollier, P.; Mayr, L. M.; Woelcke, J., Fragment-based screening by biochemical assays: Systematic feasibility studies with trypsin and MMP12. *J. Biomol. Screen.* **2010**, *15* (9), 1029-1041.
129. Hesterkamp, T.; Barker, J.; Davenport, A.; Whittaker, M., Fragment based drug discovery using fluorescence correlation: spectroscopy techniques: challenges and solutions. *Curr. Top. Med. Chem.* **2007**, *7* (16), 1582-1591.
130. Petros, A. M.; Huth, J. R.; Oost, T.; Park, C. M.; Ding, H.; Wang, X.; Zhang, H.; Nimmer, P.; Mendoza, R.; Sun, C.; Mack, J.; Walter, K.; Dorwin, S.; Gramling, E.;

- Ladror, U.; Rosenberg, S. H.; Elmore, S. W.; Fesik, S. W.; Hajduk, P. J., Discovery of a potent and selective Bcl-2 inhibitor using SAR by NMR. *Bioorg. Med. Chem. Lett.* **2010**, *20* (22), 6587-6591.
131. Vivat Hannah, V.; Atmanene, C.; Zeyer, D.; Van Dorsselaer, A.; Sanglier-Cianfèrani, S., Native MS: an 'ESI, way to support structure- and fragment-based drug discovery. *Future Med. Chem.* **2010**, *2* (1), 35-50.
132. Hartshorn, M. J.; Murray, C. W.; Cleasby, A.; Frederickson, M.; Tickle, I. J.; Jhoti, H., Fragment-based lead discovery using X-ray crystallography. *J. Med. Chem.* **2005**, *48* (2), 403-413.
133. Neumann, T.; Junker, H. D.; Schmidt, K.; Sekul, R., SPR-based fragment screening: advantages and applications. *Curr. Top. Med. Chem.* **2007**, *7* (16), 1630-1642.
134. Hubbard, R. E.; Murray, J. B., Experiences in fragment-based lead discovery. *Methods Enzymol.* 2011, pp 509-531.
135. Pellecchia, M., Solution nuclear magnetic resonance spectroscopy techniques for probing intermolecular interactions. *Chem. Biol.* **2005**, *12* (9), 961-971.
136. Lepre, C. A., Practical aspects of NMR-based fragment screening. *Methods Enzymol.* **2011**, *493*, 219-239.
137. Sun, C.; Petros, A. M.; Hajduk, P. J., Fragment-based lead discovery: challenges and opportunities. *J. Comput. Aided Mol. Des.* **2011**.
138. Klages, J.; Coles, M.; Kessler, H., NMR-based screening: a powerful tool in fragment-based drug discovery. *Mol. BioSyst.* **2006**, *2* (6-7), 318-332.
139. Pellecchia, M.; Meininger, D.; Dong, Q.; Chang, E.; Jack, R.; Sem, D. S., NMR-based structural characterization of large protein-ligand interactions. *J. Biomol. NMR* **2002**, *22* (2), 165-173.
140. Meyer, B.; Peters, T., NMR spectroscopy techniques for screening and identifying ligand binding to protein receptors. *Angew. Chem. Int. Ed.* **2003**, *42* (8), 864-890.
141. Lepre, C. A.; Moore, J. M.; Peng, J. W., Theory and applications of NMR-based screening in pharmaceutical research. *Chem. Rev.* **2004**, *104* (8), 3641-3676.
142. Meyer, B.; Peters, T., NMR spectroscopy techniques for screening and identifying ligand binding to protein receptors. *Angew. Chem. Int. Ed. Engl.* **2003**, *42* (8), 864-890.
143. Hajduk, P. J.; Meadows, R. P.; Fesik, S. W., NMR-based screening in drug discovery. *Q. Rev. Biophys.* **1999**, *32* (3), 211-240.
144. Eaton, H. L.; Wyss, D. F., Effective progression of nuclear magnetic resonance-detected fragment hits. *Methods Enzymol.* **2011**, *493*, 447-468.
145. Bartoli, S.; Fincham, C.; Fattori, D., The fragment-approach: An update. *Drug Discov. Today: Technologies* **2006**, *3* (4), 425-431.

- 
146. Mayer, M.; Meyer, B., Characterization of ligand binding by saturation transfer difference NMR spectroscopy. *Angew. Chem. Int. Ed.* **1999**, *38* (12), 1784-1788.
147. Wielens, J.; Headey, S. J.; Deadman, J. J.; Rhodes, D. I.; Le, G. T.; Parker, M. W.; Chalmers, D. K.; Scanlon, M. J., Fragment-based design of ligands targeting a novel site on the integrase enzyme of human immunodeficiency virus 1. *ChemMedChem* **2011**, *6* (2), 258-261.
148. Rohrig, C. H.; Loch, C.; Guan, J. Y.; Siegal, G.; Overhand, M., Fragment-based synthesis and SAR of modified FKBP ligands: influence of different linking on binding affinity. *ChemMedChem* **2007**, *2* (7), 1054-1070.
149. Wyss, D. F.; Arasappan, A.; Senior, M. M.; Wang, Y. S.; Beyer, B. M.; Njoroge, F. G.; McCoy, M. A., Non-peptidic small-molecule inhibitors of the single-chain hepatitis C virus NS3 protease/NS4A cofactor complex discovered by structure-based NMR screening. *J. Med. Chem.* **2004**, *47* (10), 2486-2498.
150. Congreve, M.; Murray, C. W.; Blundell, T. L., Structural biology and drug discovery. *Drug Discov. Today* **2005**, *10* (13), 895-907.
151. Nienaber, V. L.; Richardson, P. L.; Klighofer, V.; Bouska, J. J.; Giranda, V. L.; Greer, J., Discovering novel ligands for macromolecules using X-ray crystallographic screening. *Nat. Biotechnol.* **2000**, *18* (10), 1105-1108.
152. Ochi, T.; Bolanos-Garcia, V. M.; Stojanoff, V.; Moreno, A., Perspectives on protein crystallisation. *Prog. Biophys. Mol. Biol.* **2009**, *101* (1-3), 56-63.
153. Chayen, N. E.; Saridakis, E., Protein crystallization: from purified protein to diffraction-quality crystal. *Nat. Methods* **2008**, *5* (2), 147-153.
154. Ciulli, A.; Abell, C., Fragment-based approaches to enzyme inhibition. *Curr. Opin. Biotechnol.* **2007**, *18* (6), 489-496.
155. Jahnke, W.; Florsheimer, A.; Blommers, M. J.; Paris, C. G.; Heim, J.; Nalin, C. M.; Perez, L. B., Second-site NMR screening and linker design. *Curr. Top. Med. Chem.* **2003**, *3* (1), 69-80.
156. Howard, N.; Abell, C.; Blakemore, W.; Chessari, G.; Congreve, M.; Howard, S.; Jhoti, H.; Murray, C. W.; Seavers, L. C.; van Montfort, R. L., Application of fragment screening and fragment linking to the discovery of novel thrombin inhibitors. *J. Med. Chem.* **2006**, *49* (4), 1346-1355.
157. Huth, J. R.; Park, C.; Petros, A. M.; Kunzer, A. R.; Wendt, M. D.; Wang, X.; Lynch, C. L.; Mack, J. C.; Swift, K. M.; Judge, R. A.; Chen, J.; Richardson, P. L.; Jin, S.; Tahir, S. K.; Matayoshi, E. D.; Dorwin, S. A.; Lador, U. S.; Severin, J. M.; Walter, K. A.; Bartley, D. M.; Fesik, S. W.; Elmore, S. W.; Hajduk, P. J., Discovery and design of novel HSP90 inhibitors using multiple fragment-based design strategies. *Chem. Biol. Drug Des.* **2007**, *70* (1), 1-12.
158. Chung, S.; Parker, J. B.; Bianchet, M.; Amzel, L. M.; Stivers, J. T., Impact of linker strain and flexibility in the design of a fragment-based inhibitor. *Nat. Chem. Biol.* **2009**, *5* (6), 407-413.

- 
159. Hajduk, P. J.; Greer, J., A decade of fragment-based drug design: strategic advances and lessons learned. *Nat. Rev. Drug Discov.* **2007**, *6* (3), 211-219.
160. Murray, C. W.; Rees, D. C., The rise of fragment-based drug discovery. *Nat. Chem.* **2009**, *1* (3), 187-192.
161. de Kloe, G. E.; Bailey, D.; Leurs, R.; de Esch, I. J., Transforming fragments into candidates: small becomes big in medicinal chemistry. *Drug Discov. Today* **2009**, *14* (13-14), 630-646.
162. Chessari, G.; Woodhead, A. J., From fragment to clinical candidate-a historical perspective. *Drug Discov. Today* **2009**, *14* (13-14), 668-675.
163. Hubbard, R. E., Structure-based drug discovery and protein targets in the CNS. *Neuropharmacology* **2011**, *60* (1), 7-23.
164. Flaherty, K. T.; Yasothan, U.; Kirkpatrick, P., Vemurafenib. *Nat. Rev. Drug Discov.* **2011**, *10* (11), 811-812.
165. Tsai, J.; Lee, J. T.; Wang, W.; Zhang, J.; Cho, H.; Mamo, S.; Bremer, R.; Gillette, S.; Kong, J.; Haass, N. K.; Sproesser, K.; Li, L.; Smalley, K. S.; Fong, D.; Zhu, Y. L.; Marimuthu, A.; Nguyen, H.; Lam, B.; Liu, J.; Cheung, I.; Rice, J.; Suzuki, Y.; Luu, C.; Settachatgul, C.; Shellooe, R.; Cantwell, J.; Kim, S. H.; Schlessinger, J.; Zhang, K. Y.; West, B. L.; Powell, B.; Habets, G.; Zhang, C.; Ibrahim, P. N.; Hirth, P.; Artis, D. R.; Herlyn, M.; Bollag, G., Discovery of a selective inhibitor of oncogenic B-Raf kinase with potent antimelanoma activity. *Proc. Natl. Acad. Sci. U.S.A.* **2008**, *105* (8), 3041-3046.
166. Bollag, G.; Hirth, P.; Tsai, J.; Zhang, J.; Ibrahim, P. N.; Cho, H.; Spevak, W.; Zhang, C.; Zhang, Y.; Habets, G.; Burton, E. A.; Wong, B.; Tsang, G.; West, B. L.; Powell, B.; Shellooe, R.; Marimuthu, A.; Nguyen, H.; Zhang, K. Y.; Artis, D. R.; Schlessinger, J.; Su, F.; Higgins, B.; Iyer, R.; D'Andrea, K.; Koehler, A.; Stumm, M.; Lin, P. S.; Lee, R. J.; Grippo, J.; Puzanov, I.; Kim, K. B.; Ribas, A.; McArthur, G. A.; Sosman, J. A.; Chapman, P. B.; Flaherty, K. T.; Xu, X.; Nathanson, K. L.; Nolop, K., Clinical efficacy of a RAF inhibitor needs broad target blockade in BRAF-mutant melanoma. *Nature* **2010**, *467* (7315), 596-599.
167. Miroux, B.; Walker, J. E., Over-production of proteins in Escherichia coli: mutant hosts that allow synthesis of some membrane proteins and globular proteins at high levels. *J. Mol. Biol.* **1996**, *260* (3), 289-298.
168. Froger, A.; Hall, J. E., Transformation of plasmid DNA into E. coli using the heat shock method. *J. Vis. Exp.* **2007**, (6), 253.
169. Studier, F. W., Protein production by auto-induction in high density shaking cultures. *Protein Expr. Purif.* **2005**, *41* (1), 207-234.
170. Marley, J.; Lu, M.; Bracken, C., A method for efficient isotopic labeling of recombinant proteins. *J. Biomol. NMR* **2001**, *20* (1), 71-75.
171. Sambrook, J.; Fritsch, E. F.; Maniatis, T., *Molecular Cloning: A Laboratory Manual*. Cold Spring Harbor Laboratory Press: Cold Spring Harbor, NY, 1989; Vol. 3.

- 
172. Zhao, H. T. A fragment based approach to the identification of ketopantoate reductase inhibitors. Honours thesis, Monash Institute of Pharmaceutical Sciences, Monash University, Parkville, 2006.
173. Headey, S. J.; Vom, A.; Simpson, J. S.; Scanlon, M. J., Backbone assignments of the 34 kDa ketopantoate reductase from *E. coli*. *Biomol. NMR Assign.* **2008**, *2* (1), 93-96.
174. Krzeminski, M.; Loth, K.; Boelens, R.; Bonvin, A. M., SAMPLEX: automatic mapping of perturbed and unperturbed regions of proteins and complexes. *BMC Bioinformatics* **2010**, *11*, 51.
175. Krishnamoorthy, J.; Yu, V. C.; Mok, Y. K., Auto-FACE: an NMR based binding site mapping program for fast chemical exchange protein-ligand systems. *PLoS One* **2010**, *5* (2), e8943.
176. Yuriev, E.; Agostino, M.; Ramsland, P. A., Challenges and advances in computational docking: 2009 in review. *J. Mol. Recognit.* **2011**, *24* (2), 149-164.
177. Kolb, P.; Irwin, J. J., Docking screens: right for the right reasons? *Curr. Top. Med. Chem.* **2009**, *9* (9), 755-770.
178. Gonzalez-Ruiz, D.; Gohlke, H., Steering protein-ligand docking with quantitative NMR chemical shift perturbations. *J. Chem. Inf. Model* **2009**, *49* (10), 2260-2271.
179. Zhang, L.; Hermans, J., Hydrophilicity of cavities in proteins. *Proteins* **1996**, *24* (4), 433-438.
180. Davis, A. M.; St-Gallay, S. A.; Kleywegt, G. J., Limitations and lessons in the use of X-ray structural information in drug design. *Drug Discov. Today* **2008**, *13* (19-20), 831-841.
181. Friesner, R. A.; Banks, J. L.; Murphy, R. B.; Halgren, T. A.; Klicic, J. J.; Mainz, D. T.; Repasky, M. P.; Knoll, E. H.; Shelley, M.; Perry, J. K.; Shaw, D. E.; Francis, P.; Shenkin, P. S., Glide: a new approach for rapid, accurate docking and scoring. 1. Method and assessment of docking accuracy. *J. Med. Chem.* **2004**, *47* (7), 1739-1749.
182. McGovern, S. L.; Shoichet, B. K., Information decay in molecular docking screens against holo, apo, and modeled conformations of enzymes. *J. Med. Chem.* **2003**, *46* (14), 2895-2907.
183. Erickson, J. A.; Jalaie, M.; Robertson, D. H.; Lewis, R. A.; Vieth, M., Lessons in molecular recognition: the effects of ligand and protein flexibility on molecular docking accuracy. *J. Med. Chem.* **2004**, *47* (1), 45-55.
184. Verdonk, M. L.; Giangreco, I.; Hall, R. J.; Korb, O.; Mortenson, P. N.; Murray, C. W., Docking performance of fragments and druglike compounds. *J. Med. Chem.* **2011**, *54* (15), 5422-5431.
185. Instant JChem was used for structure database management, search and prediction. Instant JChem 5.2.5.1: 2009, ChemAxon (<http://www.chemaxon.com>).

186. Pfefferkorn, J. A.; Guzman-Perez, A.; Oates, P. J.; Litchfield, J.; Aspnes, G.; Basak, A.; Benbow, J.; Berliner, M. A.; Bian, J.; Choi, C.; Freeman-Cook, K.; Corbett, J. W.; Didiuk, M.; Dunetz, J. R.; Filipinski, K. J.; Hungerford, W. M.; Jones, C. S.; Karki, K.; Ling, A.; Li, J. C.; Patel, L.; Perreault, C.; Risley, H.; Saenz, J.; Song, W.; Tu, M.; Aiello, R.; Atkinson, K.; Barucci, N.; Beebe, D.; Bourassa, P.; Bourbounais, F.; Brodeur, A. M.; Burbey, R.; Chen, J.; D'Aquila, T.; Derksen, D. R.; Haddish-Berhane, N.; Huang, C.; Landro, J.; Lee, L. A.; MacDougall, M.; Perregaux, D.; Pettersen, J.; Robertson, A.; Tan, B.; Treadway, J. L.; Liu, S.; Qiu, X.; Knafels, J.; Ammirati, M.; Song, X.; DaSilva-Jardine, P.; Liras, S.; Sweet, L.; Rolph, T. P., Designing glucokinase activators with reduced hypoglycemia risk: discovery of N,N-dimethyl-5-(2-methyl-6-((5-methylpyrazin-2-yl)-carbamoyl)benzofuran-4-yloxy)pyrimidine-2-carboxamide as a clinical candidate for the treatment of type 2 diabetes mellitus. *MedChemComm* **2011**, *2* (9), 828-839.
187. Singh, R. K.; Mandal, T.; Balsubramanian, N.; Viaene, T.; Leedahl, T.; Sule, N.; Cook, G.; Srivastava, D. K., Histone deacetylase activators: N-acetylthioureas serve as highly potent and isozyme selective activators for human histone deacetylase-8 on a fluorescent substrate. *Bioorg. Med. Chem. Lett.* **2011**, *21* (19), 5920-5923.
188. Copeland, R. A., *Evaluation of enzyme inhibitors in drug discovery. A guide for medicinal chemists and pharmacologists*. Wiley-Interscience: Hoboken, N.J. : 2005; Vol. 46, p 1-265.
189. Monod, J.; Changeux, J. P.; Jacob, F., Allosteric proteins and cellular control systems. *J. Mol. Biol.* **1963**, *6*, 306-329.
190. Christopoulos, A.; May, L. T.; Avlani, V. A.; Sexton, P. M., G-protein-coupled receptor allosterism: the promise and the problem(s). *Biochem. Soc. Trans.* **2004**, *32* (Pt 5), 873-877.
191. Whittamore, P. R. O.; Bennett, S. N. L.; Simpson, I. Preparation of heterocyclic amide derivatives having glycogen phosphorylase inhibitory activity. WO2003074531A1, 2003.
192. Ivashchenko, A. A.; Lavrovsky, Y. V.; Lakner, F.; Malyarchuk, S. V.; Okun, I. M.; Savchuk, N. F.; Tkachenko, S. E.; Khvat, A. V.; Ivashchenko, A. V. Preparation of heterocyclic compounds as inhibitors of an Hh-signal cascade for treatment of oncological diseases caused by the aberrant activity of an Hh-signal system and pharmaceutical compositions containing them. WO2009077956A2, 2009.
193. Rohde, J.; Peng, B.; Nakai, T.; Sprott, K.; Mermerian, A.; Schairer, W. C. Preparation of thieno[3,2-b]pyrrole derivatives as agonists of the cannabinoid receptors. WO2011100359A1, 2011.
194. Litvinov, V. P.; Fraenkel, G., Thiophthenes. XII. Synthesis of thieno[3,4-b]thiophene-2-carboxylic acid and the NMR-spectra of isomeric thienothiophenes. *Izv. Akad. Nauk SSSR, Ser. Khim.* **1968**, *8*, 1828-1835.
195. Litvinov, V. P.; Shchedrinskaya, T. V.; Konstantinov, P. A.; Gol'dfarb, Y. L., Condensed heteroaromatic systems containing thiophene rings. XXXIII. Catalytic liquid-phase oxidation of 3-methyl derivatives of thieno[2,3-b]thiophene and thieno[3,2-b]thiophene. *Khim. Geterotsikl. Soedin.* **1975**, *4*, 492-498.

196. Prugh, J. D.; Hartman, G. D.; Mallorga, P. J.; McKeever, B. M.; Michelson, S. R.; Murcko, M. A.; Schwam, H.; Smith, R. L.; Sondey, J. M.; Springer, J. P.; Sugrue, M. F., New isomeric classes of topically active ocular hypotensive carbonic anhydrase inhibitors: 5-substituted thieno[2,3-b]thiophene-2-sulfonamides and 5-substituted thieno[3,2-b]thiophene-2-sulfonamides. *J. Med. Chem.* **1991**, *34* (6), 1805-1818.
197. Comel, A.; Sommen, G.; Kirsch, G., Thienothiophenes: Synthesis and applications. *Mini-Rev. Org. Chem.* **2004**, *1* (4), 367-374.
198. Moretto, A. F.; Kirincich, S. J.; Xu, W. X.; Smith, M. J.; Wan, Z. K.; Wilson, D. P.; Follows, B. C.; Binnun, E.; Joseph-McCarthy, D.; Foreman, K.; Erbe, D. V.; Zhang, Y. L.; Tam, S. K.; Tam, S. Y.; Lee, J., Bicyclic and tricyclic thiophenes as protein tyrosine phosphatase 1B inhibitors. *Bioorg. Med. Chem.* **2006**, *14* (7), 2162-2177.
199. Fuller, L. S.; Iddon, B.; Smith, K. A., Thienothiophenes. Part 2.1 Synthesis, metallation and bromine - lithium exchange reactions of thieno[3,2-b]thiophene and its polybromo derivatives. *J. Chem. Soc., Perkin Trans. 1* **1997**, (22), 3465-3470.
200. Prugh, J. D.; Hartman, G. D.; Mallorga, P. J.; McKeever, B. M.; Michelson, S. R.; Murcko, M. A.; Schwam, H.; Smith, R. L.; Sondey, J. M.; Springer, J. P.; et al., New isomeric classes of topically active ocular hypotensive carbonic anhydrase inhibitors: 5-substituted thieno[2,3-b]thiophene-2-sulfonamides and 5-substituted thieno[3,2-b]thiophene-2-sulfonamides. *J. Med. Chem.* **1991**, *34* (6), 1805-1818.
201. He, M.; Zhang, F., Synthesis and structure of alkyl-substituted fused thiophenes containing up to seven rings. *J. Org. Chem.* **2007**, *72* (2), 442-451.
202. Valeur, E.; Bradley, M., Amide bond formation: beyond the myth of coupling reagents. *Chem. Soc. Rev.* **2009**, *38* (2), 606-631.
203. Miyaura, N.; Suzuki, A., Palladium-Catalyzed Cross-Coupling Reactions of Organoboron Compounds. *Chem. Rev.* **1995**, *95* (7), 2457-2483.
204. Wolfe, J. P.; Li, J. J., Chapter 1 An introduction to palladium catalysis. In *Tetrahedron Organic Chemistry Series*, Li, J. J.; Gribble, G. W., Eds. Elsevier: 2007; Vol. 26, pp 1-35.
205. Lipinski, C. A., Overview of Hit to Lead: The Medicinal Chemist's Role from HTS Retest to Lead Optimisation Hand Off. In *Topics in medicinal chemistry*, Hayward, M. M.; Bikker, J. A., Eds. Springer: Heidelberg, Berlin, 2009; Vol. 5, pp 1-24.
206. Jadhav, A.; Ferreira, R. S.; Klumpp, C.; Mott, B. T.; Austin, C. P.; Inglese, J.; Thomas, C. J.; Maloney, D. J.; Shoichet, B. K.; Simeonov, A., Quantitative analyses of aggregation, autofluorescence, and reactivity artifacts in a screen for inhibitors of a thiol protease. *J. Med. Chem.* **2010**, *53* (1), 37-51.
207. Coan, K. E.; Shoichet, B. K., Stoichiometry and physical chemistry of promiscuous aggregate-based inhibitors. *J. Am. Chem. Soc.* **2008**, *130* (29), 9606-9612.
208. Shoichet, B. K., Screening in a spirit haunted world. *Drug Discov. Today* **2006**, *11* (13-14), 607-615.

- 
209. McGovern, S. L.; Caselli, E.; Grigorieff, N.; Shoichet, B. K., A common mechanism underlying promiscuous inhibitors from virtual and high-throughput screening. *J. Med. Chem.* **2002**, *45* (8), 1712-1722.
210. Baker, M., Academic screening goes high-throughput. *Nat. Meth.* **2010**, *7* (10), 787-792.
211. Coan, K. E.; Maltby, D. A.; Burlingame, A. L.; Shoichet, B. K., Promiscuous aggregate-based inhibitors promote enzyme unfolding. *J. Med. Chem.* **2009**, *52* (7), 2067-2075.
212. McGovern, S. L.; Helfand, B. T.; Feng, B.; Shoichet, B. K., A specific mechanism of nonspecific inhibition. *J. Med. Chem.* **2003**, *46* (20), 4265-4272.
213. Shoichet, B. K., Interpreting steep dose-response curves in early inhibitor discovery. *J. Med. Chem.* **2006**, *49* (25), 7274-7277.
214. Feng, B. Y.; Simeonov, A.; Jadhav, A.; Babaoglu, K.; Inglese, J.; Shoichet, B. K.; Austin, C. P., A high-throughput screen for aggregation-based inhibition in a large compound library. *J. Med. Chem.* **2007**, *50* (10), 2385-2390.
215. Fasano, M.; Curry, S.; Terreno, E.; Galliano, M.; Fanali, G.; Narciso, P.; Notari, S.; Ascenzi, P., The extraordinary ligand binding properties of human serum albumin. *IUBMB Life* **2005**, *57* (12), 787-796.
216. Bertucci, C.; Domenici, E., Reversible and covalent binding of drugs to human serum albumin: methodological approaches and physiological relevance. *Curr. Med. Chem.* **2002**, *9* (15), 1463-1481.
217. Coan, K. E.; Shoichet, B. K., Stability and equilibria of promiscuous aggregates in high protein milieus. *Mol. Biosyst.* **2007**, *3* (3), 208-213.
218. Feng, B. Y.; Shoichet, B. K., A detergent-based assay for the detection of promiscuous inhibitors. *Nat. Protoc.* **2006**, *1* (2), 550-553.
219. Feng, B. Y.; Shelat, A.; Doman, T. N.; Guy, R. K.; Shoichet, B. K., High-throughput assays for promiscuous inhibitors. *Nat. Chem. Biol.* **2005**, *1* (3), 146-148.
220. Ryan, A. J.; Gray, N. M.; Lowe, P. N.; Chung, C. W., Effect of detergent on "promiscuous" inhibitors. *J. Med. Chem.* **2003**, *46* (16), 3448-3451.
221. Ouellet, M.; Falgueyret, J. P.; Percival, M. D., Detergents profoundly affect inhibitor potencies against both cyclo-oxygenase isoforms. *Biochem. J.* **2004**, *377* (Pt 3), 675-684.
222. Leach, A. R.; Hann, M. M., Molecular complexity and fragment-based drug discovery: ten years on. *Curr. Opin. Chem. Biol.* **2011**, *15* (4), 489-496.
223. Blundell, T. L.; Patel, S., High-throughput X-ray crystallography for drug discovery. *Curr. Opin. Pharmacol.* **2004**, *4* (5), 490-496.
224. Nwaka, S.; Hudson, A., Innovative lead discovery strategies for tropical diseases. *Nat. Rev. Drug Discov.* **2006**, *5* (11), 941-955.

225. Wanger, A., Disk Diffusion Test and Gradient Methodologies. In *Antimicrobial Susceptibility Testing Protocols*, Schwalbe, R.; Steele-Moore, L.; Goodwin, A. C., Eds. CRC Press: Boca Raton, Florida, 2007; pp 53-73.
226. Motulsky, H. J.; Christopoulos, A., *Fitting models to biological data using linear and nonlinear regression. A practical guide to curve fitting*. GraphPad Software Inc.: San Diego CA, [www.graphpad.com](http://www.graphpad.com), 2003.
227. Piotto, M.; Saudek, V.; Sklenar, V., Gradient-tailored excitation for single-quantum NMR spectroscopy of aqueous solutions. *J. Biomol. NMR* **1992**, *2* (6), 661-665.
228. Goddard, T. D.; Kneller, D. G., SPARKY 3. University of California: San Francisco, 2006.
229. DeLano, W. L., *The PyMOL molecular graphics system*. DeLano Scientific LLC: San Carlos, California, U.S.A. (<http://www.delanoscientific.com>), 2006.
230. Gottlieb, H. E.; Kotlyar, V.; Nudelman, A., NMR chemical shifts of common laboratory solvents as trace impurities. *J. Org. Chem.* **1997**, *62* (21), 7512-7515.
231. Still, W. C.; Kahn, M.; Mitra, A., Rapid chromatographic technique for preparative separations with moderate resolution. *J. Org. Chem.* **1978**, *43* (14), 2923-2925.
232. Barbosa, M. L.; Melo, G. M.; da Silva, Y. K.; Lopes Rde, O.; de Souza, E. T.; de Queiroz, A. C.; Smaniotto, S.; Alexandre-Moreira, M. S.; Barreiro, E. J.; Lima, L. M., Synthesis and pharmacological evaluation of *N*-phenyl-acetamide sulfonamides designed as novel non-hepatotoxic analgesic candidates. *Eur. J. Med. Chem.* **2009**, *44* (9), 3612-3620.
233. Baraldi, P. G.; Moorman, A. R.; Borea, P. A. Novel adenosine A3 receptor agonists. WO 2005028489, 2005.
234. Patel, P. R.; Ramalingan, C.; Park, Y. T., Synthesis and antimicrobial evaluation of guanylsulfonamides. *Bioorg. Med. Chem. Lett.* **2007**, *17* (23), 6610-6614.
235. Salvino, J. M.; Gerard, B.; Ye, H. F.; Sauvagnat, B.; Dolle, R. E., The solid-phase synthesis and use of *N*-monosubstituted piperazines in chemical library synthesis. *J. Comb. Chem.* **2003**, *5* (3), 260-266.
236. Winikoff, D.; Trikojus, V. M., *N*-Diethylsulphanilamide: a reagent for the colorimetric estimation of thyroxine. *Biochem. J.* **1948**, *42* (3), 475-480.
237. Cass, W. E., Sulfanilyl pyrrolidine and pyrroline. *J. Am. Chem. Soc.* **1940**, *62* (11), 3255-3267.
238. Ilyin, A. P.; Dmitrieva, I. G.; Kustova, V. A.; Manaev, A. V.; Ivachtchenko, A. V., Synthesis of heterocyclic compounds possessing the 4H-thieno[3,2-b]pyrrole moiety. *J. Comb. Chem.* **2007**, *9* (1), 96-106.
239. Carpino, L. A.; Abdel-Maksoud, A. A.; Ionescu, D.; Mansour, E. M.; Zewail, M. A., 1,1-dioxonaphtho[1,2-b]thiophene-2-methyloxycarbonyl (alpha-Nsmoc) and 3,3-dioxonaphtho[2,1-b]thiophene-2-methyloxycarbonyl (beta-Nsmoc) amino-protecting groups. *J. Org. Chem.* **2007**, *72* (5), 1729-1736.

- 
240. Mangini, A., Sulfonamides V. *Chem. Zentr.* **1941**, *1*, 146-147.
241. Pool, D. H.; DuBois, D. L., [Ni(PPh<sub>2</sub>NAr<sub>2</sub>)<sub>2</sub>(NCMe)][BF<sub>4</sub>]<sub>2</sub> as an electrocatalyst for H<sub>2</sub> production: PPh<sub>2</sub>NAr<sub>2</sub> = 1,5-(di(4-(thiophene-3-yl)phenyl)-3,7-diphenyl-1,5-diaza-3,7-diphosphacyclooctane). *J. Organomet. Chem.* **2009**, *694* (17), 2858-2865.
242. Lameijer, E. W.; Tromp, R. A.; Spanjersberg, R. F.; Brussee, J.; Ijzerman, A. P., Designing active template molecules by combining computational de novo design and human chemist's expertise. *J. Med. Chem.* **2007**, *50* (8), 1925-1932.
243. Guizzardi, B.; Mella, M.; Fagnoni, M.; Albini, A., Easy photochemical preparation of 2-dimethylaminophenylfurans, -pyrroles and -thiophenes. *Tetrahedron* **2000**, *56* (47), 9383-9389.
244. Molander, G. A.; Canturk, B.; Kennedy, L. E., Scope of the Suzuki-Miyaura cross-coupling reactions of potassium heteroaryltrifluoroborates. *J. Org. Chem.* **2009**, *74* (3), 973-980.

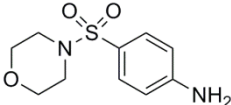
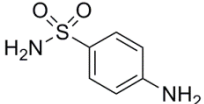
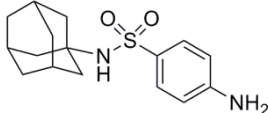
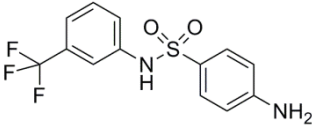
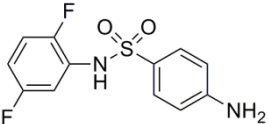
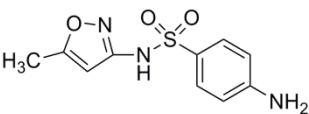
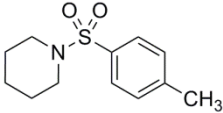
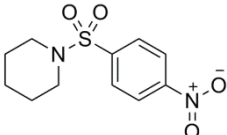
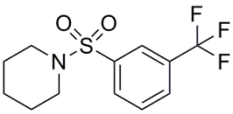
# Appendices

---

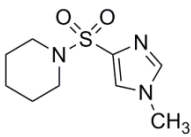
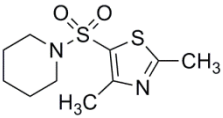
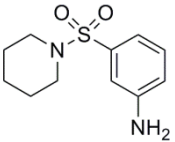
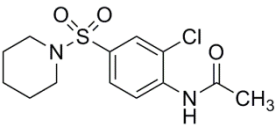
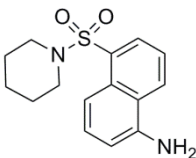
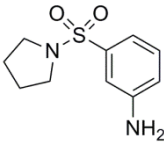
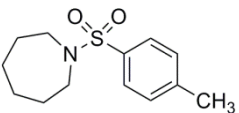
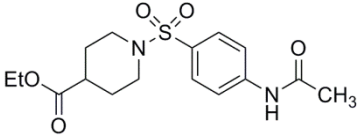
# Appendices

## Appendix I

**Table A.** Summary of inhibitory data for the sulfonamide analogues obtained from internal library or purchased. ‘\*’ Indicates inhibitory activity could not be measured due to low compound solubility.

	Structure	Inhibition (%)	
		500 $\mu$ M	300 $\mu$ M
124		85	-
125		9	-
126*		-	-
127		-	43
128		-	3
129		-	17
130		-	5
131		-	16
132		-	11

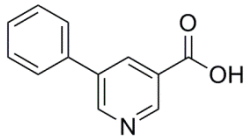
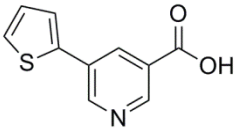
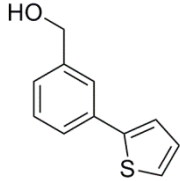
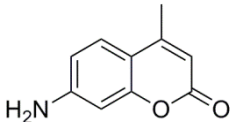
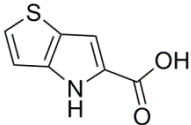
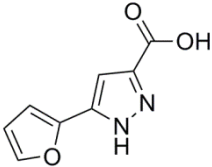
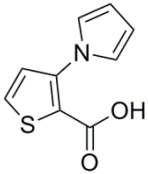
---

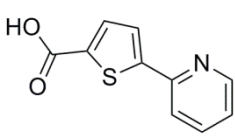
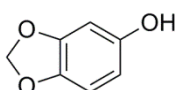
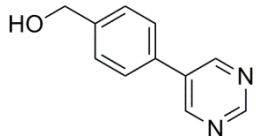
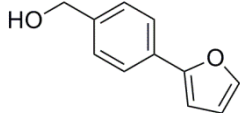
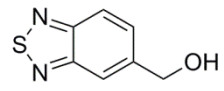
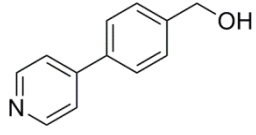
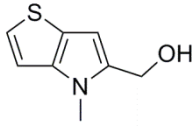
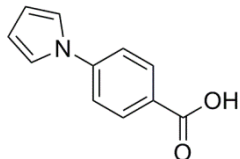
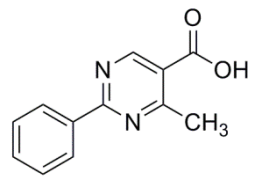
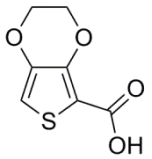
133		5	-
134		10	-
135		28	-
136		-	- 49
137*		-	-
138		4	-
139		-	17
139		-	- 44

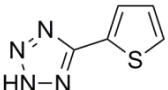
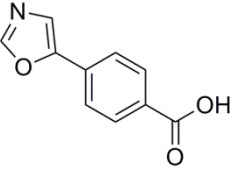
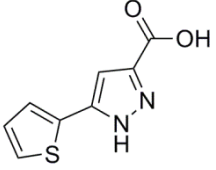
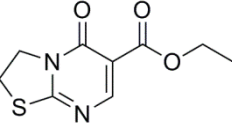
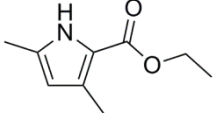
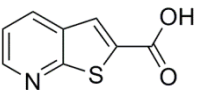
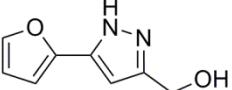
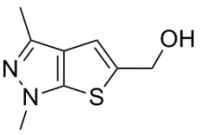
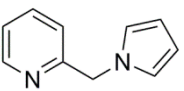
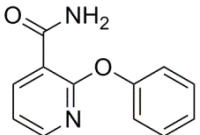
---

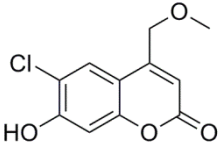
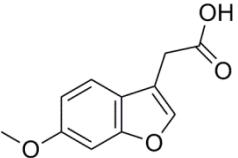
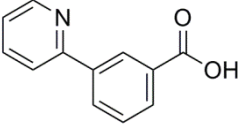
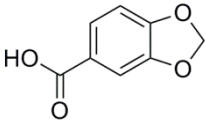
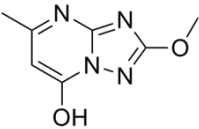
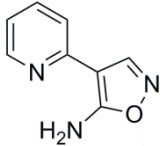
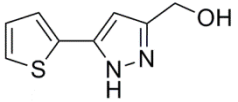
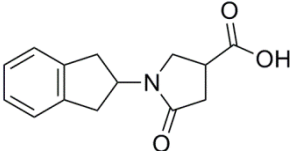
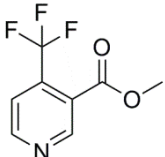
## Appendix II

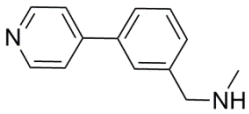
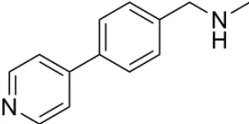
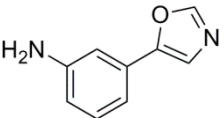
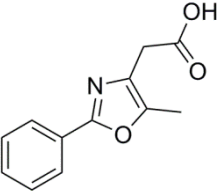
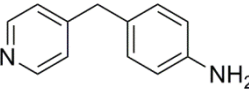
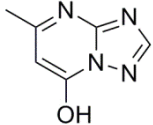
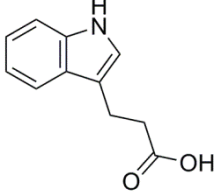
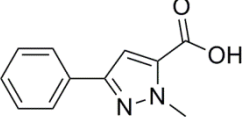
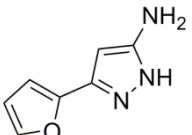
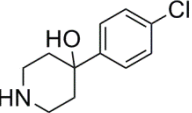
**Table B.** Summary of rescreened fragment hits with their STD-NMR,  $^1\text{H}/^{15}\text{N}$ -HSQC, single concentration inhibition and  $\text{IC}_{50}$  values tabulated. For the STD summary the letters: S = strong, M = medium, W = weak; HSQC score is the magnitude of CSPs observed in the  $^1\text{H}/^{15}\text{N}$ -HSQC experiment: 3 = significant change, 2 = definite hit, 1 = maybe, 0 = no change. ‘\*’ Indicates inhibitory activity could not be measured due to low compound solubility or the compound had degraded based on LCMS or HPLC analysis.

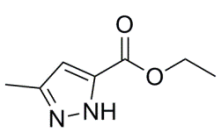
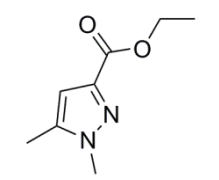
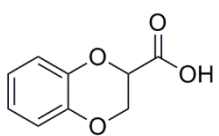
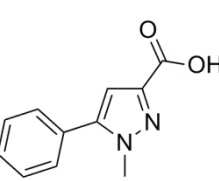
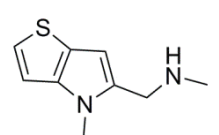
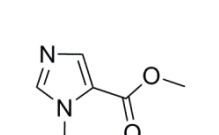
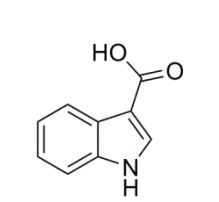
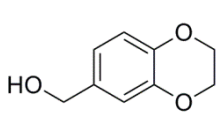
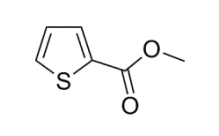
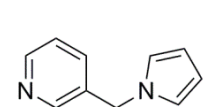
	Fragment	STD (S/M/W)	HSQC Score (0-3)	% Inhibition (1 mM)	$\text{IC}_{50}$ ( $\mu\text{M}$ )
220		S	2	69	13
221		W	3	76	6
71		S	3	89	292
222		W	0	63	664
150		M	2	45	> 1000
90		M	2	44	> 1000
223		M	1	66	> 1000

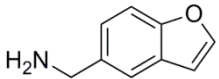
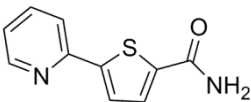
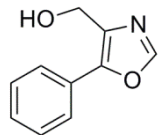
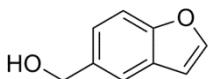
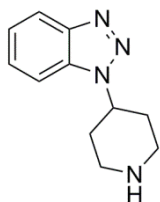
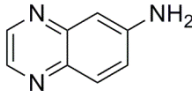
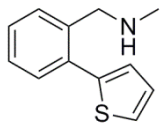
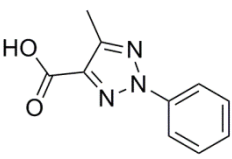
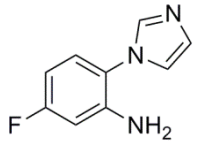
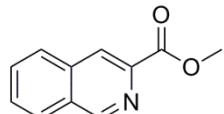
224		W	3	42	> 1000
110		S	3	44	> 1000
225		W	1	73	> 1000
203*		W	1	-	
226		W	2	51	> 1000
247		W	0	39	
147		W	1-0	37	
77		S	3	33	
248		W	2	32	
249		W	0	28	

250		M	3	24
251		M	3	23
252		M	3	22
253		W	0	22
117		M	3	21
102		W	2	20
254		W	1	20
255		W	0	19
256		W	0	17
257		W	0	17

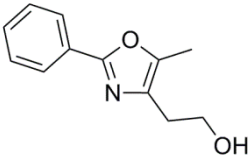
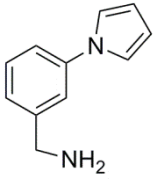
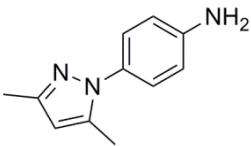
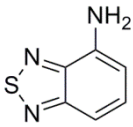
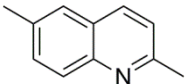
107		W	2	17
105		M	3	17
258*		W	3	-
259		W	0	14
260*		M	1	-
261		S	0	12
89		W	2	12
262		W	0	12
263		W	1	11

264		W	0	11
265		W	3	10
266		W	2	9
267		W	1	9
268		W	0	8
269*		W	3	-
94		W	3	7
270		M	2	7
271		M	2	7
272*		W	0	-

273		W	1	6
274		W	1	6
275		W	1	6
276		M	2	5
146		W	1	5
277		M	0	5
278		W	1-0	5
279		W	1-0	5
280		W	0	4
281		W	0	4

282		W	0	4
283		M	0	3
284		W	0	3
104		M	2	3
285		W	0	2
286		W	0	2
186		W	0	2
86		M	2	2
287		W	1-0	2
288		W	0	1

---

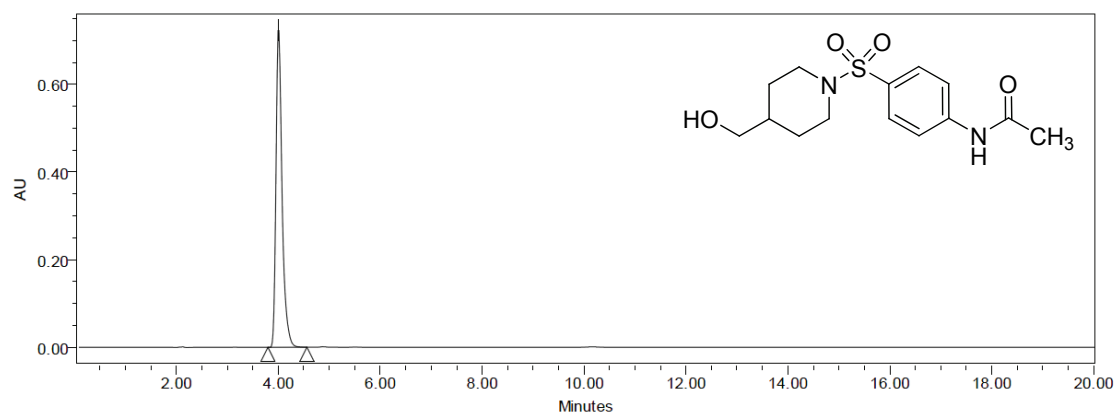
82		S	2	0
289*		M	1-0	-
290		S	0	-2
291		W	2	-5
292		W	1-0	-6

---

## Appendix III

### A: HPLC chromatograms for synthesised sulfonamide analogues

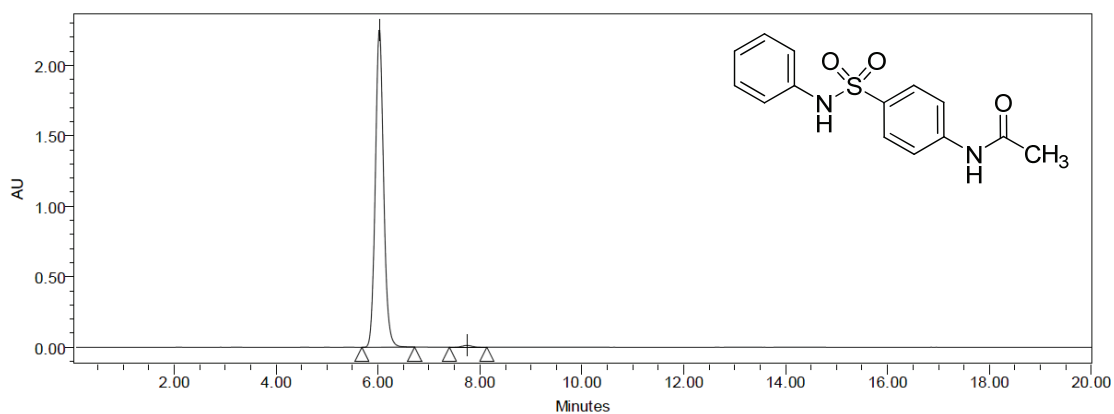
#### *N*-{4-[4-(Hydroxymethyl)piperidine-1-sulfonyl]phenyl}acetamide (143e)



Conditions: Isocratic elution: 0-20 min, 70% A, 30% B

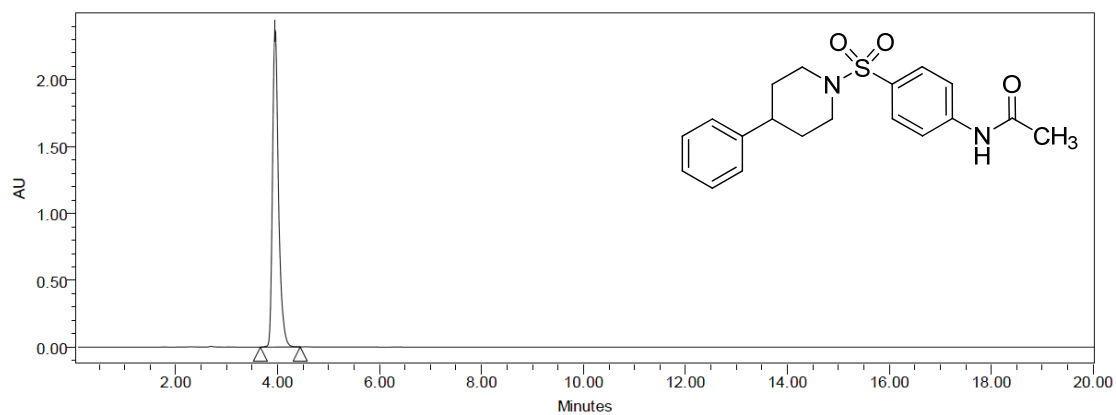
Peak	RT (min)	Area	% Area	Height
1	4.006	5949978	100.00	726599

#### *N*-[4-(Phenylsulfonyl)phenyl]acetamide (143g)



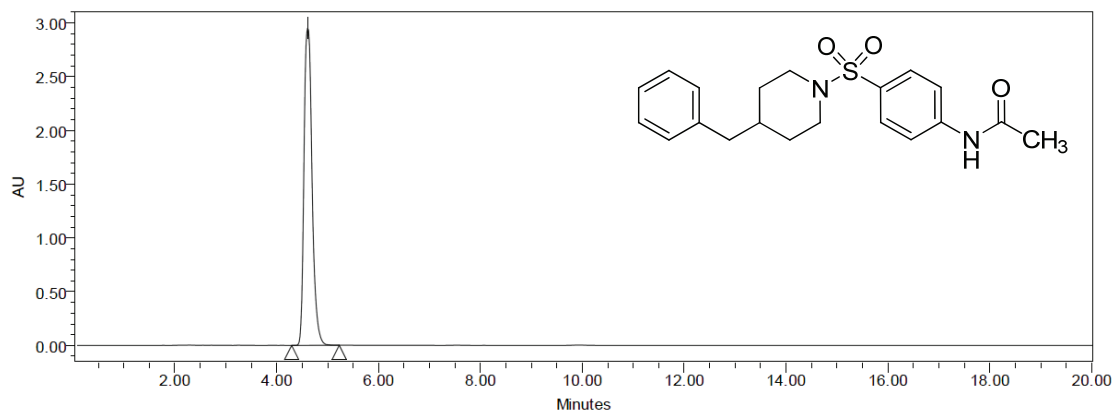
Conditions: Isocratic elution: 0-20 min, 70% A, 30% B

Peak	RT (min)	Area	% Area	Height
1	6.026	25681631	99.33	2259863
2	7.745	173023	0.67	12348

***N*-[4-(4-Phenylpiperidine-1-sulfonyl)phenyl]acetamide (143j)**

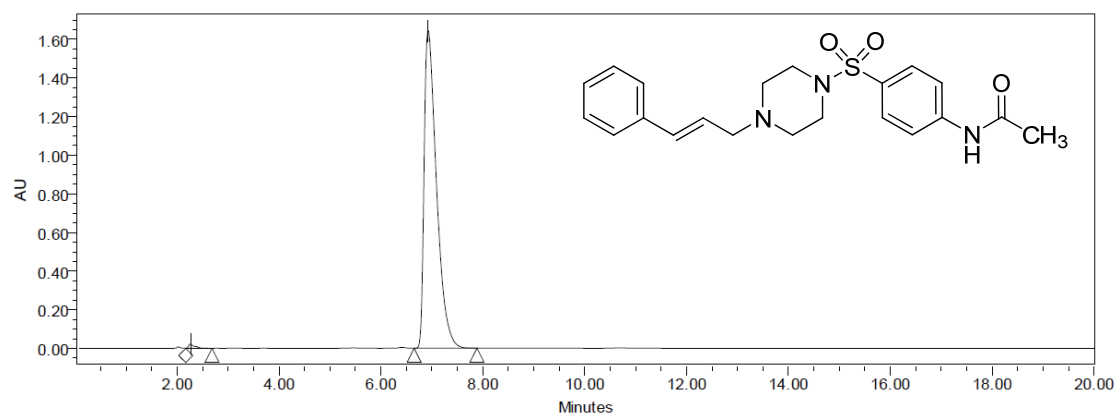
Conditions: Isocratic elution: 0-20 min, 50% A, 50% B

Peak	RT (min)	Area	% Area	Height
1	3.953	19389246	100.00	2395099

***N*-[4-(4-Benzylpiperidine-1-sulfonyl)phenyl]acetamide (143k)**

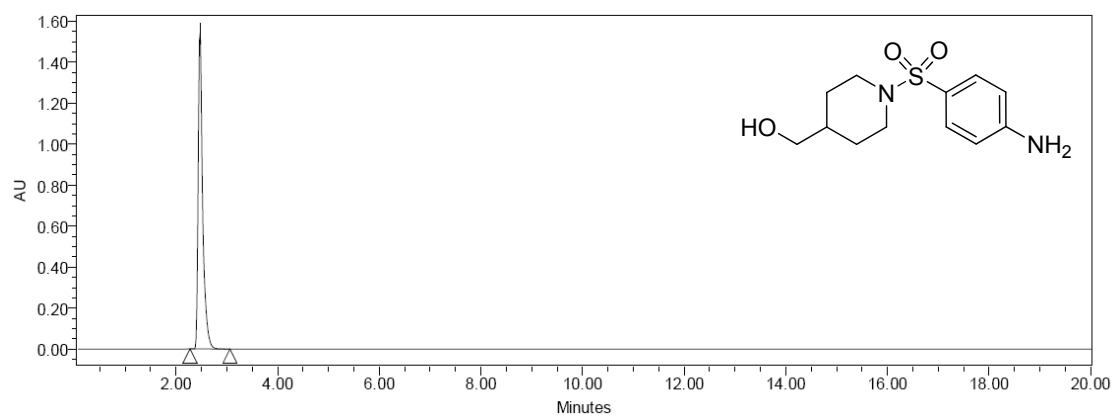
Conditions: Isocratic elution: 0-20 min, 50% A, 50% B

Peak	RT (min)	Area	% Area	Height
1	4.610	32249837	100.00	2957292

***N*-[4-(4-Cinnamylpiperazine-1-sulfonyl)phenyl]acetamide (143m)**

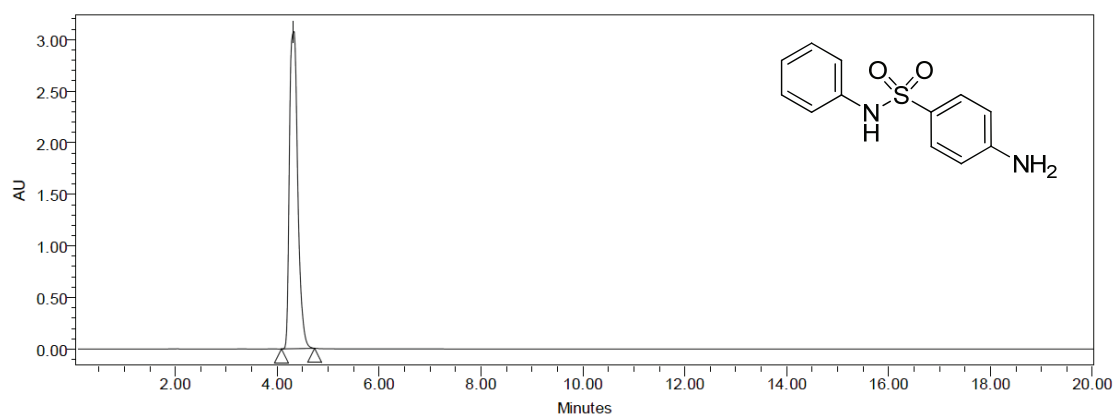
Conditions: Isocratic elution: 0-20 min, 70% A, 30% B

Peak	RT (min)	Area	% Area	Height
1	2.264	182139	0.66	22411
2	6.928	27623117	99.34	1653700

**{1-[(4-Aminobenzene)sulfonyl]piperidin-4-yl}methanol (144e)**

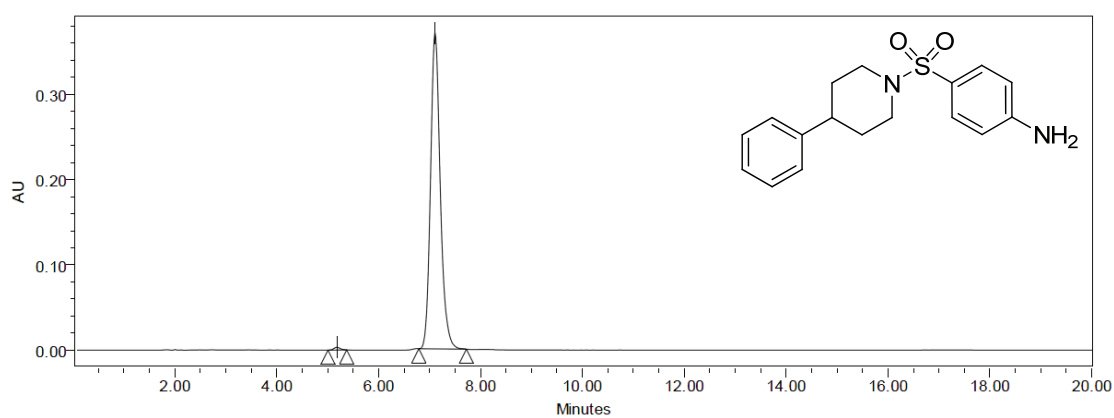
Conditions: Isocratic elution: 0-20 min, 60% A, 40% B

Peak	RT (min)	Area	% Area	Height
1	2.473	9479117	100.00	1538595

**4-Amino-N-phenylbenzene-1-sulfonamide (144g)**

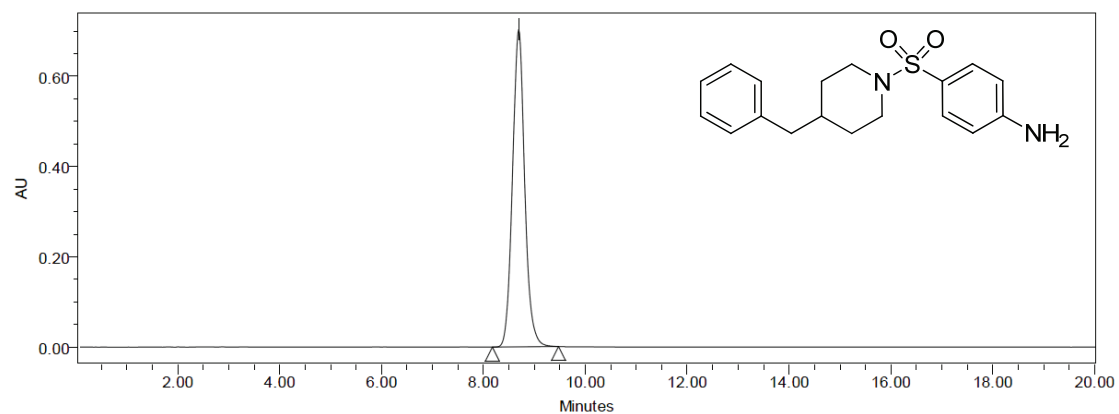
Conditions: Isocratic elution: 0-20 min, 60% A, 40% B

Peak	RT (min)	Area	% Area	Height
1	4.315	35100468	100.00	3084434

**4-(4-Phenylpiperidine-1-sulfonyl)aniline (144j)**

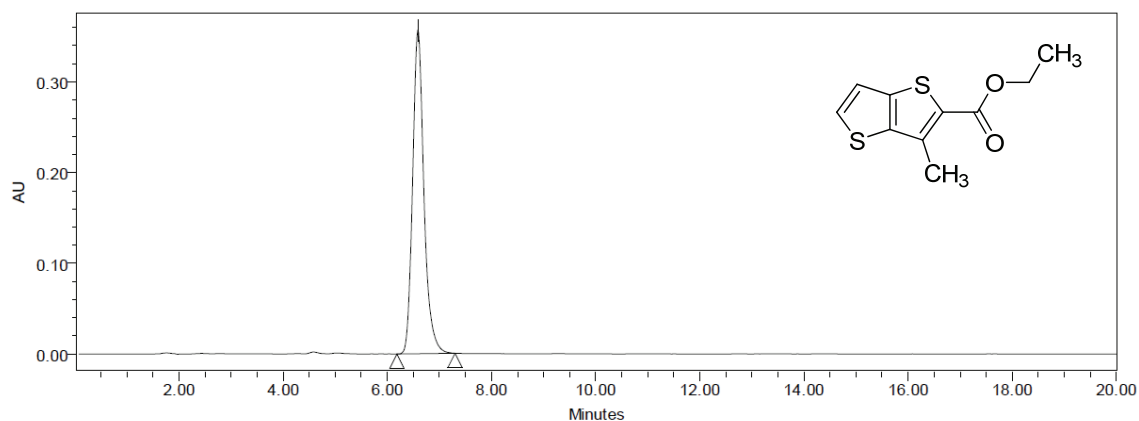
Conditions: Isocratic elution: 0-20 min, 50% A, 50% B

Peak	RT (min)	Area	% Area	Height
1	5.180	28136	0.57	3150
2	7.107	4951329	99.43	370816

**4-(4-Benzylpiperidine-1-sulfonyl)aniline (144k)**

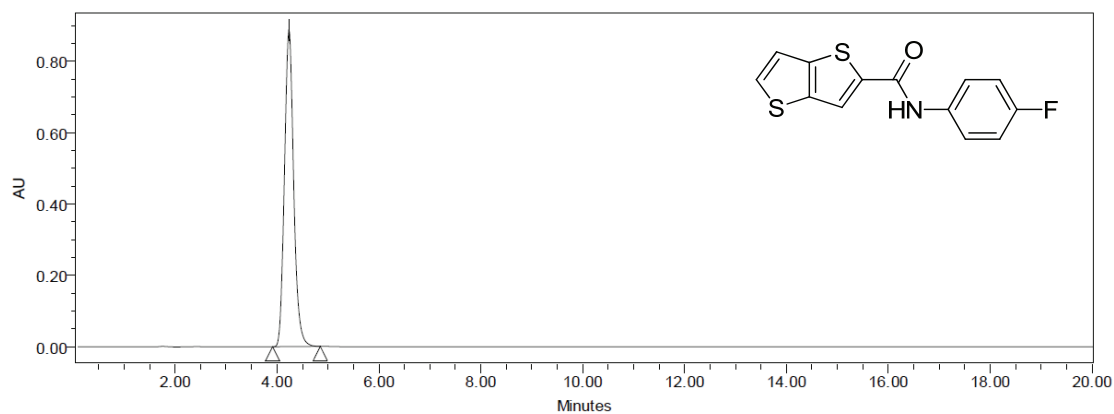
Conditions: Isocratic elution: 0-20 min, 50% A, 50% B

Peak	RT (min)	Area	% Area	Height
1	8.691	11724450	100.00	703061

**B: HPLC chromatograms for synthesised thienothiophene analogues****Ethyl 3-methylthieno[3,2-*b*]thiophene-2-carboxylate (162a)**

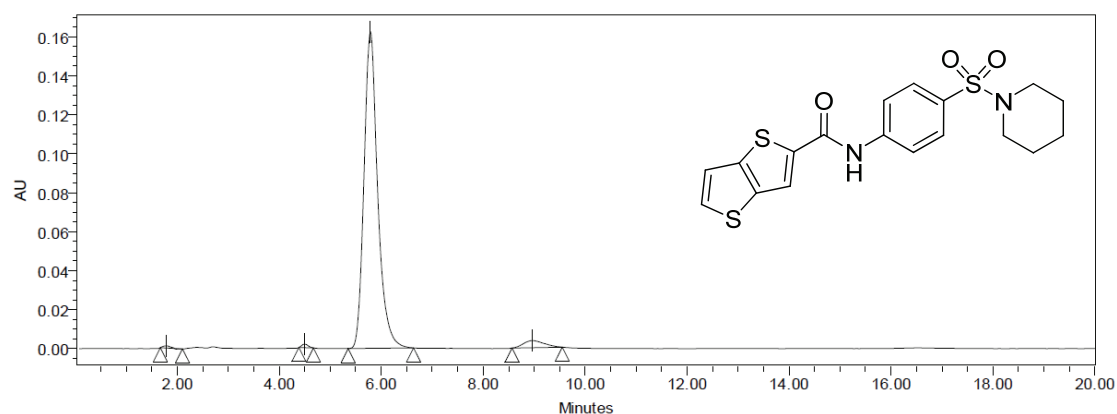
Conditions: Isocratic elution: 0-20 min, 40% A, 60% B

Peak	RT (min)	Area	% Area	Height
1	6.588	5412820	100.00	357110

***N*-(4-Fluorophenyl)thieno[3,2-*b*]thiophene-2-carboxamide (166)**

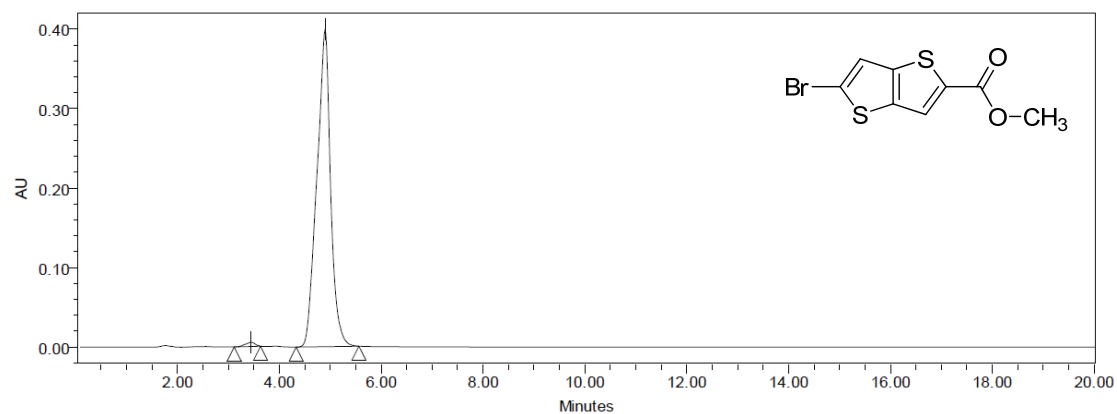
Conditions: Isocratic elution: 0-20 min, 40% A, 60% B

Peak	RT (min)	Area	% Area	Height
1	4.235	11225183	100.00	888394

***N*-[4-(Piperidine-1-sulfonyl)phenyl]thieno[3,2-*b*]thiophene-2-carboxamide (167)**

Conditions: Isocratic elution: 0-20 min, 40% A, 60% B

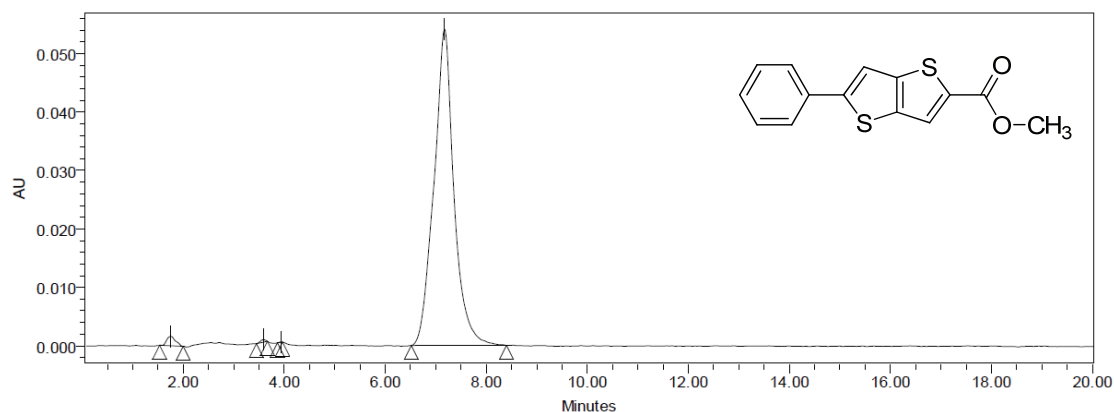
Peak	RT (min)	Area	% Area	Height
1	1.781	12832	0.41	1138
2	4.499	15893	0.50	1806
3	5.787	3017386	95.82	162692
4	8.968	103049	3.27	3626

**Methyl 5-bromothieno[3,2-*b*]thiophene-2-carboxylate (172)**

Conditions: Isocratic elution: 0-20 min, 50% A, 50% B

Peak	RT (min)	Area	% Area	Height
1	3.446	68250	0.90	5265
2	4.896	7493671	99.10	398791

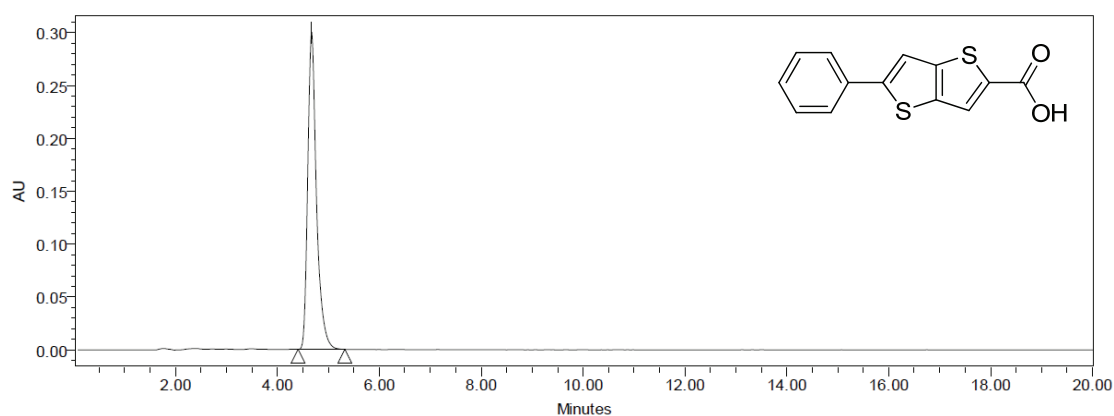
### Methyl 5-phenylthieno[3,2-*b*]thiophene-2-carboxylate (174)



Conditions: Isocratic elution: 0-20 min, 40% A, 60% B

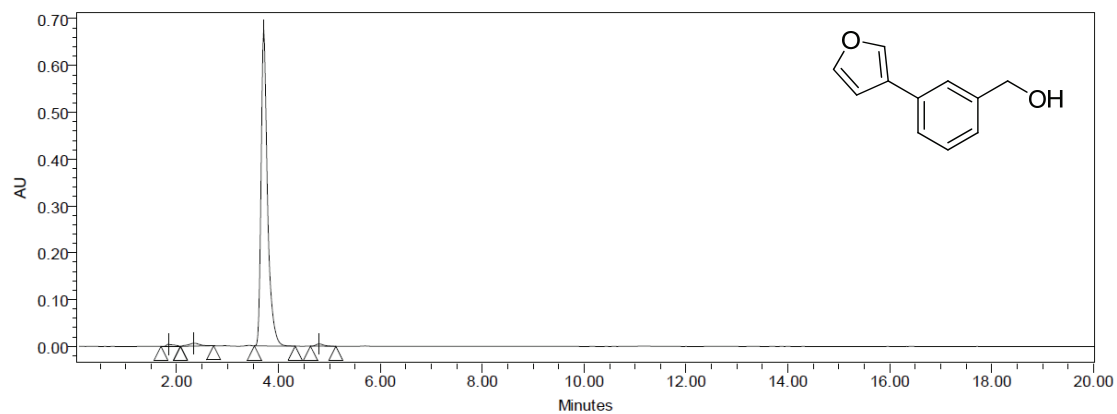
Peak	RT (min)	Area	% Area	Height
1	1.750	19301	1.28	1605
2	3.584	2906	0.19	424
3	3.941	242	0.02	59
4	7.173	1483247	98.51	54102

### 5-Phenylthieno[3,2-*b*]thiophene-2-carboxylic acid (175)



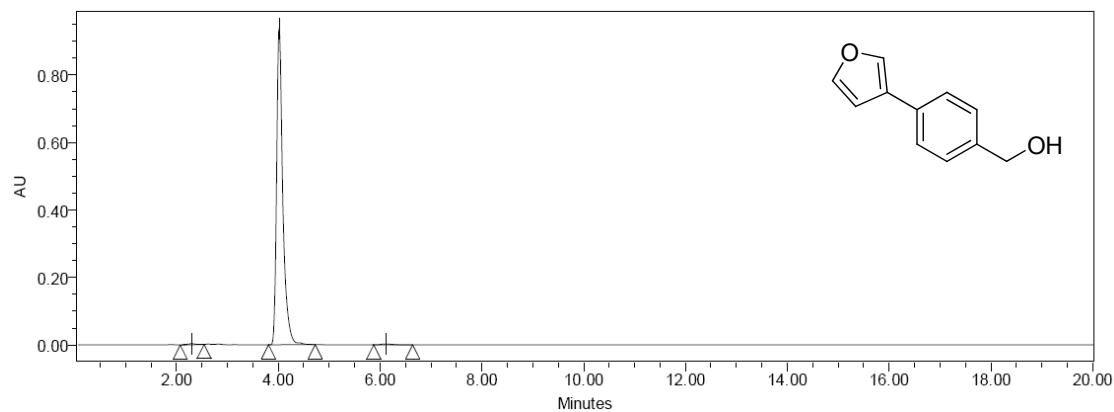
Conditions: Isocratic elution: 0-20 min, 40% A, 60% B

Peak	RT (min)	Area	% Area	Height
1	4.670	3569305	100.00	300187

**C: HPLC chromatograms for synthesised phenylfuran analogues****[3-(Furan-3-yl)phenyl]methanol (200)**

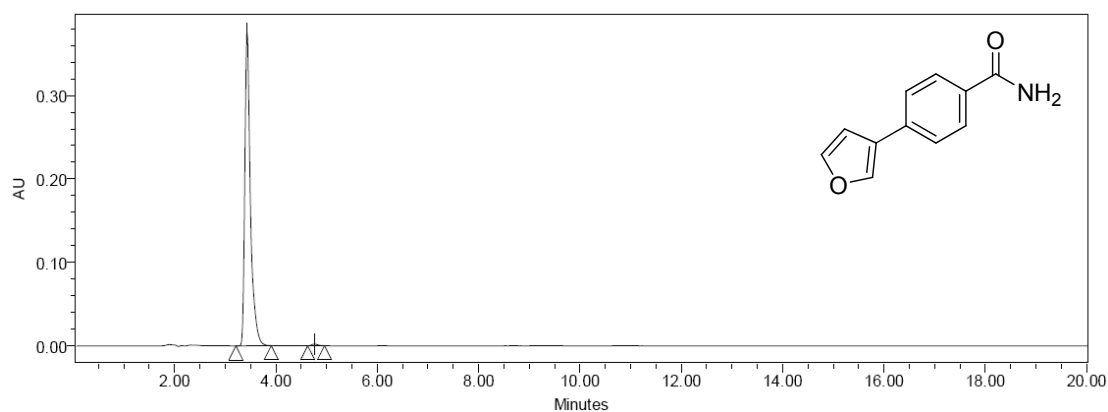
Conditions: Isocratic elution: 0-20 min, 60% A, 40% B

Peak	RT (min)	Area	% Area	Height
1	1.847	49582	0.81	4305
2	2.339	96473	1.57	6203
3	3.711	5931917	96.79	675012
4	4.801	50679	0.83	4868

**[4-(Furan-3-yl)phenyl]methanol (204)**

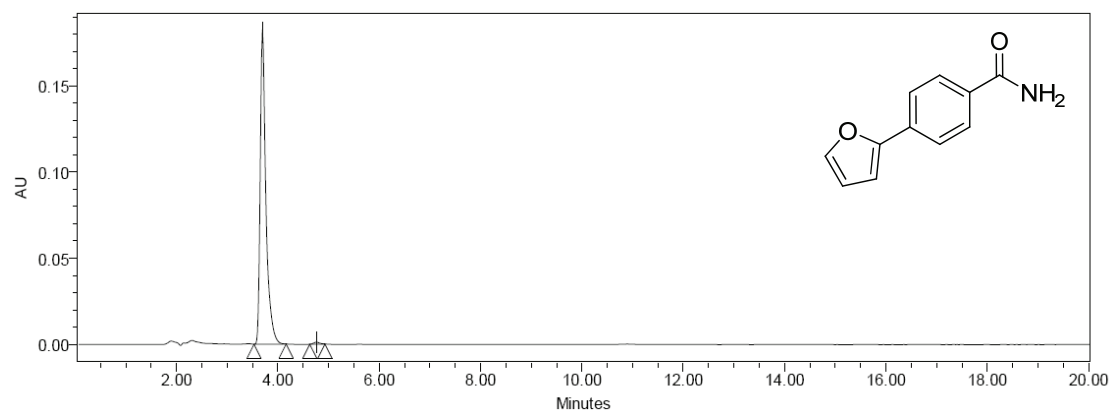
Conditions: Isocratic elution: 0-20 min, 60% A, 40% B

Peak	RT (min)	Area	% Area	Height
1	2.298	39577	0.50	3228
2	4.020	7881479	99.07	941341
3	6.111	34347	0.43	2414

**4-(Furan-3-yl)benzamide (215)**

Conditions: Isocratic elution: 0-20 min, 60% A, 40% B

Peak	RT (min)	Area	% Area	Height
1	3.433	2852380	99.40	378385
2	4.761	17144	0.60	2007

**4-(Furan-2-yl)benzamide (216)**

Conditions: Isocratic elution: 0-20 min, 60% A, 40% B

Peak	RT (min)	Area	% Area	Height
1	3.698	1438370	99.36	181858
2	4.761	9291	0.64	1141



---

